SYNTHESIS, REACTIVITY AND CATALYTIC ACTIVITY OF METAL COMPLEXES

A THESIS

Submitted in partial fulfilment of the requirements for the award of the degree of

DOCTOR OF PHILOSOPHY

in

CHEMISTRY

by

CHANCHAL HALDAR

DEPARTMENT OF CHEMISTRY
INDIAN INSTITUTE OF TECHNOLOGY ROORKEE
ROORKEE-247 667 (INDIA)

MAY, 2012

INDIAN INSTITUTE OF TECHNOLOGY ROORKEE
ROORKEE

CANDIDATE'S DECLARATION

I hereby certify that the work which is being presented in the thesis entitled **SYNTHESIS, REACTIVITY AND CATALYTIC ACTIVITY OF METAL COMPLEXES** in partial fulfilment of the requirements for the award of the Degree of Doctor of Philosophy and submitted in the Department of Chemistry of the Indian Institute of Technology Roorkee is an authentic record of my own work carried out during a period from January, 2009 to May, 2012 under the supervision of Dr. Mannar R. Maurya, Professor, Department of Chemistry, Indian Institute of Technology Roorkee, Roorkee.

The matter presented in the thesis has not been submitted by me for the award of any other degree of this or any other Institute.

Chanchal Haldar.

(Chanchal Haldar)

This is to certify that the above statement made by the candidate is correct to the best of my knowledge.

Date: May 31, 2012

Mmaurya

(Mannar R. Maurya)
Supervisor

The Ph. D. Viva-Voce Examination of **Mr. Chanchal Haldar**, Research Scholar, has been held on ...July 04, 2012.....

Mmaurya
Signature of Supervisor

Signature of Chairman SRC

04.07.12
Signature of External Examiner

04 July 2012
Head of the Deptt. / Chairman ODC

ABSTRACT

Vanadium exhibits formal oxidation states from +V down to –III. The most stable oxidation states +IV and +V under normal conditions are generally stabilized through V-O bond and oxocations $[VO]^{2+}$, $[VO]^{3+}$ and $[VO_2]^{+}$ are most common for biological systems. Vanadium in these oxidation states comfortably binds with O, N and S donor ligands. The discovery of vanadium(V) in vanadium based enzymes e.g. vanadate-dependent haloperoxidases, attracted attention of researcher to develop coordination chemistry of vanadium(V) in search of good models for vanadium-containing biomolecules. Vanadium compounds have also been found to promote a peroxide-driven oxidation of organic substrates. Basic chemistry and potential applications of vanadium complexes in diverse fields have been discussed time to time in International Vanadium Chemistry symposium held biannually (For chemistry discussed in recent symposium please refer to Coord. Chem. Rev., 255 (2011)). In view of the above it may clearly be conceived that the coordination chemistry of vanadium is of increasing potential interest and therefore it was considered desirable to study the coordination chemistry of vanadium with the ligands that would provide structural and functional models of haloperoxidases. Stability, structural and reactivity studies have been carried out to model the role of vanadium in vanadium based enzymes. Coordination chemistry has further been extended to manganese with the idea if they would serve good functional models of haloperoxidases. At the end, looking at the importance of zeolite-Y encapsulated metal complexes (ZEMC) where these complexes are suggested as model compounds for enzyme mimicking, copper(II) complex has been prepared and encapsulated in the cavity of zeolite-Y to study its catalytic activity.

For convenient the work embodied in the thesis has been divided into following chapters:

First chapter is introductory one and deals with the general remarks on vanadium and manganese, their occurrence in nature and biological systems. Applications of vanadium complexes with particular emphasis on structural and functional models of haloperoxidases have been discussed. Applications of manganese complexes as potential catalysts have also been considered. At the end importance of zeolite-Y encapsulated metal complexes (with simple as well as macrocyclic ligands) in the catalytic field has also been presented.

$[V^{IV}O(acac)_2]$ reacts with ligands $CH_2(H_2L)_2$ in refluxing methanol to yield two neutral binuclear V^{IV}-complexes formulated as $[CH_2\{V^{IV}OL(H_2O)\}_2]$, namely **2.1** and **2.2**. Ligands $CH_2(H_2L)_2$ **2.I** and **2.II** are derived from 5,5'-methylenebis(salicylaldehyde) and S-benzyldithiocarbazate [$CH_2(H_2sal\text{-}sbdt)_2$, **2.I**] or S-methydithiocarbazate [$CH_2(H_2sal\text{-}smdt)_2$, **2.II**]. Aerial oxidation of **2.1** and **2.2** in the presence of KOH or $CsOH{\cdot}H_2O$ results in the formation of dioxidovanadium(V) complexes, $K_2[CH_2\{V^{V}O_2(sal\text{-}sbdt)\}_2]{\cdot}2H_2O$ (**2.3**), $Cs_2[CH_2\{V^{V}O_2(sal\text{-}sbdt)\}_2]{\cdot}2H_2O$ (**2.4**) $K_2[CH_2\{V^{V}O_2(sal\text{-}smdt)\}_2]{\cdot}2H_2O$ (**2.5**) and $Cs_2[CH_2\{V^{V}O_2(sal\text{-}smdt)\}_2]{\cdot}2H_2O$ (**2.6**). Characterization of these complexes, their reactivity and catalytic activity are presented in **Chapter 2**. These compounds are characterized in the solid state and in solution, namely by spectroscopic techniques (IR, UV-Vis, EPR, ^{1}H, ^{13}C and ^{51}V NMR). It is demonstrated that the $V^{V}O_2$-complexes **2.3–2.6** are efficient and selective towards the oxidative bromination by H_2O_2 of styrene yielding 1,2-dibromo-1-phenylethane, 1-phenylethane-1,2-diol and 2-bromo-1-phenylethane-1-ol, therefore acting as functional models of vanadium dependent haloperoxidases. Plausible intermediates involved in these catalytic processes are established by UV-Vis, EPR and ^{51}V NMR studies.

Chapter 3 considers vanadium chemistry with binucleating ligands derived from 2,6-diformyl-4-methylphenol and various hydrazides. These hydrazones [$H_3dfmp(inh)_2$ (**3.I**), $H_3dfmp(nah)_2$ (**3.II**) and $H_3dfmp(bhz)_2$ (**3.III**); inh = isonicotinoylhydrazide, nah = nicotinoylhydrazide and bhz = benzoylhydrazide] react with $[V^{IV}O(acac)_2]$ in refluxing methanol to give oxidovanadium(IV) complexes, $[V^{IV}O\{Hdfmp(inh)_2\}]$ (**3.1**),

$[V^{IV}O\{Hdfmp(nah)_2\}]$ (**3.2**) and $[V^{IV}O\{Hdfmp(bhz)_2\}]$ (**3.3**). Aerial oxidation of these complexes in methanol results in the formation of complexes, $[V^{V}O(OMe)\{Hdfmp(inh)_2\}(MeOH)]$ (**3.4**), $[V^{V}O(OMe)\{Hdfmp(nah)_2\}(MeOH)]$ (**3.5**) and $[V^{V}O(OMe)\{Hdfmp(bhz)_2\}(MeOH)]$ (**3.6**). In the presence of KOH, oxidation of **3.1–3.3** results in the formation of complexes $K[V^{V}O_2\{Hdfmp(inh)_2\}]$ (**3.7**), $K[V^{V}O_2\{Hdfmp(nah)_2\}]$ (**3.8**) and $K[V^{V}O_2\{Hdfmp(bhz)_2\}]$ (**3.9**). These compounds were also prepared by the reaction of aqueous KVO_3 with ligands at pH ca. 7. All compounds are characterized by IR, electronic, EPR, ^{1}H, ^{13}C and ^{51}V NMR spectroscopy and elemental analyses. Single crystal X-ray analysis of $[V^{V}O(OMe)\{Hdfmp(bhz)_2\}(MeOH)]$ (**6**) and $K[V^{V}O_2\{Hdfmp(inh)_2\}]$ (**3.7**) confirm the coordination of the ligand in the dianionic (ONO^{2-}) enolate tautomeric form and one of the hydrazide moieties remains non-coordinated. However, the nitrogen atom of the free inh moiety coordinates to the other vanadium centre in **3.7** giving a polynuclear complex. It has also been shown that the dioxidovanadium(V) complexes are active catalysts in the oxidative bromination of styrene, by H_2O_2, therefore acting as functional models of vanadium dependent haloperoxidases. Plausible intermediates involved in the catalytic process are established by UV-Vis, EPR and ^{51}V NMR studies.

Reaction of $MnClO_4$ with 2-[2-(1H-(benzo[d]imidazol-2-yl)ethylimino) methyl]phenol (Hsal-aebmz, **4.I**) under aerobic conditions results in the formation of $[Mn^{III}(sal\text{-}aebmz)_2]\cdot ClO_4$ (**4.1**). In the presence of triethylamine and using $MnCl_2$ under similar condition **4.I** forms $[Mn^{III}(sal\text{-}aebmz\text{-}H)(sal\text{-}aebmz)]$ (**4.2**). These complexes are characterised on the basis of elemental and electrochemical analyses, spectroscopic (IR and UV–Vis) data and thermogravimetric studies and results are presented in **Chapter 4**. Single crystal X-ray analysis of **4.2** shows that it is stabilized, in the solid state, through inter molecular hydrogen bonding between NH groups of the two benzimidazole moieties after losing one of the hydrogen atoms; the coordination sites of the ligand being imine nitrogen of the benzimidazole ring, the azomethine nitrogen and the deprotonated phenolic oxygen. It has been demonstrated that **4.2** is efficient catalyst for the oxidative

bromination by H_2O_2 of styrene yielding 1,2-dibromo-1-phenylethane, 1-phenylethane-1,2-diol and 2-bromo-1-phenylethane-1-ol.

Chapter 5 deals with the reaction between $CuCl_2$ and (Z)-2-(1-(2-(1H-benzo[d]imidazol-2-yl)ethylimino) ethyl)phenol (Hhap-aebmz) derived from *o*-hydroxyacetophenone (Hhap) and 2-aminoethylbenzimidazole (aebmz) which gives $[Cu^{II}(hap\text{-}aebmz)Cl]$. Elemental analysis, magnetic successibility, spectral (IR and electronic) data and single crystal X-ray studies confirm the distorted square planar structure of the complex. Complex $[Cu^{II}(hap\text{-}aebmz)Cl]$ has also been encapsulated in the nano cavity of zeolite-Y and its encapsulation ensured by various physico-chemical techniques. The encapsulated complex has been used as catalyst for the oxidation of cyclohexene and phenol in the presence of H_2O_2. With nearly quantitative oxidation of cyclohexene, the selectivity of the oxidation products obtained follows the order: 2-cyclohexene-1-ol (44 %) > 2-cyclohexene-1-one (40 %) cyclohexeneoxide (12 %) > cyclohexane-1,2-diol (4%). Oxidation of phenol (65.7%) gives two products with the selectivity order: catechol (66.1%) > hydroquinone (32.9%).

Finally, summary and over all conclusions based on the achievements are presented.

ACKNOWLEDGEMENTS

First of all, I would like to thank the almighty God, who made everything possible by giving me strength and courage to complete the most significant and scientific accomplishment in my life.

I would like to express my deepest gratitude to my advisor, Dr. M. R. Maurya, Professor, Department of Chemistry, Indian Institute of Technology Roorkee, for his excellent guidance, caring, patience, scientific knowledge and providing me with an excellent atmosphere for doing research. I am highly indebted to my guide for his enthusiastic supervision as well as for providing necessary information from the preliminary to the concluding level. My thank also goes to Mrs. Usha Maurya, for caring, kindness and generosity. I seek their pious blessing ever in my life. I would also like to thank Kshitij Maurya and Rajeshwar Maurya for giving such a homely environment.

I would like to gratefully acknowledge Prof. & Head V.K. Gupta and former HOD Prof. Kamaluddin, Department of Chemistry, Indian Institute of Technology Roorkee, for providing me essential infrastructural facilities to carry out this research work.

I am thankful to the Head, Institute Instrumentation Centre of our institute for providing me necessary instrumentation facilities for my research work. My sincere thank to Mr. A. Haque, Mr. V.P. Saxena, Mr. H. S. Panwar and, Mr. Madan Pal, who helped me from time to time during my research work. I am also grateful to all the members of Chemistry Department for their cooperation in many ways. Great deals appreciated go to the contribution of my Department - Department of Chemistry.

I am grateful to Prof. Joao Costa-Pessoa and Dr. Amit Kumar, Instituto Superior Tecnico, Portugal for carrying out the EPR studies and ^{51}V NMR spectra of some of my samples. I would also like to thanks Prof. Fernando Avecilla, Departamento de Química Fundamental, Facultad de Ciencias, Universidade da Coruña, Spain for carrying out Single crystal data of some of my samples.

I want to express my sincere gratitude to my seniors and laboratory colleagues Dr. Umesh Kumar, Dr. Maneesh Kumar, Dr. Aarti, Dr. Aftab Alam Khan, Dr. Manisha Bisht,

Dr. Priyanka saini, Ms. Ruchi Singh and juniors Mr. Nawal, Ms. Nikita, Ms. Sarita, Mr. Naveen, Mr. Naidu, Mr. Deepanjan for their lively company and motivation for the completion of my work.

I thank my friends in my home town Binoy Biswas, Israfil Dhabak, Kaushik Moni, Nishit Ghosh and Sujan biswas for their lovely company, respect and encouragement. They are simple and funny. I know they will be always with me in every stage of my life. They are my best friends and their friendship gave me a lot for which I am thankful to them.

In campus I meet Dr. Kuntal Maiti, a senior cum guide cum friend, Mr. Tapas Bhattacharya(our Tapas Sir), is a serious researcher and a food lover, Malay Jana a silent researcher and he knows everything, Suman Chandra a sportsman, likes only good food and sound sleep, Sudhir Kumar Gupta, secret researcher and also a good friend, and juniors Arijit, Kaustab, Amrit, Biplab, Venkatesh, Sourav, Naresh, Khurshid, Biswajait, Animesh, Anupam, Hasan, Mainak, Sibendu, all have helped me stay sane through these difficult years. Their support and care helped me overcome setbacks and stay focused on my research.

My special thanks goes to my M.Sc. friends Suman Kumar Barman and Pradip Kumar Dutta. I greatly value their friendship and I deeply appreciate their belief in me.

I would like to thank my teacher Mr. Ratan Majundar, and I was extraordinarily fortunate in having Mr. Alok Roy as my high school Chemistry teacher. I could never have embarked and started all of this without his prior teachings in chemistry and thus opened up unknown areas to me.

I would have not finished this thesis without the support of my family who has always been there for me whenever I need them, the encouragement they give to keep me going and their love to empower me that never fails all the time. I wish to thank my sisters Jayanti haldar, who was my first teacher and had a great role in developing confidence, enthusiasm, selfdependence, hard working nature in me. She is always there with sweet affection, extending helpful hand and cheering me up in her own special way through every thick and thin. She had been a role model for me to follow unconsciously

when I was a teenager and has always been one of my best counselors, Basanti Sarkar, Pratima Rajbanshi, Poornima Talukdar, and my brothers Utpal Haldar, Ujjwal Haldar and sisters in law Jayanti Haldar and Sumitra Haldar, for being a constant source of love, concern, support and strength all these years. I warmly appreciate the loving company of my nieces and nephews Anamika, Subho, Piali, Parthasarthi, Papiya, Payal, Ayan, Deep, Priyashi, Shreyashi. They were always supporting me and encouraging me with their best wishes.

I would like to express my eternal gratitude to my parents for their everlasting love and support. I am indebted to my father, Mr. Kanai Haldar, for his care and love. Although he is no longer with us, he is forever remembered. I am sure he shares our joy and happiness in the heaven. I cannot ask for more from my mother, Mrs. Sova Haldar, as she is simply perfect.

I would like to acknowledge the Council of scientific and Industrial Research, New Delhi for the necessary financial support for this research.

Finally, I wish to acknowledge all those, whose names have not figured above, but helped me in any form during the entire period of my research work.

Chanchal Haldar.

(Chanchal Haldar)

LIST OF PUBLICATIONS

Papers published/ accepted/ communicated for publication

1. M.R. Maurya, **C. Haldar**, S. Behl, N. Kamatham and F. Avecilla, Copper(II) complex of monobasic tridentate ONN donor ligand: synthesis, encapsulation in zeolite-Y, characterization, and catalytic activity, *J. Coord. Chem.*, **64**, 2995–3011, 2011.

2. M. R. Maurya, P. Saini, **C. Haldar**, F. Avecilla, Synthesis, characterisation and catalytic activities of manganese(III) complexes of pyridoxal-based ONNO donor tetradenatate ligands, *Polyhedron*, **31**, 710–720, 2012.

3. M. R. Maurya, **C. Haldar**, A. A. Khan, A. Azam, A. Salahuddin, A. Kumar and J. Costa Pessoa, Synthesis, characterization, catalytic and antiamoebic activity of vanadium complexes of binucleating bis(dibasic tridentate ONS donor) ligand systems, *Eur. J. Inorg. Chem.*, **15**, 2560-2577, 2012.

4. M. R. Maurya, P. Saini, **C. haldar**, A. K. Chandrakar, S. Chand, Oxidation of styrene and cyclohexene with TBHP catalyzed by Zeolite-Y encapsulated copper(II) complex, *J. Coord. Chem.*, In press (2012).

5. M.R. Maurya, **C. Haldar**, P. Saini and F. Avecilla, Mn(III) complexes of monoprotic tridentate ONN donor 2-[2-(1H-(benzo[d]imidazol-2-yl)ethylimino)methyl]phenol: Stabilisation of a neutral Mn(III) complex through intermolecular hydrogen bonding and functional mimic of haloperoxidase, Submitted for publication.

Papers presented in Symposia / Conferences

1. M. R. Maurya, **C. Haldar**, N. Kamatham and S. Behl, Copper(II) complex of monobasic tridentate ONN donor ligand: synthesis, encapsulation in zeolite-Y, characterization, and catalytic activity, *Recent Trends in Instrumental Methods of Analysis,* I.I.T. Roorkee, February 18-20, 2010.

2. M. R. Maurya and **C. Haldar**, Zeolite–encapsulated vanadium(IV) complexes as catalysts for the oxidative desulfurization of organosulfur compounds. *National Conference on Emerging Trends in Chemistry and Biology Interface*, Kumaun University, Nainital, November 03 – 05, 2011.

3. M. R. Maurya, **C. Haldar** and A. A. Khan, Synthesis, characterization, catalytic and antiamoebic activities of vanadium complexes with 5,5'-methylenebis-salicylaldehyde – dibasic tridentate ONS donor systems, *48th Annual Convention of Chemists*, Allahabad University, December 03 – 07, 2011.

4. M. R. Maurya, **C. Haldar**, A. Kumar, F. Avecilla and J. Costa Pessoa, Effect of coordination sites on vanadium complexes having $[VO]^{2+}$, $[VO]^{3+}$ and $[VO_2]^{+}$ cores with hydrazones of 2,6-diformyl-4-methylphenol: Synthesis, characterization, reactivity, and catalytic potential, *8th International Vanadium Symposium: Chemistry, Biological Chemistry & Toxicology"* Washington DC, USA, August 15-18, 2012, Accepted for presentation.

CONTENTS

CHAPTER 3

Effect of coordination sites on vanadium complexes having $[VO]^{2+}$, $[VO]^{3+}$ and $[VO_2]^{+}$ cores with hydrazones of 2,6-diformyl-4-methylphenol: Synthesis, characterization, reactivity, and catalytic potential

Chapter-1

- General introduction and literature survey

General introduction and literature survey

1.1. Vanadium: Historical background and applications of vanadium complexes

Vanadium with 136 ppm (0.0136 %) of the earth's crustal rocks is the nineteenth element in the order of abundance. It is also present at very low concentrations ($<10^{-8}$ M) in the cells of plants and animals. Vanadium exhibits formal oxidation states from –III to +V. However, the most stable oxidation states under normal conditions are IV and V, and generally stabilized through V-O bond and oxocations such as $[VO]^{2+}$, $[VO]^{3+}$ and $[VO_2]^{+}$ are most common for biological systems. The role of vanadium in biochemistry has attracted attention for the last three decades. It could be used as inhibitor for nucleases and phosphatases [1]. Cantley and coworkers revealed a potent inhibitor of Na^{+}/K^{+} – ATPase, widely used to study the mechanism of the sodium-potassium pump [2,3]. This pump is necessary for proper transport of materials across cell membranes to maintain ionic equilibrium.

Studies on the metabolism and detoxification of vanadium compounds under physiological conditions, stability and speciation of vanadium complexes in biofluides, and potential therapeutic and catalytic applications have influenced the coordination chemistry of vanadium. Vanadium is toxic both as a cation and as an anion [4]. The toxicity of vanadium has been found to be high when it is given intravenous, low when it is orally administered, and intermediate in the case of respiratory exposure. Toxicity as observed by weight lose, poor appetite, vomiting and diarrhea has been associated with ingestion of vanadium compounds therefore the therapeutic index of some vanadium complexes can be quite narrow [5]. However, the anti-parasitic activities of vanadium complexes are worth mentioning here [6].

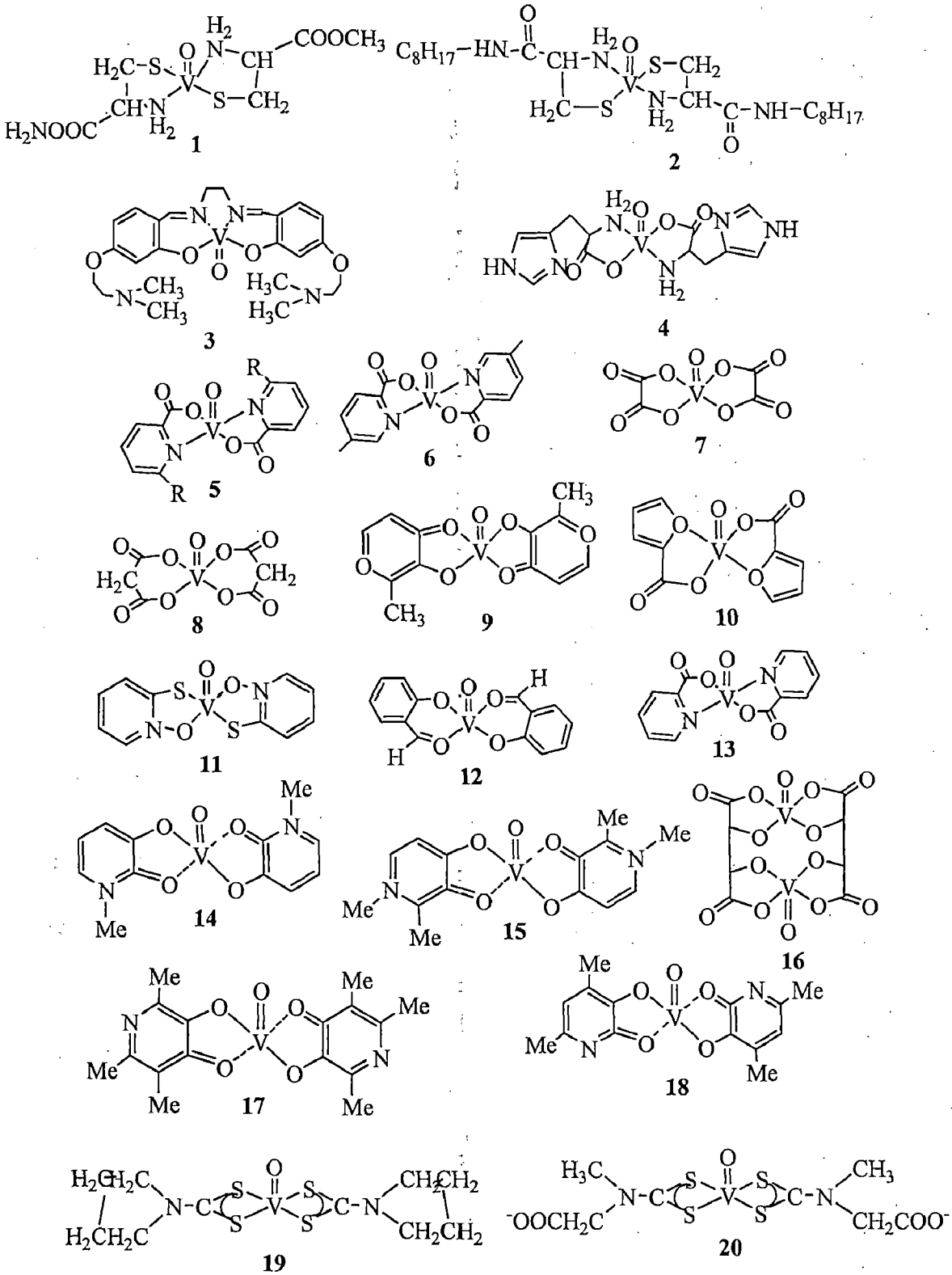

Figure 1.1. Structure of complexes studied for insulin-mimetic activity.

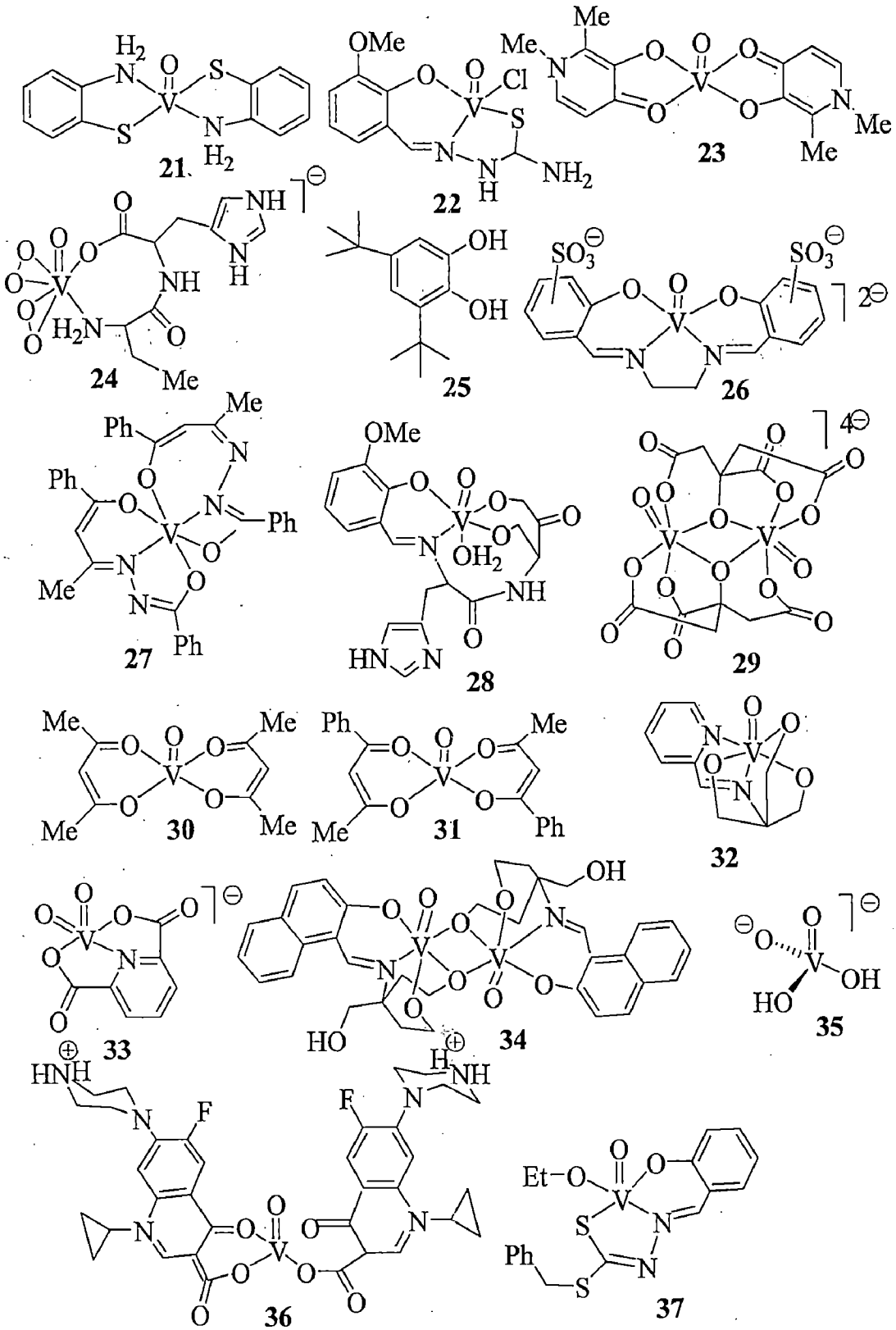

Figure 1.2. Structure of complexes studied for insulin-mimetic activity by Rehder *et al.* [12].

Several types of neutral and low molecular weight vanadium(IV) complexes with organic ligands have been designed and investigated in animal model systems for the treatment of diabetes. Figure 1.1 lists some of these complexes while review articles provide details of these complexes used in the study [7, 8, 9, 10, 11]. Rehder *et al.* have screened toxicity and insulin mimetic activity of a whole range of oxidovanadium(IV), oxidovanadium(V) and oxidoperoxidovanadium(V) complexes presented in Figure 1.2 along with some of the complexes presented in Figure 1.1 [12].

1.2. Naturally occurring vanadium-containing enzyme

Biological systems have developed haloperoxidases enzymes to catalyze the oxidation of chloride and bromide by hydrogen peroxide. In 1983, a naturally occurring vanadium-containing enzyme, vanadium bromoperoxidase (VBrPO), was discovered [13]. It has trigonal bipyramidal coordination sphere including apical histdine and a meridionally bound oxo group; Figure 1.3 [14]. Irrespective of the origin of vanadate-dependent haloperoxidases [*Ascophyllum nodosum* from brown algae [13,15], *Corallina officinalis* from red algae [16], or *Curvularia inequalis* from fungi [17], they all show a high degree of amino acid homology in their active centers and have almost identical structural features. The enzyme fluorinase has also been isolated and is proposed to act by SN_2 mechanism [18]. These enzymes catalyze the oxidation of suitable electophilic halides (X^-) to the corresponding hypohalous acid (HOX) according to equation (1) using H_2O_2 as an oxidant followed by non-enzymatically halogenation of organic compounds, equation (2).

$$X^- + H_2O_2 + H^+ \rightleftharpoons HOX + H_2O \quad \text{.....(1.1)}$$

(X^- = Cl^-, Br^- and I^-)

$$HOX + RH \rightarrow RX + H_2O \quad \text{.....(1.2)}$$

(RH = organic substrate, RX = halogenated product)

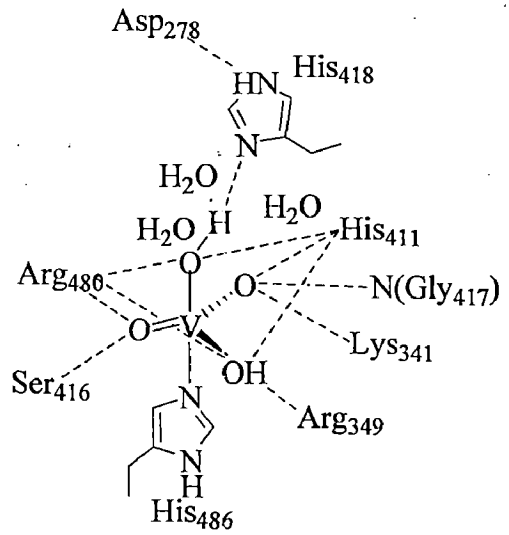

38

Figure 1.3. Active site structure of vanadate-dependent haloperoxidasese from *Ascophyllum nodosum.*

Vanadium chloroperoxidases (VClPO), in the peroxido form has also been isolated from the fungus *Curvularia inaequalis* [17,19]. The active site structure of the peroxido form is shown in Figure 1.4 [20]. In the peroxido form, the peroxide ligand is bound in a η^2-manner in the equatorial plane. The apical oxygen ligand detaches and gives a distorted tetragonal pyramid coordination geometry around the vanadium centre with the two peroxido oxygens having V-O bond length ~ 1.87 Å and O-O is 1.47 Å. The oxidation state of vanadium is +V in vanadium haloperoxidases enzymes and does not change when hydrogen peroxide binds to give activated peroxido-intermediate species.

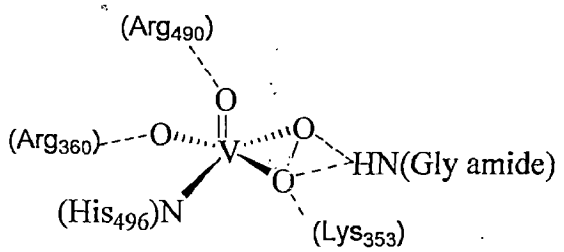

39

Figure 1.4. The peroxide site of vanadate-dependent haloperoxidasese.

Chloroperoxidases have been shown to catalyse a variety of synthetically useful oxygen transfer reactions with H_2O_2, including enantioselective oxidation of sulfides [21,22]. The vanadium-dependent bromoperoxidase from *Corallina officinalis* mediates the enantioselective oxidation of aromatic sulfides [23,24]. The brown seaweed *Ascophyllum nodosum* mediate the formation of the (R)-enantiomer of the methyl phenyl sulfoxide with 91 % enantiomeric excess, whereas the red seaweed *Corallina pilulifera* mediates formation of the (S)-enantiomer (55 % enantiomeric excess) under optimal reaction conditions [25]. Recently Butler *et al.* have reported vanadium bromoperoxidase catalyzed biosynthesis of halogenated marine natural products [26]. Isolation of bromoperoxidase, its immobilisation on magnetite and catalytic activity have been reported by Wischang *et al.* [27].

1.3. Structural and functional models of haloperoxidases

The active site structure of vanadate-dependent haloperoxidases has O_4N coordination environment where vanadate(V) is coordinated to the histidine of the protein matrix. Vanadium (V) complexes provide suitable structural and/or functional models for these enzymes [28-33] as they are stable under aerobic conditions. Model experiments show that intermediate species having $\{VO(H_2O)\}$, $\{VO_2\}$, $\{VO(OH)\}$ and $\{VO(O_2)\}$ cores form during catalytic turnover. A large number of imidazole coordinated vanadium complexes has been synthesized in order to model the active site of haloperoxidases. Complexes, [VO(acac)(sal-im)], [VO(sal)(sal-im)] and $[VO(sal\text{-}im)_2]$ (H_2sal-im = 4-(2-(salicylideneamino)ethylimidazole) represent model characters observed for the reduced form of vanadate-bromo peroxidase. Upon acidification, protonation of coordinated imidazole (in [VO(acac)(sal-im)] and [VO(sal)(sal-im)]) or non-coordinated imidazole (in $[VO(sal\text{-}im)_2]$) have been suggested in these complexes [34-36].

As a peroxidovanadium(V) intermediate has been reported to form during turnover of haloperoxidases, such complexes have also been prepared and characterized. Tetradentate glycine-derived ligands, nitrilotriacetic acid (nta), aminodiacetic acid (ada), N-(carbamoylmethyl)iminodiatetic acid (H_2cmida) and N-(carbamoylethyl) iminodiatetic acid (H_2ceida) give oxidoperoxidovanadium(V) complexes in presence of H_2O_2. The X-ray structure analyses of $Ba[VO(O_2)(nta)].3H_2O$ and $K[VO(O_2)(ceida)].2H_2O$ ((40) of Figure 1.5) reveal a mononuclear structure of the complex anions with a typical pentagonal bipyramidal arrangement around vanadium [37,38]. A glycylglycine complex of monoperoxidovanadate, $[NEt_4][VO(O_2)_2(glygly)].1.58H_2O$ (where Hglygly = glycylglycine) has been isolated by reacting glycylglycine with vanadate in presence of H_2O_2. Complex $[NEt_4][VO(O_2)_2(glygly)].1.58H_2O$ has pentagonal bipyramidal structure where axial positions are occupied by the oxo ligand and by one oxygen of the peroxido group of the adjacent anion ((41) of Figure 1.5). The equatorial positions are occupied by the peroxido group and the tridentate ligand [39]. Monoperoxido complexes, $M_2[VO(O_2)(acmaa)(H_2O)]$ (where M = K^+ and NH_4^+) and $M_2[VO(O_2)(Hacmaa)(H_2O)]$ (where M = K^+, Cs^+ and NBu_4^+, H_3acmaa = R,S-N-(carboxymethyl)aspartic acid) exist in two isomeric forms *exo* and *endo* with their ^{51}V NMR chemical shift at ca. –590 and –600 ppm, respectively. While endo-form partially decomposes with pH variations, it has no influence on the chemical shifts of the diastereomers [40]. Formation of peroxidovanadate(V) adducts with hetero ligands in presence of H_2O_2 has also been studied in solution using various techniques [41]

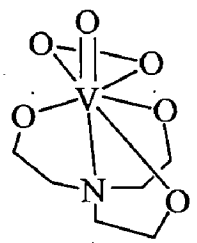

(40)

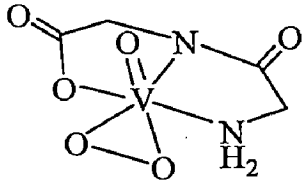

(41)

Figure 1.5. Examples of model peroxido complexes.

Several groups worldwide have prepared structural models of haloperoxidases [28-33]. From our laboratory some examples are provided here. Simple ligands derived from salicylaldehyde, substituted salicylaldehyde and isonicotinic acid hydrazide (H_2R'-sal-inh). Thus, the dioxidovanadium(V) complexes $[K(H_2O)][V^VO_2(sal\text{-}inh)]$ and $[K(H_2O)][V^VO_2(Cl\text{-}sal\text{-}inh)]$ have been isolated by the reaction of potassium vanadate and potassium salt of the corresponding ligands at pH ca. 7.5. Lowering the pH of the reaction mixture to ca. 6.5 causes the formation of oxido-bridged binuclear complexes $[\{V^VO(sal\text{-}inh)\}_2\text{–}O]$ and $[\{V^VO(Cl\text{-}sal\text{-}inh)\}_2\text{–}O]$, respectively, along with the respective expected anionic species; Figure 1.6. The mixture of anionic and neutral complexes could be separated easily by fractional crystallization from methanol [42]. Using NH_4VO_3 in place of KVO_3 results in the formation of the corresponding ammonium salt $NH_4[V^VO_2(sal\text{-}inh)(H_2O)]$ and the neutral species $[\{V^VO(sal\text{-}inh)\}_2\text{–}O]$ [42]. Aanionic and neutral –oxido binuclear complexes of the types $[V^VO_2L]^-$ and $[(VOL)_2\text{–}O]$ (H_2L = ligands) with ligands H_2sal-nah and H_2sal-fah have also been isolated similarly as reported above [43].

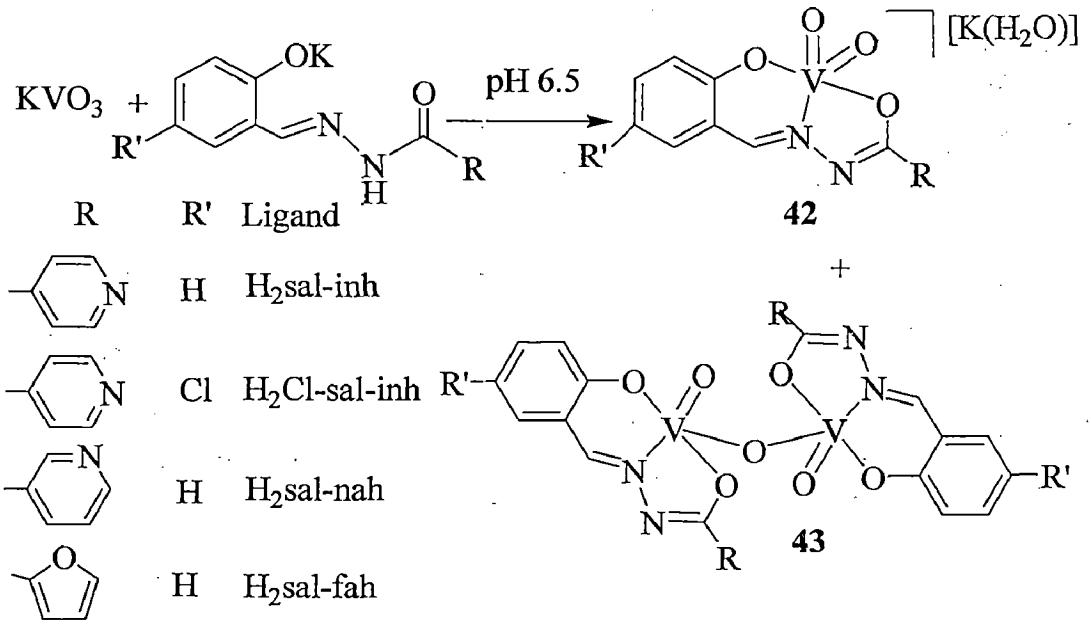

Figure 1.6. Synthetic procedure for vanadium(V) complexes.

Reaction of aqueous solution of $[V^{V}O_2(sal\text{-}nah)]^-$ and $[V^{V}O_2(sal\text{-}fah)]^-$ with $HClO_4$ or HCl yields the neutral complexes $[V^{V}O_2(Hsal\text{-}nah)]$ and $[V^{V}O_2(Hsal\text{-}fah)]$, respectively in which one of the nitrogens of the –N=N– group is protonated (Figure 1.7). Isolation and structural characterization of such complexes, e.g. $[V^{V}O_2(Hsal\text{-}bhz)]$ has been reported by Plass *et al.* [44].

Reaction of equimolar amounts of potassium salt of ligands H_2pydx-inh, H_2pydx-nah and H_2pydx-bhz with KVO_3 at pH ca. 6.5 produces $[K(H_2O)_3][VO_2(pydx\text{-}inh)]$, $[K(H_2O)_2][V^{V}O_2(pydx\text{-}nah)]$ and $[K(H_2O)_2][V^{V}O_2(pydx\text{-}bhz)]$, respectively, along with neutral species $[V^{V}O_2(Hpydx\text{-}inh)]$, $[V^{V}O_2(Hpydx\text{-}nah)]$ and $[V^{V}O_2(Hpydx\text{-}bhz)]$; Figure 1.8. All these complexes are good structural models of VHPO. IR spectroscopy suggests protonation of pyridine's nitrogen to stabilize these complexes as neutral species [45].

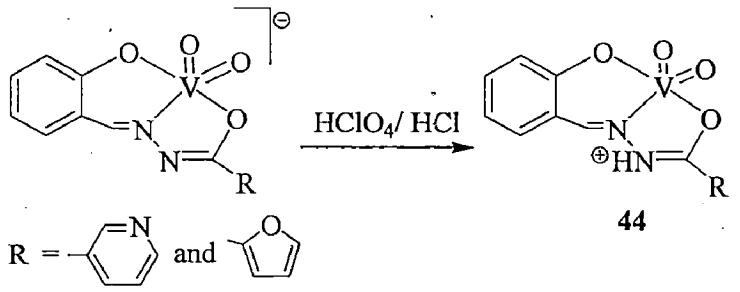

Figure 1.7. Synthesis of neutral dioxidovanadium(V) complexes.

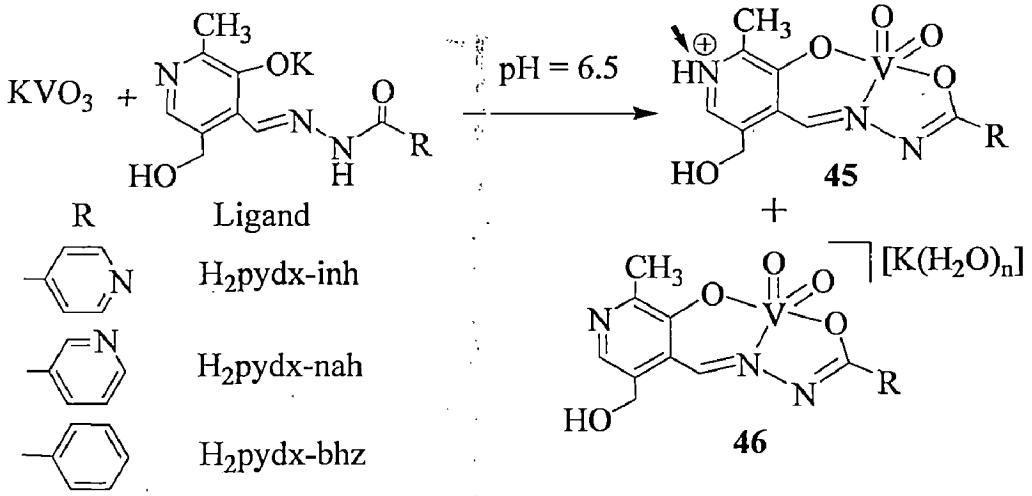

Figure 1.8. Synthetic procedure for pyridixal based vanadium(V) complexes.

Complex $[V^{V}O_2(acac\text{-}ambmz)]$ along with minor amount of $[V^{IV}O(sal\text{-}phen)]$ has been isolated from the filtrate obtained after isolating $[V^{IV}O(acac)(sal\text{-}ambmz)]$ from the reaction of equimolar amounts of $[V^{IV}O(acac)_2]$ and Hsal-ambmz in refluxing methanol; Figure 1.9. Complex $[V^{V}O_2(acac\text{-}ambmz)]$ can also be prepared directly by reacting $[V^{IV}O(acac)_2]$ with ambmz followed by aerial oxidation. Aerial oxidation of $[V^{IV}O(acac)(sal\text{-}ambmz)]$ and $[V^{IV}O(acac)(sal\text{-}aebmz)]$ gives the corresponding dioxidovanadium(V) complexes $[V^{V}O_2(sal\text{-}ambmz)]$ and $[V^{V}O_2(sal\text{-}aebmz)]$, respectively. These complexes can also be obtained from the reaction of aerially oxidized solutions of $[V^{IV}O(acac)_2]$ with the respective ligand in methanol. These complexes can be considered to be structural models of VHPO as they attain the geometry of a trigonal bipyramid, distorted toward the square pyramid. The □-parameters for $[V^{V}O_2(acac\text{-}ambmz)]$ and $[V^{V}O_2(sal\text{-}ambmz)]$ amount to 0.71 and 0.60, respectively [46].

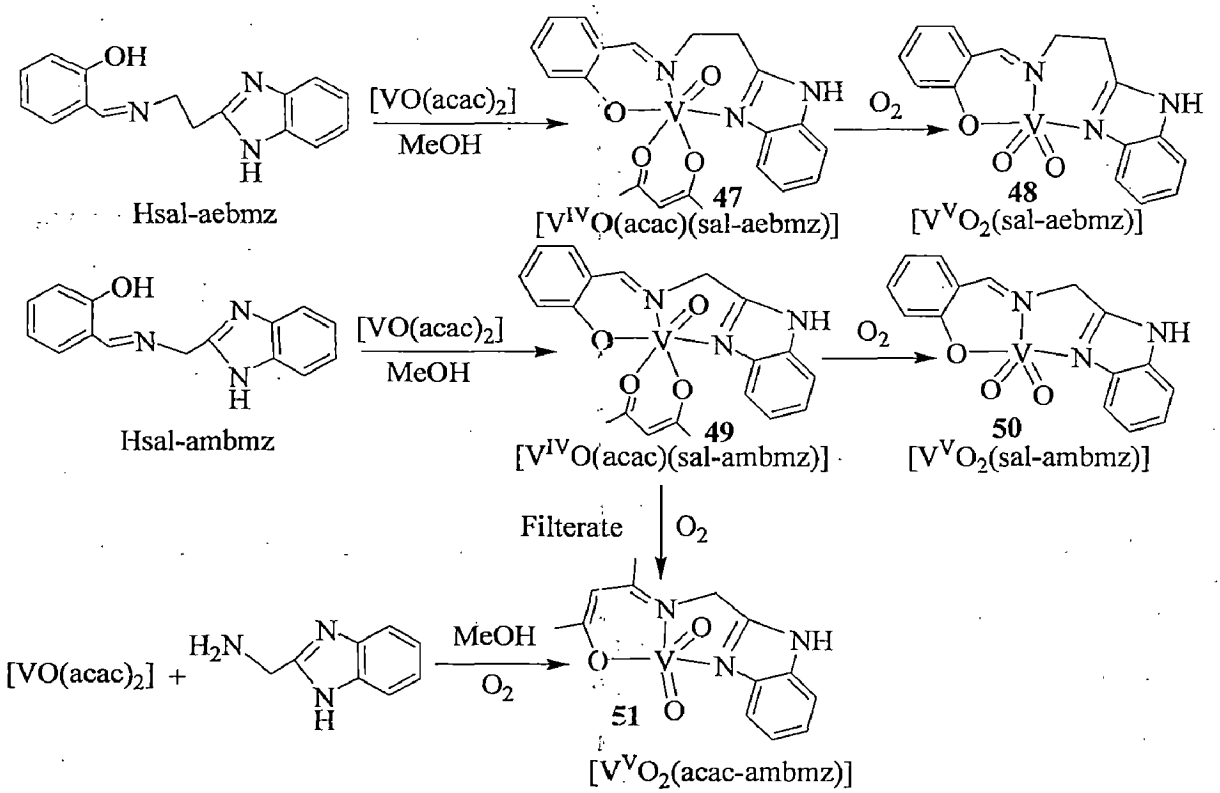

Figure 1.9. Synthesis of vanadium complexes with benzimidazole based ligands.

Similarly, the reaction of $[V^{IV}O(acac)_2]$ with equimolar amount of Hsal-aepy, Hfsal-dmen and Hsal-his in solvent yield the oxidovanadium(IV) complexes $[V^{IV}O(acac)(sal\text{-}aepy)]$, $[V^{IV}O(acac)(fsal\text{-}dmen)]$ and $[V^{IV}O(acac)(sal\text{-}his)]$, respectively. Dioxidovanadium(V) complexes $[V^{V}O_2(sal\text{-}aepy)]$, $[V^{V}O_2(fsal\text{-}dmen)]$ and $[V^{V}O_2(sal\text{-}his)]$ were obtained by the aerobic oxidation of respective oxidovanadium(IV) complexes in solvent in the presence of a small amount of H_2O_2; Figure 1.10 [47-49]. Single crystal X-ray diffraction study of $[V^{V}O_2(sal\text{-}dmen)]$ confirms the distorted square pyramidal structure[25]. The structure of this compound was also previously reported [50].

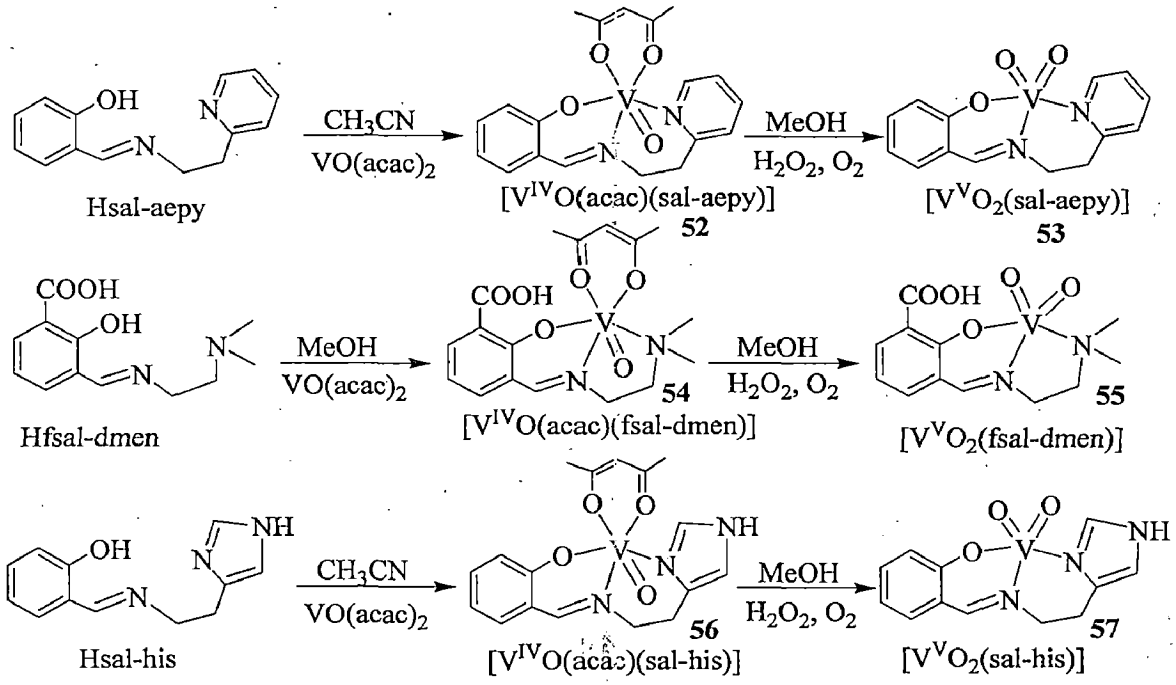

Figure 1.10. Design of dioxidovanadium(V) complexes.

Complex $[V^{V}O_2(sal\text{-}aepy)]$ exhibits two resonances at = −517 and −491 ppm in DMSO-d_6 [47]. These chemical shifts are within the values expected for dioxidovanadium(V) complexes containing a O/N donor set [51]. The first major signal at = −517 ppm (92%) is due to authentic complex i.e. $[V^{V}O_2(sal\text{-}aepy)]$. The resonance at −491 ppm gains intensity with time in DMSO (24 h), and therefore is assignable to $[V^{V}O_2(sal\text{-}aepy)(DMSO)]$. Addition of methanol to

$[V^{V}O_2(sal\text{-}aepy)]$ in DMSO results in the appearance of a single signal at –542 ppm, identical to what is obtained by recording ^{51}V NMR of $[V^{V}O_2(sal\text{-}aepy)]$ directly in MeOH only. The signal at –515 ppm is, therefore, assigned to $[V^{V}O_2(sal\text{-}aepy)(MeOH)]$. A very similar ^{51}V NMR spectrum with a strong resonance at $\delta = -503$ ppm (92.0%) and a minor resonance at –490 ppm (8.0%) for $[V^{V}O_2(fsal\text{-}dmen)]$ (ca. 4 mM) dissolved in DMSO-d_6 has also been obtained. Addition of methanol (50% v/v) to a 4 mM solution of $[V^{V}O_2(fsal\text{-}dmen)]$ in DMSO shifts the –503 ppm resonances to –515 ppm, identical to the spectrum of $[V^{V}O_2(fsal\text{-}dmen)]$ in MeOH only.

The reaction of $CH_2(H_2sal\text{-}bhz)_2$, $CH_2(H_2sal\text{-}fah)_2$, $CH_2(H_2sal\text{-}inh)_2$ and $CH_2(H_2sal\text{-}nah)_2$ (ligands derived from 5,5'-methylenebis(salicylaldehyde) and hydrazides) with $[V^{IV}O(acac)_2]$ in 1:2 molar ratio in refluxing methanol followed by aerial oxidation in the presence of KOH or $CsOH.H_2O$ yield the corresponding salt of dioxidovanadium(V) species $[CH_2\{V^{V}O_2(sal\text{-}bhz)\}_2]^{2-}$, $[CH_2\{V^{V}O_2(sal\text{-}fah)\}_2]^{2-}$, $[CH_2\{V^{V}O_2(sal\text{-}inh)\}_2]^{2-}$ and $[CH_2\{V^{V}O_2(sal\text{-}nah)\}_2]^{2-}$; Figure 1.11. In these complexes, two independent dioxidovanadium(V) units do not interact with each other [52,53].

Vanadium(V) complexes can also act as functional models of vanadate dependent haloperoxidases catalyzing the oxidative bromination of organic substrates in the presence of H_2O_2 and bromide ion in aqueous acidic medium [54-56]. Oxido- and dioxidovanadium(V) complexes of multidentate ligands (59-70) that presented the active functional models for bromoperoxidases are presented in Figure 1.12. Efforts were made to get a better understanding of the working mechanism of the vanadium haloperoxidase enzymes.

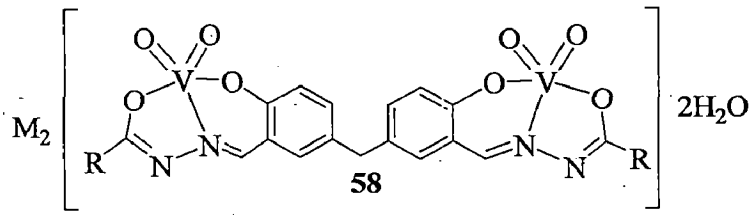

M^+	R	Complex
K^+		$K_2[CH_2\{V^VO_2(sal\text{-}bhz)\}_2]\cdot 2H_2O$
Cs^+		$Cs_2[CH_2\{V^VO_2(sal\text{-}bhz)\}_2]\cdot 2H_2O$
K^+		$K_2[CH_2\{V^VO_2(sal\text{-}fah)\}_2]\cdot 2H_2O$
Cs^+		$Cs_2[CH_2\{VO_2(sal\text{-}fah)\}_2]\cdot 2H_2O$
K^+		$K_2[CH_2\{V^VO_2(sal\text{-}inh)\}_2]\cdot 2H_2O$
Cs^+		$Cs_2[CH_2\{V^VO_2(sal\text{-}inh)\}_2]\cdot 2H_2O$
K^+		$K_2[CH_2\{V^VO_2(sal\text{-}nah)\}_2]\cdot 2H_2O$
Cs^+		$Cs_2[CH_2\{V^VO_2(sal\text{-}nah)\}_2]\cdot 2H_2O$

Figure 1.11. Structure of dinuclear dioxidovanadium(V) complexes.

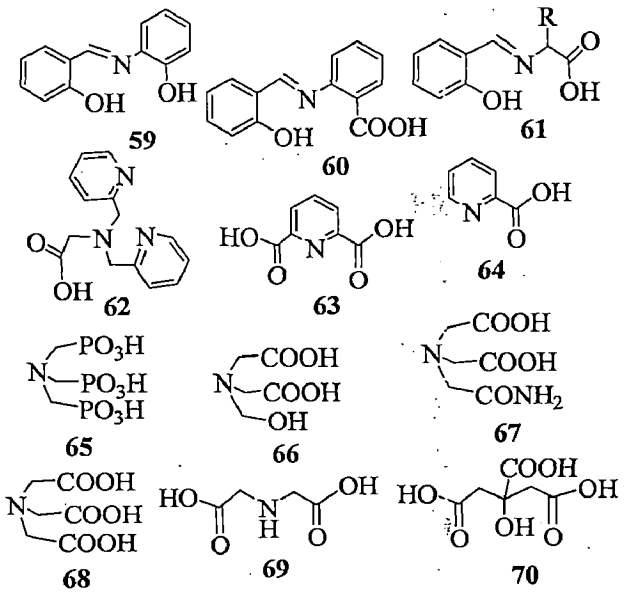

Figure 1.12. Structures of ligands that are used to design functional models of haloperoxidases.

The first functional mimic of bromoperoxidase to catalyse the bromination of 1,3,5-trimethoxybenzene (TMB) was reported by Butler *et al.* [57] using cis-dioxidovanadium(V) complex in acidic aqueous solution. The brominated product 2-bromo-1,3,5-trimethoxybenzene was obtained when the reaction was catalysed by [VO(OMe)(MeOH)(sal-oap)] using H_2O_2 as oxidant. Complexes $[VO(hybeb)]^{2-}$ and $[VO(hybeb)]^{-}$ (H_2hybeb = 1,2-bis(2-hydroxybenzylamido)benzene) have also shown catalytic activity for the bromination of 1,3,5-trimethoxybenzene to some extent [58].

Oxidative bromination of salicylaldehyde catalysed by the complexes $[K(H_2O)][V^VO_2$(sal-nah)] and $[K(H_2O)][V^VO_2$(sal-fah)], using aqueous H_2O_2/KBr in the presence of $HClO_4$, has been carried out successfully [59]. This oxidation was also catalysed by $[VO_2$(sal-inh)]$^-$ encapsulated in the cavity of zeolite-Y [60]. During this process vanadium reacts with one or two equivalents of H_2O_2, forming monoperoxido $\{VO(O_2)^+\}$ or *bis*(peroxido) $\{VO(O_2)^-\}$ species, which ultimately oxidise bromide, possibly via a hydroperoxido intermediate. The oxidised bromine species (Br_2, Br_3^- and/or HOBr) then brominates the substrate [57,61,62]. A maximum of ca. 51% conversion of salicylaldehyde was achieved with 4 mmol of $HClO_4$, 2 mmol of substrate, 15 mmol of H_2O_2, 0.020 g (ca. 0.05 mmol) of catalyst and 0.476 g (4 mmol) of KBr. The selectivity of obtained products varied in the order: 5-bromosalicylaldehyde (85.8%) > 3,5-dibromosalicylaldehyde (9.0%) > unidentified (5.2 %). Under similar conditions, $[K(H_2O)_3][V^VO_2$(pydx-inh)] gave only 46 % conversion of salicylaldehyde with almost similar selectivity of products as obtained for above complexes [45]. Other non-oxidizing acids such as H_2SO_4 were also tested successfully giving comparable results.

Oxidative bromination of salicylaldehyde to 5-bromosalicylaldehyde and 3,5-dibromosalicylaldehyde catalysed by polymeric oxidovanadium(IV) complexes (71 of Figure 1.13) [63].

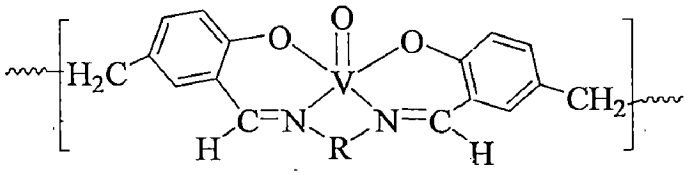

R = CH_2CH_2
$CH(CH_3)CH_2$
$CH_2CH_2CH_2$

71

Figure 1.13. Complex used for functional model study.

Dinuclear dioxidovanadium(V) complexes, $[CH_2\{V^VO_2(sal\text{-}bhz)\}_2]^{2-}$, $[CH_2\{V^VO_2(sal\text{-}fah)\}_2]^{2-}$, $[CH_2\{V^VO_2(sal\text{-}inh)\}_2]^{2-}$ and $[CH_2\{V^VO_2(sal\text{-}nah)\}_2]^{2-}$ have also been used as catalyst for the oxidative bromination of salicylaldehyde. A maximum of ca. 90 % conversion of salicylaldehyde was achieved under optimized conditions but the addition of $HClO_4$ in four equal portions during the first two hours of reaction time was necessary to improve the conversion of the substrate and to avoid decomposition of catalyst. At least three products, 5-bromosalicylaldehyde, 3,5-dibromosalicylaldehyde and 2,4,6-tribromophenol were identified; Figure 1.14 [52,53]. Increasing the amount of oxidant improves the conversion of salicylaldehyde but the selectivity of 5-bromosalicylaldehyde decreases considerably, while that of 3,5-dibromosalicylaldehyde and 2,4,6-tribromophenol increase. The presence of excess H_2O_2 facilitates the formation of more and more HOBr which ultimately helps in the further oxidative bromination of salicylaldehyde to other position(s).

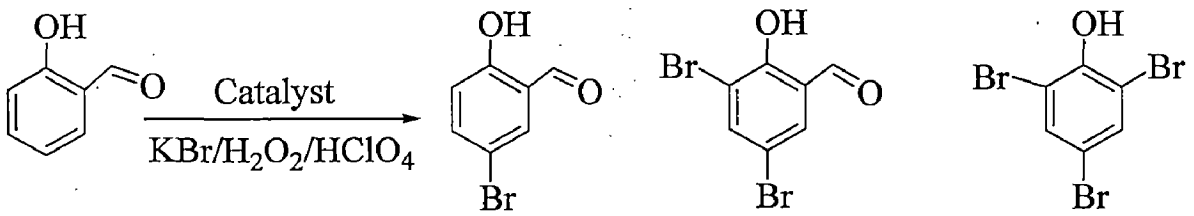

Figure 1.14. Oxidation products of salicylaldehyde.

Oxidovanadium(IV) complex supported on polystyrene, PS-[VO(hmbmz)$_2$] (Hhmbmz = 2-(-hydroxymethyl)benzimidazole) has been used for the oxidative bromination of salicylaldehyde using H_2O_2 / KBr and gives 5-bromosalicylaldehyde in quantitative yield [64]. Oxidovanadium(IV) complexes of tridentate Schiff bases (derived from salicyaldehyde and 2-aminoethanol, L-histidine or L-phenylalanine) supported on Merrifield resin (Figure 1.15) [65] or oxidovanadium(IV) complexes of pentadentate Schiff bases (derived from salicyaldehyde or its derivatives (e.g. 3-methoxysalicyaldehyde, 5-methoxysalicyaldehyde, 5-chlorosalicyaldehyde, 3,5-dichlorosalicyaldehyde and 3,5-dichlorosalicyaldehyde etc.) and 2,2'-bis(aminoethyl)amine) (Figure 1.15) [66] catalyze the oxidation of methyl phenyl sulfide to the corresponding sulfoxide in 80-90% yield by TBHP. It was found that the monomeric complexes show greater rate of reaction than the corresponding polymer supported complexes.

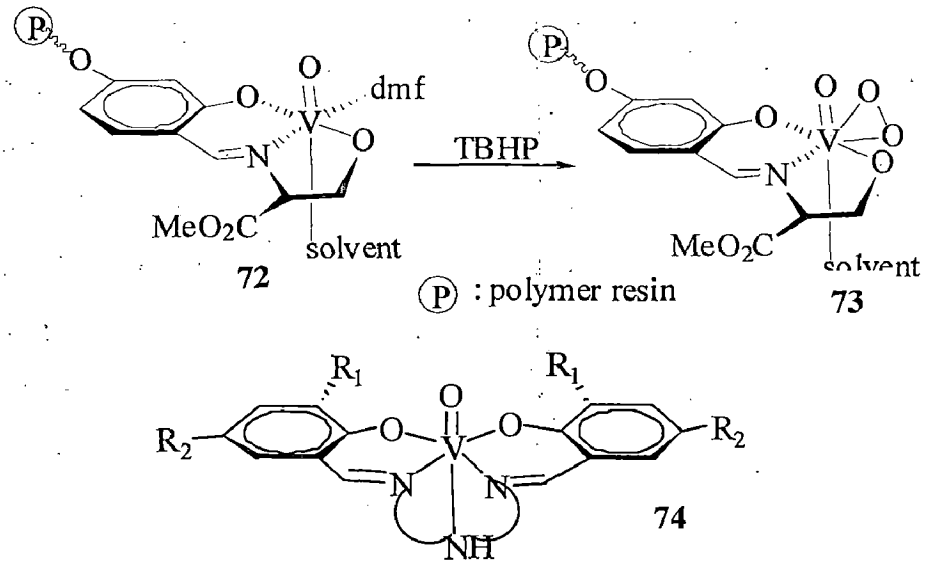

Figure 1.15. Complexes having catalytic potential for the oxidation of methyl phenyl sulfide.

Similarly, oxidation of methyl phenyl sulfide has also been catalysed by oxidovanadium(IV) complexes of ligands (Figure 1.16) derived from salicyaldehyde or its derivatives and amino acids (eg. glycine, alanine, valine etc).

All the oxidovanadium(IV) complexes having L-conformational amino acids Schiff-bases convert sulfide to sulfoxide with R conformation in excess while D-conformational amino acids Schiff bases provide the sulfoxide with S-conformation in excess (Figure 1.16) [67].

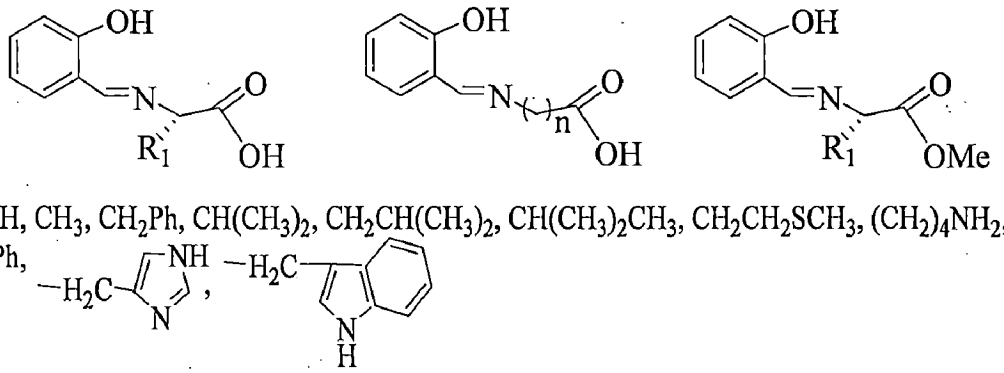

Figure 1.16. Ligands used to prepared oxidovanadium(IV) complexes having catalytic potential.

Vanadyl complexes of N-salicylidene amino acids gave moderate enantioselectivity in asymmetric sulfide oxidation with 30% aqueous hydrogen peroxide as an oxidant. These vanadyl complexes transformed thioanisole into its sulfoxide with high yield at a catalyst loading as low as 0.03 (mol) % with hydrogen peroxide. But vanadyl complexes of N-salicylidene amino alcohols did not show catalytic activity even at 0.1 (mol) % catalyst loading. This is probably because the acidity of N-salicylidene amino acids is higher than that of N-salicylidene amino alcohol, and thus the former vanadyl complexes are much more stable to excess hydrogen peroxide's attack than the latter [68]. Mechanistic aspects of vanadium catalysed oxidations with peroxides have recently been reported by Conte *et al.* [69].

1.4. Manganese complexes and their applications

Manganese with 1000 ppm (0.1%) of the earth's crustal rocks is the 12th most abundant element in the order of abundance. It is widely distributed in nature and in terms of terrestrial abundance it is second among the 3d-block transition elements [70]. There are a class of manganese catalases that have been found in bacterial organisms such as *Lactobacillus plantarum* [71,72], *Thermus thermophilus* [73], and *Thermoleophilum album* [74] that catalyze the disproportionation of H_2O_2. Besides the photosynthetic water-oxidizing complex, which is known to utilize four Mn ions for the oxidation of water to molecular oxygen [75], evidences support that the Mn site in these enzymes is comprised of two Mn ions per protein subunit. Manganese can adopt a wide variety of oxidation states (+2 to +5) and this ability is related to the redox function of the metal ion in biological systems [76].

Manganese complexes have been reported to be useful homogeneous catalysts for the oxidation of organic substrates with different oxidants [77]. For instance, the manganese based Jacobsen catalysts are known to catalyse epoxidation reactions [78]. In fact, much efforts have been made to immobilize Jacobsen's catalysts (i.e. C-2 asymmetric Mn(salen) complexes derived from *trans*-1,2-diaminocyclohexane and salicylaldehyde derivatives) (75) on to different polymer-supports [79,80]. Several other complexes have also been either immobilized on polymer or encapsulated in zeolite-Y in order to study their catalytic activities.

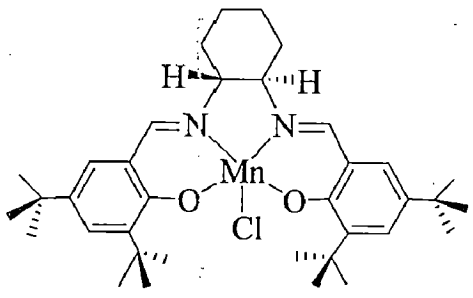

75

Jacobsen's catalyst

Manganese complexes having tetradentate ONNO donor ligands are found to be artificial mimics of some of the manganese containing enzymes [81]. In addition, they also act as catalysts for important reactions [82,83]. Manganese(II) and manganese(III) complexes of substituted *N,N'*-bis(salicylidene)-1,2-diimino-2-methylethane have been prepared and used as efficient peroxidase mimics in the presence of water-soluble trap ABTS. The rate of peroxidase activity of the present complexes is significantly higher than that of other series of Mn-Schiff base compounds, probably due to their versatility in adopting in solution a structure that allows the coordination of the hydrogen peroxide molecule to the manganese.

Complexes $[Mn^{III}(pydx\text{-}en)Cl(H_2O)]$, $[Mn^{III}(pydx\text{-}1,3\text{-}pn)Cl(CH_3OH)]$ and $[Mn^{III}(pydx\text{-}1,2\text{-}pn)Cl(H_2O)]$ (see Figure 1.17 for ligands and the corresponding complexes) have been used as catalysts for the oxidation, by H_2O_2, of methyl phenyl sulphide, styrene and benzoin [84]. Oxidation of methyl phenyl sulphide under the optimized reaction conditions gave 38 - 44 % conversion with two major products methyl phenyl sulfoxide and methyl phenyl sulfone in the ca. 70 % and 30 % selectivity, respectively. Oxidation of styrene catalyzed by these complexes gave at least five products namely styrene oxide, benzaldehyde, benzoic acid, 1-phenylethane-1,2-diol and phenylacetaldehyde with a maximum of 49 % conversion of styrene by $[Mn^{III}(pydx\text{-}en)Cl(H_2O)]$, 46 % by $[Mn^{III}(pydx\text{-}1,3\text{-}pn)Cl(CH_3OH)]$ and 47 % by $[Mn^{III}(pydx\text{-}1,2\text{-}pn)Cl(H_2O)]$ under optimized conditions. The selectivity of the obtained products followed the order: benzaldehyde > benzoic acid > styrene oxide > phenylacetaldehyde > 1-phenylethane-1,2-diol. Similarly, ca. 93% conversion of benzoin was obtained by these catalysts, where the selectivity of the products followed the order benzil > benzoic acid > benzaldehyde-dimethylacetal. Similar manganese(II)-N,N'-ethylenebis(salicylideneaminato) and analogous complexes have been reported to catalyse oxyfunctionalization of cyclohexane by tert-butyl hydroperoxide to give cyclohexanol and cyclohexanone in high yields at room temperature in

acetonitrile solution. A pathway involving oxidomanganese intermediate is suggested for the reaction [85].

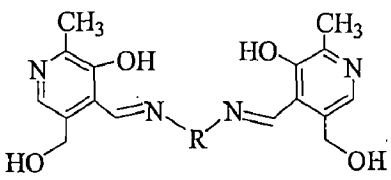

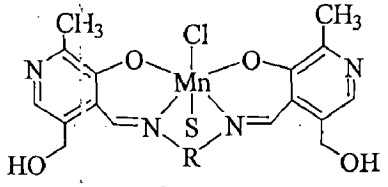

76

R	S	Complex
R = CH_2CH_2: H_2pydx-en (**I**)	CH_2CH_2	H_2O	$[Mn^{III}(pydx\text{-}en)Cl(H_2O)]$ (1)
R = $CH_2CH_2CH_2$: H_2pydx-1,3-pn (**II**)	$CH_2CH_2CH_2$	CH_3OH	$[Mn^{III}(pydx\text{-}1,3\text{-}pn)Cl(CH_3OH)]$ (2)
R = $CH(CH_3)CH_2$: H_2pydx-1,2-pn (**III**)	$CH(CH_3)CH_2$	H_2O	$[Mn^{III}(pydx\text{-}1,2\text{-}pn)Cl(H_2O)]$ (3)

Figure 1.17. Structures of tetradentate ligands and complexes.

Two chiral manganese(III) *salen* complexes, (*R,R*)-[Mn^{III}(3,5-dtButsalhd)Cl] and (*R,R*) [Mn^{III}(3,5-dtButsaldPh)Cl] (Figure 1.18) were encapsulated by in situ generation of the complexes inside of the three types of Al-pillared clays (Al-PILCs) having different structural properties [86]. One of the PILCs used was derived from Wyoming clay (Al-WYO) and the other two were from the same original clay Benavila: (i) Al-BEN, where no surfactant was used in the preparation and (ii) Al-TERG, where a polyalcohol (tergitol) was used as surfactant to act as an interlayer gallery template. These complexes were screened as heterogeneous catalysts in the epoxidation of styrene using iodosylbenzene or *m*-chloroperbenzoic acid as oxidants. The encapsulated complexes show moderate alkene conversion (16–40%) with poor enantiomeric excesses (ee % = 0–14). Nevertheless, complex (*R,R*)-[Mn^{III}(3,5-dtButsalhd)Cl] encapsulated into Al-TERG using PhIO as oxidant gave 14 ee% %, which is higher than the value found for the homogeneous catalyst under similar conditions. The clay pillars partially collapse after two runs.

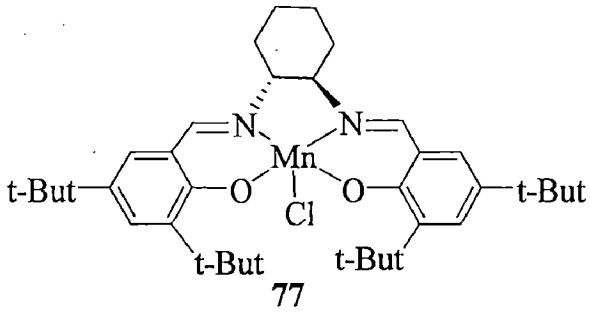

77

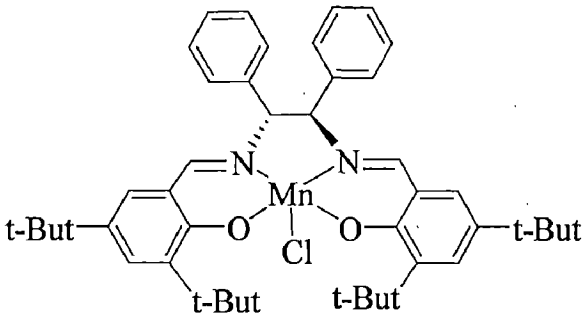

78

(*R,R*)-[Mn^{III}(3,5-dtButsalhd)Cl] (*R,R*) [Mn^{III}(3,5-dtButsaldPh)Cl]

Figure 1.18. Chiral Mn(III) complexes.

A series of manganese (III) complexes of chiral pentadentate dihydrosalen ligands, having an imidazole group as a fifth, axial donor has been synthesized (Figure 1.19) and studied for the the epoxidation of olefins with a variety of terminal oxidants, but most importantly, with dilute (1%) aqueous hydrogen peroxide and without any added co-ligands [87]. With 1,2-dihydronaphthalene as substrate and 10 mol% of catalyst, enantiomeric excesses up to 66% were achieved. This value is the highest so far reported for an asymmetric epoxidation of 1,2-dihydronaphthalene, using hydrogen peroxide as oxidant and a salen-type complex as catalyst. Control experiments using a tetradentate chelate lacking the axial imidazole donor showed that the pentacoordination of the manganese ion is crucial for the peroxidase activity.

Three manganese(II) complexes of a compartmental ligand, namely $[Mn(HL)(H_2O)_3](NO_3)_2 \cdot H_2O$, $[Mn(HL)(SCN)_2(H_2O)] \cdot H_2O$ and $[Mn(HL)\{N(CN)_2\}(H_2O)_2](NO_3) \cdot H_2O$, where HL = 2,6-bis{2-(N-ethyl)pyridineiminomethyl}-4-methylphenol, have been synthesized (Figure 1.20) and characterised by routine physicochemical techniques [88]. These complexes show excellent catecholase-like activity with both 3,5-di-tert butylcatechol and tetrachlorocatechol as substrates. In addition complexes

$[Mn(HL)(H_2O)_3](NO_3)_2 \cdot H_2O$ and $[Mn(HL)(SCN)_2(H_2O)] \cdot H_2O$ also exhibit phosphatase activity.

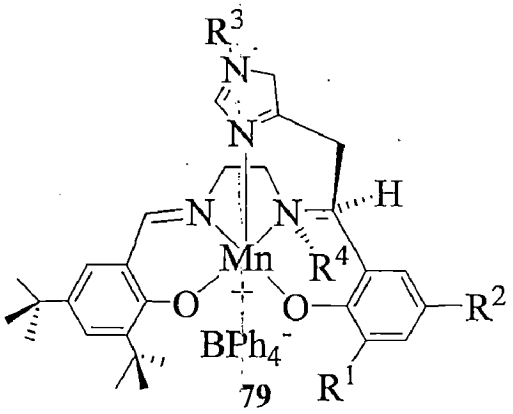

79

a: $R^1 = R^2 = R^3 = H$, $R^4 = CH_3$

b: $R^1 = R^2 = H$, $R^3 = R^4 = CH_3$

c: $R^1 = R^4 = CH_3$, $R^2 = R^3 = H$

d: $R^1 = R^3 = H$, $R^3 = OCH_3$, $R^4 = CH_3$

e: $R^1 = R^2 = R^3 = H$, $R^4 = CH_2CH_3$

Figure 1.19. Structure of Mn(III) complexes with chiral ligand having appended imidazole group.

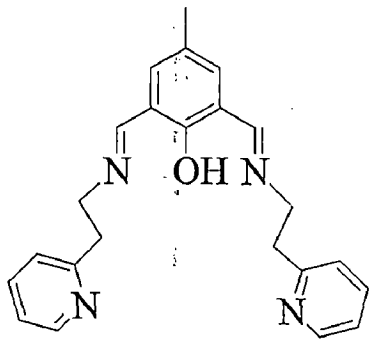

Figure 1.20. Structure of compartmental ligand.

The oxidation of ethylbenzene with 30% aqueous hydrogen peroxide (H_2O_2) in an acetone–water medium at 30 °C was investigated using $[Mn^{III}(X\text{-}hq)_3]$ (Hhq = 8-quinolinol, X = H, Cl or Br) as catalysts; Figure 1.21. The results indicated that these complexes, with ammonium acetate and acetic acid as

additives, selectively catalyze the side chain oxidation of ethylbenzene at secondary carbon atoms, affording acetophenone as a major product. Among the complexes examined, the 5,7-dibromohq catalyst was the most active, and provides ethylbenzene conversion of 26.1% under the optimum conditions [89].

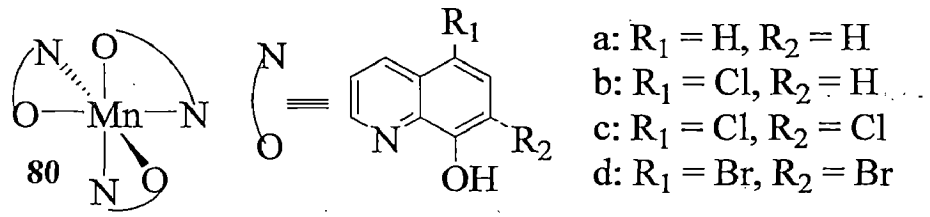

Figure. 1.21. Structure of Mn(III) complexes.

Manganese(III) complexes of 1,2-diamines and fluorous derivatives of salicylaldehyde have also been prepared and tested as catalysts in the selective oxidation of alkyl aryl sulfides with PhIO under biphasic conditions. When reactions were carried out under fluorous biphasic (FB) conditions, the selectivity for sulfoxides was improved and the catalyst could be easily recovered by simple phase separation and reused up to four times [90]. Despite their good chemoselectivity, catalytic efficiency and recyclability, chiral fluorous (salen)manganese(III) complexes showed low enantioselectivities in preliminary experiments run under fluorous biphasic conditions.

Tangestaninejad *et al.* have reported manganese(III) salophen chloride [Mn(salophen)Cl], supported on functionalized multi-wall carbon nanotubes MWCNTs (Figure 1.22) [91]. The MWCNT was modified with 1,4-diaminobenzene, 4-aminophenol and 4-aminothiophenol and [Mn(salophen)Cl] was attached to the supports via axial ligation. These new heterogenized catalysts were characterized by elemental analysis, FT-IR and diffuse reflectance spectrometery and scanning electron microscopy. These catalysts are effective for efficient epoxidation of alkenes with $NaIO_4$ at room temperature. These

heterogeneous catalysts were highly reusable in the oxidation reactions and reused several times without significant loss of their catalytic activity.

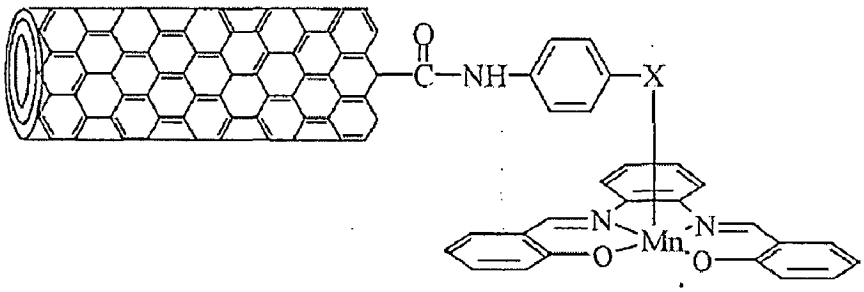

81

Figure 1.22. Multi-wall carbon nanotube supported Mn(III) complex.

1.5. Zeolite encapsulated metal complexes and their catalytic applications

Zeolites (Figure 1.23) find applications in many scientific disciplines such as inorganic and organic chemistry, biochemistry, physical chemistry, colloid chemistry, mineralogy, geology, surface chemistry, crystallography, catalysis and all types of chemical engineering process technologies. They are often called molecular sieves because the large number of small but identical pores can be used to separate small molecules from large molecules, which can pass through the pores. Thus, the separation of air components, recovery of different hydrocarbons, removing carbon dioxide and small sulfur compounds from natural gases etc. are possible by using zeolites. Zeolites have also been compared with metalloenzymes and hence they are referred to as "zeozymes".

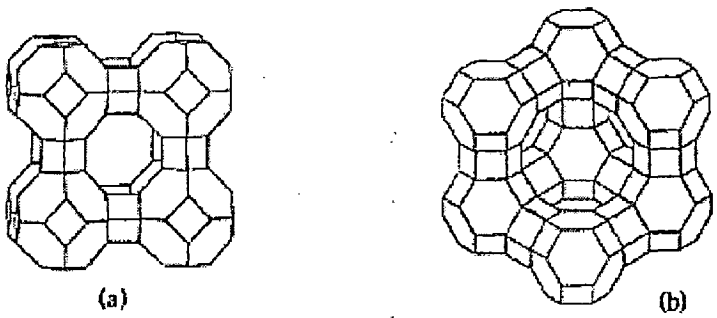

Figure 1.23. Represented zeolite structures: (a) Zeolite A and (b) Zeolite-Y (adopted from Reference [92]).

Zeolite encapsulated metal complexes having good catalytic activities possess all the advantages of solid heterogeneous catalysts as well as share many advantageous features of homogeneous catalysts. Bedioui has suggested basically three general approaches to the preparation of zeolite encapsulated metal complexes. These are: flexible ligand method, template synthesis method and zeolite synthesis method. In addition to these, other two approaches, such as, ion exchange method and adsorption method may also be considered [92, 93].

The zeolite-Y encapsulated metal complexes have shown tremendous catalytic applications. A brief account of some metal complexes (mostly copper(II)) and their applications of are given below:

Ratnasamy *et al.* have isolated copper(II) and manganese(III) complexes of salen derivatives encapsulated in the cavity of zeolite-X and zeolite-Y by zeolite synthesis method. The structures of the complexes have been characterized by FTIR, UV-visible and EPR spectroscopic techniques, XRD, SEM, thermal and elemental analysis, as well as nitrogen absorption and cyclic voltametric studies [94,95]. The oxidation of styrene using these complexes as catalysts under aerobic conditions in the presence of tert-butylhydroperoxide gave benzaldehyde, styrene and phenylacetaldehyde. The catalytic efficiency of these encapsulated complexes was much higher than that of the neat complexes. Electron withdrawing substituents such as -Cl, -Br, $-NO_2$ on the aromatic ring enhances the rate of oxidation [94, 95]. These complexes also catalyse the oxidation of phenol and p-xylene. The aerobic oxidation of p-xylene in the absence of added hydrogen promoters and using *tert*-butyl hydrpperoxide as the initiator and Mn(X-sal-1,3-pn)Cl]-X and [Mn(sal-dach)Cl]-X H_2sal-dach = Schiff derived from salicylaldehyde and 1,2-diaminocyclohexane) at low temperature showed as high as 60 % conversion [96, 97].

Chavan *et al.* have prepared dimeric $[Cu(CH_3COO)_2.H_2O]$ in the cavity of zeolite-Y. The convincing proofs of dimer comes from EPR study, which gives 7-line hyperfine structure due to the two Cu(II) nuclei. The activity of the complex

has been evaluated in the aerial oxidation of phenols, which is in natural system catalyzed by the dicopper enzyme tyrosinase [98].

Zeolite encapsulated metal complexes prepared from Schiff base ligands have been used for the oxidation of phenol using different oxidants. Cu(salen) [99], Cu(X-salen) [100], Mn(X-salen) [101] (X = H, Cl, Br or NO_2), VO(salen) [102, 103], VO(sal-1,2-pn), VO(sal-1,3-pn) and VO(saldien) (saldien = salicylidene-diethylenetriamine) [103] encapsulated in zeolite-Y have been used as catalysts. The oxidation products are mainly catechol and hydroquinone. In no case the formation of 1,4-benzoquinone was detected.

Oxidation of styrene has also been studied using tetraazamacrocycle complexes, 7,16-diacetyl[M{$Me_4(Bzo)_2$[14]tetraeneN_4}], {M= Cu(II) and Ni(II)} encapsulated in the cavity of Zeolite-Y; Scheme 1.24 [104]. These encapsulated tetraazamacrocycle complexes have been used as a heterogeneous catalyst for the oxidation of styrene and for the solvent free oxidation of benzyl alcohol using hydrogen peroxide as oxidant. The solvent free catalyzed oxidation of benzyl alcohol catalyzed by 7,16-diacetyl[Cu{$Me_4(Bzo)_2$[14]tetraeneN_4}]-Na-Y gives benzaldehyde as the major product, while that of styrene gives benzaldehyde and styrene oxide as major oxidation products when 7,16-diacetyl[Ni{$Me_4(Bzo)_2$[14]tetraeneN_4}]-Na-Y is used as catalyst.

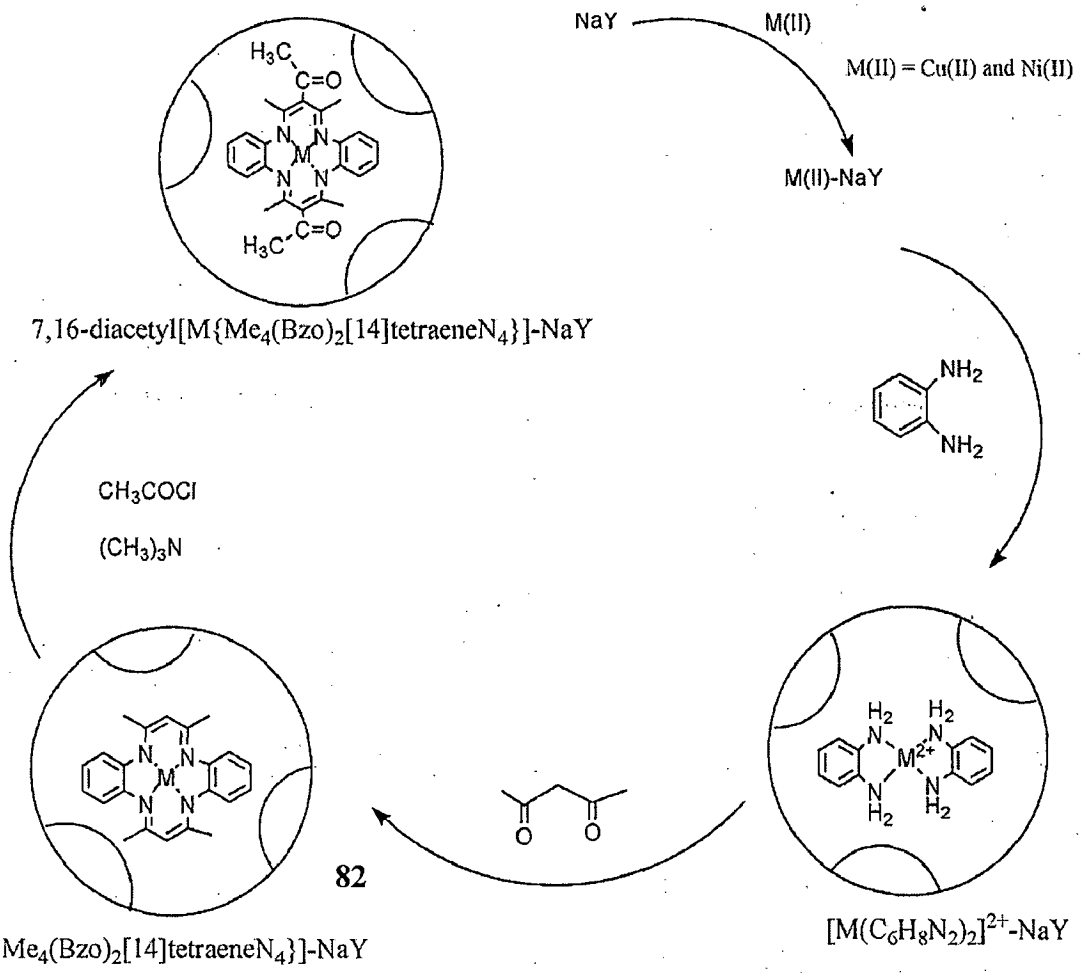

Scheme 1.24. Synthetic approach to prepare zeolite-Y encapsulated macrocyclic complexes (M = Cu(II) and Ni(II).

The Mn(II), Co(II), Ni(II) and Cu(II) complexes of the type [ML] with bis(salicyaldehyde)oxaloyldihydrazone (H_2L) have been synthesized from the reaction of metal acetate with H_2L in 1:1 molar ratio in ethanol under reflux. These metal complexes with tetradendate Schiff-base ligand have also been entrapped in the nanocavity of zeolite-Y. The new Host–Guest nano composite materials have been used as catalyst for oxidation of cyclohexane and their activity compared with the homogeneous analogues [105].

Yusuff *et al.* have reported the catalytic oxidation of ascorbic acid by atmospheric oxygen using $[Cu(dmpz)_2]$-Y (Hdmpz = 3,5-dimethyl-1H- pyrazole) as catalyst. The oxidation of ascorbic acid to dehydroascorbic acid was monitored

by continuous measurement of transmittance at 245 nm after exposing deoxygenated methanolic solution of ascorbic acid in air in the presence of catalyst. It is proposed that oxidation proceeds through Cu(I)-ascorbate intermediate [106].

Oxidation of ethylbenzene over "neat" and zeolite-Y encapsulated copper tri and tetraaza macrocyclic complexes using *tert*-butyl hydroperoxide as oxidant has been reported; Figure 1.25. C-H bond activation takes place both at benzylic and aromatic ring carbon atoms. Ring hydroxylation was better by neat complexes than the encapsulated ones. The differences in the selectivity are attributed to different types of "active" copper–oxygen intermediates formed in different proportions [107].

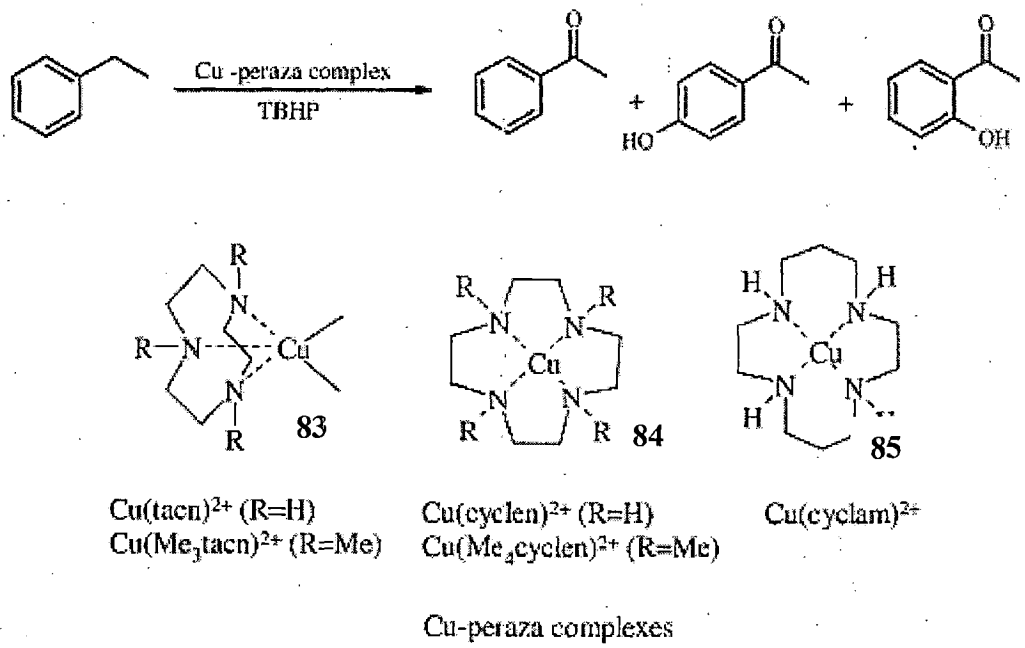

Figure 1.25. Triaza and trtraaza macrocyclic copper (II) complexes (83-85) used as catalysts.

1.6. Objective of the present investigations

It is evident from the review of the literature that vanadium complexes have provided opportunities to develop structural and functional models of haloperoxidases including the oxidative halogenation of organic substrates and oxidation of organic sulfides. Catalytic oxidation reactions by manganese complexes are also well documented but these complexes have not been used as functional mimic of haloperoxidases. Therefore, it is reasonable to consider preparing model complexes of vanadium and manganese for functional mimics of haloperoxidases.

Contributions of copper complexes encapsulated in the nano cavity of zeolite-Y are widely documented in the literature, specifically for the oxidation reactions. However, as we go through the oxidation reactions we observe that, in spite of considerable research, optimization of reaction conditions have not been set out in most papers. It was, therefore, reasonable to undertake systematic study on the synthesis and characterization of new zeolite-Y encapsulated copper(II) based catalysts and to explore their catalytic potential for the oxidation of organic substrates under optimized reaction conditions.

Present study is aimed to describe (i) the structural and functional model of haloperoxidases (ii) the synthesis of manganese complexes and their functional model of haloperoxidases and (iii) the synthesis and characterization of new zeolite-Y encapsulated copper complex catalysts to explore catalytic potential for the oxidation of organic substrates under optimized reaction conditions. The ligands selected to undertake such studies and their abbreviations are presented below:

(i) Binucleating ONS–ONS donor ligands **2.I** and **2.II** derived from 5,5'-methylenebis(salicylaldehyde) $\{CH_2(Hsal)_2\}$ and S-benzyldithiocarbazate (sbdt) or S-methyldithiocarbazate (smdt) as well simple ONS donor ligands **2.III** and **2.IV** derived from salicylaldehyde (sal) and sbdt or smdt:

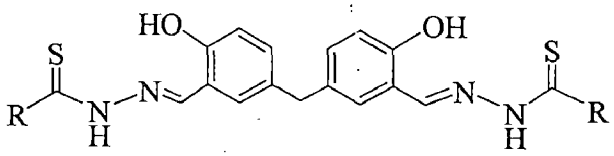

R = 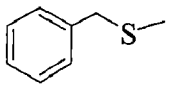 : $CH_2(H_2sal\text{-}sbdt)_2$ (**2.I**)

R = H_3C-S : $CH_2(H_2sal\text{-}smdt)_2$ (**2.II**)

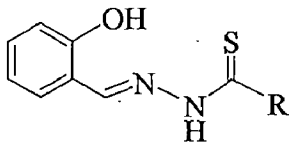

R = 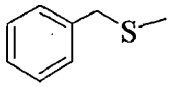 : $H_2sal\text{-}sbdt$ (**2.III**)

R = H_3C-S : $H_2sal\text{-}smdt$ (**2.IV**)

(ii) Compartmental ONO donor ligands **3.I**, **3.II** and **3.III** derived from 2,6-diformyl-4-methylphenol (dfmp) and isonicotinoylhydrazide (inh), nicotinoylhydrazide (nah) and benzoylhydrazide (bhz):

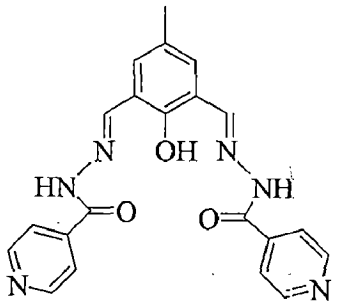

$H_3dfmp(inh)_2$ (**3.I**)

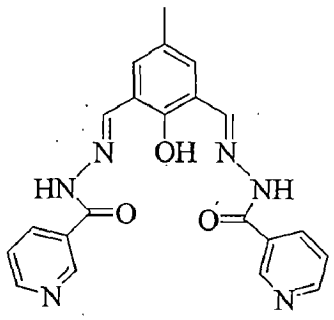

$H_3dfmp(nah)_2$ (**3.II**)

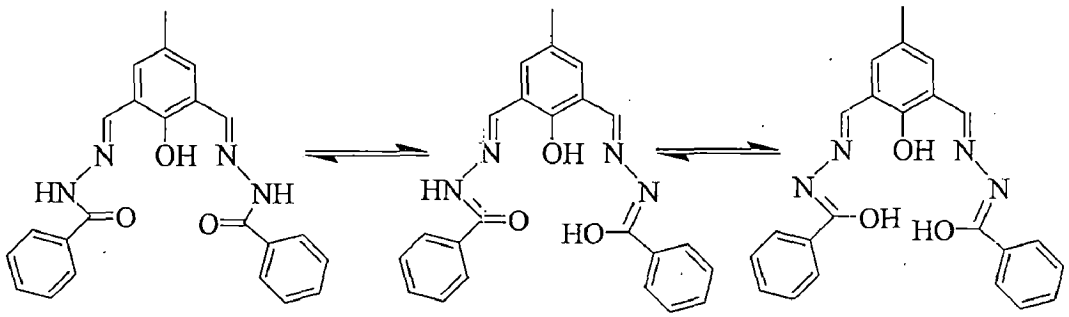

keto-form

$H_3dfmp(bhz)_2$ (**3.III**)

enol-form

(iii) Monobasic trodentate ONN donor Ligand derived from salicylaldehyde (sal) and 2-aminoethylbenzimidazole (aebmz):

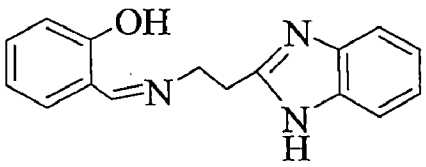

Hsal-aebmz (**4.I**)

(iv) Monobasic trodentate ONN donor Ligand derived from o-hydroxyacetophenone (hap) and 2-aminoethylbenzimidazole (aebmz):

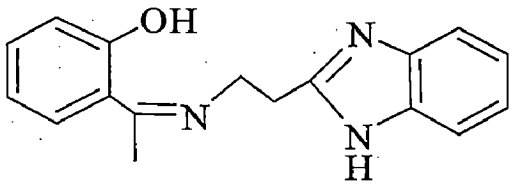

Hhap-aebmz, **5.I**

Chapter-2

◈ Oxidative bromination of styrene by mono and binuclear vanadium complexes of ONS donor ligand systems: A functional model of haloperoxidase

---

This work is published in *Eur. J. Inorg. Chem.*, 2560-2577, 2012.

Oxidative bromination of styrene by mono and binuclear vanadium complexes of ONS donor ligand systems: A functional model of haloperoxidase

2.1. Introduction

Interest in the coordination chemistry of vanadium, with particular emphasis on its biological [56,108-110] structural [30,108,109] and catalytic properties [111-115] has increased over the past two decades. The vanadate-dependent haloperoxidase enzymes (VHPO) [15-17] and the covalent bonding of the imidazole moiety of histidine residue through Nε to vanadate in the active site stimulated the design of structural models [34-36,46,116-121]. These structural models have been extended to functional similarities in that vanadium complexes also model the oxidative halogenation and sulfoxidation of organic substrates [32,33,111-115]. The homogeneous as well as their immobilized analogues of vanadium (IV and V) complexes also catalyze other organic reactions such as the epoxidation of alkenes,[122-125] the hydroxylation of hydrocarbons [126], hydro- and oxidative-amination [47,127] and the oxidation of alcohols to aldehydes and ketones [63,128], thus showing their influence on the yield and selectivity in chemical transformations.

Binuclear $V^{IV}O$- and $V^{V}O_2$-complexes of binucleating, bis(dibasic tridentate ONO donor) ligands have also been studied recently [52,53]. Their good reactivity patterns and catalytic activities encouraged to consider binucleating, bis(dibasic tridentate ONS donor) ligands and study their catalytic activities. The syntheses and partial characterization of binuclear $V^{IV}O$- and $V^{V}O_2$-complexes of ligands **2.I** and **2.II** derived from 5,5'-methylenebis(salicylaldehyde) $\{CH_2(Hsal)_2\}$ and S-benzyldithiocarbazate (sbdt) or S-methyldithiocarbazate (smdt) (Scheme 2.1) are reported recently [129] but their reactivity patterns and catalytic activities are not studied well. In this chapter, complete characterization of these complexes and their reactivity are reported. Their haloperoxidase activity is confirmed considering oxidative bromination of styrene using the $V^{V}O_2$-complexes as catalyst precursors. Mononuclear $V^{V}O_2$-complexes with ligands **2.III** and **2.IV**

have also been prepared to compare their catalytic activity with binuclear complexes.

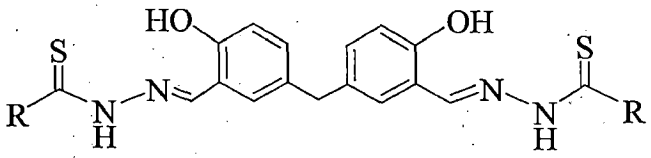

R = 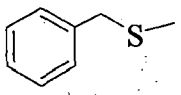 : $CH_2(H_2sal\text{-}sbdt)_2$ (**2.I**)

R = H_3C-S : $CH_2(H_2sal\text{-}smdt)_2$ (**2.II**)

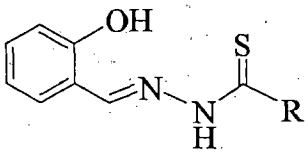

R = 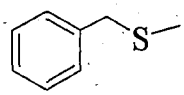 : $H_2sal\text{-}sbdt$ (**2.III**)

R = H_3C-S : $H_2sal\text{-}smdt$ (**2.IV**)

Scheme 2.1. Structure of ligands designated by **2.I – 2.IV** used in this chapter.

2.2. Experimental

2.2.1. Materials

Acetylacetone (Hacac, E. Merck, India), styrene (Acros, USA), 30% aqueous H_2O_2, KBr (E. Merck, India), salicylaldehyde, hydrazine hydrate, $CsOH{\cdot}H_2O$, benzyl chloride (S.D fine chemicals, India), methyl iodide (Himedia, India), and 70 % $HClO_4$ (Qualigens, India) were used as obtained. Other chemicals and solvents were of analytical reagent grade. S-benzyldithiocarbazate [130], S-methydithiocarbazate [131] and 5,5'-methylbis(salicylaldehyde) [132], $CH_2(H_2sal\text{-}sbdt)_2$ (**2.I**) and $CH_2(H_2sal\text{-}smdt)_2$ (**2.II**), $H_2sal\text{-}sbdt$ (**2.III**) and $H_2sal\text{-}sbdt$ (**2.IV**) [133].

2.2.2. Instrumentation and Characterization Procedures

Elemental analyses of the compounds were carried out on an Elementar model Vario-El-III. IR spectra were recorded as KBr pellets on a Nicolet NEXUS Aligent 1100 series FT-IR spectrometer. Electronic spectra were measured in

methanol with an UV-1601 PC UV-Vis spectrophotometer. ^{1}H NMR spectra were obtained on a Bruker 200, ^{13}C and ^{51}V NMR spectra on a Bruker Avance III 400 MHz spectrometer with the common parameter settings. NMR spectra were usually recorded in DMSO-d_6, and δ (^{51}V) values are referenced relative to neat $V^{V}OCl_3$ as external standard. Thermogravimetric analyses of the complexes were carried out under oxygen atmosphere using a TG Stanton Redcroft STA 780 instrument. The magnetic susceptibilities were measured by a Vibrating Sample Magnetometer model 155 supplied by Princeton Applied Research, using nickel as standard. Diamagnetic corrections were carried out using Pascal's constants.[58] EPR spectra were recorded with a Bruker ESP 300E X-band spectrometer. The spin Hamiltonian parameters were obtained by simulation of the spectra with the computer program of Rockenbauer and Korecz [134]. A Thermax Nicolet gas chromatograph fitted with a HP–1 capillary column (30 m × 0.25 mm × 0.25 μm) and FID detector was used to analyze the reaction products and their quantifications were made on the basis of the relative peak area of the respective product. Oxidation and oxidative bromination of styrene have also been normalized from the set of calibration curve for styrene to get response factors and obtained results are nearly same within experimental error. The identity of the products was confirmed using a GC-MS model Perkin-Elmer, Clarus 500 and comparing the fragments of each product with the library available.

2.2.3. Preparations

All these complexes were prepared using the procedure reported earlier [129]. However, for convenient their syntheses are reproduced here briefly. Satisfactory elemental analyses of all these complexes were also obtained.

2.2.3.1. Preparations of $[CH_2\{V^{IV}O(sal\text{-}sbdt)(H_2O)\}_2]$ (2.1) and $[CH_2\{V^{IV}O(sal\text{-}smdt)(H_2O)\}_2]$ (2.2) – General method

A filtered solution of $[V^{IV}O(acac)_2]$ (2.56 g, 10 mmol) in dry methanol (30 mL) was added to a filtered solution of appropriate ligand (5 mmol) prepared in dry hot methanol (150 mL) while shaking the reaction flask. The reaction mixture

was refluxed on a water bath for 4 h. After reducing the volume of the solvent to ca. 30 mL and keeping at room temperature for 10 h, the separated brown solid was filtered, washed with methanol and dried in desiccator over silica gel.

$[CH_2\{V^{IV}O(sal\text{-}sbdt)(H_2O)\}_2]$ (2.1): Yield 3.16 g (80.5 %). $C_{31}H_{28}N_4O_6S_4V_2$ (782.68): Calcd. C, 47.57; H, 3.61; N, 7.16. Found: C, 47.7; H, 3.5; N, 7.2%.

$[CH_2\{V^{IV}O(sal\text{-}smdt)(H_2O)\}_2]$ (2.2): Yield: 0.431 g (68.4 %). $C_{19}H_{20}N_4O_6S_4V_2$ (630.48): Calcd. C, 36.19; H, 3.20; N, 8.89. Found: C, 36.4; H, 3.0; N, 8.9%.

2.2.3.2. $K_2[CH_2\{V^{V}O_2(sal\text{-}sbdt)\}_2]\cdot 2H_2O$ (2.3)

A filtered solution of $[V^{IV}O(acac)_2]$ (0.530 g, 2 mmol) in methanol (15 mL) was added while stirring to a solution of $CH_2(H_2sal\text{-}sbdt)_2$ (0.616 g, 1 mmol) in methanol (450 mL) and refluxed for 4 h. After adding KOH (0.224 g, 4.0 mmol) to the above, the reaction mixture was further refluxed for 2 h. The obtained light brown solution was allowed to oxidize aerially along with slow evaporation at room temperature. After 2 days the color of the solution changed to yellow, its volume was reduced to ca. 10 mL and the solution kept for 12 hr at room temperature. A yellow solid of **2.3** separated out. This was filtered off, washed with methanol and dried in a desiccator over silica gel. Yield 0.786 g (72.8 %). $C_{31}H_{28}K_2N_4O_8S_4V_2$ (892.90): Calcd. C, 41.70; H, 3.16; N, 6.27. Found C, 41.8; H, 3.1; N, 6.3%.

2.2.3.3. $Cs_2[CH_2\{V^{V}O_2(sal\text{-}sbdt)\}_2]\cdot 2H_2O$ (2.4).

A filtered solution of $[V^{IV}O(acac)_2]$ (0.530 g, 2.0 mmol) in methanol (15 mL) was added while stirring to a solution of $CH_2(H_2sal\text{-}sbdt)_2$ (0.616 g, 1.0 mmol) in methanol (450 mL) and refluxed for 4 h. After adding $CsOH\cdot H_2O$ (0.403 g, 2.4 mmol), the reaction mixture was further refluxed for 2 h. The obtained light green solution was allowed to oxidize aerially while slowly evaporating at room temperature. After 2 days the green solution turned yellow, the volume reduced to ca. 10 mL and the mixture kept over night at room temperature. A yellow solid of **2.4** separated out. This was filtered off washed with methanol and dried in a

desiccator over silica gel. Yield: 0.786 g (72.8 %). $C_{31}H_{28}Cs_2N_4O_8S_4V_2$ (1080.49): Calcd. C, 34.46; H, 2.61; N, 5.19. Found C, 34.3; H, 2.5; N, 5.3%.

2.2.3.4. Preparation of $K_2[CH_2\{V^VO_2(sal\text{-}smdt)_2\}]\cdot 2H_2O$ (2.5)

This complex was prepared by the procedures outlined for $K_2[CH_2\{V^VO_2(sal\text{-}sbdt)_2\}]\cdot 2H_2O$ (**2.3**): Yield: 0.513 g (73.9 %) . $C_{19}H_{20}K_2N_4O_8S_4V_2$ (740.71) : Calcd. C, 30.81; H, 2.72; N, 7.56. Found: C, 30.9; H, 2.7; N, 7.5%.

2.2.3.5. Preparation of $Cs_2[CH_2\{V^VO_2(sal\text{-}smdt)_2\}]\cdot 2H_2O$ (2.6)

This complex was prepared by the procedure outlined as for $Cs_2[CH_2\{V^VO_2(sal\text{-}sbdt)_2\}]\cdot 2H_2O$(**2.4**). Yield: 0.735 g (79.2 %). $C_{19}H_{20}Cs_2N_4O_8S_4V_2$ (928.29): Calcd. C, 24.6; H, 2.2; N, 6.0. Found C, 24.5; H, 2.1; N, 6.2%.

2.2.3.6. $K[V^VO_2(sal\text{-}sbdt)]\cdot H_2O$ (2.7) [135]

Starting precursor, $[VO(acac)_2]$ (0.53 g, 2 mmol) was added to a solution of H_2sal-sbdt (0.604 g, 2 mmol) dissolved in methanol (30 mL) containing KOH (0.056 g, 1 mmol). The reaction mixture was refluxed on a water bath under aerobic condition for 6 h. After cooling to room temperature, 1 mmol of additional KOH was added, and the solution was kept for 2 days at ambient temperature to allow for slow evaporation of the solvent. The yellow precipitate thus obtained was filtered, washed with cold methanol and dried. Finally it was recrystallised from methanol to afford 0.40 g (45%) of crystalline complex. $C_{15}H_{14}KN_2O_4S_2V$ (440): Calcd. C, 40.9; H, 3.2; N, 6.4. Found C 40.8, H 3.2, N 6.4%.

2.2.3.7. $Na[V^VO_2(sal\text{-}smdt]\cdot 2H_2O$ (2.8) [119]

A solution of $[VO(acac)_2]$ (0.530 g, 2.0 mmol) dissolved in acetonitrile (30 mL) was added to a solution of H_2sal-smdt (0.452 g, 2.0 mmol) dissolved in the same solvent (20 mL) and the reaction mixture was refluxed for 1 h. After addition of an aqueous solution (5 mL) of sodium carbonate (0.12 g), the resulting solution was further refluxed for 2 h. The green solution obtained at this point was filtered and passed air through the filtrate until the green solution turned into light yellow

solution. After keeping the solution for two days yellow colour crystals slowly separated which was filtered washed with methanol and dried. Yield : 0.501 g (68%). $C_9H_{12}N_2O_5S_2VNa$ (366): Calcd. C, 29.51; H, 3.3; N, 7.65. Found C, 29.71; H, 3.88; N, 7.32%.

2.2.4. Oxidative bromination of styrene

Compounds $Cs_2[CH_2\{V^VO_2(sal\text{-}sbdt)_2\}]\cdot 2H_2O$ (**2.4**) and $Cs_2[CH_2\{V^VO_2(sal\text{-}smdt)_2\}]\cdot 2H_2O$ (**2.6**) were used as catalyst precursors to carry out the oxidative bromination of styrene. In a typical reaction, styrene (1.04 g, 10 mmol) was added to an aqueous solution (20 mL) of KBr (3.57 g, 30 mmol), followed by addition of 20 mL CH_2Cl_2 and 30% aqueous H_2O_2 (3.40 g, 30 mmol) in a 100 mL reaction flask. The catalyst (0.0010 g) and 70% $HClO_4$ (1.43 g, 10 mmol) were added, and the reaction mixture was stirred at room temperature. Three additional 10 mmol portions of 70% $HClO_4$ were further added after every 15 minutes with continuous stirring. In all batches the experimental conditions (e.g. stirring speed, size of magnetic bar and reaction flask) were kept as similar as possible. After 1 h the orange colored organic layer was separated using a separatory funnel, washed with water and dried. The crude mass was redissolved in CH_2Cl_2; insoluble material, if any, was removed by filtration, and the solvent evaporated. The reaction products were separated using a silica gel column. Elution of the column with 1% CH_2Cl_2 in n-hexane first separated a mixture of bromo derivatives followed by 1-phenylethane-1,2-diol. The two bromo derivatives were finally separated from each other using the silica gel column again by eluting with pure n-hexane. The products were identified by GC–MS [Perkin-Elmer Clarus 500 using an Elite-5 column (30 m × 0.25 mm × 0.25 μm)] and ^{1}H NMR.

1,2-Dibromo-1-phenylethane: ^{1}H-NMR ($CDCl_3$, δ/ ppm): 7.29–7.39 (m, 5 H, aromatic), 5.11–5.13 (q, 1H, CH), 3.97–4.06 (septet, 2 H, CH_2).

1-Phenylethane-1,2-diol: ^{1}H-NMR ($CDCl_3$, δ/ ppm): 7.29–7.39 (m, 5 H, aromatic), 4.9 (q, 1 H, CH), 3.5 (q, 1 H of CH_2), 3.6 (q, 1 H of CH_2), 2.7 (broad, 1 H, OH).

2-Bromo-1-phenylethane-1-ol: ^{1}H-NMR ($CDCl_3$ δ/ ppm): 7.29–7.39 (m, 5H, aromatic), 5.1 (q, 1 H, CH), 3.9 (septate, 2H, CH_2).

2.3. Results and discussion

$[V^{IV}O(acac)_2]$ reacts with the binucleating ligands $CH_2(H_2sal\text{-}sbdt)_2$ (**2.I**) or $CH_2(H_2sal\text{-}smdt)_2$ (**2.II**) in 2:1 molar ratio in refluxing methanol to give the binuclear oxidovanadium(IV) complexes: $CH_2\{V^{IV}O(sal\text{-}sbdt)(H_2O)\}_2$ (**2.1**) and $CH_2\{V^{IV}O(sal\text{-}smdt)(H_2O)\}_2$ (**2.2**), respectively. Oxidation of $[CH_2\{V^{IV}O(sal\text{-}sbdt)(H_2O)\}_2]$ and $[CH_2\{V^{IV}O(sal\text{-}smdt)(H_2O)\}_2]$ in the presence of KOH or $CsOH{\cdot}H_2O$ gave the corresponding V^VO_2-species $K_2[CH_2\{V^VO_2(sal\text{-}sbdt)_2\}]{\cdot}2H_2O$ (**2.3**), $Cs_2[CH_2\{V^VO_2(sal\text{-}sbdt)_2\}]{\cdot}2H_2O$ (**2.4**), $Cs_2[CH_2\{V^VO_2(sal\text{-}smdt)_2\}]{\cdot}2H_2O$ (**2.5**) and $Cs_2[CH_2\{V^VO_2(sal\text{-}smdt)_2\}]{\cdot}2H_2O$ (**2.6**). These complexes were also isolated directly by the reaction of $[V^{IV}O(acac)_2]$ with **2.I** or **2.II** in 2:1 ratio in refluxing methanol followed by aerial oxidation in the presence of the corresponding hydroxides. Here, the reaction probably proceeds through the formation of the $V^{IV}O$-complexes **2.1** and **2.2**. Equations (2.1) to (2.3) summarize the synthetic procedures considering $CH_2(H_2sal\text{-}sbdt)_2$ as a representative ligand.

$$2[V^{IV}O(acac)_2] + CH_2(H_2sal\text{-}sbdt)_2 + 2H_2O \rightarrow [CH_2\{V^{IV}O(sal\text{-}sbdt)(H_2O)\}_2] + 4Hacac \quad (2.1)$$

$$[CH_2\{V^{IV}O(sal\text{-}sbdt)(H_2O)\}_2] + 2KOH + \tfrac{1}{2}O_2 \rightarrow K_2[CH_2\{V^VO_2(sal\text{-}sbdt)\}_2]{\cdot}2H_2O + H_2O \quad (2.2)$$

$$[CH_2\{V^{IV}O(sal\text{-}sbdt)(H_2O)\}_2] + 2CsOH + \tfrac{1}{2}O_2 \rightarrow Cs_2[CH_2\{V^VO_2(sal\text{-}sbdt)\}_2]{\cdot}2H_2O + H_2O \quad (2.3)$$

$[VO(acac)_2]$ also reacts with the potassium salt of $H_2sal\text{-}sbdt$ (**2.III**) or $H_2sal\text{-}smdt$ (**2.IV**) in the presence of Na_2CO_3 under aerobic conditions to give dioxidovanadium(V) complexes, $K[VO_2(sal\text{-}sbdt)]{\cdot}H_2O$ (**2.7**) or $Na[VO_2(sal\text{-}smdt)]{\cdot}2H_2O$ (**2.8**). All complexes are soluble in methanol, DMSO and DMF. Proposed structures of these complexes (Scheme 2.2) are based on the spectroscopic characterization (IR, electronic, EPR, ^{1}H and ^{51}V NMR) and

elemental analyses. The ligands coordinate through each of their dianionic $(ONS)^{2-}$ thioenolate tautomeric forms.

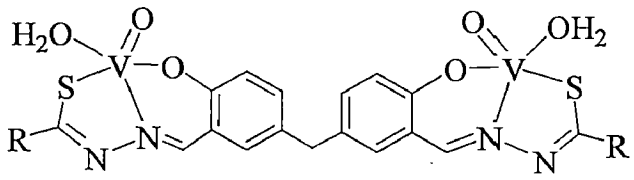

R	Complex
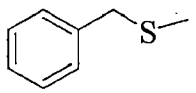	$[CH_2\{V^{IV}O(sal\text{-}sbdt)(H_2O)\}_2]$ **(2.1)**
H_3C-S	$[CH_2\{V^{IV}O(sal\text{-}smdt)(H_2O)\}_2]$ **(2.2)**

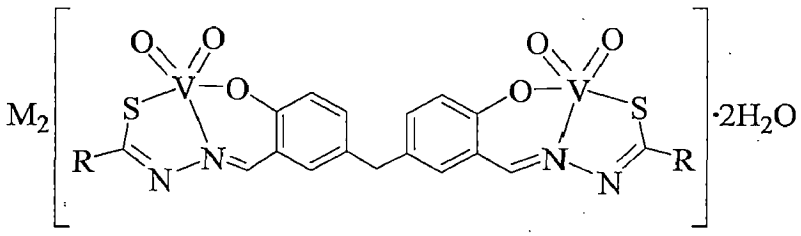

M^+	R	Complex
K^+	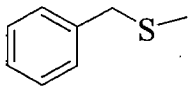	$K_2[CH_2\{V^{V}O_2(sal\text{-}sbdt)\}_2]\cdot 2H_2O$ **(2.3)**
Cs^+	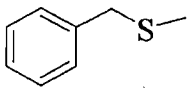	$Cs_2[CH_2\{V^{V}O_2(sal\text{-}sbdt)\}_2]\cdot 2H_2O$ **(2.4)**
K^+	H_3C-S	$K_2[CH_2\{V^{V}O_2(sal\text{-}smdt)\}_2]\cdot 2H_2O$ **(2.5)**
Cs^+	H_3C-S	$Cs_2[CH_2\{VO_2(sal\text{-}smdt)\}_2]\cdot 2H_2O$ **(2.6)**

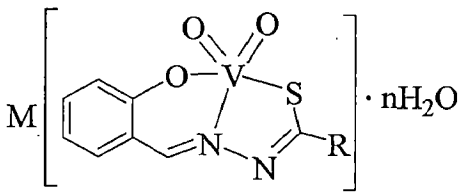

M^+	R	Complex
K^+	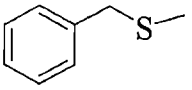	$K[V^{V}O_2(sal\text{-}sbdt)]\cdot H_2O$ **(2.7)**
Na^+	H_3C-S	$Na[V^{V}O_2(sal\text{-}smdt)]\cdot 2H_2O$ **(2.8)**

Scheme 2.2. Schematic structural formulae of the $V^{IV}O$- and $V^{V}O_2$-complexes prepared.

2.3.1. IR spectral studies

The IR spectra of a representative ligand and of the corresponding $V^{V}O_2$-complex are presented in Figures 2.1 to 2.3 while a partial list of IR spectral data of ligands and complexes is presented in Table 2.1. Detailed discussion on the IR spectral studies is presented elsewhere [119,136,130]. The IR spectra of the complexes have all characteristic bands of the coordinated tridentate system. The $V^{IV}O$-complexes exhibit bands at 994 (**2.1**) and 996 cm^{-1} (**2.2**), due to ν(V=O) stretch. The $V^{V}O_2$-complexes exhibit one sharp band in the 888–887 cm^{-1} region and a weaker one at ca. 928–965 cm^{-1} due to ν_{sym}(O=V=O) and ν_{asym}(O=V=O). These bands confirm the cis-$V^{V}O_2$ structure in complexes [30]. The weakening of one the bands may be considered to suggest that the O-atoms of the $V^{V}O_2$-units are probably involved in binding to $Na^+/K^+/Cs^+$ in the crystal structure; such binding was confirmed in anionic dioxidovanadium(V) complexes [136,137].

Table 2.1. IR data of the compounds prepared (ν in cm^{-1}) and the corresponding assignments.

Compounds	ν(C=S)	ν(C=N)	ν(V=O)	ν(N–N)
$CH_2(H_2sal\text{-}sbdt)_2$	1030	1625		948
$CH_2(H_2sal\text{-}smdt)_2$	1039	1624	-	936
$[CH_2\{V^{IV}O(sal\text{-}sbdt)(H_2O)\}_2]$		1609	994	1034
$K_2[CH_2\{V^{V}O_2(sal\text{-}sbdt)\}_2]\cdot 2H_2O$		1613	884, 935	1027
$Cs_2[CH_2\{V^{V}O_2(sal\text{-}sbdt)\}_2]\cdot 2H_2O$		1612	887, 928	1027
$[CH_2\{V^{IV}O(sal\text{-}smdt)(H_2O)\}_2]$		1609	996	1034
$K_2[CH_2\{V^{V}O_2(sal\text{-}smdt))\}_2]\cdot 2H_2O$		1612	886, 939	1030
$Cs_2[CH_2\{V^{V}O_2(sal\text{-}smdt)\}_2]\cdot 2H_2O$		1612	887, 927	1033
$H_2sal\text{-}sbdt$	1041	1619	-	950
$K[VO_2(sal\text{-}sbdt)]\cdot H_2O$		1601	888, 921	1020
$H_2sal\text{-}smdt$	1044	1610	-	946
$Na[VO_2(sal\text{-}smdt)]\cdot 2H_2O$		1600	900, 970	1027

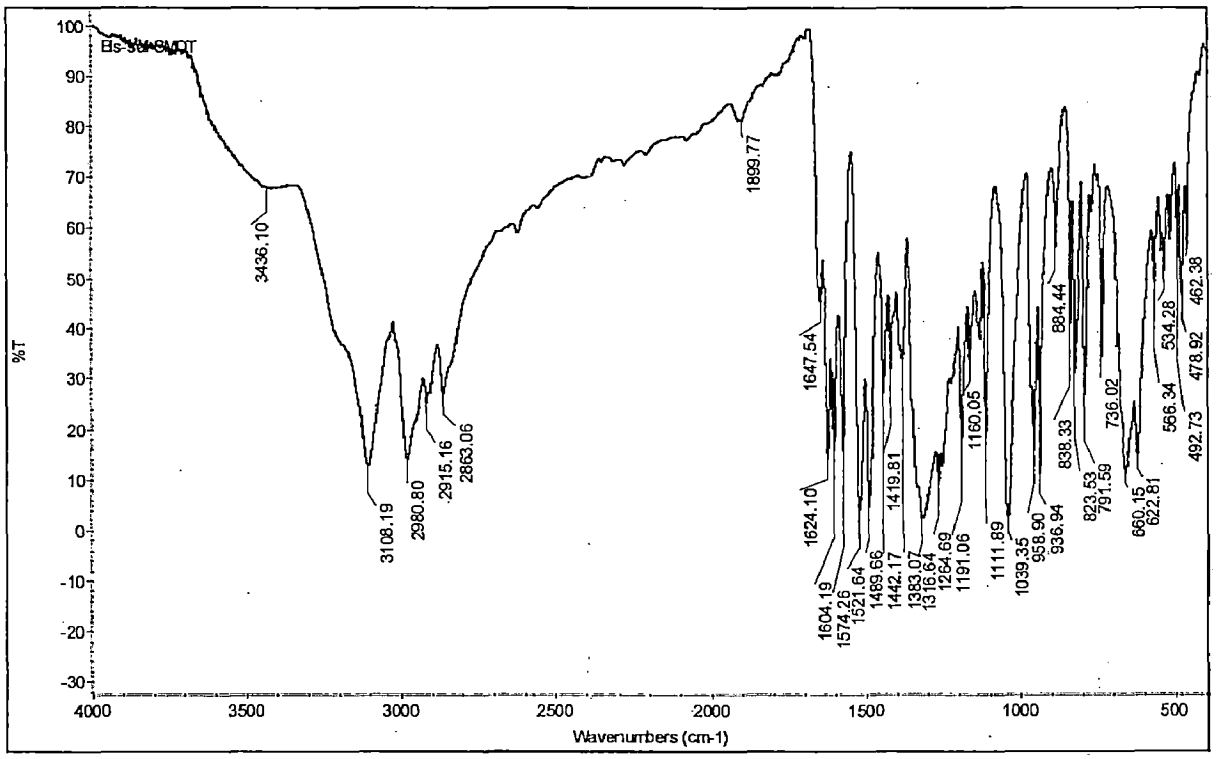

Figure 2.1. FT-IR Spectrum of $CH_2(H_2sal\text{-}smdt)_2$ (**2.II**).

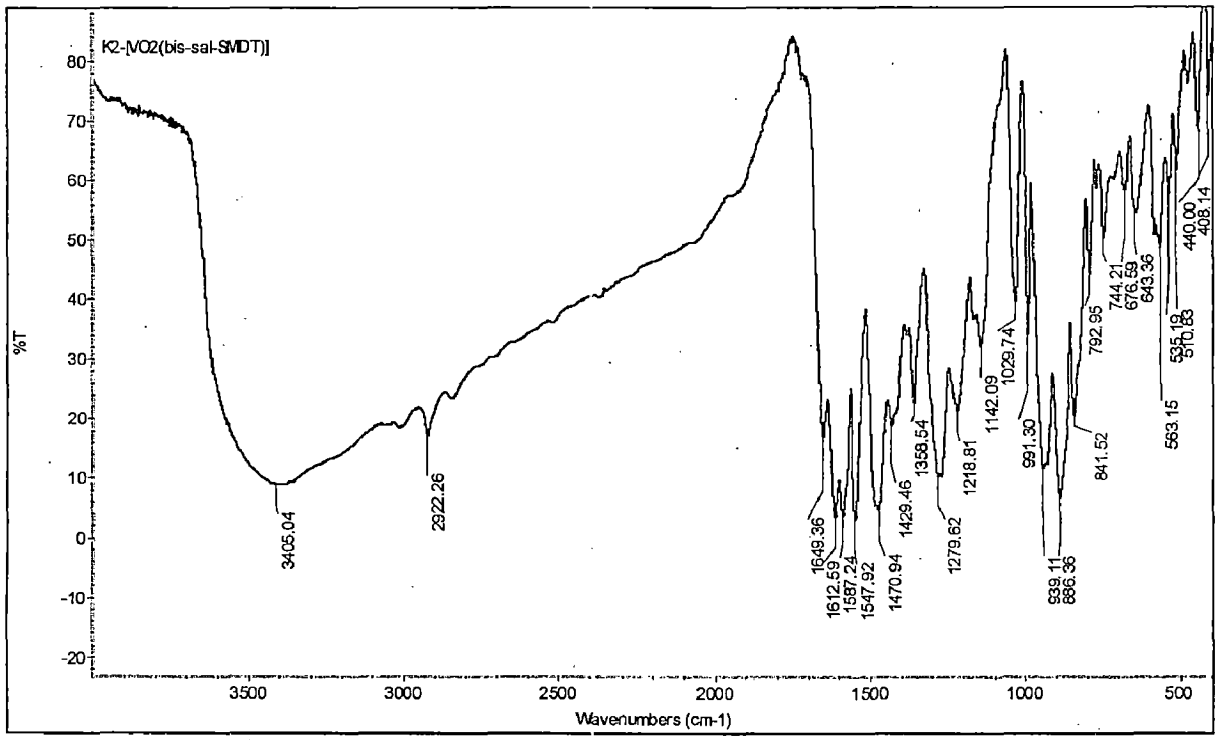

Figure 2.2. FT-IR Spectrum of $K_2[CH_2\{V^VO_2(sal\text{-}smdt)\}_2]\cdot 2H_2O$ (**2.5**).

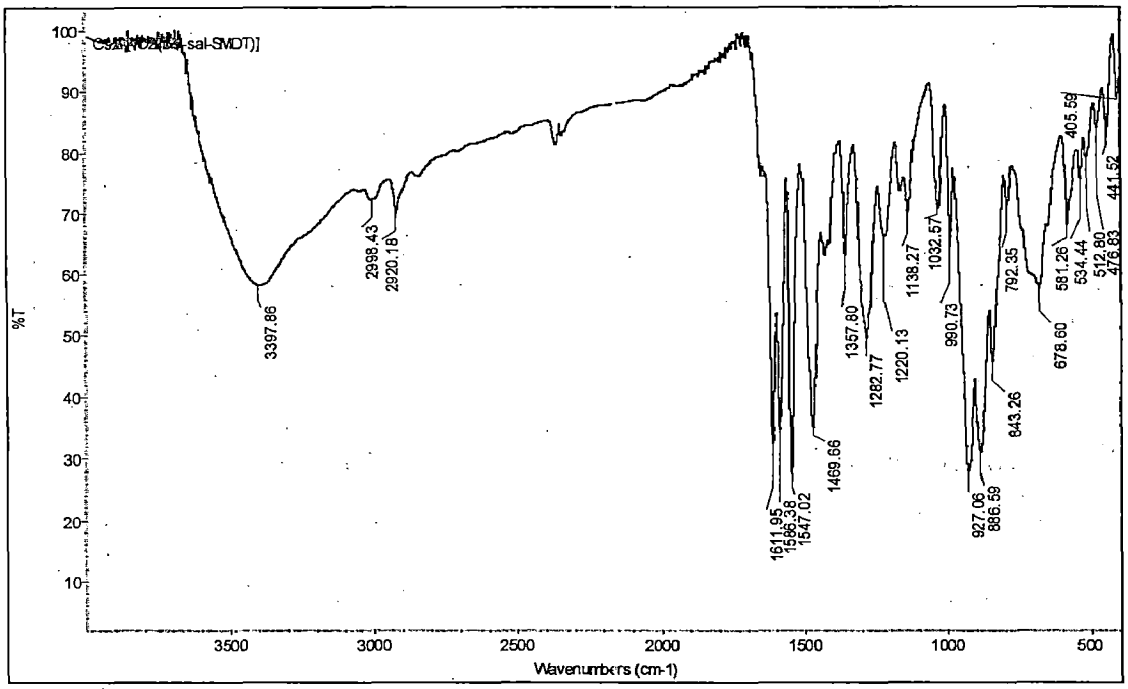

Figure 2.3. FT-IR Spectrum of $Cs_2[CH_2\{V^VO_2(sal\text{-}smdt)\}_2]\cdot 2H_2O$ (**2.6**).

2.3.2. Electronic Spectral Studies

Ligands $CH_2(H_2sal\text{-}sbdt)_2$ and $CH_2(H_2sal\text{-}smdt)_2$ exhibit absorption bands at ca. 206, 255, 328 and 360 nm which are assigned to $\varphi \rightarrow \varphi^*$, $\pi \rightarrow \pi_1^*$, $\pi \rightarrow \pi_2^*$, and $n \rightarrow \pi^*$ transitions, respectively. Similar slightly shifted bands are also observed in the corresponding complexes (Table 2.2). In addition, a new band of medium intensity appears at ca. 405 nm, which is assigned to a ligand to metal charge transfer (LMCT) band.

Upon dissolution the $V^{IV}O$-complexes have tendency to hydrolise and oxidize (see below). Three bands at 575, 680 and 845 nm (in **2.1**) and at 565, 675 and 875 nm (in **2.2**), observed at higher concentration, are assigned to d–d transitions. However it is probable that these bands might be due to the presence of more than one type of $V^{IV}O$-complex in solution. For the V^VO_2-complexes no such bands were detected.

Table 2.2. Electronic spectral data (in methanol) of the compounds.

Compounds	λ/nm (ε/ litre $mole^{-1}$ cm^{-1})
$CH_2(H_2sal\text{-}sbdt)_2$ **(2.I)**	362(5.07×10^4), 328(3.23×10^4), 254 (1.54×10^4), 213(5.15×10^4)
$CH_2(H_2sal\text{-}smdt)_2$ **(2.II)**	361(4.8×10^4), 327(3.14×10^4), 256(1.48×10^4), 215(3.53×10^4)
$[CH_2\{V^{IV}O(sal\text{-}sbdt)(H_2O)\}_2]$ **(2.1)**	845(32), 680(62), 575(84), 417(8.16×10^3), 352sh(2.52×10^4), 297(3.36×10^4), 210(1.80×10^4)
$K_2[CH_2\{V^VO_2(sal\text{-}sbdt)\}_2]\cdot2H_2O$ **(2.3)**	410 (1.52×10^4), 352(1.73×10^4), 302 (3.88×10^4)
$Cs_2[CH_2\{V^VO_2(sal\text{-}sbdt)\}_2]\cdot2H_2O$ **(2.4)**	410(1.64×10^4), 345(1.89×10^4), 297(4.04×10^4), 210(2.53×10^4)
$[CH_2\{V^{IV}O(sal\text{-}smdt)(H_2O)\}_2]$ **(2.2)**	875(53), 675(110), 565(187), 405(5.97×10^3), 350(2.65×10^4), 305(2.8×10^4), 215(1.52×10^4)
$K_2[CH_2\{V^VO_2(sal\text{-}smdt))\}_2]\cdot2H_2O$ **(2.5)**	403(1.15×10^4), 343(1.98×10^4), 295(3.48×10^4), 233(3.54×10^4)
$Cs_2[CH_2\{V^VO_2(sal\text{-}smdt)\}_2]\cdot2H_2O$ **(2.6)**	403(1.29×10^4), 345(1.78×10^4), 295(3.57×10^4), 238(1.96×10^4), 208(1.91×10^4)

2.3.3. ^{1}H NMR studies

Table 2.3 summarizes data of the ^{1}H NMR spectra of the ligands and V^VO_2-complexes while Figures 2.4 and 2.5 present the representative ^{1}H NMR spectra of **2.II** and of complex **2.6**. The ^{1}H NMR data are consistent with the ONS dibasic tridentate binding mode of each unit of ligands **2.I** and **2.II**. Data of monomeric **2.7** and **2.8** complexes are also compatible with the structure proposed.

Table 2.3. ^{1}H NMR spectral data (δ in ppm) of ligands and complexes recorded in DMSO-d_6

Compounds [a], [b]	–CH=N–	Aromatic H	–CH_2–	-OH	–NH	-SCH_2-	-CH_3
2.I	8.50(s, 2H)	6.80 (d, 2H), 7.50 (d, 2H), 7.35 (m, 12H)	3.75(s, 2H)	13.35(s, 2H)	10.10(s, 2H)	4.50(s, 4H)	
2.3 (Δδ)	9.02(s, 2H) (0.52)	6.78(d, 2H), 7.0–7.80(m, 14H)	3.89(s, 2H) (0.14)			4.39(s, 4H) (-0.11)	
2.4 (Δδ)	9.03 (s, 2H) (0.53)	6.77 (d, 2H), 7.35-7.75 (m, 14H)	3.89 (s, 2H) (0.14)			4.39 (s, 4H) (-0.11)	
2.II	8.45 (s, 2H)	6.8 (d, 2H), 7.4 (d, 2H), 7.55 (d, 2H)	3.80 (s, 2H)	13.32 (s, 2H)	10.11 (s, 2H)		2.5 (s, 6H)
2.5 (Δδ)	8.96 (s, 2H) (0.51)	6.77 (d, 2H), 7.26 (d, 2H), 7.51 (d, 2H)	3.87 (s, 2H) (0.07)				2.50 (s, 6H) (0.03)
2.6 (Δδ)	8.96 (s, 2H) (0.52)	6.7 (d, 2H), 7.26 (d, 2H), 7.50 (d, 2H)	3.86 (s, 2H) (0.08)				2.50 (s, 6H) (0.03
2.III	8.55 (s, 1H)	6.89 (m, 2H), 7.28 (m, 4H), 7.40 (d, 2H), 7.64 (d, 1H)		13.40 (s, 1H)	10.24 (s, 1H)	4.50 (s, 2H)	
2.7 (Δδ)	9.07 (s,1H) (0.52)	6.86 (q, 2 H), 7.23 (q, 1 H), 7.32 (t, 2 H), 7.43 (q, 3 H), 7.65 (d, 1 H)				4.40 (s, 2H) (-0.10)	
2.IV	8.51(s, 1H)	6.87 (m, 2 H), 7.26 (t, 1 H), 7.63 (d, 1 H)		13.31 (s, 1H)	10.22 (s, 1H)		2.41 (s, 3H)
2.8 (Δδ)	8.82(s, 1H) (0.31)	6.84 (m, 2 H), 7.22 (t, 1 H), 7.75 (d, 1 H)					3.18(s, 3H) (0.77)

[a] Letters given in parentheses indicate the signal structure: s = singlet, b = broad (unresolved), m = multiplet.

[b] $\Delta\delta = \delta$ (complex) – δ (ligand).

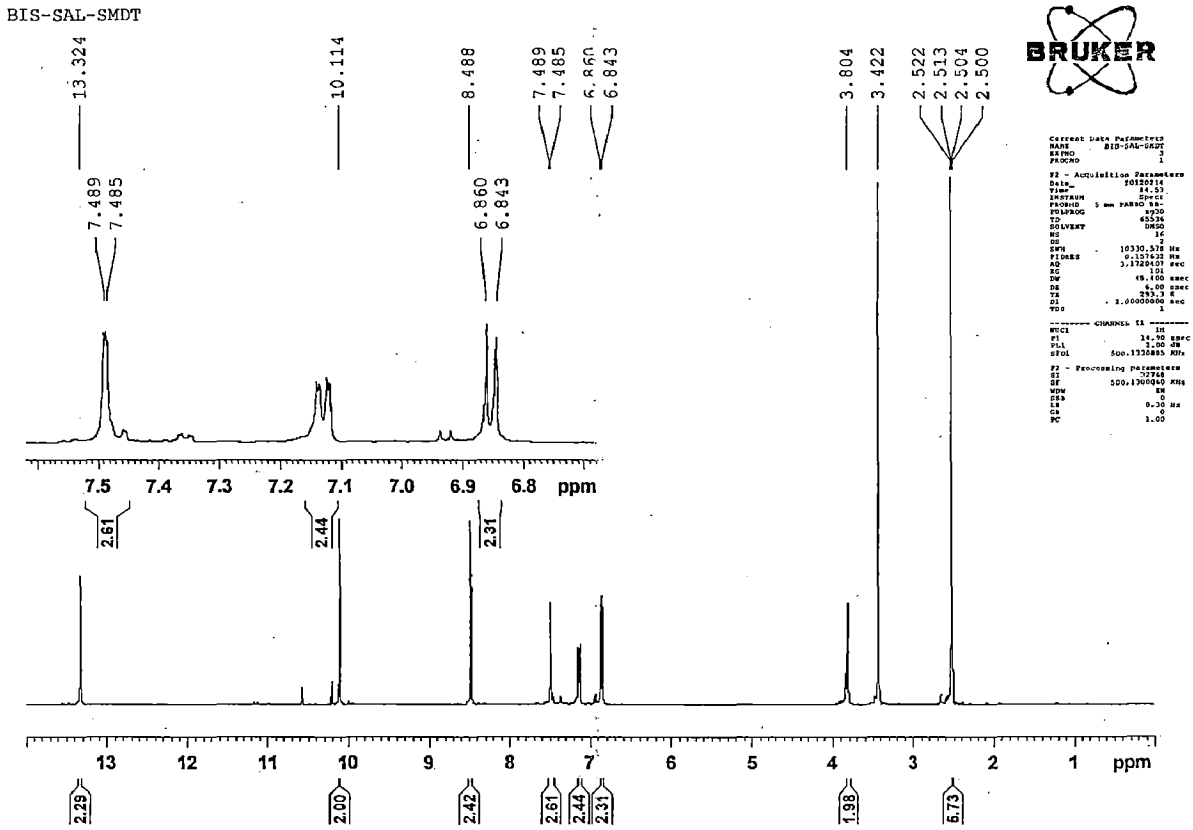

Figure 2.4. ^{1}H NMR Spectrum of $CH_2(H_2sal\text{-}smdt)_2$ (**2.II**).

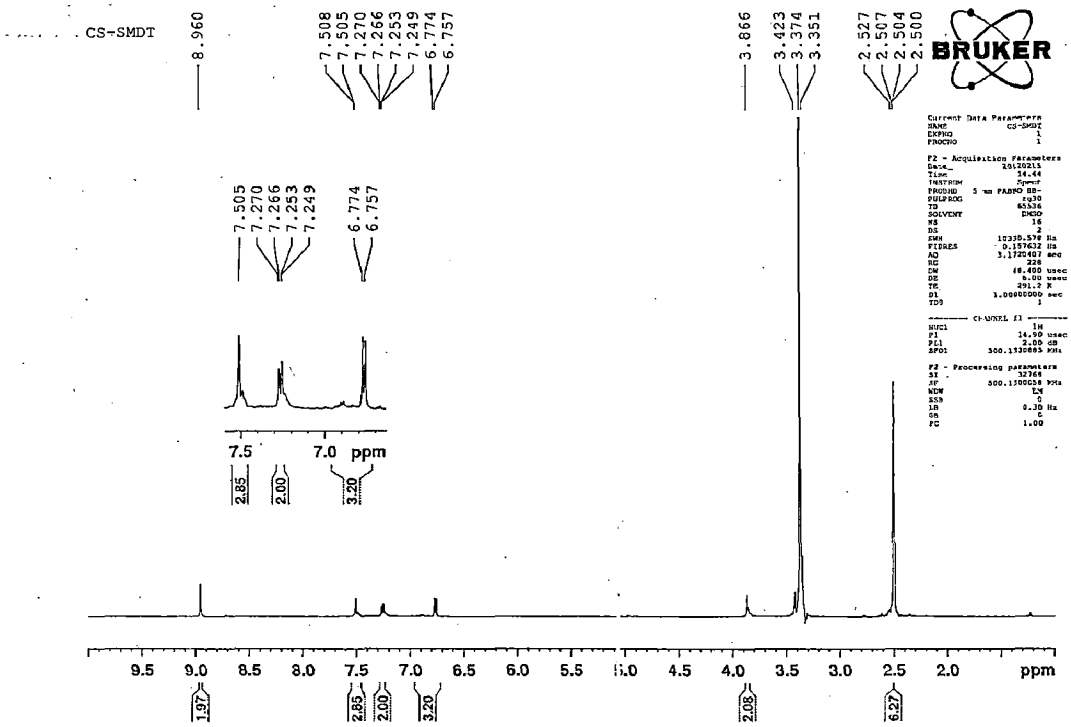

Figure 2.5. ^{1}H NMR spectrum of $Cs_2[CH_2\{V^VO_2(sal\text{-}smdt)\}_2]\cdot 2H_2O$ (**2.6**).

2.3.4. ^{13}C NMR studies

The ^{13}C NMR spectra recorded for complexes **2.3** and **2.4** contain 10 signals corresponding to the 31 carbon atoms of the molecules and, also owing to their symmetry, the spectra for complexes **2.5** and **2.6** contain 8 signals corresponding to 19 carbon atoms of the molecules. The peaks observed and their assignments are included in Tables 2.4 and 2.5, being compatible with the structures proposed.

Table 2.4. ^{13}C NMR chemical shifts observed; for the atom labelling see scheme below.

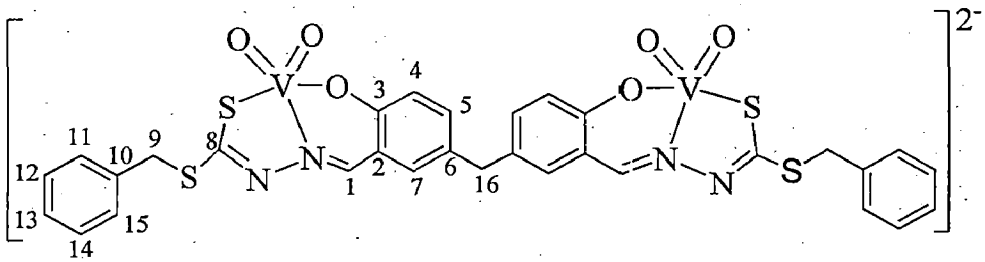

Compounds	C8	C1	C3	C2/4/5/6/7/10/11/12/13/14	C9	C16
$K_2[CH_2\{V^VO_2(sal\text{-}sbdt)\}_2]$ **(2.3)**	164	163	159.9	138.4 133.4/129.6/128.8/127.5	39.7	36.9
$Cs_2[CH_2\{V^VO_2(sal\text{-}sbdt)\}_2]$ **(2.4)**	163. 3	163.2	157	138.6 135.1/129.8/129.1/127.5	39.7	37

Table 2.5. ^{13}C NMR chemical shifts observed; for the atom labelling see scheme below.

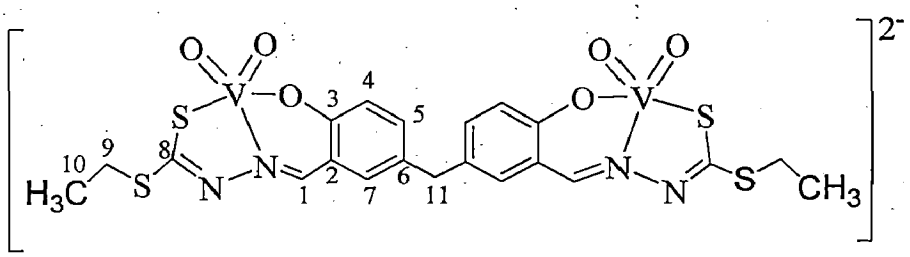

Compound	C8	C1	C3	C2/4/5/6/7	C9	C11	C10
$K_2[CH_2\{V^VO_2(sal\text{-}smdt)\}_2]$ **(2.5)**	162.4	162.2	161.7	129.6/128.8	37	56.5	12.6
$Cs_2[CH_2\{V^VO_2(sal\text{-}smdt)\}_2]$ **(2.6)**	162.4	162.2	161.7	129.6/128.8	35	38.2	19.2

2.3.5. ^{51}V NMR studies

Complexes **2.3**, **2.4**, **2.5** and **2.6** were further characterized in solution by recording their ^{51}V NMR spectra in DMSO-d_6 (see Table 2.6). The line widths at half height are ca. 200 Hz. The ^{51}V NMR spectra of complexes $[CH_2\{V^VO_2(ONS)\}_2]^{2-}$ (4 mM) in DMSO show a major resonance at δ –462/–463 ppm and a minor one at δ –494/ –497 ppm. The ^{51}V nucleus is thus less shielded than commonly observed with V^VO_2-complexes with O, N donor atoms. However, the chemical shifts are well within the range expected for vanadium(V) complexes where a soft S atom participates in coordination in addition to the O and N donor atoms [51].

Table 2.6. Summary of the ^{51}V NMR data and assignment of the vanadium complexes studied in this work (see text and Scheme 2.3)

Compounds	Chemical shifts / ppm				
	CII	**CIII**	**CIV**	**CV**	**CVI**
2.3	–463.0	–495	–445	–525	–553
2.4	–463.0	–497	–448	–521	–553
2.5	–462.0	–495		–521	
2.6	–463.0	–495	–440	–525	

2.3.6. Solution behaviour of complexes

The ^{51}V NMR spectrum of **2.4** dissolved in DMSO has a major resonance at $\delta = -463$ ppm and a minor one at $\delta = -495$ ppm [Figure 2.6(a)]. The resonance at $\delta = -463$ ppm is assigned to $[CH_2\{V^VO_2(sal\text{-}sbdt)(Sv)\}_2]^{2-}$ (**CII**, Sv = H_2O or DMSO, Scheme 2.3); the two V^VO_2-centres being equivalent. A soft S atom participates in coordination in addition to the O and N donor atoms possibly trans to one of the O_{oxido} donors, otherwise probably the peak would be detected at lower fields. The minor resonance at $\delta = -495$ ppm is tentatively assigned to species **CIII** where the $S_{thiolate}$ is not coordinated to the V^V-centre, the chemical shift corresponding to ONO coordination. Upon the stepwise addition of an aqueous 30% solution of H_2O_2 to the solution of **2.4** in DMSO (ca. 4 mM), the resonance at -463 ppm progressively decreases its intensity and a resonance at –

521 ppm progressively develops (Figure 2.6 (b-e)), which we tentatively assign to $[CH_2\{V^VO(O_2)(sal\text{-}sbdt)(Sv)\}_2]^{2-}$ **(CV)** [at least one of the V^V-centres has a coordinated peroxide ligand.

The solution corresponding to the spectrum of Figure 2.6(d) was then divided in two portions: Portion (i): the tube was left open for ca. 36 h. The resonance at –521 ppm almost disappeared, indicating that, as far as V^V-species are concerned, these were converted back to **CII**, with signal at –463 ppm, indicating the reversibility of the process. Additionally the ^{51}V NMR signals show broadening indicating the probable presence of $V^{IV}O$-species in the solution. This was confirmed by recording the EPR spectra for both solutions of Figures 2.6 (f) and (e). The spectra are reasonably intense with reasonable sharp lines, and the spin Hamiltonian parameters obtained for the solution of Figure 2.6(f) are $g_{\|} = 1.974$; $g_{\perp} = 1.934$; $A_{\perp} = 59\times10^{-4}$ cm^{-1} and $A_{\|} = 178\times10^{4}$ cm^{-1}. This indicates partial hydrolysis when comparing with the $A_{\|}$ values expected for complex **2.1**.

Portion (ii): addition of styrene resulted in the disappearance of the signal at –521 ppm, the only resonance clearly detected being found at –463 ppm, giving evidence for the involvement/consumption of the peroxo-species during the catalytic process.

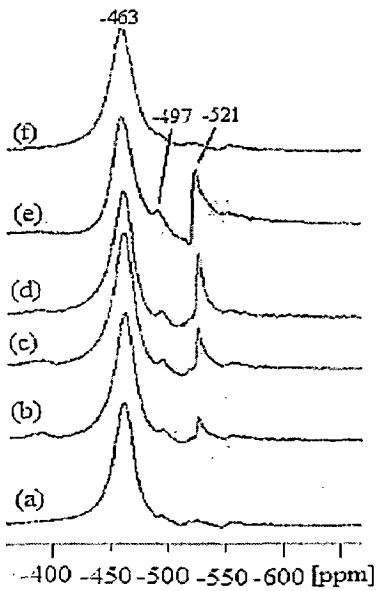

Figure 2.6. ^{51}V NMR spectra for solutions (ca. 4 mM) of $Cs_2[CH_2\{V^VO_2(sal\text{-}sbdt)\}_2]\cdot2H_2O$ (**2.4**): (a) in DMSO and (b–d) after stepwise additions of an aqueous solution of 30% H_2O_2; (b) 1.0 equiv. H_2O_2 added; (c) 2 equiv. H_2O_2 (total) added;

(d) 4.0 equiv. H_2O_2 (total) added; (e) solution of (d) after 2 h leaving the tube open; (f) solution of (e) after 36 h leaving the tube open.

Addition of acid (HCl, 11.6 M), viz. 1, 2, 3, 4 equiv. to solution of **2.4** (in DMSO, ca. 4 mM), leaded to a shift of the –463 ppm resonance to -448 ppm (see Figure 2.7); the colour of the solution turned to red and the pH was ~4.5–5.0. The addition of acid may protonate the oxo group and the resonance at δ = –463 ppm progressively shifts to –448 ppm (broad, ca. 98%) [Figure 2.7 (d)], probably corresponding to an oxido/hydroxido species **(CIV)**. An alternative plausible explanation for **CIV** is protonation of one of the coordinated donor atoms of the ligand. Addition of 4 equiv. KOH to a portion of the solution of Figure 2.7 (d) yielded a ^{51}V NMR spectrum with a main signal at –463 ppm indicating the reversibility of the processes. The other portion was left standing and spectrum (e) recorded.

Additionally the spectra (d) and (e) of Figure 2.7 show broadening of the ^{51}V NMR signals indicating the probable presence of $V^{IV}O$-species in the solution. This was confirmed by recording the EPR spectra of both solutions. Both EPR spectra are reasonably intense and the spin Hamiltonian parameters obtained are $g_{\|}$ = 1.974; $g_{\perp}$ = 1.954; $A_{\perp} = 59\times10^4$ cm^{-1} and $A_{\|} = 178\times10^4$ cm^{-1} [for solution of (e)]. The parameters are similar to those of solutions of **2.1** in DMSO (see below) indicating a O_3N or O_4 binding mode around the V^{IV} center due to the partial reduction/hydrolysis.

Similar results were obtained in case of complexes **2.3, 2.5** and **2.6**. The peaks observed and their assignments are included in the Table 2.6 and details are presented in Figures 2.8–2.12, being compatible with the structural formulae proposed.

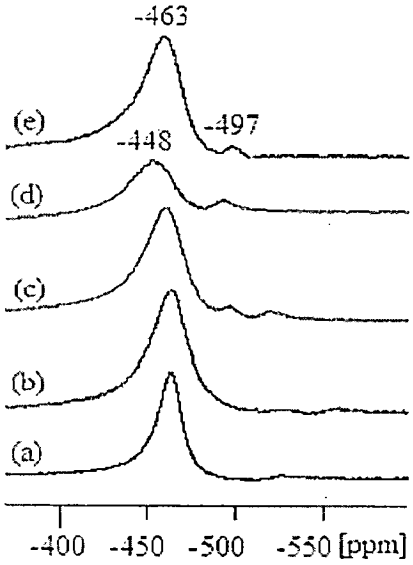

Figure 2.7. ^{51}V NMR spectra for solutions of $Cs_2[CH_2\{V^VO_2(sal\text{-}sbdt)\}_2]\cdot 2H_2O$ (**2.4**): (a) in DMSO (ca. 4 mM), (b) solution of (a) after addition of 1.0 equiv. of an aqueous solution of HCl (11.6 M), the pH being ca. 5.8; (c) solution of (b) after addition of 2.0 equiv. HCl (total) added; (d) after addition of 4.0 equiv. HCl (total) added (pH~3.5); (e) solution of spectrum (d) after leaving the sample standing for about 24 h.

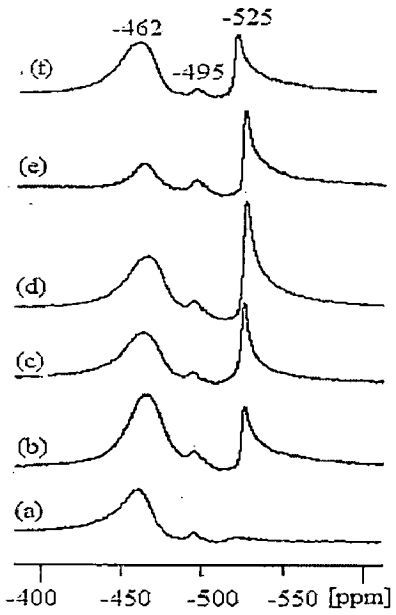

Figure 2.8. ^{51}V NMR spectra of solutions (ca. 4 mM) of $K_2[CH_2\{V^VO_2(sal\text{-}sbdt)\}_2]\cdot 2H_2O$ (**2.3**): (a) in DMSO and (b–d) after stepwise additions of an aqueous solution of 30% H_2O_2; (b) 1.0 equiv. H_2O_2 added; (c) 2 equiv. H_2O_2 (total) added; (d) 4.0 equiv. H_2O_2 (total) added; (e) solution of (d) after 2 h leaving tube open; (f) solution of (e) after 36 h leaving tube open.

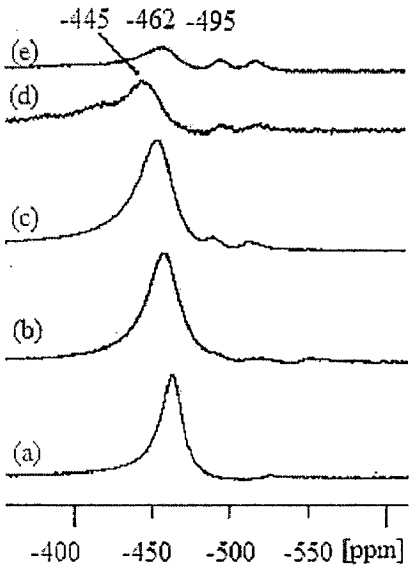

Figure 2.9. ^{51}V NMR spectra for solutions of $K_2[CH_2\{V^VO_2(sal\text{-}sbdt)\}_2]\cdot 2H_2O$ (**2.3**): (a) in DMSO (ca. 4 mM), (b) solutions of (a) after addition of 1.0 equiv. of an aqueous solution of HCl (11.6 M), the pH being about 5.8; (c) solution of (b) after addition of 2.0 equiv. HCl (total) added; (d) after addition of 4.0 equiv. HCl (total) added (pH~3.5); (e) solution of spectrum (b) after standing for about 24 h.

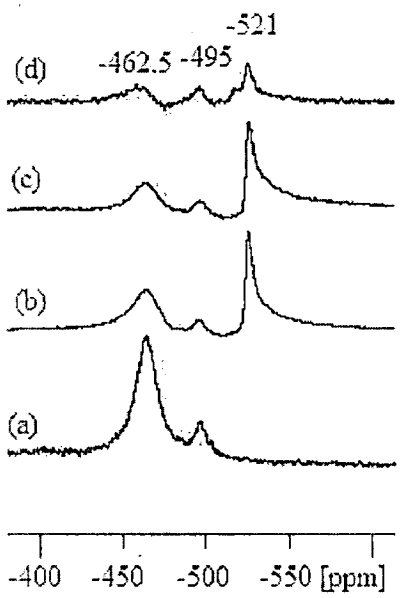

Figure 2.10. ^{51}V NMR spectra for solutions (ca. 4 mM) of $K_2[CH_2\{V^VO_2(sal\text{-}smdt)\}_2]\cdot 2H_2O$ (**2.5**): (a) in DMSO and (b–c) after stepwise additions of an aqueous solution of 30% H_2O_2; (b) 1.0 equiv. H_2O_2 added; (c) 4 equiv. H_2O_2 (total) added; (d) solution of (c) after 36 h leaving tube open.

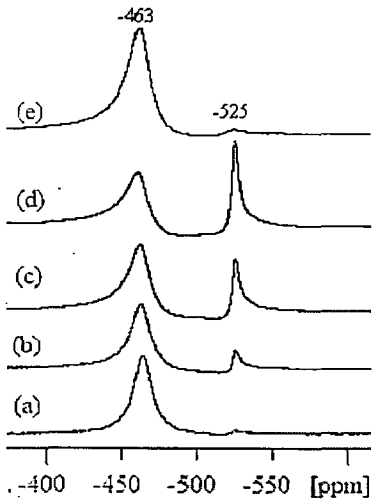

Figure 2.11. ^{51}V NMR spectra for solutions (ca. 4 mM) of $Cs_2[CH_2\{V^VO_2(sal\text{-}smdt)\}_2]\cdot 2H_2O$ (**2.6**): (a) in DMSO and (b–d) after stepwise additions of an aqueous solution of 30% H_2O_2; (b) 1.0 equiv. H_2O_2 added; (c) 2 equiv. H_2O_2 (total) added; (d) 4.0 equiv. H_2O_2 (total) added; (e) solution of (d) after 36 h leaving tube open.

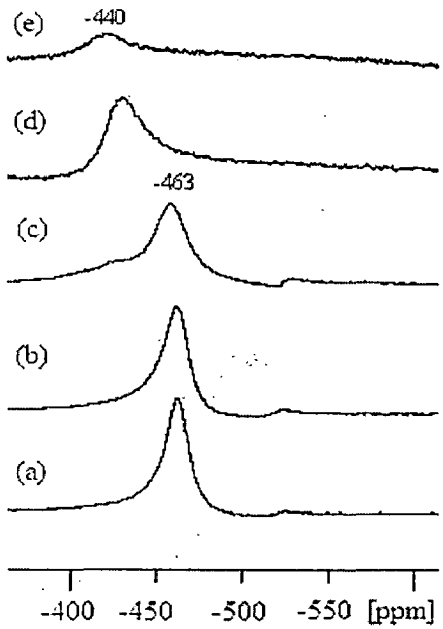

Figure 2.12. ^{51}V NMR spectra for solutions of $Cs_2[CH_2\{V^VO_2(sal\text{-}smdt)\}_2]\cdot 2H_2O$ (**2.6**): (a) in DMSO (ca. 4 mM), (b) solution of (a) after addition of 1.0 equiv. of an aqueous solution of HCl (11.6 M), the pH being about 5.8; (c) solution of (b) after addition of 2.0 equiv. HCl (total) added; (d) after addition of 4.0 equiv. HCl (total) added (pH~3.5); (e) solution of spectrum (b) after standing for about 24 h.

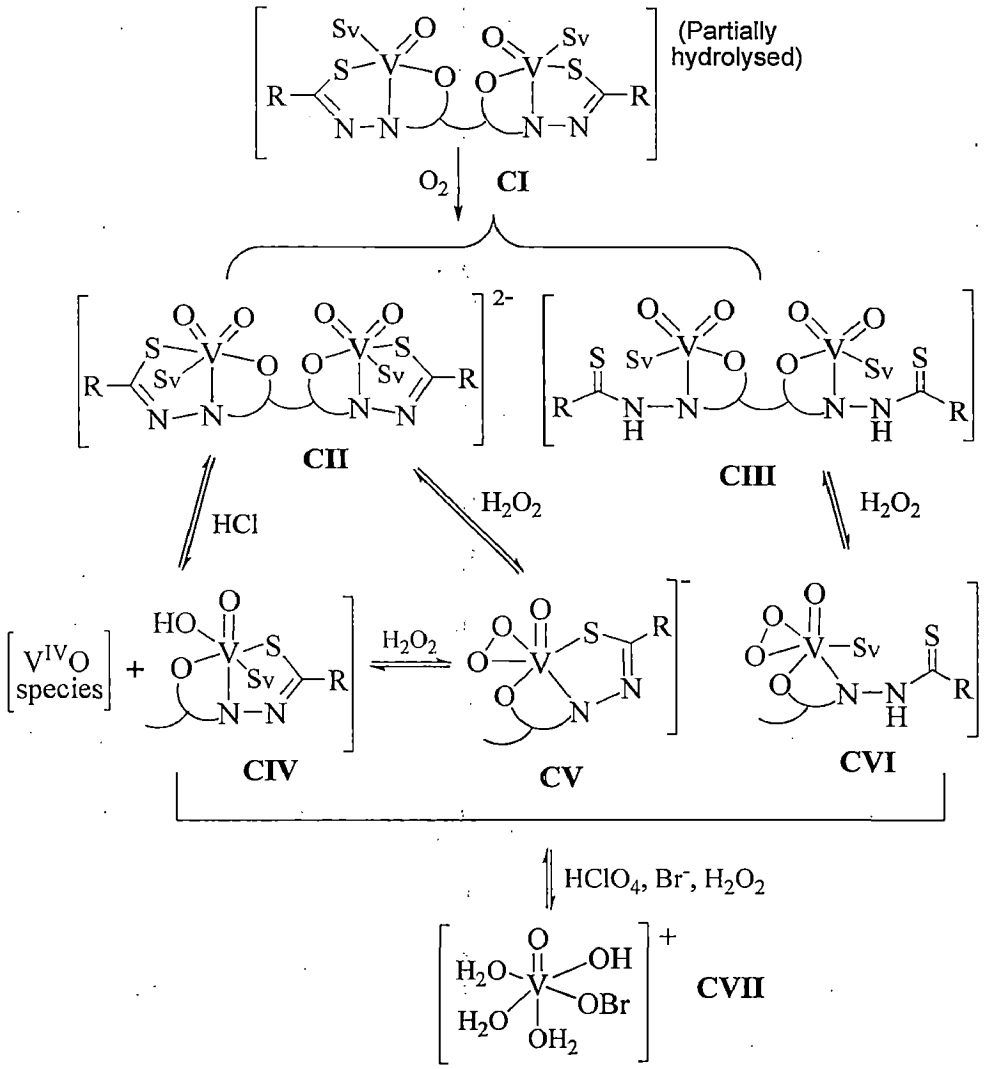

Scheme 2.3. Summary of speciation of V^V-containing species in solutions of **2.3-2.6**. In **CIV**, **CV** and **CVI** either half of the V^V-centres or both may be present as specified. For example, **CIV** may correspond to either $[\{V^VO_2(L)(Sv)\}CH_2\{V^VO(OH)(L)(Sv)\}]$ or $[\{V^VO(OH)(L)(Sv)\}CH_2\{V^VO(OH)(L)(Sv)\}]$ (Sv = solvent).

2.3.7. EPR and UV/Vis studies

The EPR spectra of "frozen" solutions (77 K) in DMSO of compounds **2.1** and **2.2** are depicted in Figure 2.13. The lines show broadening due to both: incomplete rotational averaging of the g and A tensors and probable partial precipitation of the complexes upon freezing the solutions. Apparently two sets of lines showing hyperfine splitting due to the ^{51}V nucleus are obtained. The spectra were simulated and the spin Hamiltonian parameters obtained by simulation of the

spectra are included in Table 2.7. EPR spectra were also recorded by passing He through the DMSO solutions of **2.1** and **2.2** in the presence of ascorbic acid, but the positions of the lines remained the same.

The values of $A_{\|}$ can be estimated using the additivity relationship [$A_{\|}^{est} = \Sigma A_{\|,i}$ (i = 1 to 4)], ($A_{\|,i}$ = contribution of each of the four donor atoms coordinated equatorially), proposed by Wüthrich [138] and Chasteen [55], with estimated accuracy of ± 3×10^{-4} cm^{-1}. The $A_{\|}$ values obtained for **2.1** and **2.2** (Table 2.7) agree with the $A_{\|}^{est}$ values calculated from the partial contributions of the equatorial donor groups [52,53,137,55,139-141] relevant in the present case {H_2O (45.7×10^{-4} cm^{-1}), $O_{phenolate}$ (38.9×10^{-4} cm^{-1}), N_{imine} (38.1 to 43.7×10^{-4} cm^{-1}), O_{DMSO} (41.9×10^{-4} cm^{-1}), $S_{thiolate}$ (31.9×10^{-4} cm^{-1})} either assuming a NO_3 (species II) or a O_4 (species I) equatorial binding set. If $S_{thiolate}$ is considered as an equatorial donor atom the $A_{\|}^{est}$ are much lower (ca. 157×10^{-4} cm^{-1}). Thus, at least in DMSO solution the $S_{thiolate}$ is not bound to the V^{IV}-centre (at least equatorially).

Addition of 1, 2 and 3 equiv. of H_2O_2 to solutions of **2.1** or **2.2** in DMSO acidifies the solutions, and $V^{IV}O$ species form (see Figure 2.14) with almost identical spin-Hamiltonian parameters ($g_{\|}$ = 1.939, $A_{\|}$ = 177.8×10^{-4} cm^{-1} for **2.1** and $g_{\|}$= 1.935, $A_{\|}$ = 178.0×10^{-4} cm^{-1} for **2.2**). The $V^{IV}O$ is also progressively oxidized to V^{V}. According to the $g_{\|}$ and $A_{\|}$ values obtained for these partially oxidized solutions, in these $V^{IV}O$ species the equatorial binding set is probably O_4, thus indicating the substitution of donor atoms of the ligand by DMSO and/or H_2O molecules in the coordination sphere.

Table 2.7. Spin Hamiltonian parameters obtained by simulation of the experimental 1st derivative EPR spectra recorded for DMSO solutions of complexes **2.1** and **2.2** at 77K.

Complexes in DMSO (5 mM)		$g_{\|}$	$A_{\|}$ ($\times10^{-4}$ cm^{-1})	$g_{\perp}$	$A_{\perp}$ ($\times10^{-4}$ cm^{-1})
(**2.1**)	Species I	1.936	178.1	1.976	65.0
	Species II	1.942	164.9	1.977	64.9
(**2.2**)	Species I	1.937	177.4	1.976	65.1
	Species II	1.942	165.4	1.976	65.2

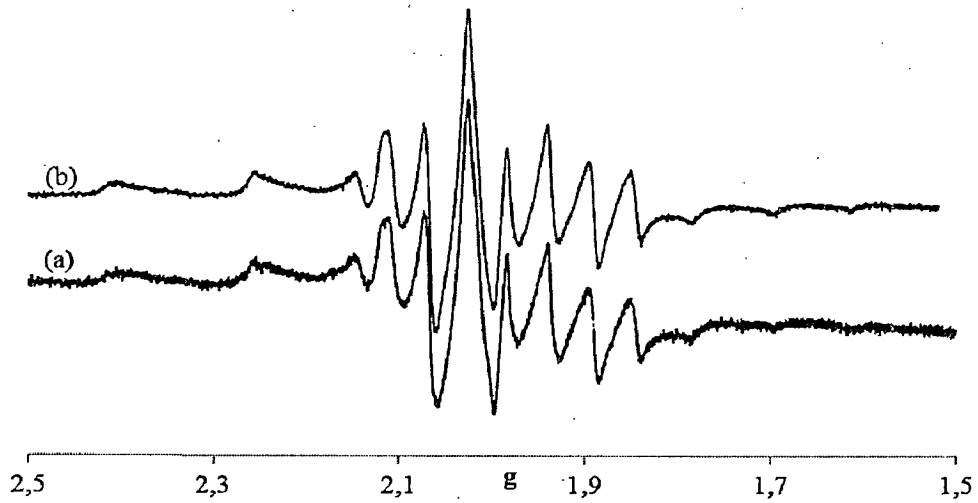

Figure 2.13. 1st derivative EPR spectra of frozen (77 K) solutions (ca. 4 mM) (a) $CH_2\{V^{IV}O(sal\text{-}sbdt)(H_2O)\}_2]$ (**2.1**) in DMSO (b) $CH_2\{V^{IV}O(sal\text{-}smdt)(H_2O)\}_2]$ (**2.2**) in DMSO. The solutions were frozen after ca. 15 min. of mixture of the solid and solvent.

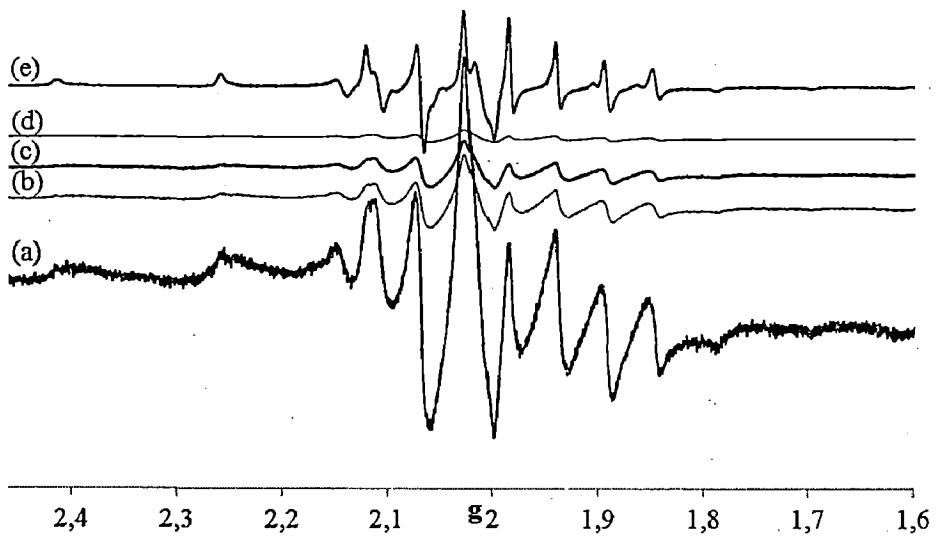

Figure 2.14. 1st derivative EPR spectra of 4 mM $[CH_2\{V^{IV}O(sal\text{-}sbdt)(H_2O)\}_2]$ (**2.1**) (a) in DMSO; (b) after addition of 1.0 equiv. of H_2O_2 [aqueous 30% solution] (c) after addition of a total of 2.0 equiv. of H_2O_2, (d) after addition of a total of 3.0 equiv. of H_2O_2 (e) after addition of a total of 10 equiv. of styrene to the solution of (d).

The EPR spectra thus indicate that upon dissolving **2.1** in DMSO, the V^{IV}-complex partly hydrolyses and oxidizes; in solution the binding set $(O_{phenolate}, N_{imine}, S_{thiolate}, O_{water})_{equatorial}$ is not detected by EPR for the $V^{IV}O$-complexes formed upon dissolution. The ^{51}V NMR spectrum of this solution depicts a resonance at δ = –463 ppm [Figure 2.15(a)]. The resonance at δ = –463 ppm is assigned to $[CH_2\{V^VO_2(sal\text{-}sbdt)(Sv)\}_2]^{2-}$ (**CII**, S = H_2O or DMSO Scheme 2.3). Typically the ^{51}V NMR spectra of the solutions of either complex **2.1** or **2.2** were measured after ca. 1 h of mixture of the solids with the solvent. Upon the stepwise addition of an aqueous 30% solution of H_2O_2 to the solution of **2.3** (in DMSO, ca. 4 mM), the resonance at –520 ppm shows up. It corresponds to the mono-peroxo species.

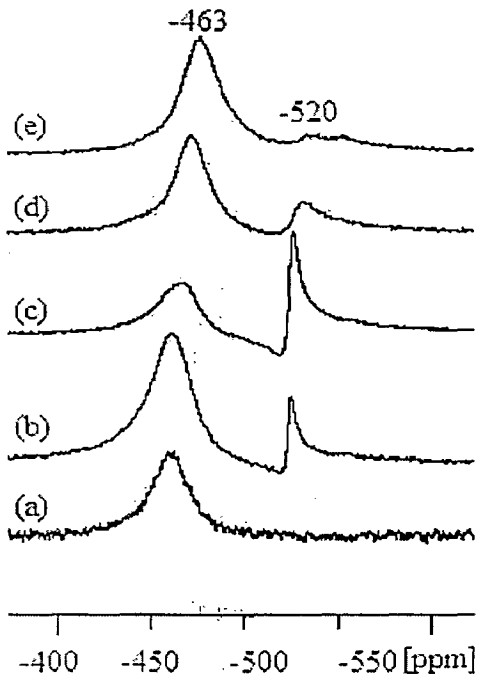

Figure 2.15. ^{51}V NMR spectra for solutions (ca. 4 mM) of complex $[CH_2\{V^{IV}O(sal\text{-}sbdt)(H_2O)\}_2]$ (**2.1**): (a) in DMSO and (b–d) after stepwise additions of an aqueous solution of 30% H_2O_2; (b) 1.0 equiv. H_2O_2 added; (c) 2 equiv. H_2O_2 (total) added; (d) 4.0 equiv. H_2O_2 (total) added; (e) solution of (d) after the addition of 10 equiv. of styrene.

Similar changes in the EPR and ^{51}V NMR spectra have also been observed for solutions of complex **2.2** (4 mM) in DMSO upon addition of H_2O_2. The spectra recorded are presented in Figures 2.16 and 2.17.

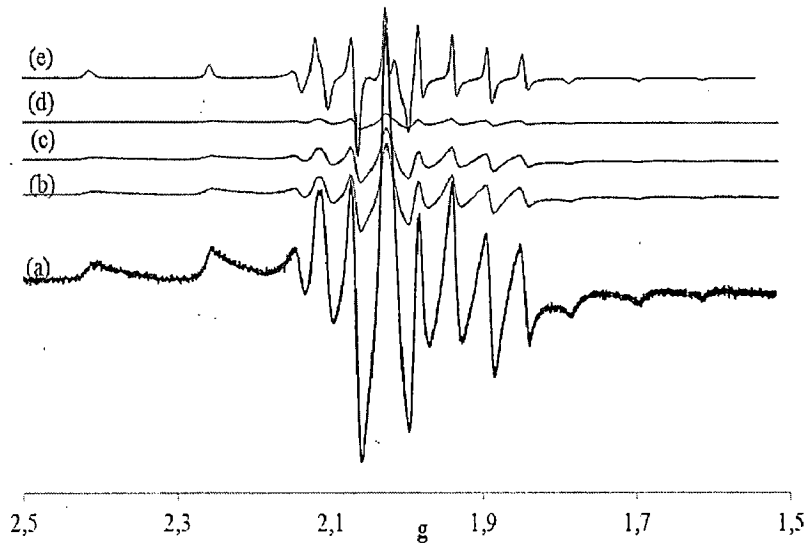

Figure 2.16. 1st derivative EPR spectra of 4 mM $[CH_2\{V^{IV}O(sal\text{-}smdt)(H_2O)\}_2]$ (**2.2**) (a) in DMSO; (b) after addition of 1.0 equiv. of H_2O_2 [aqueous 30% solution] (c) after addition of a total of 2.0 equiv. of H_2O_2, (d) after addition of a total of 3.0 equiv. of H_2O_2 (e) after addition of a total of 10.0 equiv. of styrene.

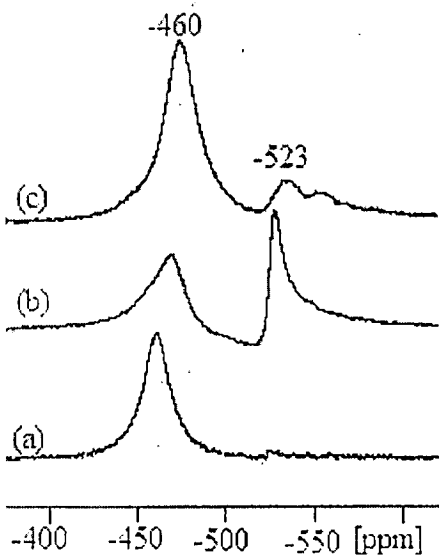

Figure 2.17. ^{51}V NMR spectra for solutions (ca. 4 mM) of $[CH_2\{V^{IV}O(sal\text{-}smdt)(H_2O)\}_2]$ (**2.1**): (a) in DMSO; (b) 3.0 equiv. H_2O_2 added; (c) solution of (b) after 10 equiv. of styrene addition.

The formation of peroxo complexes in methanol by treatment of **2.1** and **2.2** with H_2O_2 was also studied by electronic absorption spectroscopy. Thus, the addition of two drops of a dilute solution of H_2O_2 (3.21 g, 28.3 mmol of 30% aqueous H_2O_2 dissolved in 30 mL MeOH) to 20 mL of ca. 20 mL of 6.43×10^{-5} M methanolic solution of **2.1** and recording the spectra after every 15 min interval resulted in the spectral changes presented in Figure 2.18. The band at 417 nm slightly decreases in intensity, the λ_{max} slowly shifting to 400 nm. Simultaneously, the weak shoulder appearing at ca. 350 nm slowly sharpens with slightly gain in intensity. The band at 297 nm gains intensity while maintaining the position, and bands at 210 and 240 nm sharply gain intensity. The three d-d bands appearing at 575, 680 and 845 nm (in **2.1**) and at 565, 675 and 875 nm (in **2.2**) recorded with more concentrated solutions, slowly decrease their intensities and finally become non-distinguishable (Figure 2.19). Changes in the UV-Vis spectra similar to those presented here have been interpreted as involving the progressive oxidation of $V^{IV}O$-species followed by formation of oxidoperoxidovanadium(V) compound [128,142-145]. However, peroxo-to-vanadium charge transfer transitions have been reported at λ_{max} ca. 450 nm [54,146]. In the present systems, the electronic spectra of both complexes exhibit rather strong broad bands at *ca.* 410 nm, probably involving the C=N group [147-159] thus in the same range of the peroxo-to-vanadium charge transfer transition, making the detection of the latter band difficult. It is possible that the several processes taking place, namely formation of species **CV** and **CVI**, which decrease the contribution of the band involving the C=N group, precludes the observation of an increase in the absorption around 400-450 nm. Similar changes in the UV region of the absorption spectra of **2.2** could also be observed using lower concentrations.

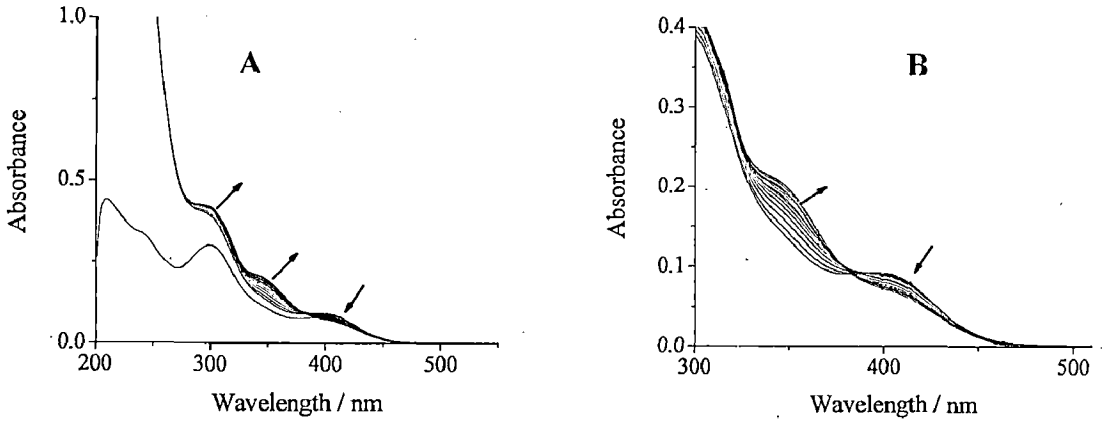

Figure 2.18. Spectral changes obtained after adding two drops of a dilute aqueous/MeOH solution of H_2O_2 (3.21 g, 28.3 mmol 30% aqueous H_2O_2 dissolved in 30 mL MeOH) to 20 mL of ca. of 6.43×10^{-5} M methanolic solution of $[CH_2\{V^{IV}O(sal\text{-}sbdt)(H_2O)\}_2]$ (**2.1**). The spectra were recorded at every 15 min. In **B** the expanded region of 300 to 500 nm is shown.

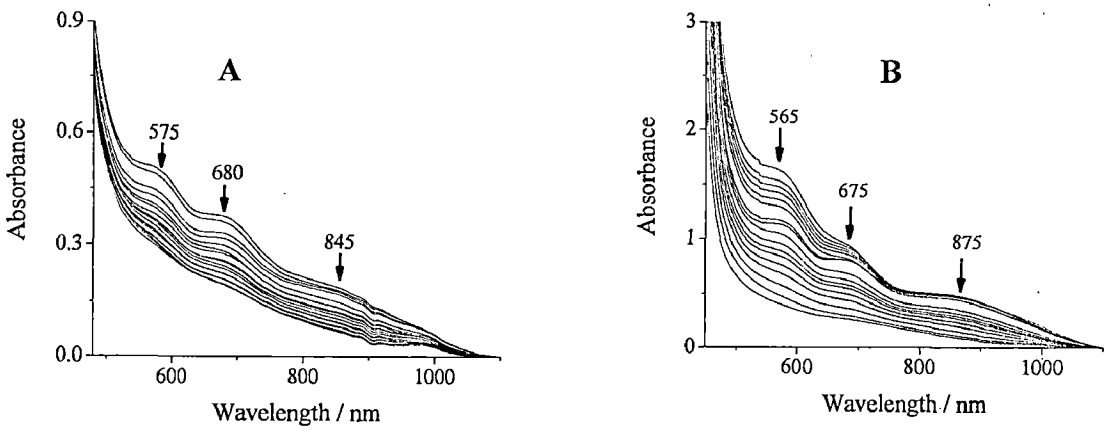

Figure 2.19. Spectral changes obtained during titration of (A) 20 mL of 5.76×10^{-3} M solution of $[CH_2\{V^{IV}O(sal\text{-}sbdt)(H_2O)\}_2]$ (**2.1**) in DMSO, (B) 20 mL of 8.76×10^{-3} M DMSO solution of $[CH_2\{V^{IV}O(sal\text{-}smdt)(H_2O)\}_2]$ (**2.2**), with a dilute solution of H_2O_2 (1.26 g, 11.1 mmol of 30% aqueous H_2O_2 in 5 mL DMSO). The spectra were recorded after the successive addition of 1-drop portions, at 2 min time intervals. The three d-d bands recorded progressively decrease their intensity as $V^{IV}O$-complexes are oxidized to V^{V}-species.

Reactivity of $Cs_2[CH_2\{V^VO_2(sal\text{-}sbdt)\}_2]\cdot 2H_2O$ (**2.4**) with H_2O_2 was also tested and spectral changes were monitored by electronic absorption spectroscopy. The spectral changes obtained upon adding successive one drop portions of an aqueous/MeOH solution of H_2O_2 (3.214 g, 28.36 mmol of 30% aqueous H_2O_2 dissolved in 30 mL MeOH) to a 20 mL solution of **2.4** (ca. 5.63×10^{-5} M in methanol) are presented in Figure 2.20. Considerable increase in the intensity of the 210 nm band and increase in the intensity of the 297 nm band was observed at the beginning, i.e. after addition of about 20 drops of H_2O_2, while the band at 410 nm remained nearly constant. On further addition of H_2O_2, the weak shoulder appearing at ca. 345 nm started to emerge, along with weakening of the band at ca. 410; nm, Figure 2.20.

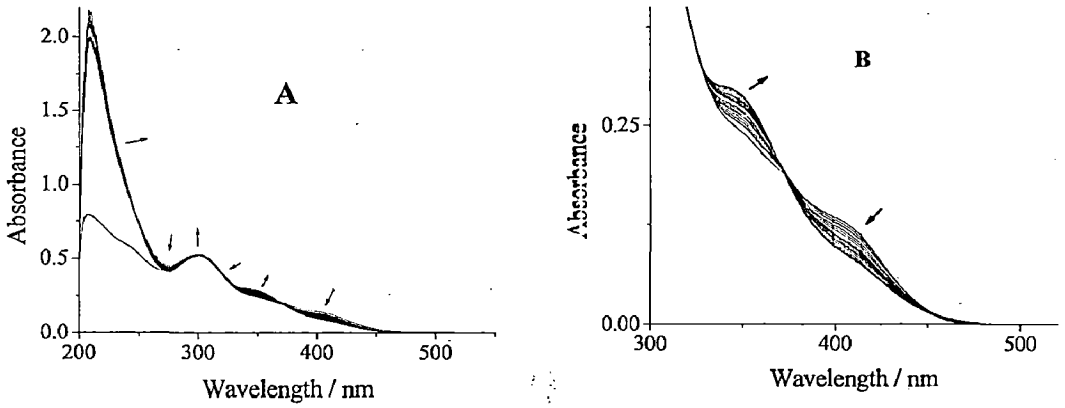

Figure 2.20. Spectral changes obtained after adding one drop of a dilute solution of 30% aqueous H_2O_2 (3.214 g, 28.36 mmol dissolved in 30 mL MeOH) to 20 mL of ca. 3.12×10^{-5} M methanolic solution of $Cs_2[CH_2\{V^VO_2(sal\text{-}sbdt)\}_2]\cdot 2H_2O$ (**2.4**). The spectra were recorded with 10 min intervals. In **B** the 300 – 500 nm range of **A** is expanded.

The behaviour of the methanolic solutions of the V^VO_2-complexes upon addition of HCl was also monitored by electronic absorption spectroscopy. Thus the drop-wise addition of HCl dissolved in methanol (3.9×10^{-3} M) to 20 mL of a

solution of $Cs_2[CH_2\{V^VO_2(sal\text{-}sbdt)\}_2]\cdot 2H_2O$ (**2.4**) (ca. 2.85×10^{-5} M) caused the darkening of the solution along with slow broadening of bands, with the spectral changes depicted in Figure 2.21. Very similar features were also similarly observed with solutions of **2.3**, **2.5** and **2.6**.

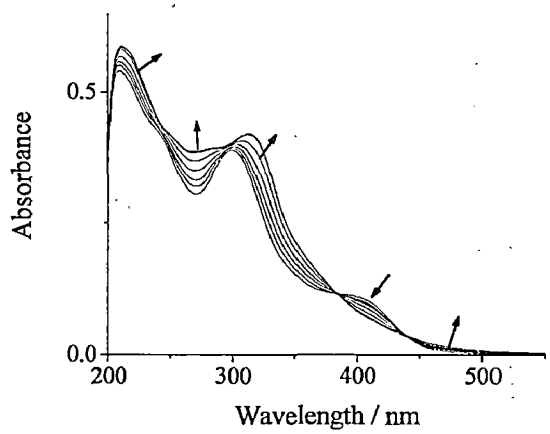

Figure 2.21. Spectral changes obtained during titration of 20 mL of a 2.85×10^{-5} M methanolic solution of $Cs_2[CH_2\{V^VO_2(sal\text{-}sbdt)\}_2]\cdot 2H_2O$ (**2.4**) upon drop wise additions of HCl dissolved in MeOH (3.9×10^{-3} M). Each spectrum was recorded upon successive additions of 1-drop portions.

As reported for other systems [52,53,54,146,150,151], besides the formation of V^{IV}-species, we interpret these results assuming the formation of oxidohydroxido species of composition $[CH_2\{V^VO(OH)(HL)\}_2]^{2+}$ via $[CH_2\{V^VO_2(HL)\}_2]$ and/or $[CH_2\{V^VO_2(OH)(HL)\}_2]$ (see Scheme 2.4). It is also possible that complexes $[CH_2\{VO_2(HL)(Sv)\}_2]$ might also form. Protonation of the hydrazone nitrogen has been reported, e.g. for the structurally characterized [VO(Hsal-bhz)] (H_2sal-bhz derives from salicylaldehyde and benzoylhydrazide), which forms upon treatment of the corresponding anionic dioxido complex with HCl [44]. EPR and ESEEM spectra recorded for [VO(salim)(acac)] (salim = a Schiff base ligand containing imidazole) upon addition of acid were explained by the protonation of the imine N-atom.[152] Very similar results were obtained for related binucleating ligands [52,53] involving a ONO binding set and interpreted similarly. Scheme 2.4 may be considered to summarize the processes taking place, with one of the =N–N= nitrogens being the site of protonation.

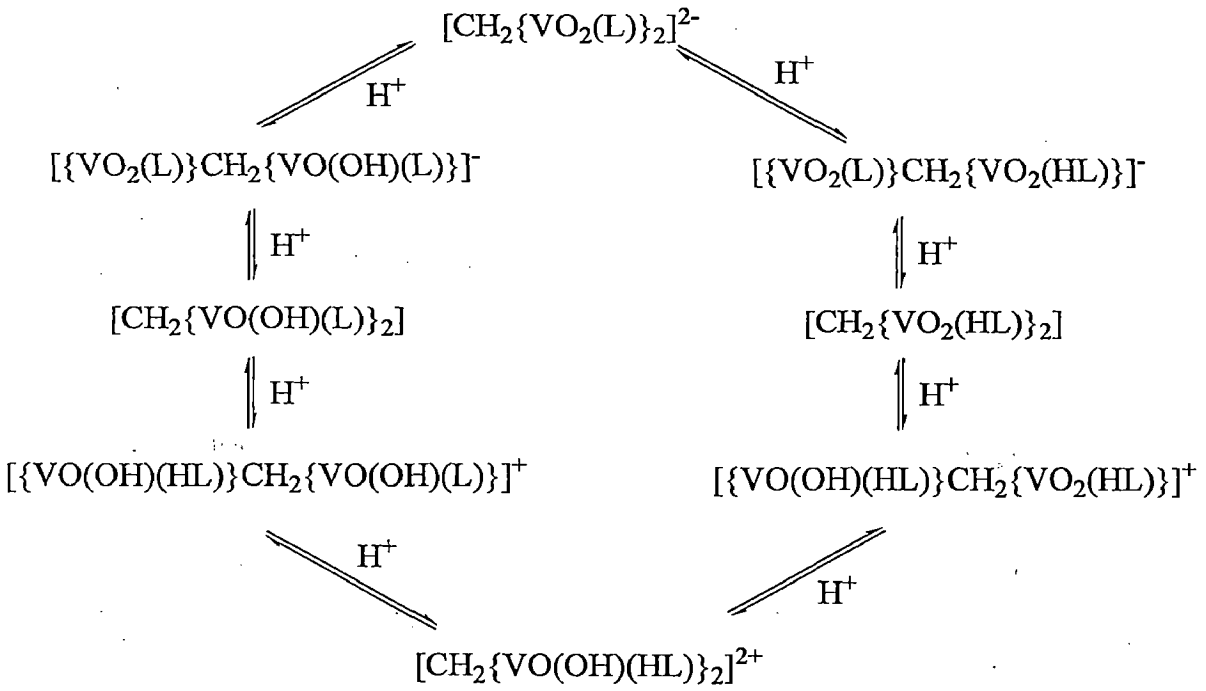

Scheme 2.4. Formation of $[CH_2\{V^VO(OH)(HL)\}_2]^{2+}$ by successive protonations starting with complexes $[CH_2\{V^VO_2(L)\}_2]^{2-}$. All included species are in equilibria. Each $V^VO_2(L)$, $V^VO_2(HL)$, $V^VO(OH)(L)$ and $V^VO(OH)(HL)$ core will probably correspond to a different chemical shift in the ^{51}V NMR spectra.

2.3.8. Oxidative bromination of styrene

Oxidative bromination of styrene under a two-phase system, using $Cs_2[CH_2\{VO^V(sal\text{-}sbdt)\}_2]\cdot 2H_2O$ and $Cs_2[CH_2\{VO^V(sal\text{-}smdt)\}_2]\cdot 2H_2O$ as catalyst precursors in the presence of KBr, $HClO_4$ and H_2O_2 gave mainly three products namely, (a) 1,2-dibromo-1-phenylethane, (b) 2-bromo-1-phenylethane-1-ol and (c) 1-phenylethane-1,2-diol; Scheme 2.5. Some minor products (benzaldehyde, styrene epoxide, benzoic acid and 4-bromostyrene) have also been detected but their overall percentage is ca. 7 of the total of the main products. The obtained products are the same as those reported by Conte *et al.* [111,112]. Addition of $HClO_4$ in four equal portions was required to obtain better oxidative bromination. All products were separated/ isolated by column chromatography and the content of each fraction was confirmed by ^1H NMR as well as GC-MS.

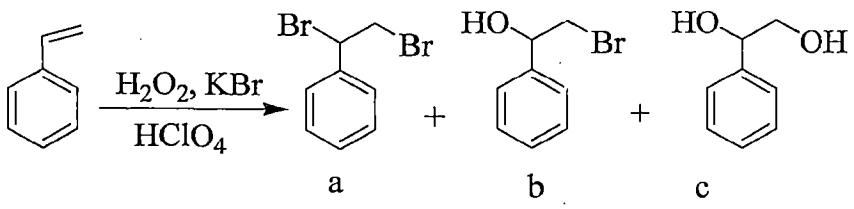

Scheme 2.5. Main products obtained by oxidative bromination of styrene. (a) 1,2-dibromo-1-phenylethane (dibromide), (b) 2-bromo-1-phenylethane-1-ol (a bromohydrin) and (c) 1-phenylethane-1,2-diol.

The following parameters were studied to optimize the reaction conditions for the maximum oxidative bromination of styrene taking $Cs_2[CH_2\{VO^V(sal\text{-}smdt)\}_2]\cdot 2H_2O$ (**2.6**) as catalyst precursor: (i) Catalyst amount, (ii) Oxidant amount and (iii) Catalyst precursor.

Three different amounts of **2.6**: 0.0010, 0.0020 and 0.0030 g of catalyst precursor were used while keeping the fixed amount of styrene (1.04 g, 10 mmol), KBr (4.76 g, 40 mmol), 30 % H_2O_2 (6.81 g, 60 mmol), aqueous 70 % $HClO_4$ (5.72 g, 40 mmol) in a 40 mL CH_2Cl_2–water (50% v/v) mixture at room temperature. As presented in Figure 2.22, a maximum of 99 % conversion was obtained after 1 h of reaction with 0.0010 g catalyst precursor, and 0.0020 and 0.0030 g of catalyst precursor gave nearly the same conversion. Therefore, 0.0010 g of **2.6** was set as optimum. Additions of $HClO_4$ were made in four portions, one immediately after the catalyst precursor (reaction time = 0), and the three other portions with 15 min. intervals.

To optimize the amount of $HClO_4$, three different amounts of 70% $HClO_4$ were used for a fixed amount of styrene (1.04 g, 10 mmol), amount of catalyst precursor (0.0010 g), KBr (4.76 g, 40 mmol), 30 % H_2O_2 (6.81 g, 60 mmol) and CH_2Cl_2-H_2O (40 mL, 50% v/v) at room temperature for 1 h. Increasing the perchloric acid amount from 1.43 g (10 mmol) to 2.86 g (20 mmol), increased the conversion from 61 % to 99 %. Only slight improvement in conversion was obtained on further increasing this amount to 4.29 g (30 mmol). Therefore, a 2.86 g of 70% $HClO_4$ was considered the more adequate one (Figure 2.23), making additions in four equal portions.

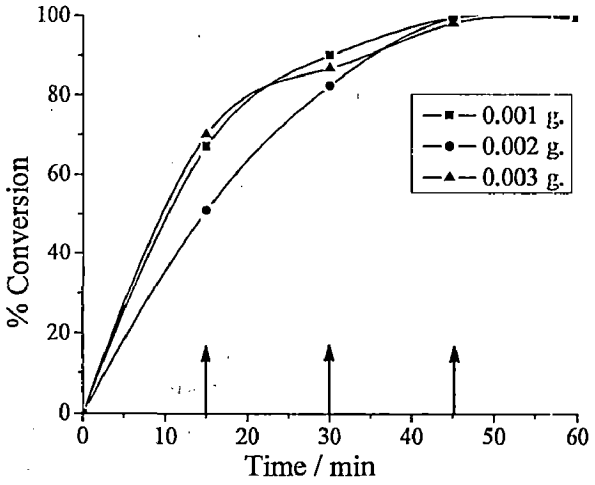

Figure 2.22. Effect of catalyst amount in oxidative bromination of styrene. Reaction conditions: styrene (1.04 g, 10 mmol), amount of catalyst precursor (0.0010 g, 0.0020 g or 0.0030 g), KBr (4.76 g, 40 mmol), aqueous 30 % H_2O_2 (6.81 g, 60 mmol), 70 % $HClO_4$ (5.72 g, 40 mmol, added in four equal portions at t = 0, 15, 30 and 45 min. of reaction time (marked with arrows in the figure), and CH_2Cl_2-H_2O (40 mL, 50% v/v) at room temperature for 1 h.

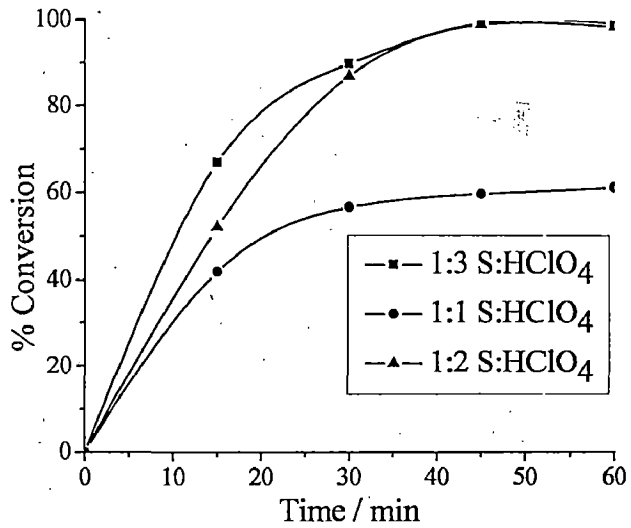

Figure 2.23. Effect of perchloric acid amount, added in four equal portions in 15 min. intervals, in the oxidative bromination of styrene.

The effect of amount of H_2O_2, added as an aqueous 30% H_2O_2 solution, was studied considering substrate to oxidant ratios of 1 : 2, 1 : 3, 1 : 4 and 1 : 5 for a fixed amount of styrene (1.04 g, 10 mmol), amount of catalyst precursor (0.0010 g), KBr (4.76 g, 40 mmol) and $HClO_4$ (2.86 g, 20 mmol) in CH_2Cl_2-H_2O (40 mL, 50% v/v), and the reaction was monitored at room temperature for 1 h. The conversion increases on increasing the substrate to oxidant ratio and 1:3 ratio is sufficient to convert 98 % styrene. Increasing this ratio further did not improve the final conversion, except to complete the reaction in a shorter time (ca. 50 min, Figure 2.24).

Similarly, three different substrate to KBr ratios were used. Increasing the amount of KBr from 1:2 to 1:3, the obtained conversion increases from ca. 84 % to 99 %, but further increment of the KBr amount gave almost the same conversion (Figure 2.25).

Table 2.8 summarizes all conditions applied to optimize the reaction conditions for the maximum oxidative bromination of styrene considering **2.6** as catalyst precursor. Entry no. 10 of this table presents the optimized reaction conditions which are: styrene (1.04 g, 10 mmol), amount of catalyst precursor (0.0010 g), 30 % aqueous H_2O_2 (3.40 g, 30 mmol), 3.56 g (30 mmol) of KBr, $HClO_4$ (2.86 g, 20 mmol) added in four equal portions in 15 min. intervals, and CH_2Cl_2-H_2O (40 mL, 50% v/v) at room temperature for 1 h.

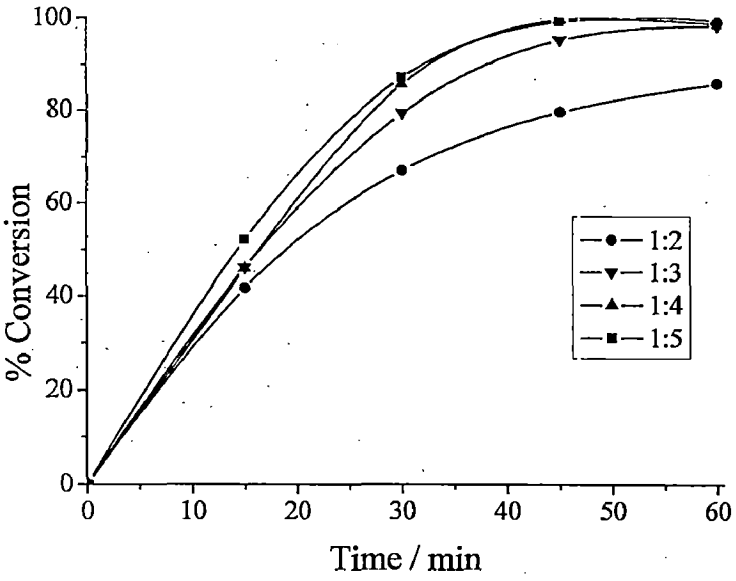

Figure 2.24. Effect of the H_2O_2 amount in the oxidative bromination of styrene.

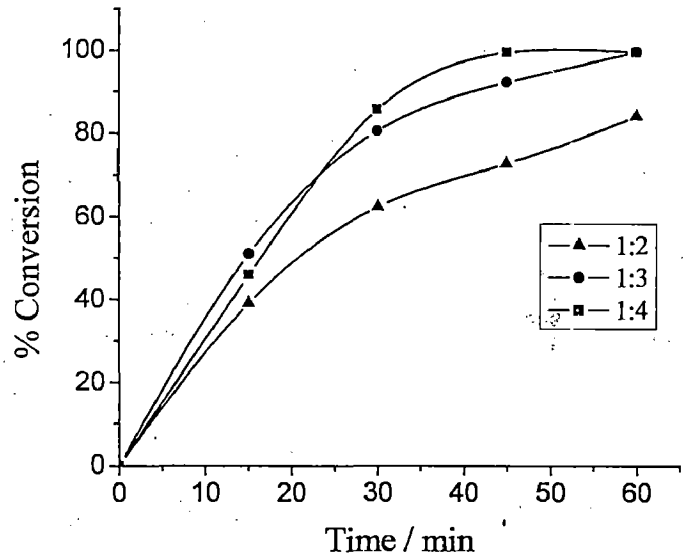

Figure 2.25. Effect of KBr amount in the oxidative bromination of styrene. Other conditions for plots (b), (c) and (d) see text.

Table 2.8. Results of oxidative bromination of styrene using $Cs_2[CH_2\{VO_2{}^V(sal\text{-}smdt)\}_2]\cdot 2H_2O$ (**2.6**) as catalyst precursor. Conversion obtained after 1 h.

SL. No.	Styrene	KBr	H_2O_2	$HClO_4$	Catalyst	Solvent (DCM/H_2O)	% Conversion
1.	1.04 g (10 mmol)	4.76 g (40 mmol)	5.67 g (50 mmol)	4.29 g (30 mmol)	0.001 g	20/20	99
2	1.04 g (10 mmol)	4.76 g (40 mmol)	5.67 g (50 mmol)	4.29 g (30 mmol)	0.002 g	20/20	99
3	1.04 g (10 mmol)	4.76 g (40 mmol)	5.67 g (50 mmol)	4.29 g (30 mmol)	0.003 g	20/20	99
4	1.04 g (10 mmol)	4.76 g (40 mmol)	5.67 g (50 mmol)	1.43 g (10 mmol)	0.001 g	20/20	61
5	1.04 g (10 mmol)	4.76 g (40 mmol)	5.67 g (50 mmol)	2.86 g (20 mmol)	0.001 g	20/20	98
6	1.04 g (10 mmol)	4.76 g (40 mmol)	2.27 g. (20 mmol)	2.86 g (20 mmol)	0.001 g	20/20	86
7	1.04 g (10 mmol)	4.76 g (40 mmol)	3.405 g (30 mmol)	2.86 g (20 mmol)	0.001 g	20/20	99
8	1.04 g (10 mmol)	4.76 g (40 mmol)	4.54 g (40 mmol)	2.86 g (20 mmol)	0.001 g	20/20	98
9	1.04 g (10 mmol)	2.38 g (20 mmol)	3.405 g (30 mmol)	2.86 g (20 mmol)	0.001 g	20/20	84
10	1.04 g (10 mmol)	3.56 g (30 mmol)	3.405 g (30 mmol)	2.86 g (20 mmol)	0.001 g	20/20	99

Figure 2.26 represents the consumption of styrene and the selectivity of the formation of major products with time for these experimental conditions. The formation of all three products starts with the consumption of styrene. However, among the three products formed, the selectivity of 1-phenylethane-1,2-diol reaches 75 % at the end of 1 h, while that of 1,2-dibromo-1-phenylethane is only 6 %. The selectivity of the formation of 2-bromo-1-phenylethane-1-ol (bromohydrin) initially increases, reaching ca. 23 %, and after ca. 40 min. of reaction decreases, being ca. 18 % at the end of 1 h. Increasing the reaction time beyond 1 h increases the formation of the dibromide, but decreases that of the

bromohydrin, while 1-phenylethane-1,2-diol remains almost constant. It should be noted here that for the catalytic oxidation of styrene the experimental conditions were set up for maximum conversion of styrene, and the product obtained in higher relative amount was 1-phenylethane-1,2-diol, not the bromohydrin.

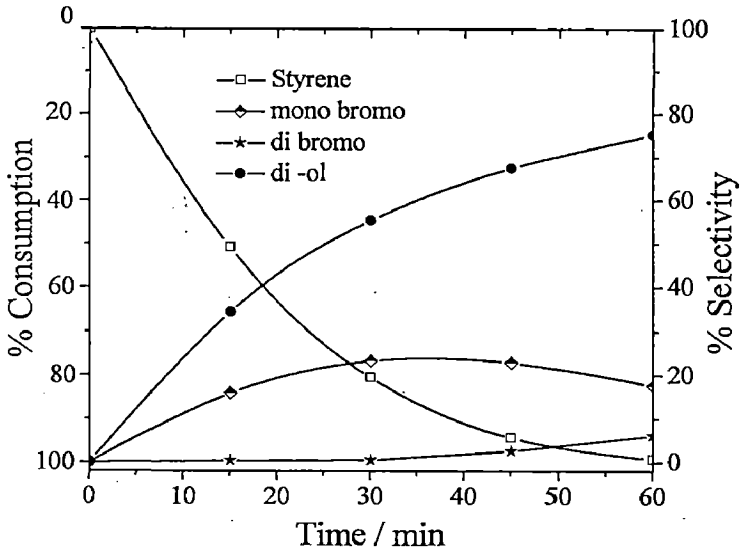

Figure 2.26. Percentage consumption of styrene and selectivity of the formation of products with time using $Cs_2[CH_2\{VO^V(sal\text{-}smdt)\}_2]\cdot 2H_2O$ (**2.6**) as catalyst precursor and the optimized conditions specified in the text.

We have also obtained oxidative bromination of styrene using mononuclear complexes $K[V^VO_2(sal\text{-}sbdt)(H_2O)]$ (**2.7**) and $Na[V^VO_2(sal\text{-}smdt)(H_2O)_2]$ (**2.8**) using 0.0010 g of each under the above optimized conditions. Conversions obtained after 1 h of reaction time are 98 and 97 %, respectively. Taking 0.0010 g of mononuclear complexes approximately corresponds to the same number of moles of metal centres as for binuclear complexes; hence their catalytic potential is almost the same as that of the binuclear complexes.

2.3.9. Mechanism of oxidative bromination

The mode of action of V-dependent bromoperoxidase enzymes (V-BrPOs) has received much attention [56,111,112,146,153-157]. The accepted mode of action of V-BrPOs involves the presence of vanadium in their active sites, this

metal in the presence of hydrogen peroxide forms a peroxido vanadium derivative which oxidizes a bromide ion, thus forming a bromine equivalent intermediate. Such an intermediate may then either brominate an appropriate organic substrate or react with another molecule of Br^- to form bromine. The role of the V^V ion is to serve as a strong Lewis acid in the activation of the primary oxidant, H_2O_2.

The suggestion that the high efficacy of this process is related to the formation of the intermediate, the bromination reaction occurring in two different compartments of the enzymes, the first step in a hydrophilic region of the protein and the second in a hydrophobic region, has led to model the reaction by the development of two-phase systems [111]: (i) the vanadium precursor, H_2O_2 and KBr are dissolved in water, where the formation of a peroxido V^V derivative and the oxidation of Br^- take place forming an intermediate; (ii) this intermediate is then transferred to the organic phase, a chlorinated solvent i.e. $CHCl_3$ or CH_2Cl_2, where the bromination of the substrate takes place. The processes occurring in the aqueous phase require acidic conditions, probably to promote the protonation of the peroxido moiety.

From the mechanistic point of view, there have been several attempts to elucidate the reaction pathways involving the oxybromination reactions, by combining reactivity analysis with e.g. spectroscopic techniques, mainly ^{51}V NMR, and theoretical calculations [111,155-157]. A mechanistic proposal [111,155-157] included two intermediates, a vanadium bound hypobromite ion, responsible for the formation of the bromohydrin, and the second one, bromine, which is responsible for the formation of the dibromo products. Both pathways start from a hypobromite-like vanadium intermediate, formed in the reaction between the monoperoxido vanadium complex and Br^-. However, direct evidence on the formation of either the hydroperoxido or the hypobromite-type vanadium intermediates, has not yet been obtained, although the involvement of a V^V-containing brominating species has been confirmed in the two-phase reaction with

adamantylideneadamantane, where a salt containing the bromiranium cation, together with the vanadate anion, was isolated and characterized [158].

The catalytic oxidative bromination of styrene described in this study also follows the approach of using a two phase system. In our systems we believe we have been able to identify the monoperoxido complexes **CV** and **CVI** (Scheme 2.3), which probably act as the oxidant of the Br^- ion. Thus, during oxidation vanadium in complexes **2.3 – 2.6** may coordinate with H_2O_2 forming V^V-oxidomonoperoxido species, e.g. **CV** (and **CVI**), Scheme 3. In acidic conditions oxidohydroxido complexes may form, such as **CIV**, and in the presence of H_2O_2 **CVI** may also form. By adding KBr to these solutions, a new ^{51}V NMR resonance appears at –586 ppm, Figure 2.27. We suggest that this resonance may correspond to species **CVII** (with a vanadium bound hypobromite ion), or to a similar species including donor atoms of the ligand also bound to V^V. This species **CVII** may be responsible for the formation of the bromohydrin. Accordingly, the hypobromite-like species formed would be directly involved in the "Br^+" transfer process or, at least, it is one of the active species in the bromination process [111,154].

The occurrence, during the catalytic cycle, of a species where the equatorial peroxido oxygen is protonated and the Br^- is prone to interact with the other peroxidic oxygen has been proposed [155], weak interactions between Br^- and V^V being also plausible prior to the oxo-transfer step [155]. In e.g. the VHPO of the fungus *Curvularia inaequalis*, a lysine side chain (from Lys353) also helps in the polarization of the V-bound peroxido moiety, and tunes its reactivity [155]. It is possible that in **CV** and/or **CVI** a similar type of effect may operate, but the data available does not allow discussing this further.

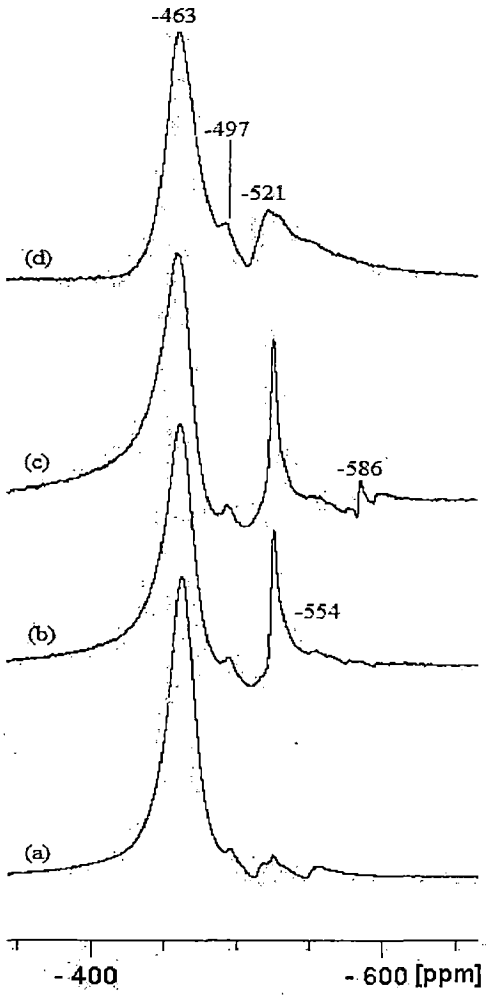

Figure 2.27. ^{51}V NMR spectra for solutions (ca. 4 mM) of $Cs_2[CH_2\{V^VO_2(sal\text{-}sbdt)\}_2]\cdot 2H_2O$ (**2.4**): (a) in DMSO; (b) 4.0 equiv. of H_2O_2 [added as an aqueous solution of 30% H_2O_2]; (c) 5 equiv. KBr (total) added to the solution of (b); (d) solution of (c) after 24 h leaving the tube open.

2.4. Conclusions

The hydrazones $CH_2(H_2sal\text{-}sbdt)_2$ (**2.I**) and $CH_2(H_2sal\text{-}smdt)_2$ (**2.II**) derived from 5,5'-methylenebis(salicylaldehyde) [$CH_2(Hsal)_2$] and S-benzyldithiocarbazate $CH_2(Hsal\text{-}sbdt)_2$ **2.I**, or S-methydithiocarbazate $CH_2(Hsal\text{-}smdt)_2$ **2.II**, and their $V^{IV}O$- and $V^{V}O_2$-complexes were synthesized and characterized. The complexes are binuclear in the solid state and in solution, but no significant interactions were detected between the vanadium centres.

Solutions of the $V^{IV}O$-complexes $CH_2\{V^{IV}O(L)\}_2 \cdot 2H_2O$ [$CH_2(HL)_2$= **2.I** (**2.1**) and **2.II** (**2.2**)] were studied by UV/Vis, EPR and ^{51}V NMR spectroscopy, and also by adding H_2O_2 or acid (HCl). The speciation of solutions of the V^{V}-complexes in MeOH and DMSO was also studied by the same spectroscopic techniques. The formation of several species was established, some of them probably being intermediates in the catalytic processes studied, namely $[CH_2\{V^{V}O(O_2)(L)\}_2]^{2-}$ and $[CH_2\{V^{V}O(OH)(L)\}_2]$. On addition of acid (HCl) the V^{V} species present are partly reduced/hydrolysed, yielding several species, namely the oxidohydroxido complex.

The $V^{V}O_2$-complexes **2.3**-**2.6** were shown to be functional models of vanadium-dependent haloperoxidases, satisfactorily catalyzing the oxidative bromination of styrene. Plausible intermediates involved in the catalytic process were established by UV-Vis, EPR and ^{51}V NMR studies, namely monoperoxido-V^{V}-complexes. A ^{51}V NMR peak detected at –586 ppm was assigned as probably being due to a V^{V}-complex containing coordinated hypobromite ion.

Chapter-3

- Effect of coordination sites on vanadium complexes having $[VO]^{2+}$, $[VO]^{3+}$ and $[VO_2]^{+}$ cores with hydrazones of 2,6-diformyl-4-methylphenol: Synthesis, characterization, reactivity, and catalytic potential

Effect of coordination sites on vanadium complexes having $[VO]^{2+}$, $[VO]^{3+}$ and $[VO_2]^{+}$ cores with hydrazones of 2,6-diformyl-4-methylphenol: Synthesis, characterization, reactivity, and catalytic potential

3.1. Introduction

The coordination chemistry of vanadium complexes with multidentate ligands has received considerable interest over the past two decades due to the design of structural models of vanadate-dependent haloperoxidases (VHPO) enzymes [34-36, 46,117-119,121,122,159,160] and the catalytic potential of several model vanadium complexes in the oxidation and oxygen-transfer reactions, including the oxidative halogenation of organic substrates and oxidation of organic sulfides [32,33,112-116].

Phenol-based polynucleating ligands, with particular emphasis on ligands derived from 2,6-diformyl-4-methylphenol have attracted a great number of researchers because such class of ligands are able to simultaneously bind two or more metal ions thus forming bi- or polynuclear metal complexes [161]. The binuclear metal complexes normally allow the understanding of the basic metal–metal interactions if they are in close proximity while polynuclear complexes may constitute supramolecular assembly through intermolecular hydrogen bonding if suitable electronegative atoms are present on the ligand.

Mondal et al. have reported phenoxide bridged binuclear ($V^{IV}V^{V}$) complexes of general formula $[V_2O_3L]$ with binucleating, 2,6-bis[{{(2-hydroxybenzyl)(N',N'-(dimethylamino)ethyl)}amino}methyl]-4-methylphenol (H_3L) and related ligands. Each unit has distorted octahedral geometry with two terminal V=O groups trans to each other where the mixed-valence complex contains two indistinguishable vanadium atoms and is the only characterized complex of H_3L amongst six such complexes reported [162].

Recently we observed that the binucleating ligand, benzoylhydrazone of 5,5-methylenebis(salicylaldehyde) [$CH_2(H_2$sal-bhz)] forms binuclear dioxidovanadium(V) complex $Cs_2[CH_2\{V^{V}O_2(\text{sal-bhz})\}_2]\cdot 2H_2O$ but the two units do not interact to each other. However, the cluster formed by the oxygen atoms

and Cs^+ ions along with $\square^2$-cation lateral π-interaction with two carbon atoms of the phenyl ring produces supramolecular assembly [53].

In continuation of our efforts on the development of vanadium chemistry with binucleating ligands [52,163], we have now prepared and characterized oxidovanadium(IV), oxidovanadium(V), dioxovanadium(V), and oxidoperoxidovanadium(V) complexes of hydrazones of 2,6-diformyl-4-methylphenol (Scheme 3.1). Designs of these ligands are such that they can result in the formation of mononuclear, dinuclear or polynuclear complexes depending up on the non-participation or coordination of additional atom present on the ligand. In addition, the additional coordinating atom(s) may or may not participate in coordination with the same metal. Novel structural features and the reactivity patterns of the complexes reported here also present model character for VHPO. The catalytic potential of V^VO_2-complexes as mimics for the oxidative bromination activity of VHPO by peroxide has also been studied.

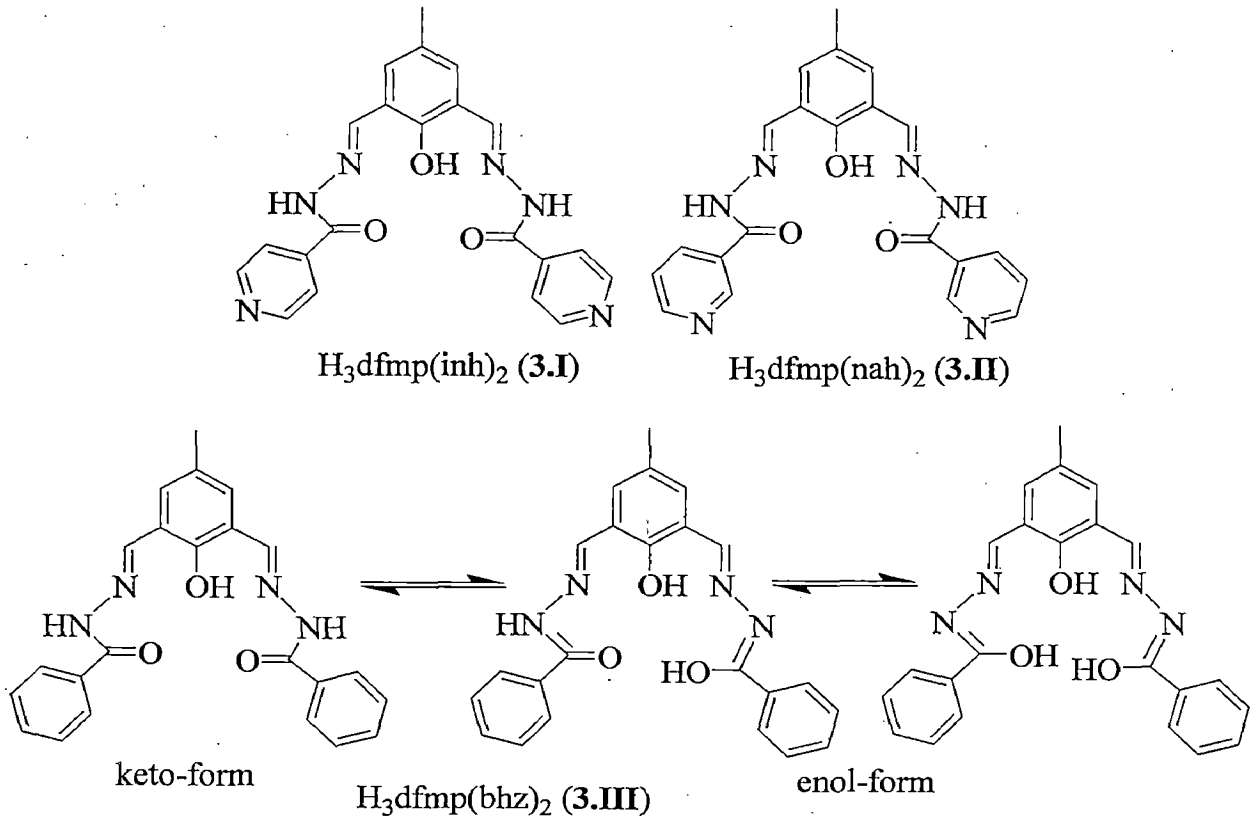

Scheme 3.1. Structure of ligands designated by **3.I**, **3.II** and **3.III** used in this work. Tautomerism shown for **3.III** only.

3.2. Experimental Section

3.2.1. Materials

Analytical reagent grade V_2O_5, ethyl benzoate, hydrazine hydrate, isonicotinic acid hydrazide, (Loba Chemie, Mumbai, India), styrene, nicotinic acid hydrazide (Acros organics, New Jersey, USA), acetylacetone (Aldrich Chemicals Co., U.S.A), 30 % aqueous H_2O_2 and 70 % $HClO_4$ (Rankem, New Delhi, India) were used as obtained. Other chemicals and solvents were of analytical reagent grade. $[V^{IV}O(acac)_2]$ [164] and 2,6-diformyl-4-methylphenol [165] were prepared according to methods reported in the literature. Benzoyl hydrazide was prepared by the reaction of a two fold excess of hydrazine hydrate with ethyl benzoate in ethanol.

3.2.2. Instrumentation and Characterization Procedures

Instrumentation details are presented in Chapter 2. A Shimadzu 2010 plus gas-chromatograph with a Rtx-1 capillary column (30 m × 0.25 mm × 0.25 μm) was used to analyze the reaction products. The identity of the products was confirmed using GC–MS, model Perkin-Elmer Clarus 500 by comparing the fragments of each product with the library that was available. All theoretical calculations were performed using Gaussian 09 package. The geometry optimization of the ligand was carried out with B3LYP functional using 6-311g basis set for all the atoms.

3.2.3. Preparations

3.2.3.1 H_3dfmp(inh)$_2$ (3.I)

A solution of isonicotinic acid hydrazide (8.238 g, 60 mmol) in methanol (80 mL) was added to a filtered solution of 2,6-diformyl-4-methylphenol (4.920 g, 30 mmol) in methanol (30 mL) with stirring. The obtained reaction mixture was refluxed on a water bath for 2 h. After reducing the solvent volume to ca. 20 mL, the flask was kept at room temperature for ca. 10 h. The separated light yellow solid of **3.I** was filtered, washed with methanol (2 × 5 mL) followed by petroleum ether and dried over silica gel under vacuum. Yield 11.87 g (98.3%). Anal. calcd.

for $C_{21}H_{18}N_6O_3$ (402.41): C, 62.68; H, 4.51; N, 20.88 %. Found: C, 62.47; H, 4.87; N, 20.52%.

3.2.3.2. H_3dfmp(nah)$_2$ (3.II) and H_3dfmp(bhz)$_2$ (3.III)

These ligands were synthesized by following the procedure outlined for **3.I.**

H_3dfmp(nah)$_2$ (3.II): Yield 11.52 g (95.4%). Anal. calcd. for $C_{21}H_{18}N_6O_3$ (402.41): C, 62.68; H, 4.51; N, 20.88 %. Found: C, 62.89; H, 4.35; N, 20.52%.

H_3dfmp(bhz)$_2$ (3.III): Yield 11.23 g (93.5%). Anal. calcd. for $C_{23}H_{20}N_4O_3$ (400.44): C, 68.99; H, 5.03; N, 13.99 %. Found: C, 68.80; H, 5.27; N, 13.62%.

3.2.3.3. [V^{IV}O{Hdfmp(inh)$_2$}] (3.1)

A solution of H_3dfmp-inh (**3.I**) (0.402 g, 1 mmol) was prepared in absolute methanol (20 mL) by heating and filtered. A solution of [V^{IV}O(acac)$_2$] (0.265 g, 1 mmol) prepared in methanol (15 mL) was added to the above solution with stirring where orange solid started to precipitate immediately. After 1 h of stirring the solid was filtered, washed with methanol followed by petrolium ether (b.p. 60 °C) and dried in a desiccator over silica gel. Yield 0.447 g (95.7 %). Anal. calcd. for $C_{21}H_{16}N_6O_4V$ (467.34): C, 53.97; H, 3.45; N, 17.98 %. Found: C, 53.53; H, 3.57; N, 17.52%.

3.2.3.4. [V^{IV}O{Hdfmp(nah)$_2$}] (3.2) and [V^{IV}O{Hdfmp(bhz)$_2$}] (3.3)

Complexes **3.2** and **3.3** were prepared similarly by reacting [V^{IV}O(acac)$_2$] (0.265 g, 1 mmol) with ligands **3.II** (0.402 g, 1 mmol) and **3.III** (0.400 g, 1 mmol), respectively.

3.2. Yield 0.419 g (89.7 %). Anal. calcd. for $C_{21}H_{16}N_6O_4V$ (467.34): C, 53.97; H, 3.45; N, 17.98 %. Found: C, 53.73; H, 3.60; N, 17.71%.

3.3. Yield 0.431 g (92.6 %). Anal. calcd. for $C_{23}H_{18}N_4O_4V$ (465.36): C, 59.35; H, 3.90; N, 12.04 %. Found: C, 59.19; H, 4.07; N, 11.82%.

3.2.3.5. $[V^{V}O(OMe)(MeOH)\{Hdfmp(inh)_2\}]$ (3.4)

Complex **3.1** (0.234 g, 0.5 mmol) was dissolved in 50 mL of methanol while heating and filtered. The clear solution was allowed to stand for slow evaporation in open air where upon dark brown crystals of **3.4** slowly separated out within ca. 2 weeks. These crystals were filtered off, washed with methanol and dried in a desiccator over silica gel. Yield 0.198 g (75 %). Anal. calcd. for $C_{23}H_{23}N_6O_6V$ (530): C, 52.08; H, 4.37; N, 15.84 %. Found: C, 52.19; H, 4.26; N, 15.52%.

3.2.3.6. $[V^{V}O(OMe)(MeOH)\{Hdfmp(nah)_2\}]$ (3.5) and $[V^{V}O(OMe)(MeOH)$-$\{Hdfmp(bhz)_2\}]$ (3.6)

Complexes **3.5** and **3.6** were isolated similarly by dissolving $[V^{IV}O\{Hdfmp(nah)_2\}]$ (**3.2**) and $[V^{IV}O\{Hdfmp(bhz)_2\}]$ (**3.3**) (0.5 mmol each) in methanol (50 mL) and crystallized as mentioned for **3.4**.

3.5. Yield 0.174 g (66 %). Anal. calcd. for $C_{23}H_{23}N_6O_6V$ (530): C, 52.08; H, 4.37; N, 15.84 %. Found: C, 52.31; H, 4.54; N, 15.73%.

3.6. Yield 0.175 g (66 %). Anal. calcd. for $C_{25}H_{25}N_4O_6V$ (528): C, 56.82; H, 4.77; N, 10.60 %. Found: C, 57.01; H, 4.42; N, 10.52%.

3.2.3.7. $[V^{V}O_2\{H_2dfmp(inh)_2\}]$ (3.7)

Vanadium(V) oxide (0.182 g, 0.001 mol) was suspended in aqueous KOH (0.112 g, 2 mmol in 5 mL H_2O) and stirred for 2 h with occasional heating at 50 °C. The resulting solution was filtered. A filtered solution of **3.I** (0.804 g, 2 mmol), dissolved in 50 mL of aqueous KOH (0.224 g, 4 mmol), was added to the above solution with stirring, and the pH of the reaction mixture was slowly adjusted to *ca.* 7.5 with 4 M HCl. The yellowish-orange solid of **3.4** started to separate and after initial stirring for 2 h the resulting reaction mixture kept undisturbed. Within 2-3 days the brown-red X-ray quality crystals that had separated was filtered, washed with cold methanol (2×5 mL) and dried in a desiccator over silica gel. Yield 0.580 g (60 %). Anal. calcd. for $C_{21}H_{17}N_6O_5V$ (484): C, 52.08; H, 3.54; N, 17.35 %. Found: C, 52.29; H, 3.77; N, 17.52%.

3.2.3.8. $K[V^{V}O_2\{Hdfmp(nah)_2\}]$ (3.8) and $K[V^{V}O_2\{Hdfmp(bhz)_2\}]$ (3.9)

Complexes **3.8** and **3.9** were prepared analogously to **3.7**, taking H_3dfmp(nah)$_2$ (**3.II**) and H_3dfmp(bhz)$_2$ (**3.III**) in place of H_3dfmp(inh)$_2$ (**3.I**).

3.8. Yield 0.514 g (49 %). Anal. calcd. for $C_{21}H_{16}N_6O_5KV$ (522): C, 48.28; H, 3.09; N, 16.09 %. Found: C, 48.49; H, 3.17; N, 16.00%.

3.9. Yield 0.532 g (51 %). Anal. calcd. for $C_{23}H_{18}N_4O_5KV$ (520): C, 53.08; H, 3.49; N, 10.76 %. Found: C, 53.59; H, 3.97; N, 10.51%.

3.2.3.9. $[\{V^{V}O_2\{Hdfmp(inh)_2\}\}_2\mu\text{–}O]$ (3.10)

Complex $[V^{V}O(OMe)(MeOH)\{Hdfmp(inh)_2\}]$ (**3.4**) (0.265 g, 0.5 mmol) was dissolved in 50 mL of CH_3CN and the clear solution was refluxed in an oil bath for ca. 4 days. After reducing the solvent volume to ca. 20 mL, flask was kept in refrigerator (ca. 10 °C) for over night where dark brown solid of **3.10** slowly separated out. This was filtered, washed with CH_3CN and dried in a desiccator over silica gel. Yield 0.200 g (42 %). Anal. calcd. for $C_{42}H_{32}N_{12}O_9V_2$ (950): C, 53.06; H, 3.39; N, 17.68%. Found: C, 52.89 H, 3.27; N, 17.55%.

3.2.3.10. $[\{V^{V}O_2\{Hdfmp(nah)_2\}\}_2\mu\text{–}O]$ (3.11) and $[\{V^{V}O_2\{Hdfmp(bhz)_2\}\}_2\mu\text{–}O]$ (3.12)

Complex **3.11** and **3.12** were prepared as outlined for **3.10** using 0.5 mmol of **3.5** or **3.6** in 50 mL of acetonitrile.

3.11. Yield: 0.0.212 g (45 %). Anal. Calcd for $C_{42}H_{32}N_{12}O_9V_2$ (950.67): C, 53.06; H, 3.39; N, 17.68. Found: C, 53.00; H, 3.28; N, 17.46.

3.12. Yield: 0.192 g (40 %). Anal. Calcd for $C_{46}H_{36}N_8O_9V_2$ (946.72): C, 58.36; H, 3.83; N, 11.84. Found: C, 58.0; H, 3.77; N, 11.56.

3.2.3.11. $[V^{V}O(O_2)\{Hdfmp(inh)_2\}]$ (3.13)

Complex $[V^{IV}O\{Hdfmp(inh)_2\}]$ (0.467g, 1 mmol) was dissolved in methanol (30 mL) and cooled with ice. Aqueous 30% H_2O_2 (2 mL) was added drop wise to the above solution with stirring. The stirring was continued for next 2 h while the reaction mixture kept cool and the separated yellow-orange **3.13** was

filtered, washed with cold methanol and dried in a desiccator over silica gel. Yield 0.280 g (56%). Anal. calcd. for $C_{21}H_{16}N_6O_6V$ (499.34): C, 50.51; H, 3.23; N, 16.83 %. Analysis could not be recorded dure to poor stability.

3.2.3.12. $[V^VO(O_2)\{Hdfmp(nah)_2\}]$ (3.14) and $[V^VO(O_2)\{Hdfmp(bhz)_2\}]$ (3.15)

Complexes **3.14** and **3.15** were prepared as outlined for **3.13** using 1 mmol of **3.2** or **3.3** in 30 mL of methanol.

3.14. Yield: 0.310 g (62%). Anal. Calcd for $C_{21}H_{16}N_6O_6V$ (499.34): C, 50.51; H, 3.23; N, 16.83. Analysis could not be recorded dure to poor stability.

3.15. Yield: 0.351 g (70%). Anal. Calcd for $C_{23}H_{18}N_4O_6V$ (497.36): C, 55.54; H, 3.65; N, 11.26. Analysis could not be recorded dure to poor stability.

3.2.4. Oxidative bromination of styrene

Complexes **3.4** to **3.9** were used as catalyst precursors to carry out the oxidative bromination of styrene. In a typical reaction, styrene (1.04 g, 10 mmol), aqueous solution (20 mL) of KBr (3.57 g, 30 mmol), 30% aqueous H_2O_2 (3.40 g, 30 mmol) and 20 mL CH_2Cl_2 were mixed in a 100 mL reaction flask. The catalyst (0.001 g) and 70% $HClO_4$ (1.43 g, 10 mmol) were added, and the reaction mixture was stirred at room temperature. Additional 20 mmol of 70% $HClO_4$ were further added in three equal portions after every 15 minutes with continuous stirring. In all reactions, experimental conditions (e.g. stirring speed, size of magnetic bar and reaction flask) were kept as similar as possible. After 1 h the orange colored organic layer was separated using a separatory funnel, washed with water and dried. The crude mass was re-dissolved in CH_2Cl_2; insoluble material, if any, was removed by filtration, and the solvent evaporated. The reaction products were separated and analysed as mentioned in Chapter 2. The identity of all products was confirmed by GC–MS and ^1H NMR.

3.2.5. X-Ray crystal structure determination of $[V^{V}O(OMe)(MeOH)\{Hdfmp(bhz)_2\}]\cdot 2MeOH$ (3.6·2MeOH) and $[V^{V}O_2\{H_2dfmp(inh)_2\}]\cdot 5H_2O$ (3.7·5H_2O)

Three-dimensional room temperature X-ray data were collected on a Bruker Kappa Apex CCDC diffractometer at low temperature by the ϕ-ω scan method. Reflections were measured from a hemisphere of data collected from frames each of them covering 0.3° in ω. Of the 29831 in **3.6** and 27082 in **3.7** reflections measured, all were corrected for Lorentz and polarization effects and for absorption by multi-scan methods based on symmetry-equivalent and repeated reflections, 3858 in **3.6** and 2879 in **3.7** independent reflections exceeded the significance level ($|F|/\sigma|F|$) > 4.0. Complex scattering factors were taken from the program package SHELXTL [166]. The structures were solved by direct methods and refined by full matrix least-squares on F^2. Hydrogen atoms were left to refine freely with isotropic thermal parameters, except hydrogen atoms of O(3W), O(5W) and C(20) in **3.7** which were localized in residual electronic density map and fixed to the corresponding atoms. Hydrogen atoms of O(1W) and one hydrogen atom of O(2W) were not localized in **3.7**. Refinement was done with allowance for thermal anisotropy of all non-hydrogen atoms. Further details of the crystal structure determination are given in Table 3.1.

Table 3.1. Crystal data and structure refinement for $[V^{V}O(OMe)(MeOH)\{Hdfmp(bhz)_2\}]\cdot MeOH$ (**3.6**·2MeOH) and for $[V^{V}O_2\{H_2dfmp(inh)_2\}]\cdot 5H_2O$ (**3.7**·$5H_2O$).

Table 1. Crystal data and structure refinement for **6** and **7**

	3.6	**3.7**
Formula	$C_{27}H_{33}N_4O_8V$	$C_{21}H_{27}N_6O_{10}V$
Molecular weight	592.51	574.43
Crystal system	Triclinic	Orthothombic
Space group	P $\bar{1}$	Pbca
T/K	100(2)	100(2)
a/Å	7.9044(2)	16.115(5)
b/Å	13.4380(4)	12.857(5)
c/Å	14.3137(4)	23.586(5)
α/°	64.434(2)	90.000(5)
β/°	86.071(2)	90.000(5)
γ/°	84.930(2)	90.000(5)
V/Å^3	1365.38(7)	4887(3)
F_{000}	620	2384
Z	2	8
D_{calc}/g cm^{-3}	1.441	1.562
μ/mm^{-1}	0.420	0.475
θ/°	1.58-25.15	2.14-25.04
R_{int}	0.0574	0.0745
Goodness-of-fit on F^2	1.120	1.037
R_1[a]	0.0377	0.0515
wR_2 (all data)[b]	0.1238	0.1568
Largest differences peak and hole (eÅ^{-3})	-0.407 and 0.706	-0.555 and 0.841

[a] $R_1 = \Sigma ||F_o| - |F_c|| / \Sigma |F_o|$. [b] $wR_2 = \{\Sigma[w(|F_o|^2 - |F_c|^2)^2]\} / \Sigma[w(F_o^4)]\}^{1/2}$

3.3. Results and discussion

3.3.1. Synthesis, reactivity and solid-state characteristics

Scheme 3.2 provides an overview of the complexes described in this contribution. Structures of these complexes are based on elemental analyses, spectroscopic (IR, UV/Vis, EPR, ^{1}H, ^{13}C, and ^{51}V NMR) data, and X-ray diffraction analyses of complexes **3.6** and **3.7**.

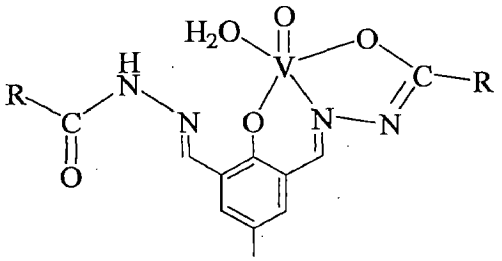

R = 4-pyridyl **3.1**
R = 3-pyridyl **3.2**
R = benzene **3.3**

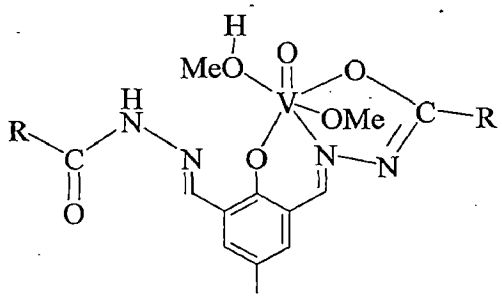

R = 4-pyridyl **3.4**
R = 3-pyridyl **3.5**
R = benzene **3.6**

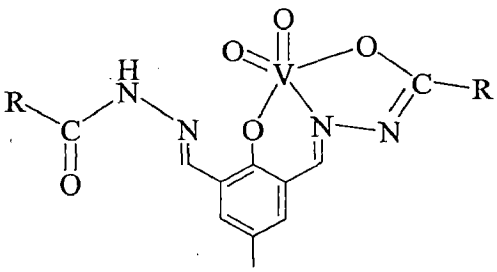

R = 3-pyridyl **3.8**
R = benzene **3.9**

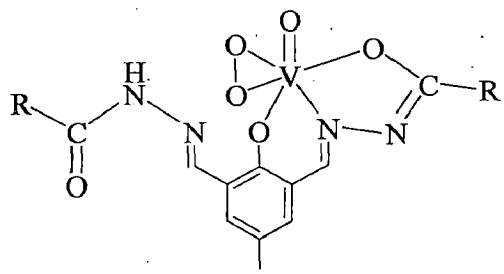

R = 4-pyridyl **3.10**
R = 3-pyridyl **3.11**
R = benzene **3.12**

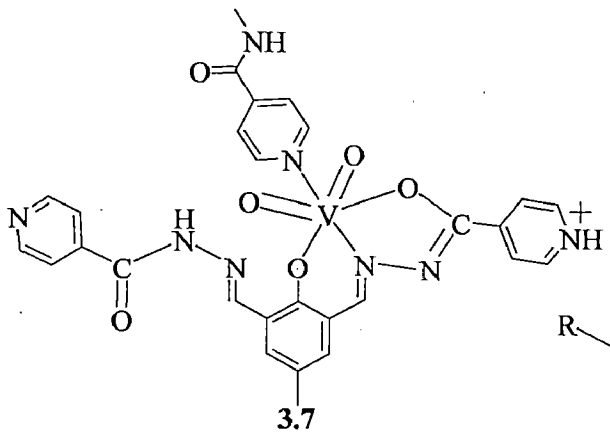

3.7

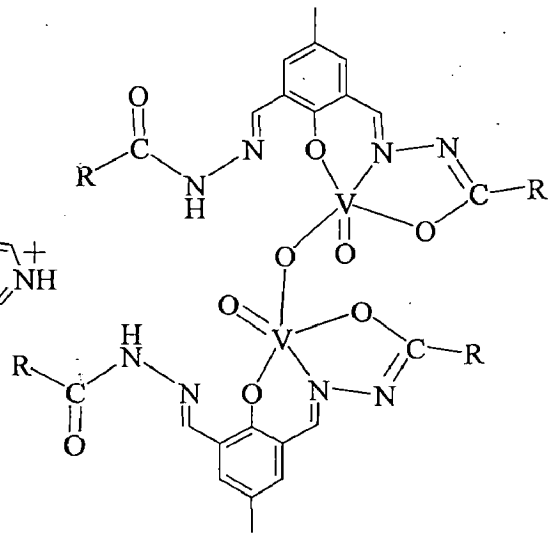

R = 4-pyridyl **3.13**
R = 3-pyridyl **3.14**
R = benzene **3.15**

Scheme 3.2. Structures of complexes reported in this chapter.

Reaction of $[V^{IV}O(acac)_2]$ with an equimolar amount of the ligands $H_3dfmp(inh)_2$ (**3.I**), $H_3dfmp(nah)_2$ (**3.II**) and $H_3dfmp(bhz)_2$ (**3.III**) (c.f. Scheme 3.1) in methanol yields the oxidovanadium(IV) complexes, $[V^{IV}O\{Hdfmp(inh)_2\}\cdot H_2O]$ (**3.1**) $[V^{IV}O\{Hdfmp(nah)_2\}\cdot H_2O]$ (**3.2**) and $[V^{IV}O\{Hdfmp(bhz)_2\}\cdot H_2O]$ (**3.3**), respectively. The ligands coordinate out of their dianionic (ONO(2−)) enolate tautomeric form leaving other coordination site free from coordination; *cf.* Scheme 3.2. These complexes can further be transformed into $[V^{V}O(OMe)(MeOH)\{Hdfmp(inh)_2\}]$(**3.4**), $[V^{V}O(OMe)(MeOH)$-$\{Hdfmp(nah)_2\}]$ (**3.5**) and $[V^{V}O(OMe)(MeOH)\{Hdfmp(bhz)_2\}]$(**3.5**) on prolonged crystallization in excess of methanol in air atmosphere. Equations (3.1), and (3.2) represent the overall synthetic procedures.

$$[V^{IV}O(acac)_2] + H_3dfmp(inh)_2 \rightarrow [V^{IV}O\{Hdfmp(inh)_2\}\cdot H_2O]\ (\mathbf{3.1}) + 2\ Hacac \qquad (3.1)$$

$$2[V^{IV}O\{Hdfmp(inh)_2\}\cdot H_2O] + 4MeOH + \tfrac{1}{2}\ O_2 \rightarrow 2[V^{V}O(OMe)(MeOH)\{Hdfmp(inh)_2\}]\ (\mathbf{3.4}) + 2\ H_2O \qquad (3.2)$$

A reaction of potassium vanadate generated *in situ* by dissolving V_2O_5 in an aqueous solution of KOH, with solutions of the potassium salts of $H_3dfmp(inh)_2$ at pH ca. 7.5 gave neutral dioxidovanadium(V) complex **3.7** (equation 3.3), while other ligands $H_3dfmp(nah)_2$ and $H_3dfmp(bhz)_2$ result in the formation of potassium salts of dioxidovanadium(V) complexes **3.8** and **3.9**, respectively (equation 3.4).

$$KVO_3 + K_2Hdfmp(inh)_2 + H^+ \rightarrow [V^{V}O_2\{H_2dfmp(inh)_2\}] + H_2O + K^+ \qquad (3.3)$$

Their dinuclear oxidovanadium(V) analogues e.g. complexes $[\{V^{V}O\{Hdfmp(inh)_2\}\}_2\mu\text{-}O]$ (**3.10**), $[\{V^{V}O\{Hdfmp(nah)_2\}\}_2\mu\text{-}O]$ (**3.11**), and $[\{V^{V}O\{Hdfmp(bhz)_2\}\}_2\mu\text{-}O]$ (**3.12**) were obtained by refluxing the corresponding oxidomethoxido complexes in dry acetonitrile (equation 3.4).

$$2[V^{V}O(OMe)(MeOH)\{Hdfmp(inh)_2\}] \rightarrow$$
$$[\{V^{V}O\{Hdfmp(inh)_2\}\}_2\mu\text{-}O] + 2MeOH + MeOMe \quad (3.4)$$

Peroxidovanadium(V) complexes **3.13, 3.14** and **3.15** were obtained by the reaction of the respective oxidovanadium(IV) complex with H_2O_2 in methanol.

These complexes are soluble in methanol, DMSO and DMF. Complexes **3.1, 3.2** and **3.3** exhibit effective magnetic moment values of 1.72 - 1.74 μ_B at 298 K, which is normal for magnetic dilute complexes with a d^1 (S=1/2) system. Other complexes are diamagnetic as expected for the $3d^0$ system.

3.3.2. Computational studies

Ligands H_3dfmp(inh)$_2$ (**3.I**), H_3dfmp(nah)$_2$ (**3.II**) and H_3dfmp(bhz)$_2$ (**3.III**) have two functionalized arms and are expected to form bi-nuclear metal complexes. However, in the complexes isolated and characterized, all ligands used their only one of the functionalized arms to coordinate with the metal ions in the enolate form. To investigate the reason we performed the theoretical calculation using Gaussian 09 package. Since the coordinating atoms as well as environment are similar in all the three ligands, we have considered H_3dfmp(bhz)$_2$ (**3.III**) as a representative for the quantum calculation. The geometry optimization of the ligand was carried out with B3LYP functional using 6-311g basis set for all the atoms. The optimized structure is shown in Figure 3.1.

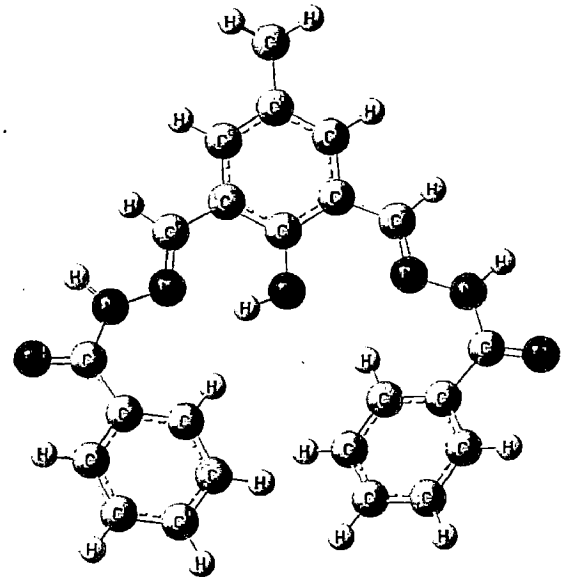

Figure 3.1. Fully optimized structure of the ligand H_3dfmp(bhz)$_2$ (**3.III**).

The generated highest occupied molecular orbital (HOMO) and lowest unoccupied molecular orbital (LUMO) from the optimized structure using GaussView 5 are presented in Figure 3.2. These figures clearly show that more electron density lies in only one of the arms while other arm has very small electron density. Hence, vanadium ion preferentially binds to that coordinating arm which has more electron cloud while other arm remains silent.

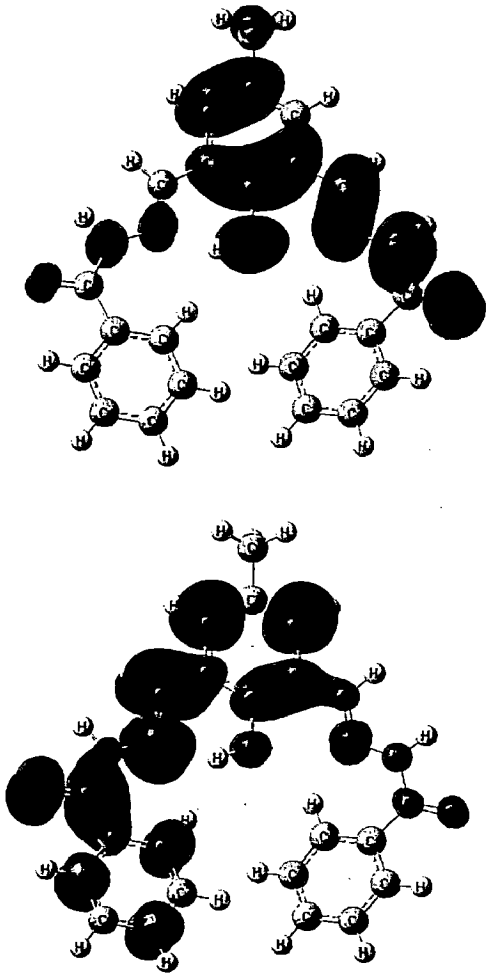

Figure 3.2. HOMO (upper) and LUMO (lower) of H_3dfmp(bhz)$_2$ (**3.III**).

3.3.3. Description of structures of [V^VO(OMe)(MeOH){Hdfmp(bhz)$_2$}] ·2MeOH (3.6·2MeOH) and [$V^V O_2${H_2dfmp(inh)$_2$}]·5H_2O (3.7·5H_2O)

Figure 3.3 shows an ORTEP representation of [V^VO(OMe){Hdfmp(bhz)$_2$}(MeOH)] (**3.6**) and Figure 3.4 an ORTEP representation of [$V^V O_2${H_2dfmp(inh)$_2$}]$_2$ (**3.7**). In **3.6**, the asymmetric unit contains one neutral vanadium complex and two methanol molecules and in **3.7**

one neutral vanadium complex and five water molecules. In the molecular structure of **3.6**, the vanadium centers adopt a distorted six-coordinated octahedral geometry with the (Hdfmp(bhz)$_2$) ligand coordinated through the one $O_{hydroxyl}$, one $N_{hydrazone}$, and one O_{keto} atoms; the oxo and, two oxygen (one of methoxy group and one of methanol group) atoms complete the coordination sphere. In **3.7**, the vanadium centers adopt a distorted six-coordinated octahedral geometry too, with the [H_2dfmp(bhz)$_2$, which is protonated in one py group] ligand coordinated through the one $O_{hydroxyl}$, one $N_{hydrazone}$, and one O_{keto} atoms; two oxo and one deprotonated N_{py} (of the other complex) atoms complete the coordination sphere. Protonation of ring nitrogen and stabilization of neutral species has previously been observed in other complexes [137]. The structure corresponds to a polymeric compound.

The V=O bonds [V(1)-O(1): 1.5910(18) Å in **3.6** and V(1)-O(3): 1.650(3)Å and V(1)-O(4): 1.621(3) in **3.7**] are characteristic of oxo-type O atoms with strong π bonding (see Table 3.2). The V-$O_{methanol}$ bond, which is trans to the oxo atom, is significantly longer [V(1)-O(2M): 2.265(2) Å] than the V-$O_{methoxy}$ bond [V(1)-O(1M): 1.7851(18) Å] in **3.6.** Such elongation has previously been observed in other complexes with similar structures [167-169]. In **3.7**, those bonds which are trans to the oxo atoms [V(1)-N(3): 2.168(3) Å and V(1)-N(6)#1: 2.494(3)Å] are longer too [170].

The tetragonal plane are best defined by N(3)-O(2)-O(3)-O(1M) (mean deviation from the plane = 0.1078(9) Å) in **3.6**, and by N(3)-O(1)-O(3)-O(5) (mean deviation from the plane = 0.0344(13) Å) in **3.7**, leaving the oxo atom, O(1), and the $O_{methanol}$ atom, O(2M), in **3.6**, or the other oxo atom, O(4), and the N_{py} of the other molecule, in the axial position, in **3.7**. The torsion angles of the plane containing hydrazone group are close to 180°: N(1)-N(2)-C(7)-C(1) is 177.6(2)° and N(3)-N(4)-C(17)-C(18) is 173.3(2)° in **3.6** and N(3)-N(2)-(C(6)-C(3) is 178.1(3)° and N(4)-N(5)-C(14)-C(15) is 179.5(3)° in **3.7**. The molecular structure in the supramolecular assembly is partly determined by the intermolecular interactions involving hydrogen bonds between the methanol molecules in **3.6** and water molecules in **3.7**, and the other heteroatom's present in the ligand. Distances

and angles of hydrogen bonds in the compounds $[V^{V}O(OMe)$-$\{Hdfmp(bhz)_2\}(MeOH)]\cdot 2MeOH$ (**3.6**) and for $[V^{V}O_2\{H_2dfmp(inh)_2\}]\cdot 5H_2O$ (**3.7**) are given in the Table 3.3. The space filling representation of compounds **3.6** and **3.7** are presented in Figure 3.5.

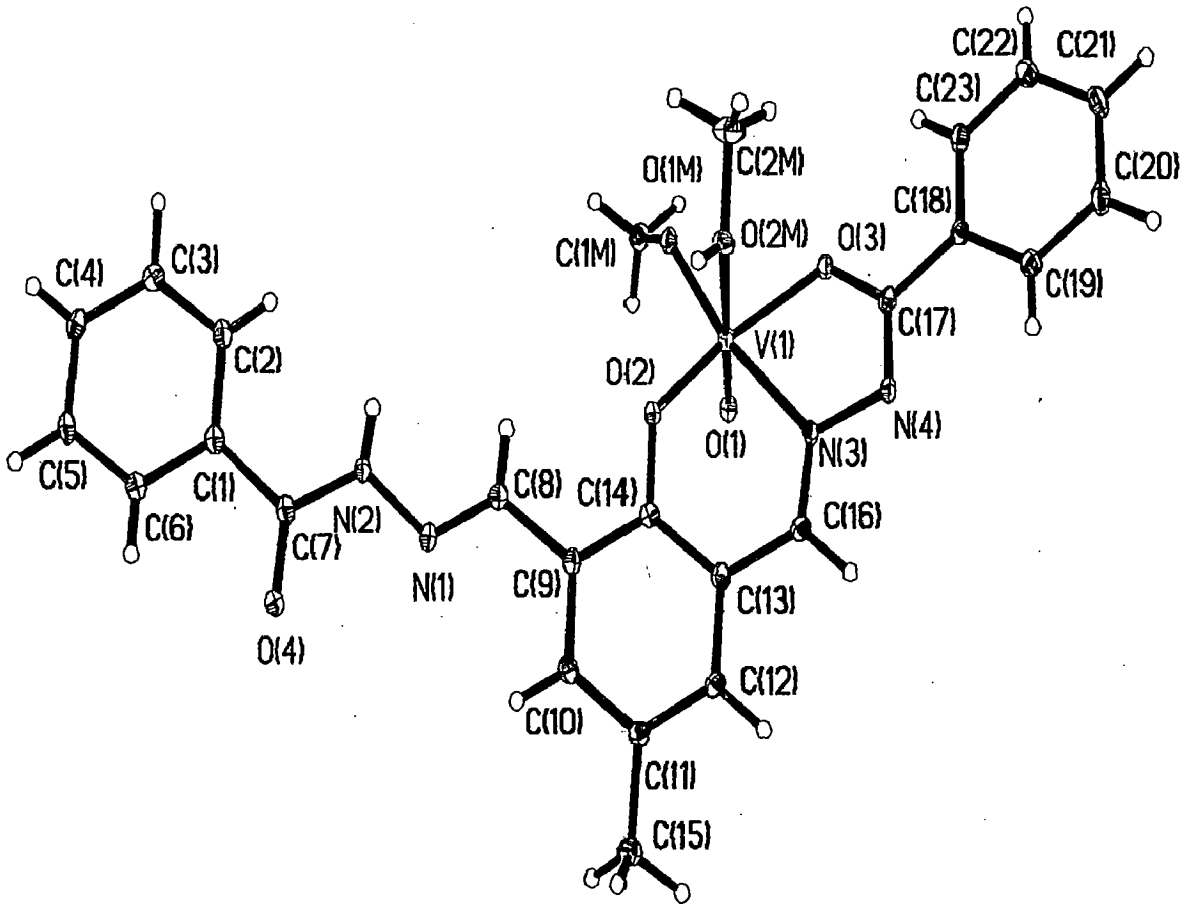

Figure 3.3. ORTEP plot of $[V^{V}O(OMe)(MeOH)\{Hdfmp(bhz)_2\}]\cdot 2MeOH$ (**3.6**·2MeOH). All the non-hydrogen atoms are represented by their 30 % probability ellipsoids. Hydrogen atoms are included.

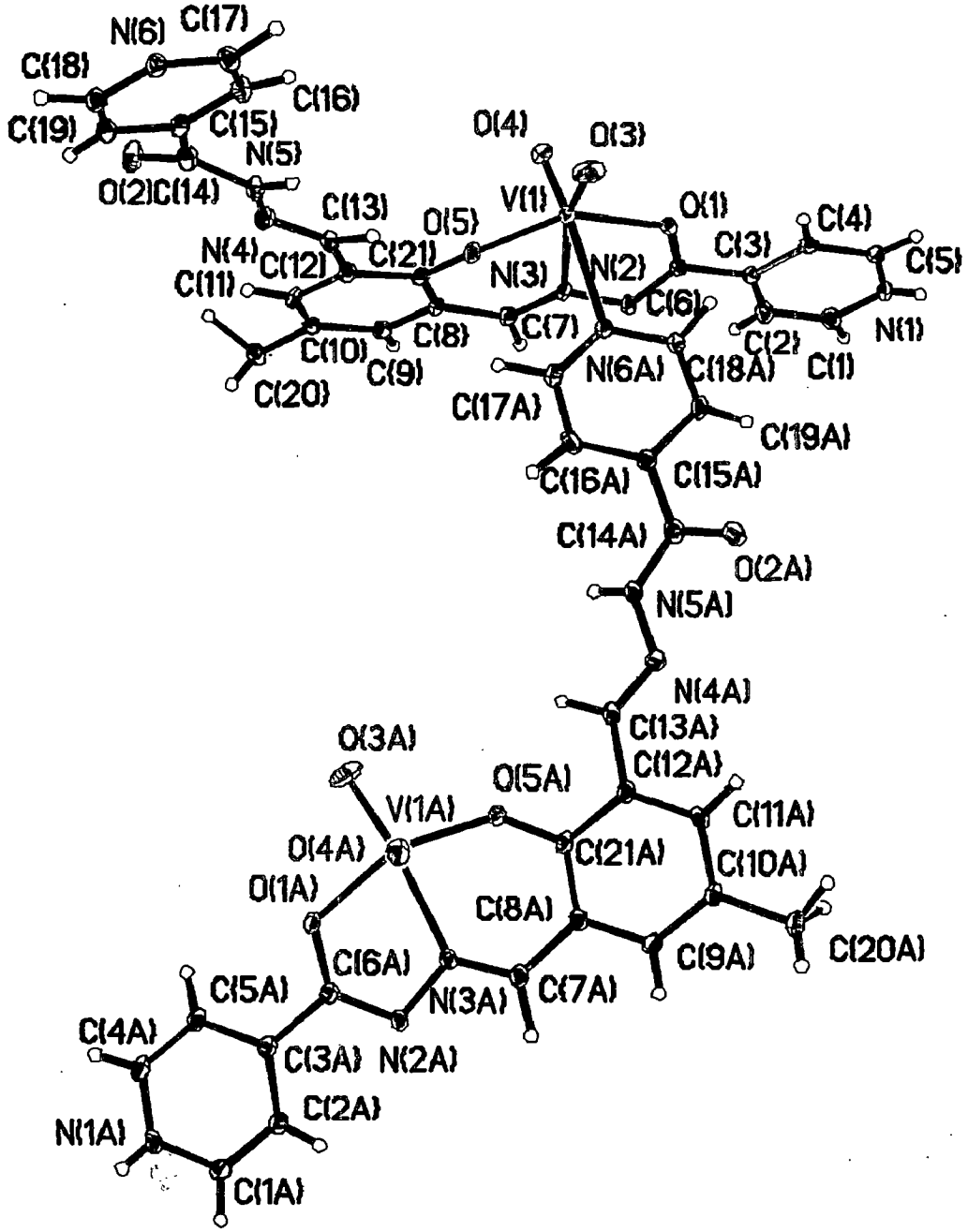

Figure 3.4. ORTEP plot of $[V^{V}O_2\{H_2dfmp(inh)_2\}]\cdot 5H_2O$ (**3.7**·$5H_2O$). All the non-hydrogen atoms are represented by their 30 % probability ellipsoids. Hydrogen atoms are included.

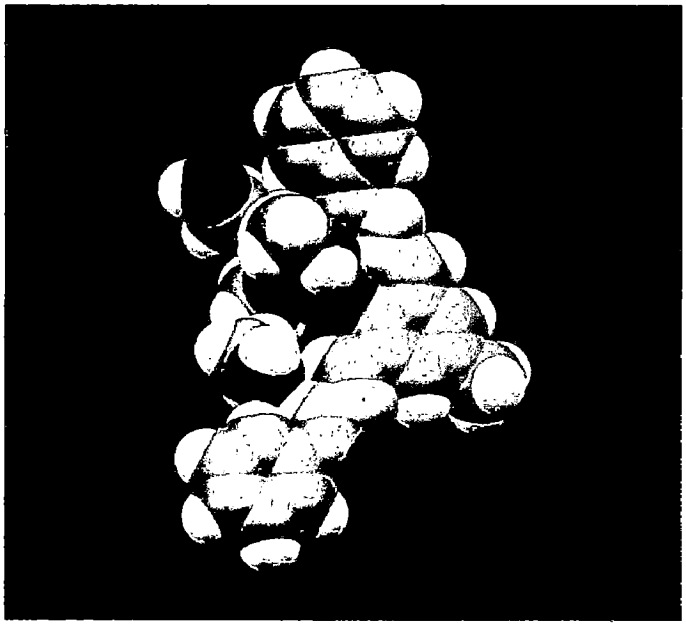

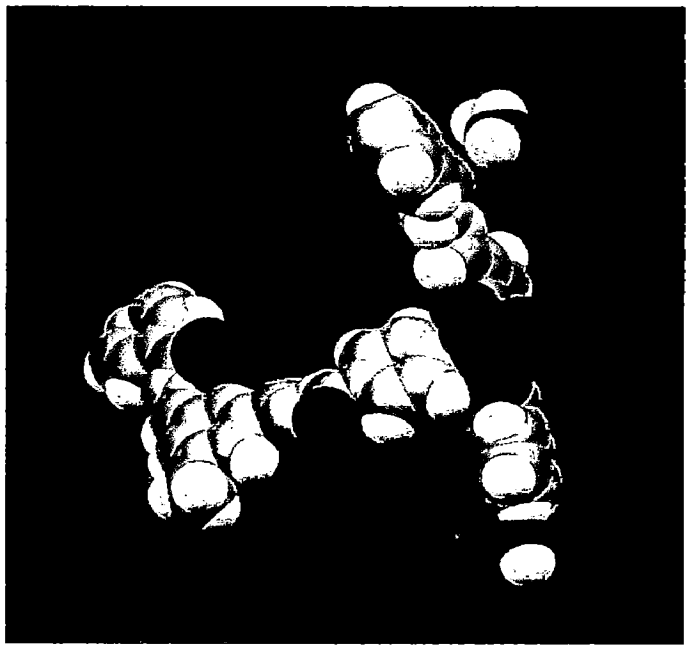

Figure 3.5. Above: Space-filling representation of compound **3.6** colored by atom type where we can observe the hydrogen bond interaction between methanol molecule and protonated hydrazone group occupying the position of the VO group (up) in the down part of the ligand showed in the figure. Below: Space-filling representation of compound **3.7** colored by atom type where we can observe the sixth coordinate position occupied by the py group of the other complex

Table 3.2. Selected bond lengths (Å) and bond angles (°) for **3.6** and **3.7**.

Bond lengths **3.6**		Bond lengths **3.7**	
V(1)-O(1)	1.5910(18)	V(1)-O(1)	1.986(3)
V(1)-O(1M)	1.7851(18)	V(1)-O(3)	1.650(3)
V(1)-O(2)	1.8630(17)	V(1)-O(4)	1.621(3)
V(1)-O(3)	1.9489(17)	V(1)-O(5)	1.913(3)
V(1)-N(3)	2.116(2)	V(1)-N(3)	2.168(3)
V(1)-O(2M)	2.265(2)	V(1)-N(6)#1	2.494(3)
N(1)-C(8)	1.274(3)	N(2)-C(6)	1.310(5)
N(1)-N(2)	1.387(3)	N(2)-N(3)	1.400(4)
N(2)-C(7)	1.352(3)	O(2)-C(14)	1.237(4)
O(2)-C(14)	1.336(3)	N(3)-C(7)	1.293(5)
N(3)-C(16)	1.286(3)	N(4)-C(13)	1.270(5)
N(3)-N(4)	1.393(3)	N(4)-N(5)	1.380(4)
O(3)-C(17)	1.315(3)	O(5)-C(21)	1.328(4)
O(4)-C(7)	1.238(3)	N(5)-C(14)	1.340(5)
N(4)-C(17)	1.303(3)	O(1)-C(6)	1.298(4)
Bond angles		Bond angles	
O(1)-V(1)-O(1M)	100.05(9)	O(4)-V(1)-O(3)	106.06(14)
O(1)-V(1)-O(2)	99.93(9)	O(4)-V(1)-O(5)	97.96(13)
O(1M)-V(1)-O(2)	103.84(8)	O(3)-V(1)-O(5)	101.56(15)
O(1)-V(1)-O(3)	103.04(8)	O(4)-V(1)-O(1)	99.13(13)
O(1M)-V(1)-O(3)	94.83(8)	O(3)-V(1)-O(1)	95.93(14)
O(2)-V(1)-O(3)	147.25(8)	O(5)-V(1)-O(1)	151.07(10)
O(1)-V(1)-N(3)	91.36(9)	O(4)-V(1)-N(3)	90.31(13)
O(1M)-V(1)-N(3)	165.83(8)	O(3)-V(1)-N(3)	162.02(13)
O(2)-V(1)-N(3)	82.21(8)	O(5)-V(1)-N(3)	83.04(11)
O(3)-V(1)-N(3)	74.26(8)	O(1)-V(1)-N(3)	73.71(10)
O(1)-V(1)-O(2M)	175.98(9)	O(4)-V(1)-N(6)#1	168.29(12)

O(1M)-V(1)-O(2M)	83.79(8)	O(3)-V(1)-N(6)#1	85.65(13)
O(2)-V(1)-O(2M)	77.87(8)	O(5)-V(1)-N(6)#1	79.63(11)
O(3)-V(1)-O(2M)	77.69(7)	O(1)-V(1)-N(6)#1	78.91(10)
N(3)-V(1)-O(2M)	85.02(8)	N(3)-V(1)-N(6)#1	78.04(11)

Symmetry transformations used to generate equivalent atoms: #1 x+1/2,-y+1/2,-z

Table 3.3. Distances [Å] and angles [°] of hydrogen bonds for $[V^{V}O(OMe)\{Hdfmp(bhz)_2\}(MeOH)]\cdot 2MeOH$ (**3.6**) and for $[V^{V}O_2\{H_2dfmp(inh)_2\}]\cdot 5H_2O$ (**3.7**).

Compound	D-H...A	d(D-H)	d(H...A)	d(D...A)	<(DHA)
3.6	N(2)-H(2N)...O(3M)	0.84(3)	2.08(3)	2.904(3)	167(3)
3.6	O(2M)-H(2O)...O(4)#1	0.67(3)	2.08(3)	2.742(3)	172(4)
3.6	O(3M)-H(3O)...O(4M)#2	0.90(3)	1.80(3)	2.677(3)	163(3)
3.6	O(4M)-H(4O)...O(4)#3	0.84(4)	1.98(4)	2.717(3)	146(4)
3.6	O(4M)-H(4O)...N(1)#3	0.84(4)	2.45(4)	3.156(3)	142(4)
3.7	N(1)-H(1N)...O(4W)	0.75(4)	1.91(4)	2.628(5)	162(4)
3.7	O(2W)-H(2W)...O(4)#4	0.94(7)	1.90(7)	2.840(5)	174(6)
3.7	O(4W)-H(4WA)...O(1W)#5	0.88(4)	1.92(4)	2.794(5)	168(4)
3.7	O(4W)-H(4WB)...N(4)#6	0.90(7)	2.34(7)	3.185(4)	156(6)
3.7	N(5)-H(5N)...O(3W)#7	0.73(5)	2.22(5)	2.933(5)	164(5)
3.7	O(5W)-H(5WB)...O(1W)#8	1.00	2.46	3.220(6)	132.3
3.7	O(5W)-H(5WA)...O(1W)#9	1.02	1.86	2.842(6)	160.3

Symmetry transformations used to generate equivalent atoms:
#1 -x,-y+2,-z+1 #2 -x,-y+1,-z+1 #3 x,y-1,z #4 x,-y+1/2,z-1/2
#5 -x+1/2,-y,z+1/2 #6 x+1/2,y-1,-z+1/2 #7 -x-1/2,y-1/2,z
#8 -x-1/2,y+1/2,z #9 x-1/2,-y+1/2,-z

3.3.4. IR spectral studies

A partial list of IR spectral data of of ligands and complexes are presented in Table 3.4. Some of the representative spectra are presented in Figures 3.6 – 3.8. In spite of the presence of two azomethine, ketonic and NH groups, all the ligands display only single band for each. The IR spectra of the ligands exhibit $\nu_{(NH)}$ and ν(C=O) at 3020–3090 cm^{-1} and 1638–1690 cm^{-1}, respectively. These are indicative of their ketonic nature in the solid state (cf. Scheme 3.1). All the complexes retain these two bands with slight deviations along with the appearance of a new band in the region 1230-1280 cm^{-1}. The later one suggests the enolization of one of the ketonic groups and replacement of H by the metal ion while presence of former bands suggests that all the ligands have at least one ketonic group free from coordination. Similarly, the ν(C=N) (azomethine) stretch appearing at 1608 – 1629 cm^{-1} in ligands splits into two: one remains at nearly same position to that of respective ligand while other one appears at lower wave number (1582 – 1600 cm^{-1}). This is also in the line of the coordination of nitrogen atom of the only one azomethine group.

The $V^{IV}O$-complexes exhibit a band at 974–996 cm^{-1} due to ν(V=O) stretch while $V^{V}O$-complexes exhibit such band at 922–935 cm^{-1}. The $V^{V}O_2$-complexes exhibit two such sharp bands in the 893–904 cm^{-1} region due to ν_{sym}(O=V=O) and ν_{asym}(O=V=O). These bands confirm the cis-$V^{V}O_2$ structure in complexes [30]. In the dinuclear complexes, two (some time one) sharp bands arising at 956–975 cm^{-1} is assigned due to ν(V=O), and a broad band arising at 760–882 cm^{-1} is assigned due to ν[V–(μ-O)–V]. The presence of two ν(V=O) in the dinuclear complexes **3.10**, **3.11** and **3.12** supports the nonequivalence of the two oxo-bridged halves [171]. The peroxo complexes show three IR-active modes associated with the $\{V(O_2)\}^{2+}$ moiety, namely the symmetric $V(O_2)$ stretch (ν_2) at ca. 600 cm^{-1}, the antisymmetric $V(O_2)$ (ν_3) at ca. 740 cm^{-1}, and the O–O(ν_1) stretch at ca. 890 cm^{-1}, characteristic of η^2–coordination of the peroxo group [42]. In addition, these complexes display the ν(V=O) mode at ca. 970 cm^{-1}.

Table 3.4. IR spectral data (cm^{-1}) of ligands and complexes.

S. No.	Compounds	ν(NH)	ν(C=O)	ν(C=N)	ν(C-O)	ν(V=O)
1	H_3dfmp(inh)$_2$ (**3.I**)	3030	1655	1618		
2	H_3dfmp(nah)$_2$ (**3.II**)	3050	1645	1616		
3	H_3dfmp(bhz)$_2$ (**3.III**)	3050	1665	1619		
4	[V^{IV}O{Hdfmp(inh)$_2$}] (**3.1**)	3020	1672	1615, 1590	1234	996
5	[V^{IV}O{Hdfmp(nah)$_2$}](**3.2**)	3047	1643	1613, 1592	1260	974
6	[V^{IV}O{Hdfmp(bhz)$_2$}](**3.3**)	3050	1653	1612, 1590	1230	977
7	[V^{V}O(OMe)(MeOH){Hdfmp(inh)$_2$}] (**3.4**)	3040	1662	1613, 1594	1260	975
8	[V^{V}O(OMe)(MeOH){Hdfmp(nah)$_2$}] (**3.5**)	3065	1652	1609, 1592	1261	983
9	[V^{V}O(OMe)(MeOH){Hdfmp(bhz)$_2$}] (**3.6**)	3055	1642	1608	1270	990
10	[$V^{V}O_2${H_2dfmp(inh)$_2$}] (**3.7**)	3065	1668	1617, 1593	1232	935, 904
11	K[$V^{V}O_2${Hdfmp(nah)$_2$}] (**3.8**)	3065	1661	1618, 1600	1233	930, 902
12	K[$V^{V}O_2${Hdfmp(bhz)$_2$}] (**3.9**)	3055	1650	1618	1280	922, 893

S.No.	Compounds	ν (NH)	ν(C=O)	ν(C=N)	ν(C-O)	ν(V=O)	ν(V-(μ-O)-V)
13	[{V^{V}O{Hdfmp(inh)$_2$}}$_2$μ–O] (**3.10**)	3043	1661	1614, 1596	1231	975	842
14	[{V^{V}O{Hdfmp(nah)$_2$}}$_2$μ–O] (**3.11**)	3093	1676	1616 (broad)	1230	956	882
15	[{V^{V}O{Hdfmp(bhz)$_2$}}$_2$μ–O] (**3.12**)	3060	1690	1612	1234	973	760

	Samples	ν(NH)	ν(C=O)	ν(C=N)	ν(C-O)	ν(V=O)	ν(O-O) (ν_1)	ν (VO_2)	
								Asy. (ν_2)	Sy. (ν_3)
16	[$V^{V}O(O_2)${Hdfmp(inh)$_2$}] (**3.13**)	3082	1638	1617, 1582	1234	971	842	747	604
17	[$V^{V}O(O_2)${Hdfmp(nah)$_2$}] (**3.14**)	3065	1674	1616, 1589	1236	977	870	723	602
18	[$V^{V}O(O_2)${Hdfmp(bhz)$_2$}] (**3.15**)	3065	1645	1629, 1590	1240	960	897	693	567

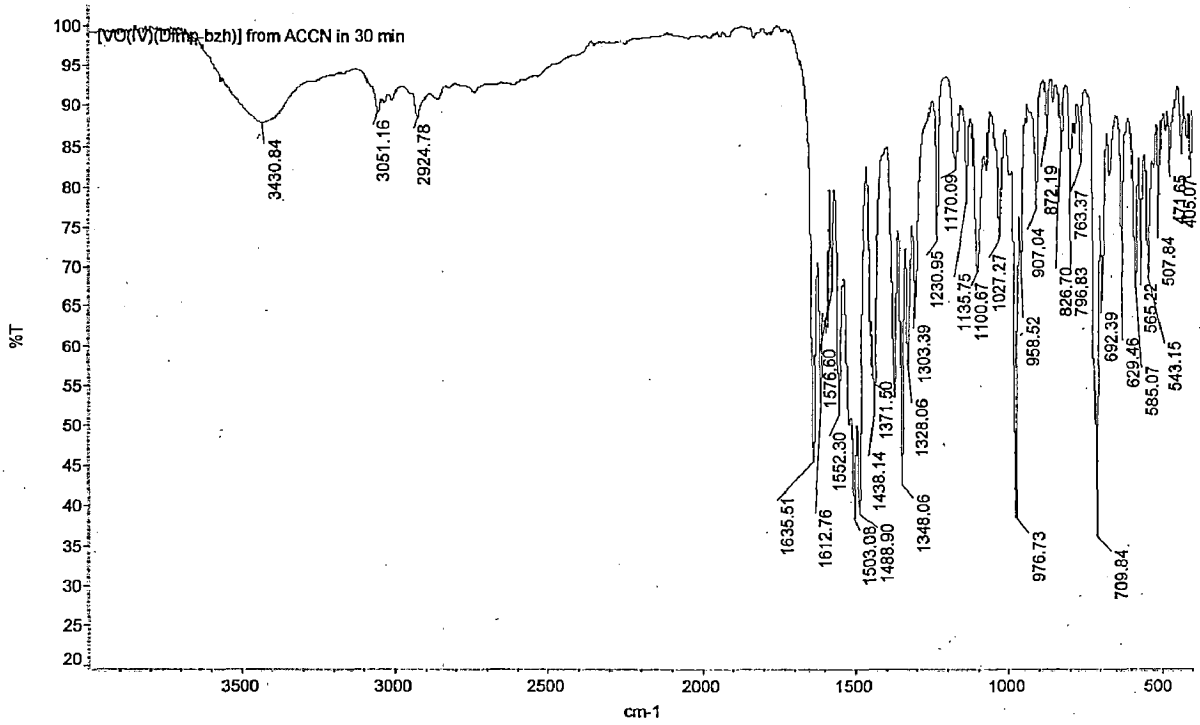

Figure 3.6. FT-IR spectra of the complex $[V^{IV}O\{Hdfmp(bhz)_2\}]$(**3.3**).

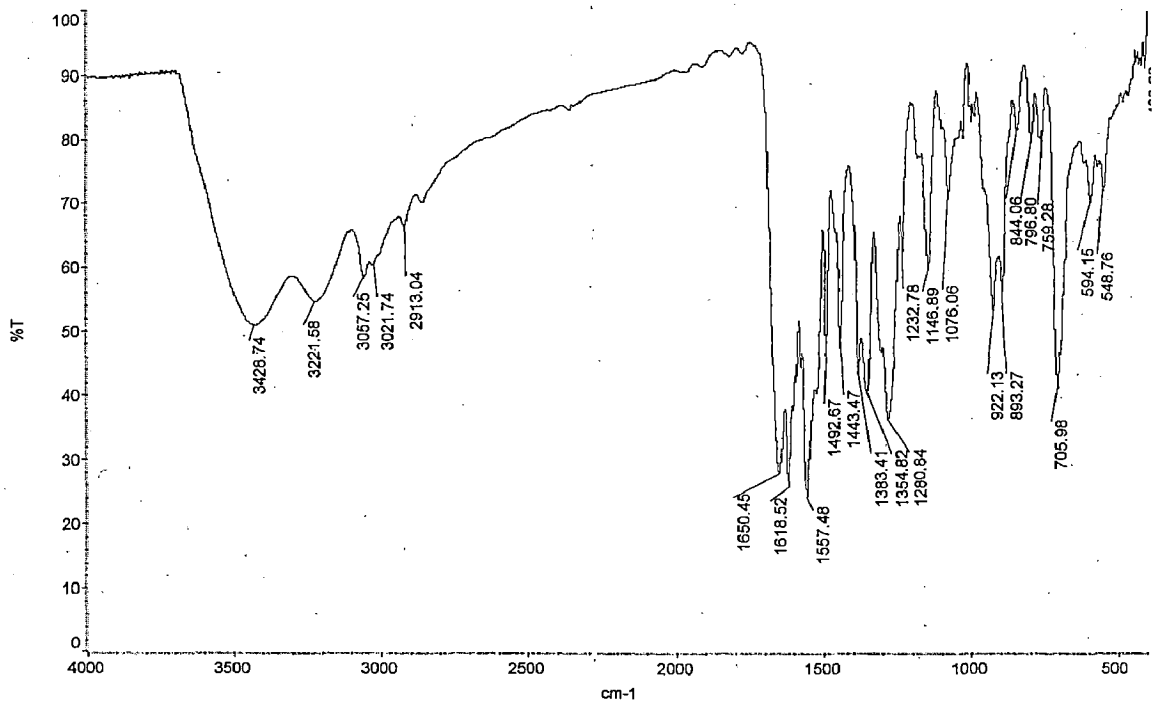

Figure 3.7. FT-IR spectra of the complex $K[V^{V}O_2\{Hdfmp(bhz)_2\}]$ (**3.9**).

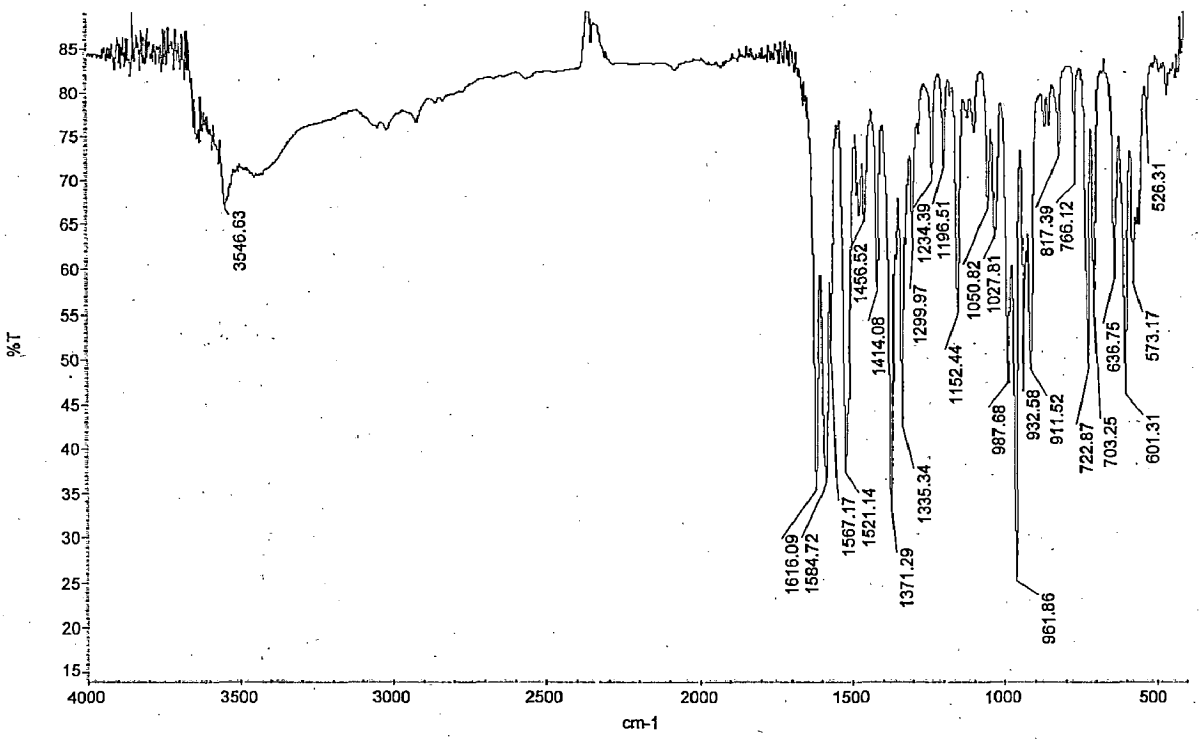

Figure 3.8. FT-IR spectra of the complex $[V^{V}O(O_2)\{Hdfmp(nah)_2\}]$ **(3.14)**.

3.3.5. Electronic spectral studies

The electronic absorption spectra of all the ligands and complexes were recorded in methanol, and the absorption maxima with their extinction coefficients are presented in Table 3.5. The UV spectra of the ligands exhibit three spectral bands at ca. 365, 300 and 200 nm. The most probable assignments for these bands are n $\rightarrow$ π^*, $\pi \rightarrow \pi^*$ and $\varphi \rightarrow \varphi^*$ transitions, respectively. All these bands are present in complexes with slight variations. The $V^{IV}O$-complexes display a medium intensity band at 775 – 837 nm at very high concentration and is assigned to d–d transitions. All the complexes display an intense to medium electronic spectral band in the visible region at ca. 425 nm. This is assigned to a ligand-to-metal charge-transfer (LMCT) transition from the phenolate oxygen atom to an empty d-orbital of the vanadium atom. Dioxidovanadium(V) complexes have a $3d^0$ configuration, and d – d bands are therefore not expected.

Table 3.5. UV-Visible spectral data of ligands and complexes.

Sl. No.	Compounds	Solvent	λ_{max}/ nm (ε/ litre mole^{-1} cm^{-1})
1	**3.I**	Methanol	453(2.804×10^3), 364(1.676×10^4), 303(3.38×10^4), 201(2.539×10^4)
2	**3.II**	Methanol	453(1.23×10^3), 363(8.76×10^3), 300(2.03×10^4), 218(1.07×10^4)
3	**3.III**	Methanol	427(3.99×10^2), 363(2.549×10^3), 300(7.02×10^3), 203(5.05×10^3)
4	**3.1**	Methanol	824(10), 409(4.14×10^3), 337(6.24×10^3), 272(7.74×10^3), 220(1.09×10^4)
5	**3.2**	Methanol	775(23), 427(2.43×10^2), 343 (9.57×10^2), 279(1.71×10^3).
6	**3.3**	Methanol	837(8), 429(5.97×10^3), 346(2.11×10^4), 298(3.68×10^4), 225(2.89×10^4), 207(2.91×10^4)
7	**3.4**	Methanol	428(2.44×10^3), 305(1.05×10^4), 283(1.02×10^4), 240(8.63×10^3)
8	**3.5**	Methanol	432(6.39×10^3), 340(2.75×10^4), 300(4.03×10^4), 250(2.94×10^4), 211(4.33×10^4)
9	**3.6**	Methanol	428(6.02×10^3), 348(2.24×10^4), 298(4.03×10^4), 223(3.17×10^4)
10	**3.7**	Methanol	430(3.44×10^3), 307(1.57×10^4), 277(1.67×10^4), 220(1.91×10^4)
11	**3.8**	Methanol	422(7.59×10^3), 302(3.63×10^4), 227(2.97×10^4), 204(2.90×10^4)
12	**3.9**	Methanol	416(1.00×10^4), 304(3.43×10^4), 225(3.12×10^4), 204(3.62×10^4)
13	**3.10**	Methanol	420(1.12×10^4), 310(3.11×10^4), 281(3.10×10^4), 220(3.70×10^4)
14	**3.11**	Methanol	414(1.25×10^4), 308(2.91×10^4), 225(3.20×10^4)
15	**3.12**	Methanol	402(1.81×10^4), 326(3.41×10^4), 261(5.76×10^4), 207(7.35×10^4)
16	**3.13**	Methanol	418(3.72×10^3), 339(8.4×10^3), 283(1.03×10^4), 220(1.89×10^4)
17	**3.14**	Methanol	418(4.19×10^3), 355(8.66×10^3), 306(1.17×10^4), 213(1.95×10^4)
18	**3.15**	Methanol	424(8.64×10^3), 302(3.00×10^4), 225(2.78×10^4), 206(3.02×10^4)

3.3.6. EPR studies

The EPR spectra of "frozen" solutions (77 K) in MeOD of complexes $[V^{IV}O\{Hdfmp(inh)_2\}]$ (**3.1**), $[V^{IV}O\{Hdfmp(nah)_2\}]$ (**3.2**) and $[V^{IV}O\{Hdfmp(bhz)_2\}]$ (**3.3**) are depicted in Figure 3.9. The spectra were simulated and the spin Hamiltonian parameters obtained by simulation of the spectra are included in Table 3.6. The value of $A_{\|}$ can be calculated using the additivity relationship [$A_z^{est} = \Sigma A_{z,i}$ (i = 1 to 4)] proposed by Wüthrich [139] and Chasteen, [55], with estimated accuracy of $\pm 3\times10^{-4}$ cm^{-1}. The $A_{\|}$ values obtained are in good (Table 3.6) agreement with the A_z^{est} values calculated from the partial contributions of the equatorial donor groups relevant in the present case {H_2O ($45.7\times10^{-4}cm^{-1}$), $O_{phenolate}$ ($38.9\times10^{-4}cm^{-1}$), N_{imine}, (38.1 to $43.7\times10^{-4}cm^{-1}$),O-enolate$^{(-1)}$ ($37.6\times10^{-4}cm^{-1}$)} assuming a NO_3 (species II) equatorial binding set.

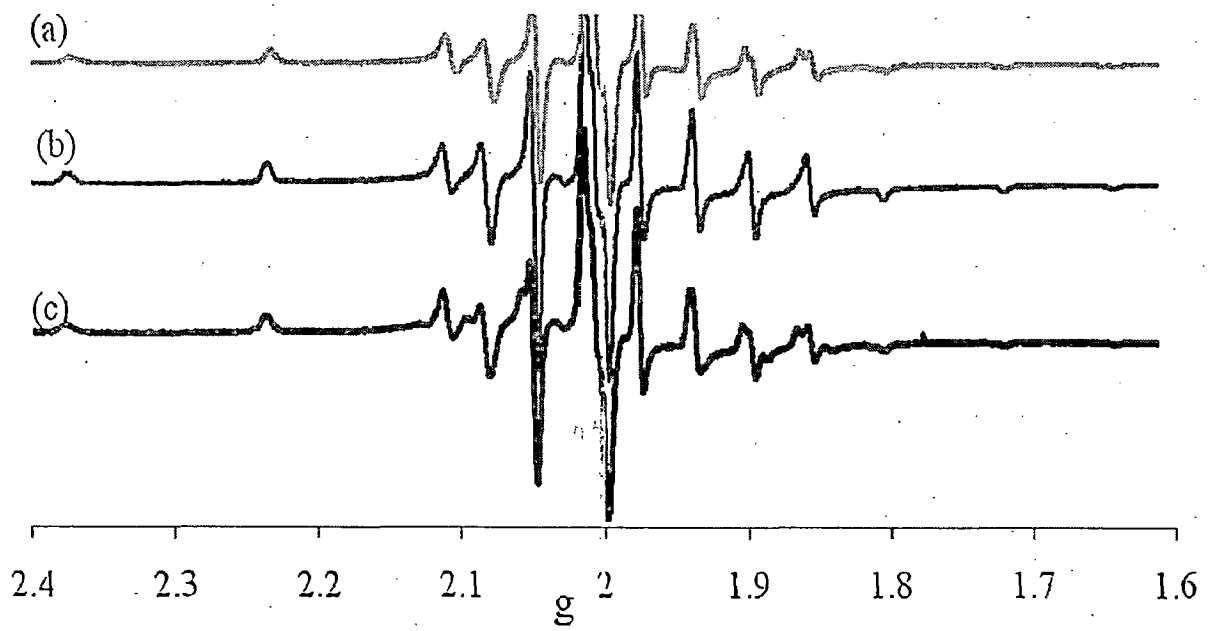

Figure 3.9. 1st derivative EPR spectra of frozen (77 K) solutions (ca. 4 mM) (a) $[V^{IV}O\{Hdfmp(inh)_2\}]$ (**3.1**), (b) $[V^{IV}O\{Hdfmp(nah)_2\}]$ (**3.2**) and (c) $[V^{IV}O\{Hdfmp(bhz)_2\}]$ (**3.3**) in MeOD.

Table 3.6. Spin Hamiltonian parameters obtained by simulation of the experimental 1st derivative EPR spectra recorded for MeOD solutions of complexes at 77K.

Complexes in MeOD (4 mM)	$g_{\|}$	$A_{\|}$ ($\times10^{-4}cm^{-1}$)	$g_{\perp}$	$A_{\perp}$ ($\times10^{-4}cm^{-1}$)
$[V^{IV}O\{H_2dfmp(inh)_2\}]$ (**3.1**)	1.950	166.1	1.981	57.7
$[V^{IV}O\{Hdfmp(nah)_2\}]$ (**3.2**)	1.952	165.6	1.982	57.3
$[V^{IV}O\{Hdfmp(bhz)_2\}]$ (**3.3**)	1.953	165.5	1.984	57.5

3.3.7. ^{1}H NMR spectral studies

^{1}H NMR spectra of the ligands and complexes were recorded to confirm the coordinating modes of the ligands. The relevant spectral data are collected in Table 3.7 and confirm the IR evidence. Some representative ^{1}H NMR spectra are presented in Figure 3.10 – 3.14. The broad signal appearing at δ = 12.21-12.34 ppm, due to the phenolic OH group, disappears in the spectra of the complexes and is in accord with the coordination of the phenolate oxygen. The appearance of a new signal at significantly down field equivalent to one proton in the complexes along with the original signal of the ligands equivalent to one proton demonstrates the coordination of the only one of the azomethine nitrogen atom. Similarly, signal due to the hydrogen of -NH protons (equivalent to two protons) remains at nearly same position but equivalent to only one proton supports the enolization of only one of the NH groups and consequent replacement of H by the metal ion. Aromatic protons appear in the expected regions in spectra of the ligands as well as of the complexes, with slight shifts in their positions. Signal due to the protons of the methyl appears well within the expected range and do not shift significantly with respect to those of the free ligands. Complexes **3.4**, **3.5** and **3.6** display an additional signal due to the methyl protons of the methoxy group. Generally, the dinuclear complexes give rise to relatively broad signals for all of the protons, indicating that the halves of the molecule and thus the coordinated ligands are slightly inequivalent also in solution.

Table 3.7. ^{1}H NMR spectral data of ligands and complexes.

Compounds	–CH=N–	Aromatic H	-OH	–NH	-CH_3
3.I	8.74(s, 2H)	7.61(s, 2H), 7.86(d, 4H), 8.81(b, 4H)	12.21(s, 1H)	12.43(s. 2H)	2.39(s,3H)
3.II		Not recorded			
3.III	8.73(s, 2H)	7.57(m, 6H), 7.64(m, 2H), 7.95(d, 4H)	12.34(s, 1H)	12.15(s, 2H)	2.31(s, 3H)
3.4	8.83 (s,1H), 8.87 (s, 1H)	7.53(m, 1H), 8.02(m, 5H), 8.9.05(m, 4H)		12.28(s, 1H)	2.35(s, 3H), 3.17(s, 3H)
3.5	8.88(s, 1H), 8.97(s, 1H),	7.63(m, 3H), 7.90(s,1H), 8.37(m, 2H), 8.79(s,2H), 9.21(d, 2H)		12.19(s, 1H)	2.32(s, 3H), 3.12(s, 3H)
3.6	8.91(b, 2H)	7.55(m,7H), 7.97(m, 5H)		12.04(s, 1H)	2.31(s, 3H), 3.13(s, 3H)
3.7	Merged with 8.90 signal	7.59(s, 1H), 7.89(m, 5H), 8.90(m, 6H)		12.23(s,1H)	2.32(s, 3H)
3.8	8.87(s, 1H), 8.97(s, 1H)	7.63(d, 3H), 7.88(s, 1H), 8.43(d, 2H), 8.78(s, 2H), 9.16(s, 2H)		12.13(s,1H)	2.32(s, 3H)
3.9	8.96(b, 2H)	7.53(m, 8H), 8.04(m, 4)		12.07(t, 1H)	2.33(s,3H)
3.10		Not recorded			
3.11		Not recorded			
3.12	9.01(s, 2H)	7.52(b, 16H), 8.01(b, 8H),		10.42(s, 2H)	2.34(s, 6H)
3.13	9.42(s, 1H)	7.92(d, 1H), 8.00(s, 1H), 8.07(s, 1H), 8.22(d, 3H), 8.88(d, 5H)		12.24(s, 1H)	2.46(s, 3H)
3.14	8.87(b, 2H)	7.80(s, 2H), 7.97(s, 2H), 8.80(s, 2H), 9.38(d, 3H)		12.22(s, 1H)	2.46(s, 3H)
3.15		Not recorded			

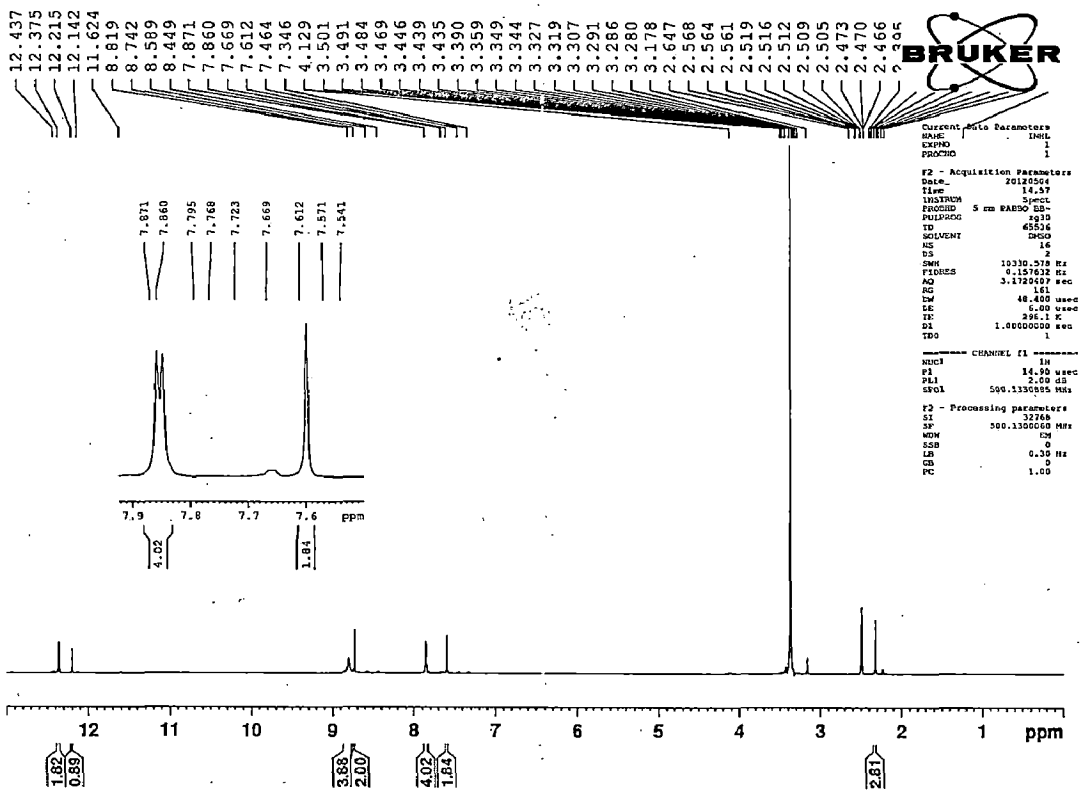

Figure 3.10. ^{1}H NMR spectra of the ligand H_3dfmp(inh)$_2$.

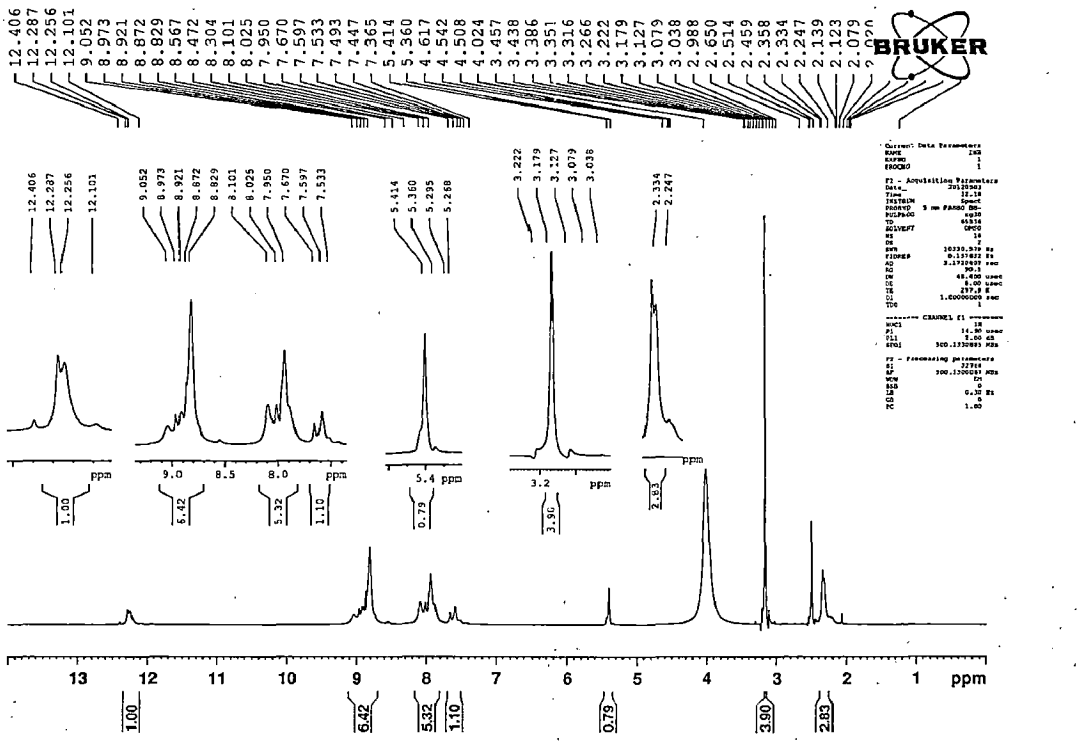

Figure 3.11. ^{1}H NMR spectra of $[V^{V}O(OMe)(MeOH)\{Hdfmp(inh)_2\}]$(**3.4**).

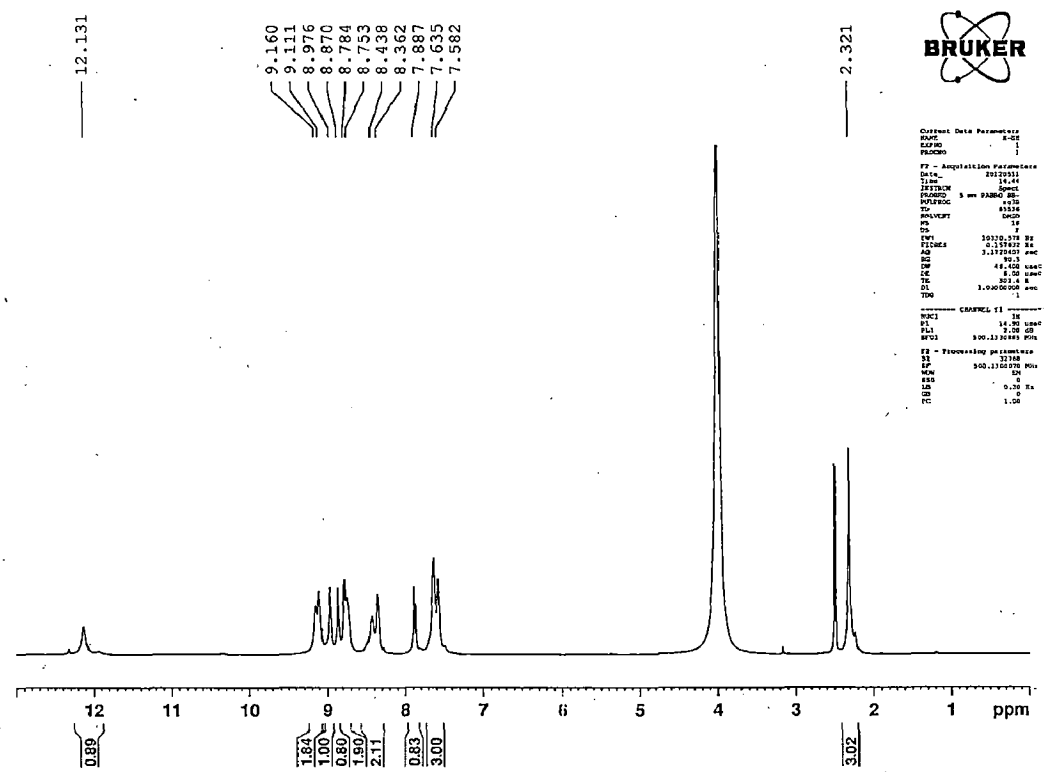

Figure 3.12. ^{1}H NMR spectra of $[V^{V}O_2\{Hdfmp(nah)_2\}]$ (**3.8**).

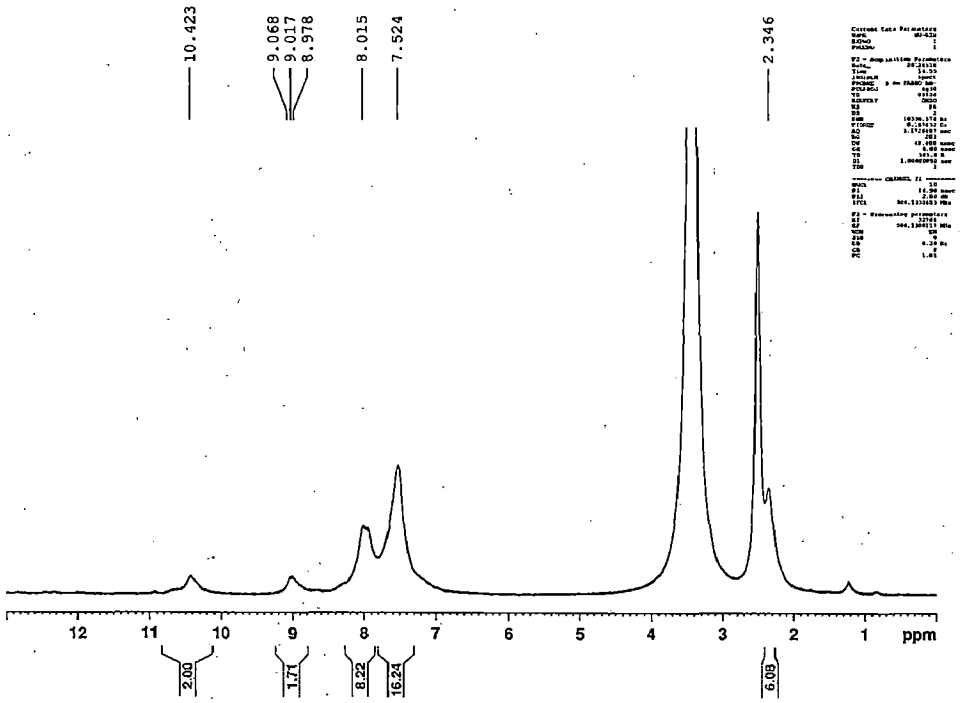

Figure 3.13. ^{1}H NMR spectra of [{$V^{V}O${Hdfmp(bhz)$_2$}}$_2\mu$ –O] (**3.12**).

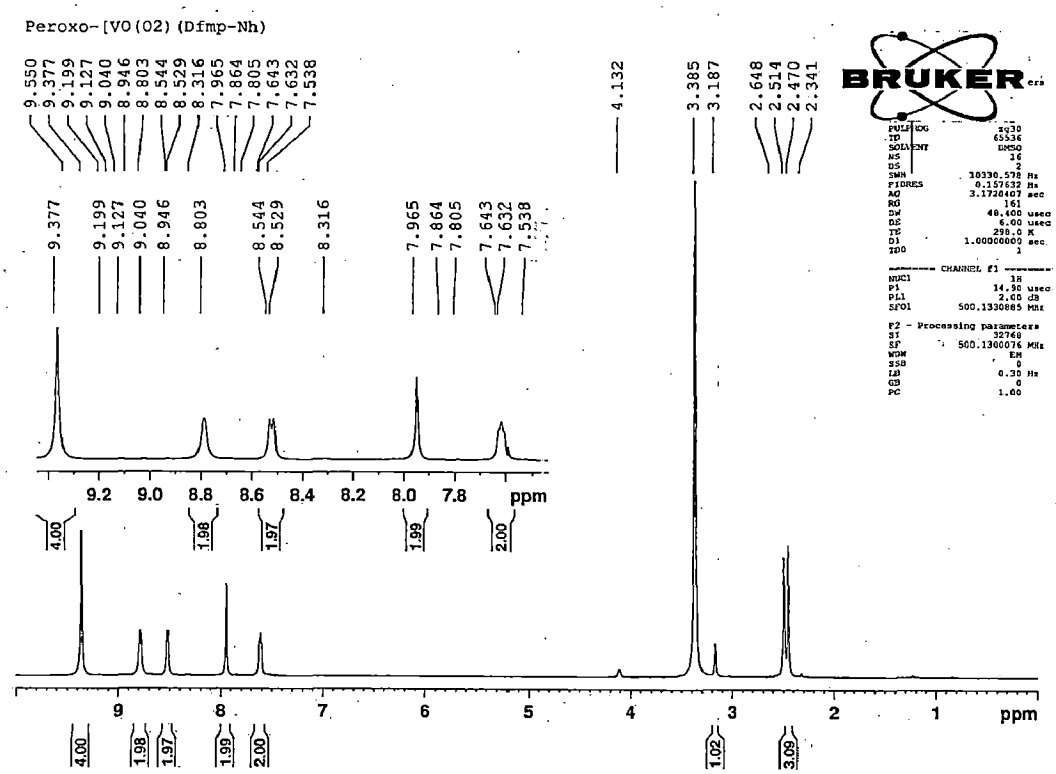

Figure 3.14. ^{1}H NMR spectra of $V^{V}O(O_2)${Hdfmp(nah)$_2$}] (**3.14**)

3.3.8. ^{13}C NMR Studies

^{13}C NMR spectra of the ligands and metal complexes were recorded in MeOD. All the spectra are in good agreement with the proposed structure. For examples, complex K[$V^{V}O_2${Hdfmp(nah)$_2$}] (**3.8**, Figure 3.15) shows 21 signals corresponding to the 21 C present in the system. All are well matched with predicted value of C atoms getting from Chemdraw 11.0.

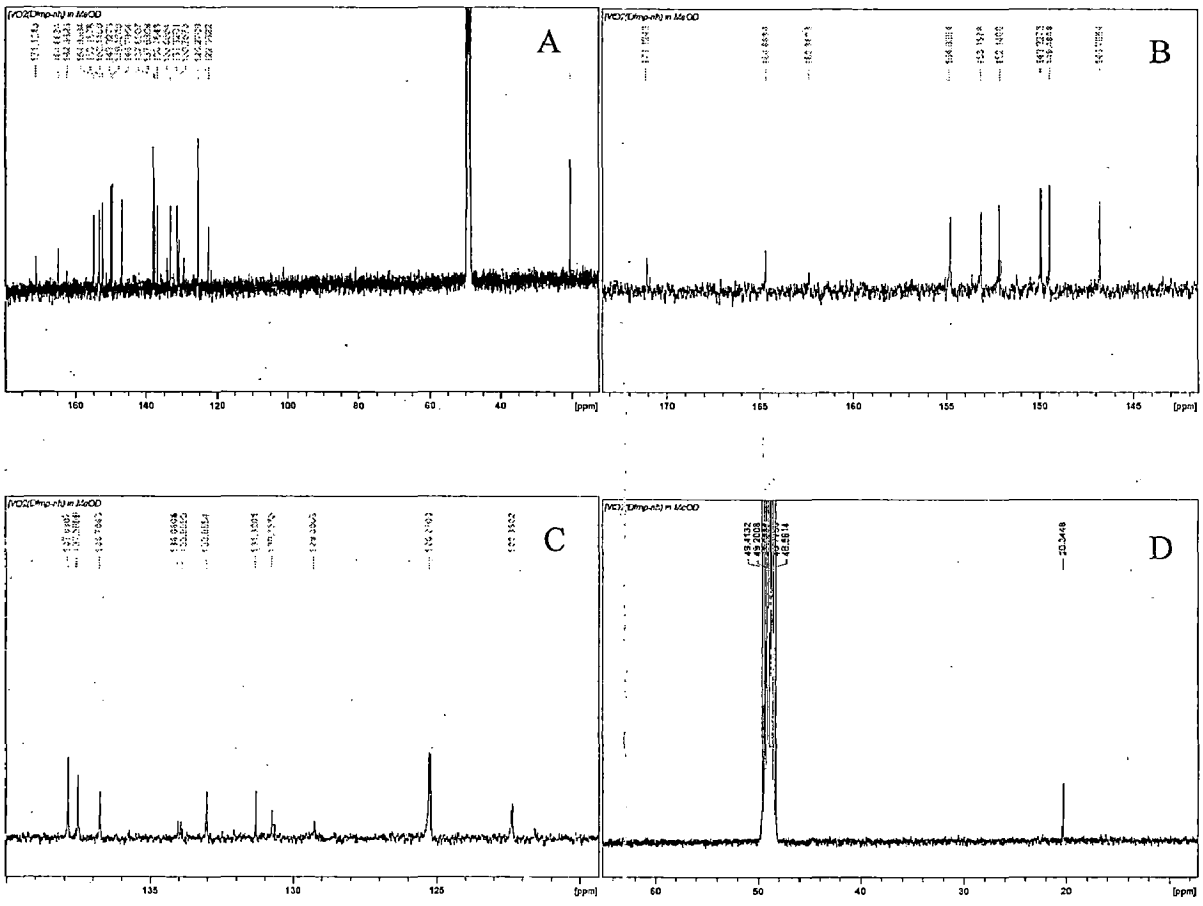

Figure 3.15. ^{13}C NMR spectra of the complex K[$V^{V}O_2${Hdfmp(nah)$_2$}] (**3.8**) in MeOD. A: complete spectrum, while B, C and D are the part of enlarged spectrum of A in different ranges.

3.3.9. ^{51} V NMR Spectra studies

Further characterization of the vanadium(V) complexes were obtained from ^{51}V NMR spectra; $\delta(^{51}V)$ values of specific compounds recorded in CD_3OD are presented Table 3.8 and some relevant spectra are presented in Figure 3.16. Owing to the quadrupole moment (spin 7/2) of the ^{51}V nucleus, the resonances are somewhat broadened; the line widths at half-height are typically ca. 200 Hz which may be considered comparatively narrow [172,173]. The dioxidovanadium(V) complexes $K[V^VO_2\{Hdfmp(nah)_2\}]$ (**3.8**) and $K[V^VO_2\{Hdfmp(bhz)_2\}]$ (**3.9**) exhibit a strong resonance at $\delta = -541$ and -534.6 ppm, respectively. These values are well within the expected shift for a dioxidovanadium(V) complexes having mixed O/N donor set [172,173,174]. Complex $[V^VO_2\{H_2dfmp(inh)_2\}]$ (**3.7**) exhibits two minor resonances at δ -544 and -549 ppm along with the major one at $\delta = -540$ ppm. Presence of the former two bands in $[V^VO(OMe)(MeOH)\{Hdfmp(inh)_2\}]$ (**3.4**) is in line to interpret these bands due to isomeric forms of methoxo complexes as complexes $[V^VO(OMe)(MeOH)\{Hdfmp(nah)_2\}]$ (**3.5**) and $[V^VO(OMe)(MeOH)\{Hdfmp(bhz)_2\}]$ (**3.6**) also exhibit two bands in the similar region. Peroxido complexes $[V^VO(O_2)\{Hdfmp(inh)_2\}]$ (**3.13**), $[V^VO(O_2)\{Hdfmp(nah)_2\}]$ (**3.14**) and $[V^VO(O_2)\{Hdfmp(bhz)_2\}]$ (**3.15**) show a minor resonance at $\delta = -603.5$ to -607 ppm due to the authentic peroxido complex and the major one at the position of dioxidovanadium(V) complexes. This indicates the poor stability of peroxido complexes and their conversion to the corresponding dioxido complexes.

Table 3.8. ^{51}V NMR data of the complexes recorded in MeOD.

Sl.No.	Compounds/ assignments →	VO_2	[VO(OMe)	[VO(O_2)
1	[V^{V}O(OMe)(MeOH){Hdfmp(inh)$_2$}] (**3.4**)		–545, –550	
2	[$V^{V}O_2${H_2dfmp(inh)$_2$}] (**3.7**)	–540	–544, –549	
3	[V^{V}O(O_2){Hdfmp(inh)$_2$}] (**3.13**)	–540		–606.4
4	[V^{V}O(OMe)(MeOH){Hdfmp(nah)$_2$}] (**3.5**)		–545, –549	
5	K[$V^{V}O_2${Hdfmp(nah)$_2$}] (**3.8**)	–541		
6	[V^{V}O(O_2){Hdfmp(nah)$_2$}] (**3.14**)	–541	–549	–603.5
7	[V^{V}O(OMe)(MeOH){Hdfmp(bzh)$_2$}] (**3.6**)		–540, –542	
8	K[$V^{V}O_2${Hdfmp(bzh)$_2$}] (**3.9**)	–534.6		
9	[V^{V}O(O_2){Hdfmp(bzh)$_2$}] (**3.15**)		–540	–607, –615

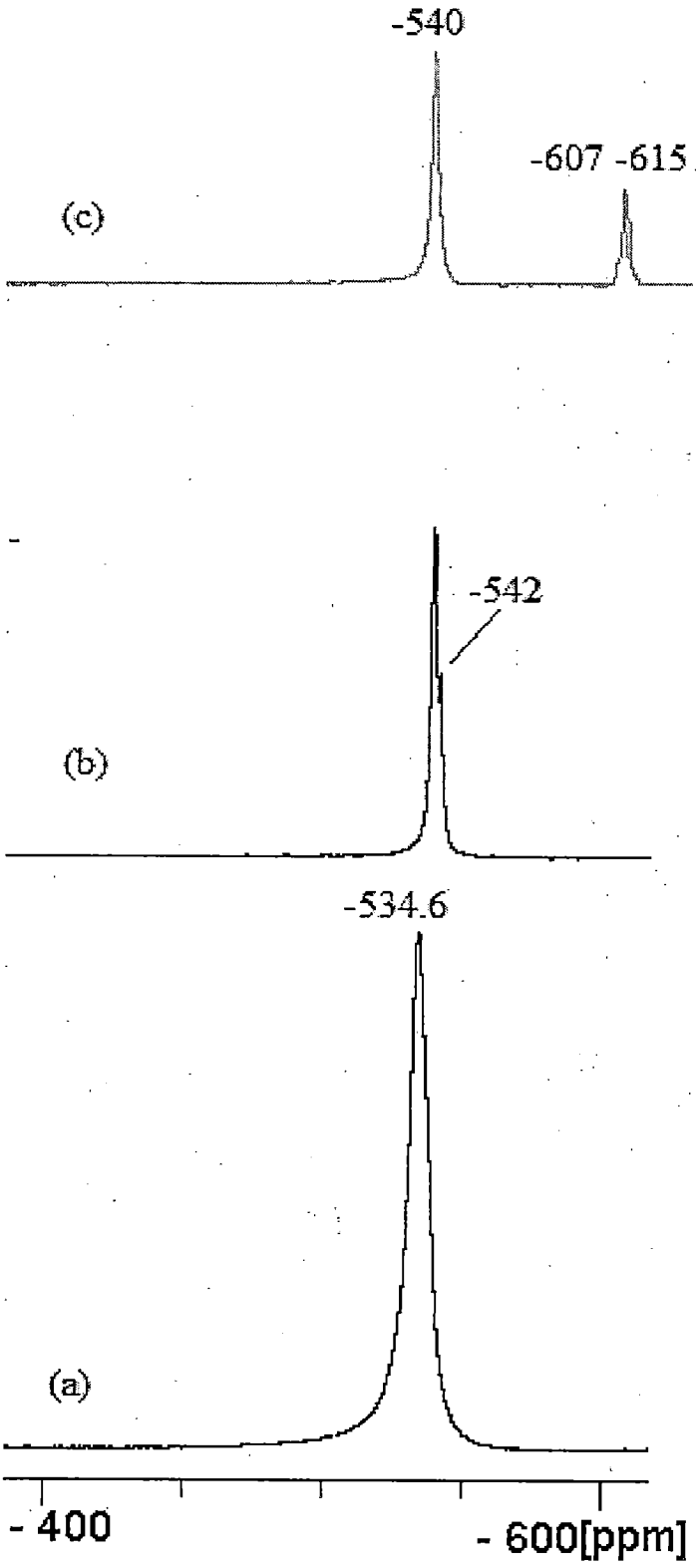

Figure 3.16. ^{51}V NMR Spectra of the Complex in MeOD. (a) $K[V^{V}O_2\{Hdfmp(bhz)_2\}]$ (**3.9**), (b) $[V^{V}O(OMe)(MeOH)\{Hdfmp(bzh)_2\}]$(**3.6**) and (c) $[V^{V}O(O_2)\{Hdfmp(bzh)_2\}]$ (**3.15**).

3.3.10. Reactivity of complexes

3.3.10.1. Reactivity of oxidovanadium(IV) and dioxidovanadium(V) complexes with H_2O_2

Solutions of $[V^{IV}O\{Hdfmp(inh)_2\}H_2O]$ (**3.1**), $[V^{IV}O\{Hdfmp(nah)_2\}H_2O]$ (**3.2**) $[V^{IV}O\{Hdfmp(bhz)_2\}H_2O]$ (**3.3**) in methanol are sensitive toward aqueous 30% H_2O_2, as monitored by electronic absorption spectroscopy. The d – d band is most sensitive to observe the changes and is presented in Figures 3.17. Thus, the progressive addition of a dilute 30% H_2O_2 solution in methanol to a solution of $[V^{IV}O\{Hdfmp(nah)_2\}H_2O]$ (**3.2**) in methanol results in the flattening of bands that appear at ca. 775 nm. Appearance of this band indicates the oxidation of oxidivanadium(IV) complex to higher oxidation state. At lower concentration, the intensity of the band at 427 nm slowly increases with a slight shift towards higher wavelength and stabilizes at 430 nm (in set of Figure 3.18), whereas the intensity of the band that appears in the UV region at 279 nm increases considerably and finally disappears. Simultaneously, the weak shoulder band at 343 nm slowly becomes further week. These changes indicate the interaction of $[V^{IV}O\{Hdfmp(nah)_2\}H_2O]$ (**3.2**) with H_2O_2 in methanol and formation of $[V^{V}O(O_2)\{Hdfmp(nah)_2\}]$. Very similar observations were recorded with other complexes **3.1** and **3.3**.

A methanolic solution of dioxidovanadium(V) complexes are also sensitive toward H_2O_2 dissolved in methanol. The reaction of a representative complex $[V^{V}O_2\{H_2dfmp(inh)_2\}]$ (**3.7**) with H_2O_2, as monitored by electron absorption spectroscopy (Figure 3.19), exhibits an increase in intensity and shift of the 427 nm band to 435 nm. Other medium intensity band at 280 nm of **3.7** gradually disappears with sharp increase in intensity. The relative stability of the peroxido species at approximately 10 °C in the presence of excess of H_2O_2 enabled us to isolate complexes $[V^{V}O(O_2)\{Hdfmp(inh)_2\}]$ (**3.13**), $[V^{V}O(O_2)\{Hdfmp(nah)_2\}]$ (**3.14**) and $[V^{V}O(O_2)\{Hdfmp(bhz)_2\}]$ (**3.15** (see Exp. Sect.), which showed that UV/Vis spectrum of $[V^{V}O_2\{H_2dfmp(inh)_2\}]$ (**3.7**) is similar to that observed here during spectroscopic studies. Other $[VO_2]^+$- complexes also have shown similar results. Interestingly, methoxido complexes (e.g. $[V^{V}O(OMe)(MeOH)\{Hdfmp(inh)_2\}]$ (**3.4**); Figure 3.20) show very similar spectral changes during their titrations with H_2O_2.

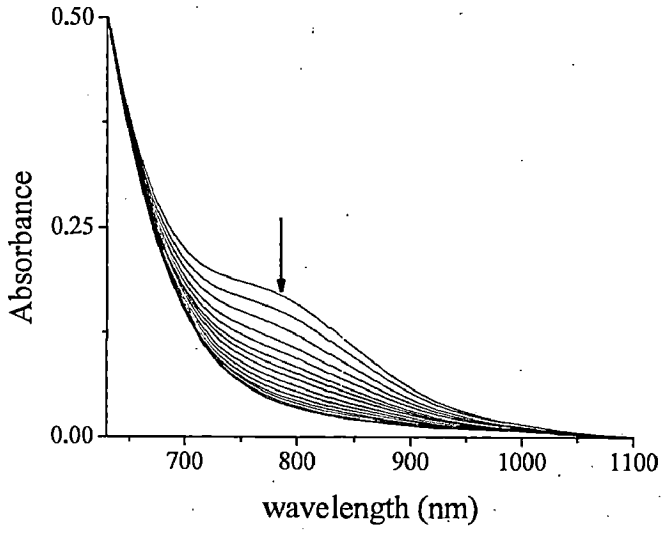

Figure 3.17. Spectral changes observed during titration of $[V^{IV}O\{Hdfmp(nah)_2\}H_2O]$ **(3.2)** with H_2O_2. The spectra were recorded upon stepwise additions of five drops portions of H_2O_2 [1.178 g (10.39 mmol) of 30% H_2O_2 dissolved in 10 mL of MeOH] to 40 mL of 7.5×10^{-3} M solution in MeOH.

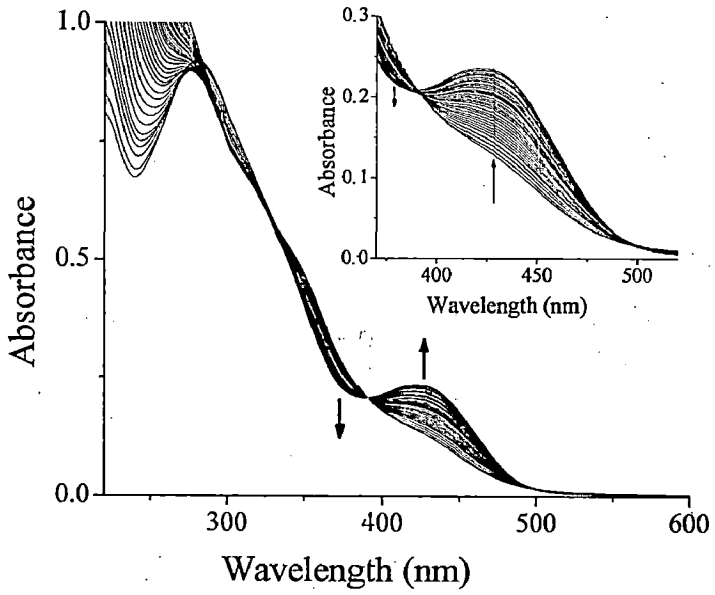

Figure 3.18. UV/Vis spectral changes observed during titration of $[V^{IV}O\{Hdfmp(nah)_2\}H_2O]$ **(3.2)** with H_2O_2. The spectra were recorded upon stepwise additions of five drops portions of H_2O_2 [1.178 g (10.39 mmol) of 30% H_2O_2 dissolved in 10 mL of MeOH] to 20 mL of 3.357×10^{-4} M solution in MeOH. The inset shows expanded spectral region (340 – 550 nm).

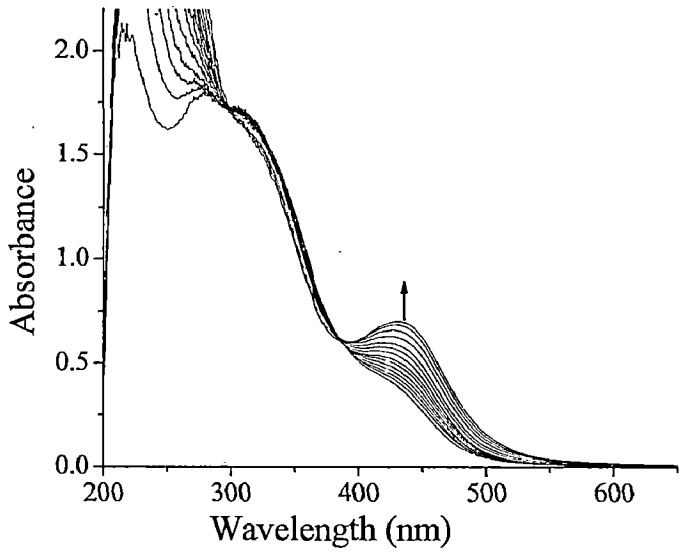

Figure 3.19. Titration of methanolic solution of $[V^{V}O_2\{H_2dfmp(inh)_2\}]$ (**3.7**) with H_2O_2. The spectra were recorded upon stepwise additions of five drops portions of H_2O_2 [1.178 g (10.39 mmol) of 30% H_2O_2 dissolved in 5 mL of MeOH] to 25 mL of 8.00 $\times 10^{-4}$ M solution in MeOH.

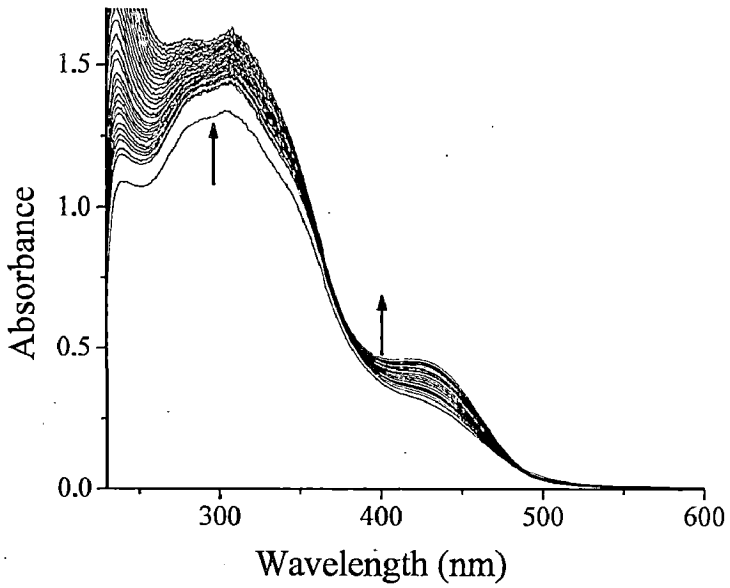

Figure 3.20. Spectral changes observed during titration of methanolic solution of $[V^{V}O(OMe)(MeOH)\{Hdfmp(inh)_2\}]$ (**3.4**) by 30% H_2O_2 dissolved in methanol. The spectra were recorded upon stepwise additions of five drops portions of H_2O_2 [1.178 g (10.39 mmol) of 30% H_2O_2 dissolved in 10 mL of MeOH] to 25 mL of 1.27 $\times 10^{-4}$ M solution in MeOH.

3.3.10.2.Titration with HCl saturated methanol

The reactivity of a methanolic solution of $[V^{V}O_2\{H_2dfmp(inh)_2\}]$ (**3.7**) with HCl was studied by drop wise addition of a methanolic solution saturated with HCl gas to 15 mL of a solution of **3.7** (ca. 6.86 $\times 10^{-5}$ M) and the observed changes are presented in Figure 3.21. The band appearing at 430 nm gains slight intensity and shifts to 448 nm. Simultaneously, the broad weak band appearing at 340 nm sharpens with slight gain in intensity. Band at 307 nm loses its intensity while the band at 277 nm shifts to 258 nm with gain in intensity. The solution became dark at the end. Such changes have been interpreted in term of the formation of oxidohydroxido species [52,53,54,147,151,152]. We also interpret our results assuming the formation of oxidohydroxido vanadium(V) species. Other complexes have very similar results.

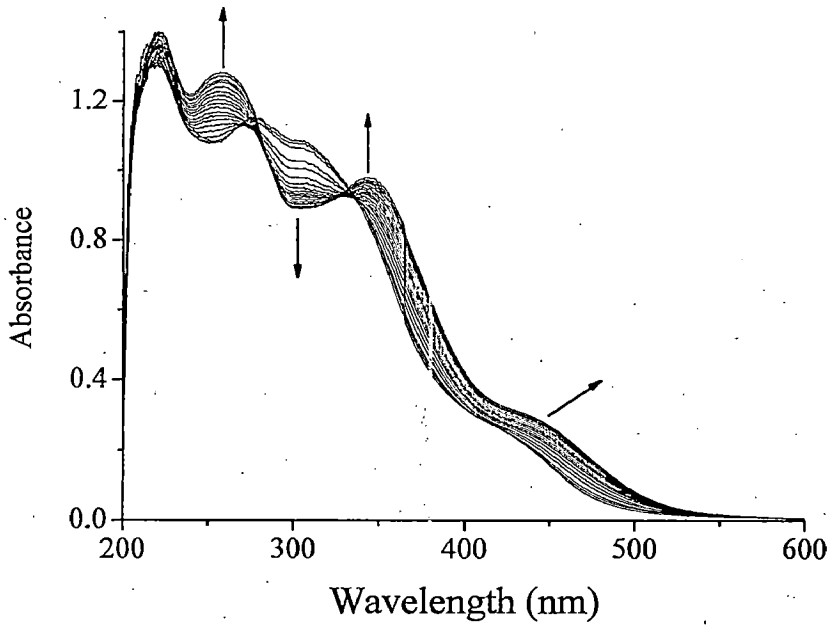

Figure 3.21. Titration of methanolic solution of $[V^{V}O_2\{H_2dfmp(inh)_2\}]$ (**3.7**) by HCl. The spectra were recorded upon stepwise additions of two drops portions of HCl saturated MeOH dissolved in 10 mL of MeOH to 15 mL of 6.86 $\times 10^{-5}$ M solution in MeOH.

3.3.11. Oxidative bromination of styrene

Oxidative bromination of styrene gave mainly three products i) 1,2-dibromo-1-phenylethane, ii) 2-bromo-1-phenylethane-1-ol and iii) 1-phenylethane-1,2-diol; Scheme 3.3, along with some minor products (benzaldehyde, styrene epoxide, benzoic acid and 4-bromostyrene). These are the normal oxidation products of styrene observed previously but are always forming in very less amount.

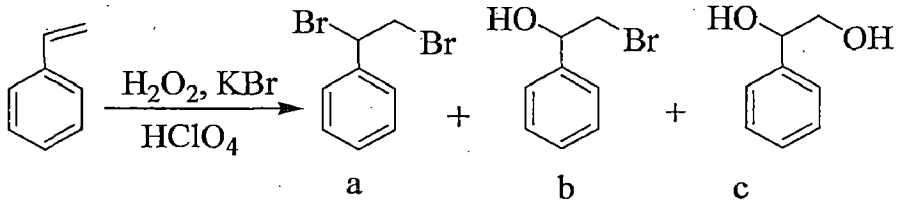

Scheme 3.3. Products on oxidative bromination of styrene.

In order to maximize the oxidative bromination of styrene the effects of following parameters have been studied in detail using $[V^{V}O_2\{H_2dfmp(inh)_2\}]$ as a representative catalyst:

i. Amount of catalyst
ii. Amount of H_2O_2
iii Amount of KBr and
iv. Amount of $HClO_4$

The effect of amount of catalyst on the oxidative bromination of styrene is shown in Figure 3.22. Three different amounts of catalyst were considered where the mixture of styrene (1.04 g, 10 mmol), catalyst (0.001 g), KBr (3.57 g, 30 mmol) and $HClO_4$ (1.43 g, 10 mmol) were taken in 40 mL dichloromethane-water (1:1 v/v) mixture and the reaction was carried out at room temperature. Another three extra 10 mmol of $HClO_4$ was added to the reaction mixture after every 15 min intervals. As shown in Figure 3.22, increasing the amount of catalyst from 0.001 g to 0.002 g and then to 0.003 g did not improve much the over all percentage conversion of the substrate but a major change in the selectivity of the products was observed. An amount of 0.001 g of catalyst gave 12% selectivity of

monobromo, 7% di-bromo and 74% di-ol derivatives at the end of 1 h. In case of 0.002 g catalyst, the selectivity of products followed the order: di-ol (75%) > mono-bromo (9%) = di-bromo (9%) while a selectivity order of di-ol (74%) > di-bromo (19%) > mono-bromo (2%) was obtained with 0.004 g of catalyst. Therefore, we have fixed 0.001 g of catalyst to optimized other conditions.

The effect of amount of oxidant (30% aqueous H_2O_2) on the oxidative bromination of styrene is illustrated in Figure 3.23. Under above condition, substrate to oxidant ratio of 1:1 gave 73% conversion with 63% selectivity of mono-bromo and 35% of di-ol derivatives. Increasing this ratio to 1:2 improved the conversion to 98% and this conversion remains almost constant on further increasing this ratio. Therefore, a substrate to H_2O_2 ratio of 1:2 was considered suitable to optimize other conditions.

Similarly, three different amount of KBr (10 mmol, 20 mmol and 30 mmol) were used while other reaction parameters such as 0.001 g catalyst $[V^{V}O_2\{H_2dfmp(inh)_2\}]$, styrene (1.04 g, 10 mmol), 30% H_2O_2 (2.27 g, 20 mmol), and $HClO_4$ (4.29 g, 30 mmol, added as described above) in 40 mL dichloromethane-water (1:1 v/v) mixture were kept constant and reaction was monitored at room temperature for 1 h. As shown in Figure 3.24, increasing the KBr amount from10 mmol to 20 mmol resulted in the rapid improvement in conversion from 49% to 97%. But further increament of KBr amount mainly reduced the time period to ca 50 min to complete the reaction and altered the selectivity of the products with no considerable improvement in the conversion. Analyses of reaction products show that 20 mmol KBr gives mono-bromo derivative with 60% selectivity and di-ol derivative with 38% selectivity, while 30 mmol KBr gives three products with the following order of selectivity: di-ol 75% > di-bromo (11%) > mono-bromo (9%).

Acid (here $HClO_4$) was found to be essential to carry out catalytic bromination. Its way of addition to the reaction mixture controls the stability of the substrate while its amount has great influence on the conversion and selectivity of products. The complexes slowly decompose during the reaction; decomposition is slowed down, if $HClO_4$ is successively added in four portions (first 10 mmol

portion at 0 time, other 20 mmol in three equal portions and second after 15 min and so on) during 1 h of reaction time. The effect of various amount of $HClO_4$ added in the reaction mixture as a function of the conversion of substrate is shown in the Figure 3.25. It is clear from the plot that 30 mmol of $HClO_4$ under above optimized reaction conditions are the best to achieve 96% conversion. Further increment of the $HClO_4$ only speeds up the reaction but does not make significant change on the product conversion.

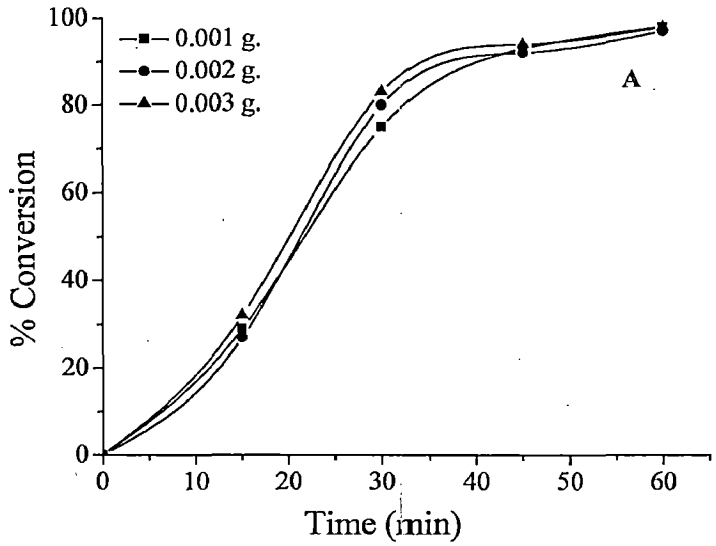

Figure 3.22. Effect of amount of catalyst on the oxidative bromination of styrene.

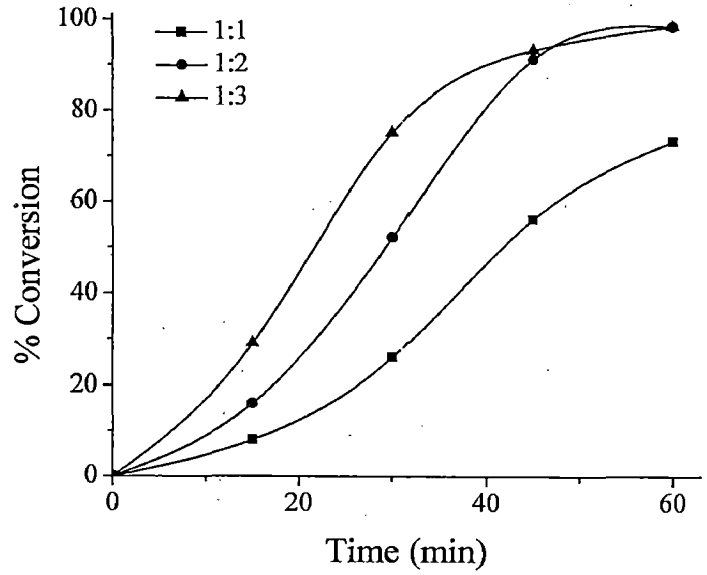

Figure 3.23. Effect of amount of styrene to oxidant ratio on the oxidative bromination of styrene.

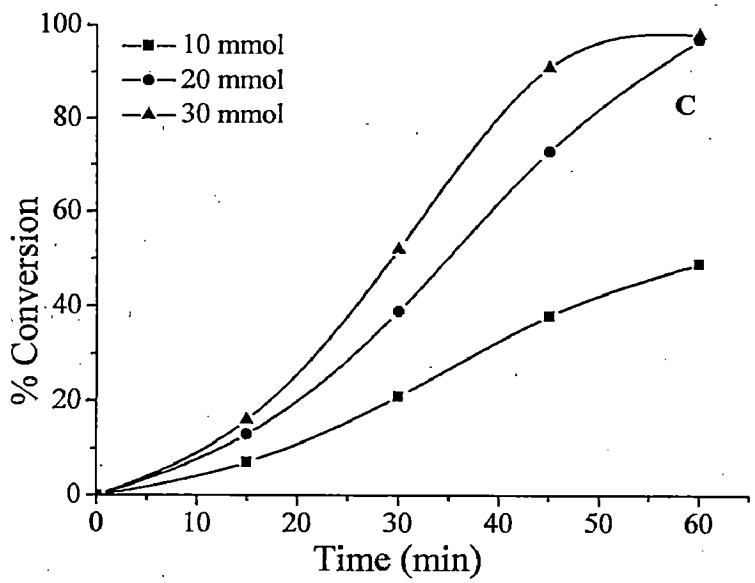

Figure 3.24. Effect of amount of KBr on the oxidative bromination of styrene.

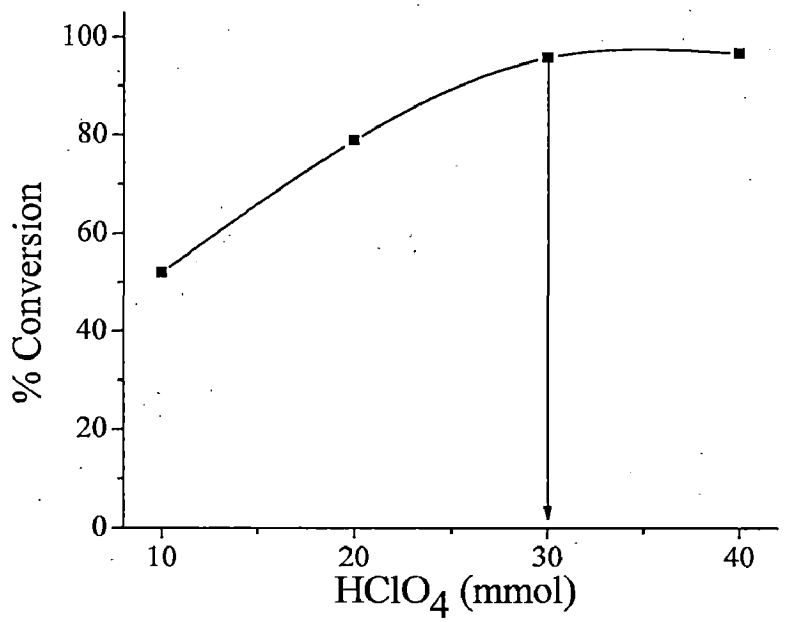

Figure 3.25. Effect of amount of $HClO_4$ on the oxidative bromination of styrene.

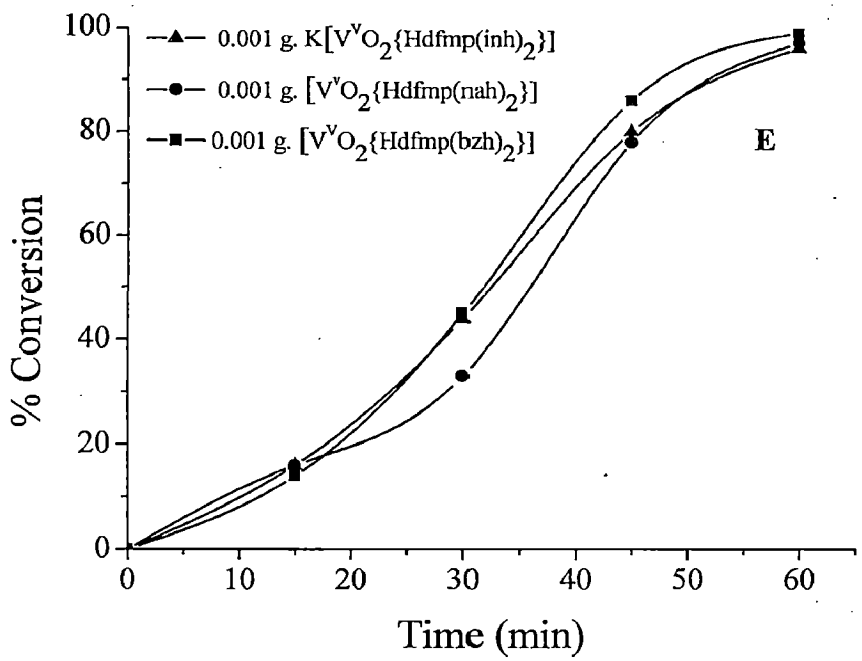

Figure 3.26. Effect of different catalyst on the conversion of oxidative bromination of styrene.

Table 3.9 provides all experimental details and conversion of styrene at different conditions. Figure 3.26 compares the catalytic potential of the three dioxidovanadium(V) complexes, $[V^{V}O_2\{H_2dfmp(inh)_2\}]$, $K[V^{V}O_2\{Hdfmp(nah)_2\}]$ and $K[V^{V}O_2\{Hdfmp(bhz)_2\}]$ under the optimised reaction conditions i.e. 0.001 g catalyst, 1.04 g (10 mmol) styrene, 2.27 g (20 mmol) 30% H_2O_2, 2.38 g (20 mmol) KBr and 4.29 g (30 mmol) $HClO_4$ in in 40 mL dichloromethane-water (1:1 v/v) mixture. Catalysts $K[V^{V}O_2\{Hdfmp(nah)_2\}]$ and $[V^{V}O_2\{H_2dfmp(inh)_2\}]$, show almost same conversion (ca. 97%) along with almost similar reaction curve but $K[V^{V}O_2\{Hdfmp(bhz)_2\}]$ shows a slightly better conversion (99 %).

Table 3.9. % conversion obtained at different conditions by using $[V^{V}O_2\{H_2dfmp(inh)_2\}]$ as catalyst in oxidative bromination of styrene.

Entry No.	Styrene	KBr	H_2O_2	$HClO_4$	Catalyst	Solvent (DCM/H_2O)	% Conv.
1.	1.04 g (10 mmol)	3.57 g (30 mmol)	3.405 g (30 mmol)	5.72 g (40 mmol)	0.001 g	20/20	98
2	1.04 g (10 mmol)	3.57 g (30 mmol)	3.405 g (30 mmol)	5.72 g (40 mmol)	0.002 g	20/20	97
3	1.04 g (10 mmol)	3.57 g (30 mmol)	3.405 g (30 mmol)	5.72 g (40 mmol)	0.003 g	20/20	98
4	1.04 g (10 mmol)	3.57 g (30 mmol)	1.135 g (10 mmol)	5.72 g (40 mmol)	0.001 g	20/20	73
5	1.04 g (10 mmol)	3.57 g (30 mmol)	2.27 g (20 mmol)	5.72 g (40 mmol)	0.001 g	20/20	98
6	1.04 g (10 mmol)	1.19 g (10 mmol)	2.27 g (20 mmol)	5.72 g (40 mmol)	0.001 g	20/20	49
7	1.04 g (10 mmol)	2.38 g (20 mmol)	2.27 g (20 mmol)	5.72 g (40 mmol)	0.001 g	20/20	97
8	1.04 g (10 mmol)	2.38 g (20 mmol)	2.27 g (20 mmol)	2.86 g (20 mmol)	0.001 g	20/20	79
9	1.04 g (10 mmol)	2.38 g (20 mmol)	2.27 g (20 mmol)	4.29 g (30 mmol)	0.001 g	20/20	96

We have also analysed the consumption of styrene and the formation of major products with time under the optimized experimental conditions for the catalyst $K[V^{V}O_2\{Hdfmp(bhz)_2\}]$; Figure 3.27. The formation of two products starts with the consumption of styrene. However, among the products formed, the formation of 1-phenylethane-1,2-diol reaches 40% (with 41% selectivity) at the end of 1 h. The formation of 2-bromo-1-phenylethane-1-ol (bromohydrin) initially increases and reaches to 61% (with 70% selectivity), and after ca. 45 min. of reaction it starts decreasing, being ca. 53% (with 54.0% selectivity) at the end of 1 h. Increasing the reaction time beyond 1 h, initiates the formation of the dibromide at the expense of bromohydrin while 1-phenylethane-1,2-diol remains almost constant. It should be noted here that for the catalytic oxidation of styrene the experimental conditions were set up for maximum conversion of styrene and the product obtained in higher relative amount was bromohydrin.

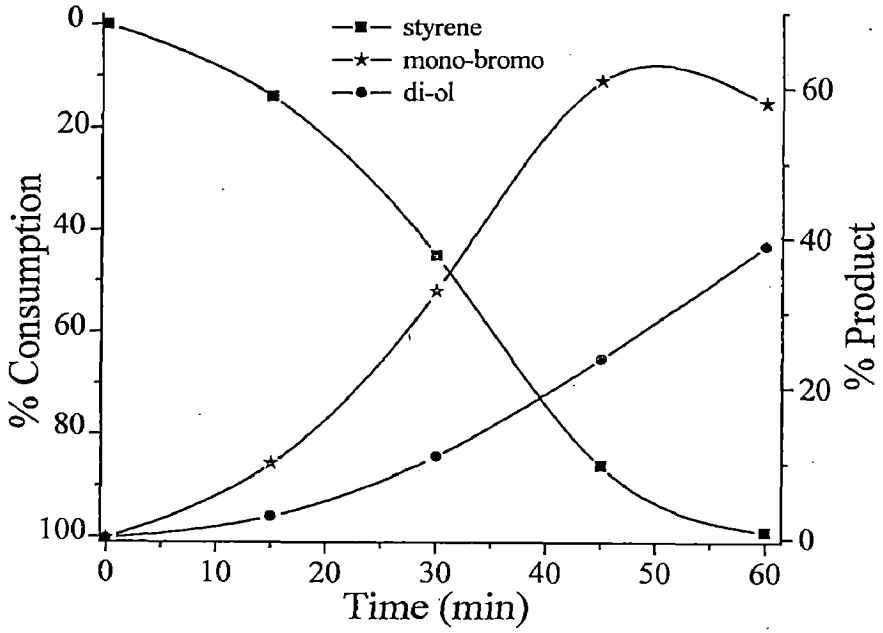

Figure 3.27. Diagram showing the % consumption of styrene with the % selectivity of the products for catalyst $K[V^{V}(O_2)\{Hdfmp(bhz)_2\}]$.

We have also tested the catalytic activity of methoxido complexes, $[V^{V}O(OMe)(MeOH)\{Hdfmp(inh)_2\}]$, $[V^{V}O(OMe)(MeOH)\{Hdfmp(nah)_2\}]$ and $[V^{V}O(OMe)(MeOH)\{Hdfmp(bhz)_2\}]$ for the oxidative bromination of styrene and optimized the various reaction conditions considering all factors mentioned above. Figure 3.28 show conditions applied and corresponding results. It is clear from the figures that nearly similar conditions are required for these complexes and that percentage conversions are also nearly same with all three complexes along with the selectivity of different products. The only difference is that 0.003 g of catalyst was required to obtain maximum conversion.

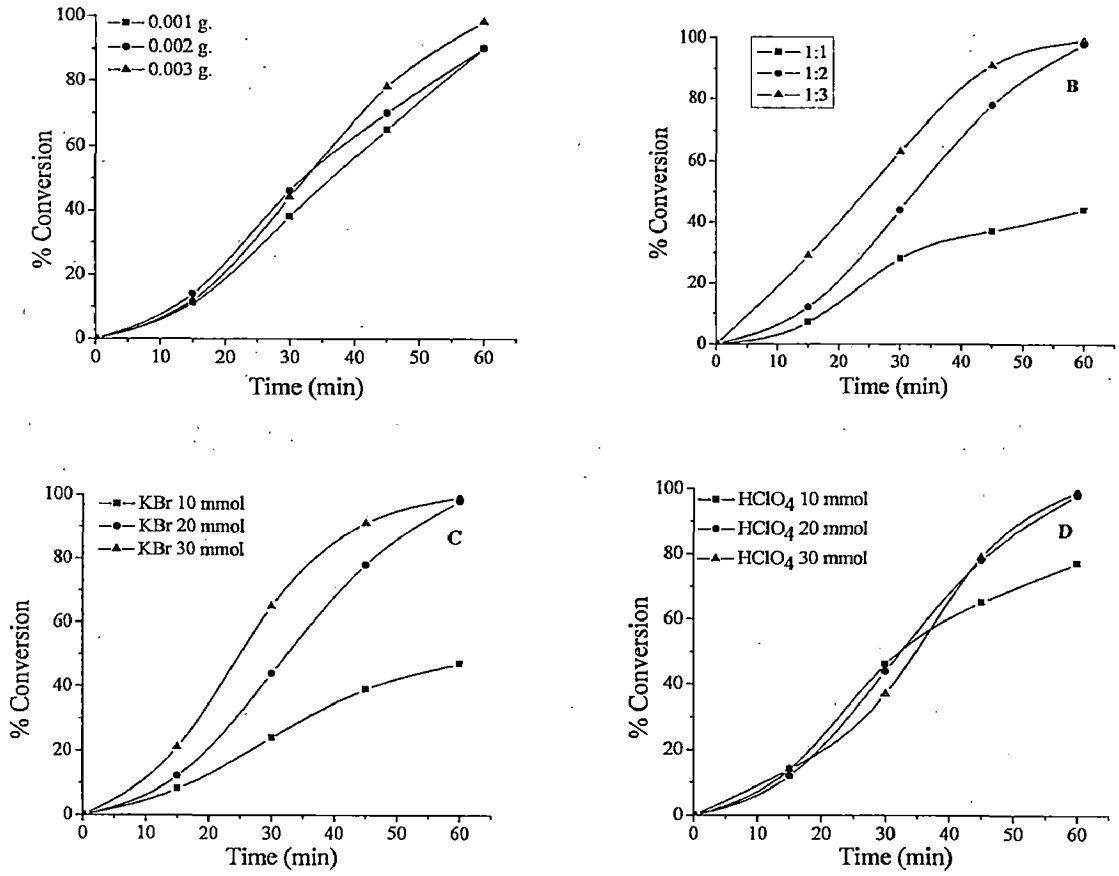

Figure 3.28. A) Effect of catalyst amount, B) effect of oxidant amount, C) effect of KBr and D) effect of $HClO_4$ on the oxidative bromination of styrene using $[V^{V}O(OMe)(MeOH)\{Hdfmp(nah)_2\}]$ as catalyst .

Table 3.10 compares the conversion of styrene and selectivity of products using methoxido and dioxido vanadium(V) complexes as catalysts.

Table 3.10. Product selectivity and % conversion at optimum reaction condition.

SL. No.	Catalyst	Catalyst amount	% Conv.	Selectivity (%)	
				Mono-bromo	di-ol
1.	$[V^{V}O(OMe)(MeOH)\{Hdfmp(nah)_2\}]$	0.003 g	98	58	40
2.	$K[V^{V}O_2\{Hdfmp(nah)_2\}]$	0.001 g	97	59	39

3.4. Conclusions

Three binucleating ligands H_3dfmp(inh)$_2$, H_3dfmp(nah)$_2$ and H_3dfmp(bhz)$_2$ derived from 2,6-diformyl-4-methylphenol and various hydrazides have been designed to prepare variety of vanadium complexes. All ligands utilize only one site of the coordinating functions. Concentrations of electron density on one site of the ligands promote only one site of functions in coordination. Oxidovanadium(IV) complexes, $[V^{IV}O\{Hdfmp(inh)_2\}\cdot H_2O]$ (**3.1**), $[V^{IV}O\{Hdfmp(nah)_2\}\cdot H_2O]$ (**3.2**) and $[V^{IV}O\{Hdfmp(bhz)_2\}\cdot H_2O]$ (**3.3**) undergo aerial oxidation in methanol with the formation of oxidomethoxido complexes $[V^{V}O(OMe)(MeOH)\{Hdfmp(inh)_2\}]$ (**3.4**), $[V^{V}O(OMe)(MeOH)\{Hdfmp(nah)_2\}]$ (**3.5**) and $[V^{V}O(OMe)(MeOH)\{Hdfmp(bhz)_2\}]$ (**3.6**). Neutral complex $[V^{V}O_2\{H_2dfmp(inh)_2\}]$ (**3.7**) has been prepared by the reaction of KVO_3 with potassium salt of inh based ligand at ca. pH 7. The presence of additional ring nitrogen in inh based ligand promotes the stabilization of neutral oxidovanadium(V) complex, $[V^{V}O_2\{H_2dfmp(inh)_2\}]$ (**3.7**) through protonation of ring nitrogen and coordination of the ring nitrogen of the second unit of ligand to vanadium. This has been confirmed by single crystal X-ray analysis of **3.7**. The nah and bhz based ligands provide potassium salts, $K[V^{V}O_2\{Hdfmp(nah)_2\}]$ (**3.8**) and $K[V^{V}O_2\{Hdfmp(bhz)_2\}]$ (**3.9**). The steric hindrance is possibly prevalent in nah based ligand to prevent the coordination of ring nitrogen. The methoxido complexes can be converted into the corresponding dinuclear complexes, e.g. **$[\{V^{V}O_2\{Hdfmp(inh)_2\}\}_2\mu$–O]** (**3.10**), $[\{V^{V}O_2\{Hdfmp(nah)_2\}\}_2\mu$–O] (**3.11**) and $[\{V^{V}O_2\{Hdfmp(bhz)_2\}\}_2\mu$–O] (**3.12**) on refluxing in dry acetonitrile.

The vanadium(V) complexes, **3.4** to **3.9** can be considered partly to be structural models of VHPO. These model characters extend to functional similarities, in that these complexes catalyse the oxidative bromination of styrene. These complexes can also be converted, by treatment with H_2O_2, to the corresponding peroxido complexes, $[V^{V}O(O_2)\{Hdfmp(inh)_2\}]$ (**3.13**), $[V^{V}O(O_2)\{Hdfmp(nah)_2\}]$ (**3.14**) and $[V^{V}O(O_2)\{Hdfmp(bhz)_2\}]$ (**3.15**) and thus to an intermediate in the catalytic cycle representing the activity of VHPO.

Chapter-4

- Mn(III) complexes of monoprotic tridentate ONN donor 2-[2-(1H-(benzo[d]imidazol-2-yl)ethylimino)methyl]phenol as functional mimic of haloperoxidases.

Mn(III) complexes of monoprotic tridentate ONN donor 2-[2-(1H-(benzo[d]imidazol-2-yl)ethylimino)methyl]phenol as functional mimic of haloperoxidases

4.1. Introduction

Benzimidazole or its derivatives are present in Vitamin B_{12} and related biomolecules. Additionally, ring nitrogen of benzimidazole group containing lignads in metal complexes partly provides model for the coordination of imidazole of histidine in several enzymes [175,176,46], Ligand 2-[2-(1H-(benzo[d]imidazol-2-yl)ethylimino)methyl]phenol (Hsal-aebmz, **4.I**), derived from salicylaldehyde and 2-aminoethylbenzimidazole, Scheme **4.1**) is a monobasic tridentate ligand having appended benzimidazole group. Structural and functional models for haloperoxidases have been prepared successfully using **4.I**. Such one or two ligands can coordinate to the metal ions depending upon the requirement of coordination number of metal ions and stabilize its complexes in different coordination geometry. [46,177]. Additionally, same metal in different oxidation states can also be stabilized depending upon whether deprotonation of ring -NH, no protonation, protonation of only one of the two ring nitrogens or both. Its vanadium complexes are known to undergo protonation/ deprotonation of ring nitrogen stabilizing the complexes in both forms.

In the present chapter we report two manganese(III) complexes with monoprotic tridentate ONN donor ligand **4.I**. While complex $[Mn^{III}(sal\text{-}aebmz)_2]ClO_4$ is the expected one, the intriguing feature of the other complex $[(sal\text{-}aebmz\text{-}H)Mn^{III}(sal\text{-}aebmz)_2]$ is the compensation of three units of cationic charge by two molecules of the ligand, giving indications that the complexation behavior of this traditionally tridentate monoprotic ligands is not straightforward and demands complete investigation. Therefore, we report the synthesis, crystal and molecular structures, spectroscopic characterization, and redox properties of these complexes, showing the diversities in their coordination properties. Manganese complexes with a mixed ON coordination sphere have been studied extensively due to their potential as (i) SOD mimics [178,179], (ii) structural models for manganese containing enzymes [81,180-184] and (iii) catalytic activities [82,84].

Oxidative bromination of styrene catalyzed by the neutral complex, a functional mimic of haloperoxidases, has also been reported here.

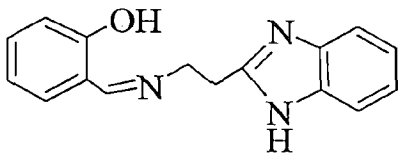

Hsal-aebmz (**4.I**)

Scheme 4.1. Structure of Hsal-aebmz (**4.I**).

4.2. Experimental Section

4.2.1. Materials

Analytical reagent grade maganese(II) chloride, manganese(II) perchlorate hexhydrate, 30 % aqueous H_2O_2 (E. Merck, India), *β*-alanine (Spectrochem, Mumbai, India), styrene (Acros Organics, U.S.A.), *o*-phenylenediamine and salicylaldehyde (Qualigens, Mumbai, India) were used as obtained. 2-Aminoethylbenzimidazole dihydrochloride (aebmz·2HCl) [185] and Hsal-aebmz (**4.I**) [46] were prepared according to methods reported in the literature. All other chemicals and solvents used were of AR grade.

4.2.2. Physical Method and Analysis

Magnetic susceptibilities of complexes were determined at 298 K with a Vibrating Sample Magnetometer model 155, using nickel as a standard. Diamagnetic corrections were carried out with Pascal's increments [186]. Cyclic voltammograms of the complexes were recorded in the potential range of –0.3 to 0.6 V in DMF (dried over molecular sieves), using 0.1 M tetrabutylammonium perchlorate (TBAP) as a supporting electrolyte. Ag/AgCl as reference electrode, glassy carbon as working electrode and platinum wire as auxillary electrode were used while scan rate was fixed at 0.1 V/s. Thermogravimetric analyses of the complexes were carried out using Perkin-Elmer (Pyris Diamond) instrument in air with a heating rate of 10 °C/min. Other experimental details are given in chapter 2.

4.2.3. Preparations

4.2.3.1. $[Mn^{III}(sal\text{-}aebmz)_2]\cdot ClO_4$ (4.1)

A solution of $MnClO_4\cdot 6H_2O$ (1.81 g, 5 mmol) in methanol (25 ml) was added to a stirred solution of Hsal-aebmz (2.65 g, 10 mmol) in methanol (40 mL) and the reaction mixture was stirred for ca. 5 h. Air was slowly passed through the resulting brown solution for 1 day. After reducing the solvent volume to ca. 10 ml and keeping the flask at room temperature complex **4.1** separated out within over night. This was filtered, washed with methanol and dried. Yield: 2.225 g (65.2 %). *Anal.* Calc. for $C_{32}H_{28}N_6O_6ClMn$ (683.00): C, 56.2; H, 4.1; N, 12.3. Found: C, 56.42; H, 4.13; N, 12.02%.

4.2.3.2. $[Mn^{III}(sal\text{-}aebmz\text{-}H)(sal\text{-}aebmz)]$ (4.2)

A stirred solution of Hsal-aebmz (1.060 g, 4 mmol) and trietylamine (0.404 g, 4 mmol) in methanol (30 ml) was treated with a solution of $MnCl_2.4H_2O$ (0.396 g, 2 mmol) in methanol (20 ml) and the reaction mixture was stirred for 5 h. Air was slowly passed through the resulting brown solution for 1 day. After reducing the solvent volume to ca. 10 ml, flask was kept at room temperature where **4.2** separated out within over night. This was filtered, washed with methanol and dried. Yield: 0.525 g (45.1 %). *Anal.* Calc. for $C_{32}H_{27}N_6O_2Mn$(582.54): C, 65.9; H, 4.6; N, 14.4. Found: C, 65.66; H, 4.72; N, 14.27%.

4.2.4. Oxidative bromination of styrene

Complex $[Mn^{III}$(sal-aebmz-H)(sal-aebmz)] (**4.2**) is used catalyst to carry out the oxidative bromination of styrene. Styrene (1.04 g, 10 mmol) was added to an aqueous solution (20 mL) of KBr (3.57 g, 30 mmol), followed by addition of 20 mL CH_2Cl_2 and 30% aqueous H_2O_2 (3.40 g, 30 mmol) in a 100 mL reaction flask. The catalyst (0.001 g) and 70% $HClO_4$ (1.43 g, 10 mmol) were added, and the reaction mixture was stirred at room temperature. Three additional 10 mmol portions of 70% $HClO_4$ were further added after every 15 minutes with continuous stirring. In all batches the experimental conditions (e.g. stirring speed, size of magnetic bar and reaction flask) were kept as similar as possible. After 1 h the

orange colored organic layer was separated by separatory funnel, washed with water and dried. The crude mass was redissolved in CH_2Cl_2 and after filtering the solvent evaporated. The reaction products were separated using a silica gel column. Elution of the column with 1% CH_2Cl_2 in n-hexane first separated a mixture of bromo derivatives followed by 1-phenylethane-1,2-diol. The two bromo derivatives were finally separated from each other using the silica gel column again by eluting with pure n-hexane. The identity of all products was confirmed by GC–MS and ^{1}H NMR.

1,2-Dibromo-1-phenylethane: ^{1}H-NMR ($CDCl_3$, δ/ ppm): 7.29-7.39 (m, 5H), aromatic), 5.11-5.13 (q, 1H, CH), 3.97-4.06 (septet, 2H, CH_2).

1-Phenylethane-1,2-diol: ^{1}H-NMR ($CDCl_3$, δ/ ppm) 7.29-7.39 (m, 5H, aromatic), 4.9 (q, 1H, CH), 3.5 (q, 1H of CH_2), 3.6 (q, 1H of CH_2), 2.7 (b, OH).

2-Bromo-1-phenylethane-1-ol: ^{1}H-NMR ($CDCl_3$, δ/ ppm): 7.29-7.39 (m, 5H, aromatic), 5.1 (q, 1H, CH), 3.9 (septet, 2H, CH_2.

4.2.5. X-Ray crystal structure determination of 4.2

Three-dimensional X-ray data were collected on a Bruker Kappa Apex CCDC diffractometer at low temperature for [Mn^{III}(sal-aebmz-H)(sal-aebmz)] (**4.2**) by the ϕ-ω scan method. Reflections were measured from a hemisphere of data collected from frames each of them covering 0.3° in ω. Of the 40784 reflections measured, all were corrected for Lorentz and polarization effects and for absorption by multi-scan methods based on symmetry-equivalent and repeated reflections, 3195 independent reflections exceeded the significance level ($|F|/\sigma|F|$) > 4.0. Complex scattering factors were taken from the program package SHELXTL [166]. The structures were solved by direct methods and refined by full matrix least-squares on F^2. Hydrogen atoms were left to refine freely with isotropic thermal parameters, except hydrogen atoms of C(31), which was included in calculated positions and refined in the riding mode. Refinement

was done with allowance for thermal anisotropy of all non-hydrogen atoms. Further details of the crystal structure determination are given in Table **4.1.**

Table 4.1. Crystal data and structure refinement for [Mn^{III}(sal-aebmz-H)(sal-aebmz)] (**4.2**).

	4.2
Formula	$C_{32}H_{27}MnN_6O_2$
Molecular weight	582.54
Crystal system	Orthorhombic
Space group	Pbca
T/K	100(2)
a/Å	18.0517(9)
b/Å	14.6821(6)
c/Å	20.1716(7)
V/Å^3	5346.2(4)
F_{000}	2416
Z	8
D_{calc}/g cm^{-3}	1.447
μ/mm^{-1}	0.537
θ	2.02-25.14
R_{int}	0.0990
Goodness-of-fit on F^2	1.003
R_1[a]	0.0402
wR_2 (all data)[b]	0.1227
Largest differences peak and hole (eÅ^{-3})	-0.554 and 0.526

[a] $R_1 = \Sigma||F_o|-|F_c||/\Sigma|F_o|$. [b] $wR_2 = \{\Sigma[w(|F_o|^2-|F_c|^2)^2]/\Sigma[w(F_o^4)]\}^{1/2}$

4.3. Results and discussion

Reaction of $Mn(ClO_4)_2$ with Hsal-aebmz (**4.I**) in 1 : 2 molar ratio in methanol under aerobic conditions yields an ionic complex , $[Mn^{III}(sal\text{-}aebmz)_2]\cdot ClO_4$ (**4.1**). In the presence of triethylamine and using $MnCl_2$ under similar condition ligand forms $[Mn^{III}(sal\text{-}aebmz\text{-}H)(sal\text{-}aebmz)]$ (**4.2**), which is a neutral species apparently stabilized, in the solid state, through inter molecular hydrogen bonding between NH groups of the two benzimidazole moieties after losing one of the hydrogen atoms. Equations (4.1) and (4.2) show the reaction involved.

$$2Mn^{II}(ClO_4)_2 + 4Hsal\text{-}aebmz + \tfrac{1}{2}\,O_2 \rightarrow 2[Mn^{III}(sal\text{-}aebmz)_2]\cdot ClO_4 + 2HClO_4 + H_2O \qquad (4.1)$$

$$2MnCl_2 + 4Hsal\text{-}aebmz + 4NEt_3 + \tfrac{1}{2}\,O_2 \rightarrow 2[Mn^{III}(sal\text{-}aebmz\text{-}H)(sal\text{-}aebmz)] + 4NEt_3HCl + H_2O \qquad (4.2)$$

Characterization of these complexes are based on spectroscopic (IR, and UV-vis) data, elemental analyses, and X-ray diffraction analysis of complex **4.2.** Both complexes are soluble in methanol, ethanol, acetonitrile, DMF and DMSO. Complex **4.1** is 1:1 electrolyte in DMF with molar conductance of 23.1 $ohm^{-1}\ cm^2\ mol^{-1}$ while **4.2** is a non-electrolyte (Λ_M = 1.6 $ohm^{-1}\ cm^2\ mol^{-1}$). The room temperature magnetic moment value of 4.87 μ_B (for **4.1**) and 4.93 μ_B (for **4.2**) are well within the range of magnetic moment reported for a magnetically dilute octahedral high-spin d^4 manganese (III) complexes [187,188].

4.3.1. Description of structure of $[Mn^{III}(sal\text{-}aebmz\text{-}H)(sal\text{-}aebmz)]$ (4.2)

Figure 4.1 shows the ORTEP diagram of the complex $[Mn^{III}(sal\text{-}aebmz\text{-}H)(sal\text{-}aebmz)]$ (**4.2**). Selected bond distances and angles are given in Table 4.2. The structure contain neutral complex of Mn(III) with two sal-aebmz ligands occupying the six coordination positions in a distorted octahedral geometry. One of the ligands (sal-aebmz-H) is deprotonated in the two benzimidazole nitrogen atoms. The ligands coordinate to the Mn(III) across of the deprotonated phenolic

oxygen, the imine nitrogen and the deprotonated benzimidazole nitrogen atoms acting as tridentate. The sal-aebmz ligands are meridionally bound, so that the imine nitrogen atoms are in trans to each other and the deprotonated phenolic oxygen atoms are in trans with respect to the deprotonated benzimidazole nitrogen atoms of the same ligand (Figure 4.2). The meridional coordination is directed by the C=N imine group, and is common to structures with this bond [189]. The N(2)-Mn(1)-N(6) interligand angle of 175.45(10)° is below the theoretical value of 180°. In addition the cis angles comprised between 84.16° and 96.49° are above 90°. The average bond distances for each set of Mn-$O_{phenolic}$, Mn-$N_{benzimidazole}$ and Mn-N_{imine} in this complex are 1.903(2), 2.044(3) and 2.252(3) Å, and are shorter than similar Mn(II) complexes with tridentate Schiff bases [189]. Intermolecular hydrogen bonding between protonated and deprotonated non-coordinated benzimidazole nitrogen atoms control the molecular packing (see Figure 4.3). No π-π stacking interactions are found.

4.3.2. Thermogravimetric analysis

Complex $[Mn(sal\text{-}aebmz)_2]\cdot ClO_4$ is stable upto ca. 100 °C and thereafter starts losing weight exothermically. The complete loss of perchlorate group occurs at ca. 300 °C (Obs. 14.3%; Cal. 14.6%). After this, complex decomposes in three major but overlapping steps and stabilizes with ca. 12% residue at ca. 650 °C which corresponds to Mn_2O_3 (Cal. 11.56%). Neutral complex [Mn^{III}(sal-aebmz-H)(sal-aebmz)] has extended thermal stability up to 235 °C. Further increasing temperature causes the exothermic decomposition of the complex in three steps which completes at ca. 650 °C with ca. 13% residue (Cal. for Mn_2O_3 = 13.54%). No further loss in weight for both complexes is observed beyond 650 °C. Approximation of the decomposition of particular group was not possible in both cases.

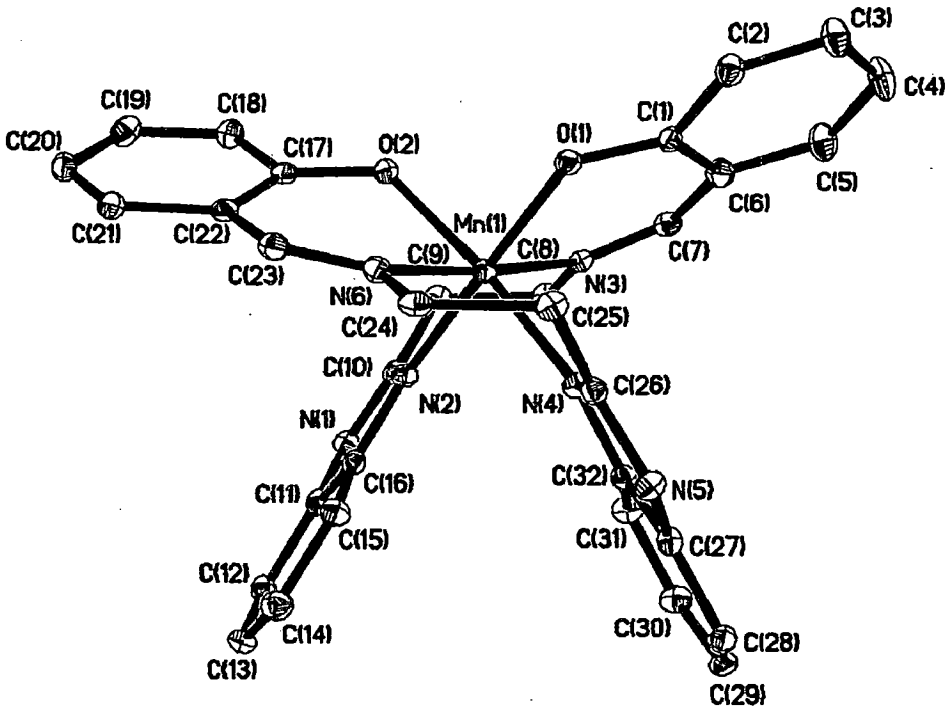

Figure 4.1. ORTEP plot of the complex [Mn^{III}(sal-aebmz-H)(sal-aebmz)] (**4.2**). All the non-hydrogen atoms are presented by their 30% probability ellipsoids. Hydrogen atoms are omitted for clarity.

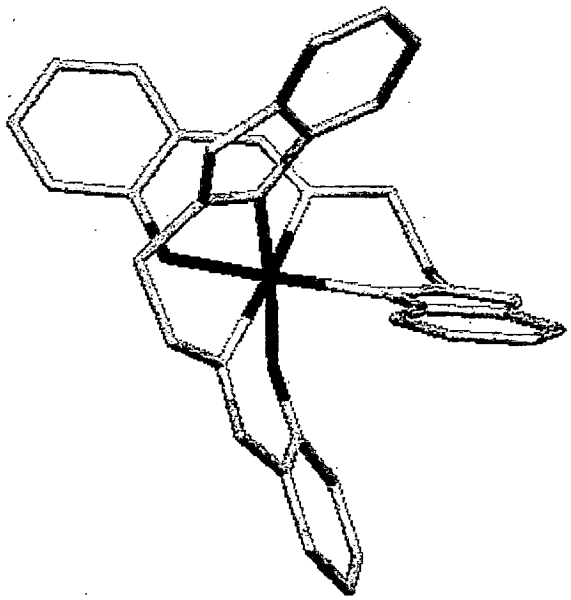

Figure 4.2. Capped sticks showing the coordination in trans of the deprotonated phenolic oxygen atoms respect to the benzimidazole nitrogen atoms of the same sal-aebmz ligand.

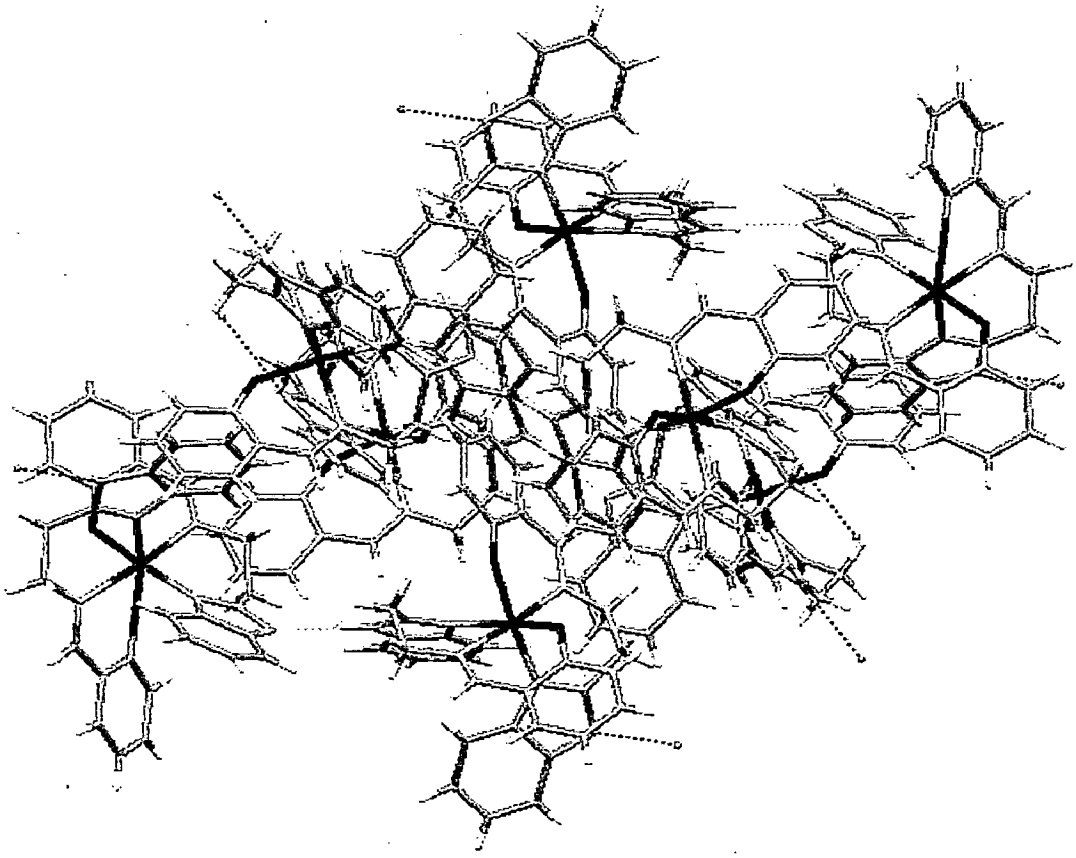

Figure 4.3. Crystal packing of the complex [Mn^{III}(sal-aebmz-H)(sal-aebmz)] (**4.2**). Hydrogen bonding interactions (dashed blue lines) as D-H, H···A, D···A (Å) and D-H···A(°): N(5)-H···N(1): 0.89(4), 1.99(4), 2.877(4) and 171(3); symmetry transformations: [x-1/2, y, -z+1/2]

Table 4.2. Selected bond lengths and bond angles for [Mn^{III}(sal-aebmz-H)(sal-aebmz)] (**4.2**).

Bond lengths (Å)		Bond angles (°)	
Mn(1)-O(1)	1.873(2)	O(1)-Mn(1)-O(2)	89.08(10)
Mn(1)-O(2)	1.934(2)	O(1)-Mn(1)-N(2)	174.88(10)
Mn(1)-N(2)	1.986(3)	O(2)-Mn(1)-N(2)	89.76(10)
Mn(1)-N(3)	2.213(3)	O(1)-Mn(1)-N(4)	90.92(10)
Mn(1)-N(4)	2.101(3)	O(2)-Mn(1)-N(4)	168.82(9)
Mn(1)-N(6)	2.290(3)	N(2)-Mn(1)-N(4)	91.19(11)
N(1)-C(10)	1.325(4)	O(1)-Mn(1)-N(3)	87.17(9)
N(1)-C(11)	1.394(4)	O(2)-Mn(1)-N(3)	94.97(9)
O(1)-C(1)	1.327(4)	N(2)-Mn(1)-N(3)	87.97(10)
O(2)-C(17)	1.322(4)	N(4)-Mn(1)-N(3)	96.20(10)
N(2)-C(10)	1.367(4)	O(1)-Mn(1)-N(6)	88.35(9)
N(2)-C(16)	1.391(4)	O(2)-Mn(1)-N(6)	84.16(9)
N(3)-C(7)	1.276(4)	N(2)-Mn(1)-N(6)	96.49(10)
N(3)-C(8)	1.474(4)	N(4)-Mn(1)-N(6)	84.66(10)
N(4)-C(26)	1.333(4)	N(3)-Mn(1)-N(6)	175.45(10)

4.3.3. IR Spectral studies

A partial list of IR spectral data is presented in Table 4.3. The ligand exhibits a broad band at ca. 3445 cm^{-1} due to ν(OH) stretch and absence of this band in complexes suggests the coordination of the phenolic oxygen atom after deprotonation. A sharp band appearing at 1634 cm^{-1} due to ν(C=N) (azomethine) moves toward lower wave numbers on coordination of the azomethine nitrogen to the manganese [46]. A strong band at 1425 cm^{-1} due to ν(-C=N-C=C-) in the free ligand shifts to 1450-1460 thereby indicating the coordination of the imine nitrogen of the benzimidazolyl group [177]. These complexes also exhibit two medium intensity bands at 455 – 457 and 576 – 629 cm^{-1} due to ν(Mn-N) and ν(M-O) stretches, respectively. The presence of several medium intensity bands between 2500 and 2700 cm^{-1} in the ligand, as well as in complexes, hints the existence of hydrogen bonding between NH of benzimidazole and other electronegative atoms. In addition, complex **4.1** exhibits two band at 1095 and 629 cm^{-1} which is well within the range reported for anionic perchlorate ion [190].

Table 4.3. IR spectral data (cm^{-1}) of ligand and complexes.

Compound	ν (C=N)	ν (Mn-N)	ν (Mn-O)	ν (ClO_4^-)
Hsal-aebmz	1634	-	-	-
$[Mn^{III}(sal\text{-}aebmz)_2]\cdot ClO_4$	1619	455	629	1095, 629
$[Mn^{III}(sal\text{-}aebmz\text{-}H)(sal\text{-}aebmz)]$	1612	457	576	

4.3.4. UV/Vis Spectral Studies

Electronic spectral data of ligand and complexes are presented in Table 4.4. Figure 4.4 presents electronic spectra of complexes. Independent of the nature of the complexes (ionic or neutral) the electronic spectra of both the complexes (recorded in methanol) exhibit two weak shoulder bands in the 620 – 480 nm region. The reflectance spectra of the complexes (see Figures. 4.5 and 4.6) also exhibit bands at nearly the same positions as of solution spectra. For the distorted

d^4 system with pseudo-C_{4V} symmetry, three spin-allowed d–d transitions $^5B_1 \rightarrow {}^5A_1$, $^5B_1 \rightarrow {}^5E$ and $^5B_1 \rightarrow {}^5B_2$ have been predicted, of which the first one involves an electron from the dz^2 orbital and is sensitive to the environment [191,192]. As electronic transitions of both the complexes are insensitive towards environments the observed bands are assigned due to $^5B_1 \rightarrow {}^5E$ and $^5B_1 \rightarrow {}^5B_2$ transitions, respectively. These complexes are also dominated by a medium intensity band at 367 nm (a near UV region) attributable to phenolate $O(p_\pi) \rightarrow Mn(d_{\pi^*})$ ligand to metal charge transfer transition. Other UV bands due to ligand in both the complexes are obtained well within the expected range reported for copper [177] and vanadium complexes [46].

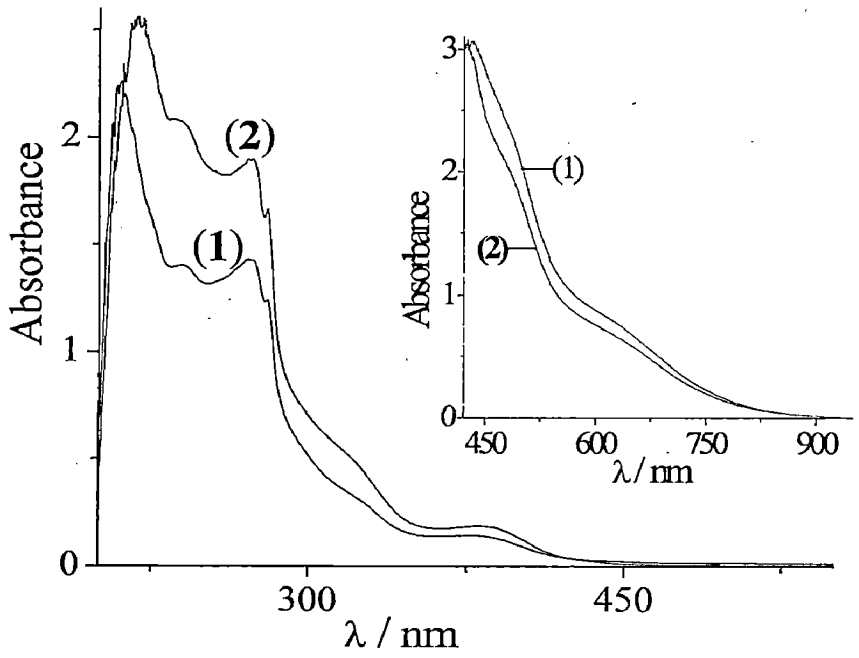

Figure 4.4. Electronic spectra of $[Mn^{III}(sal\text{-}aebmz)_2]\cdot ClO_4$ (**4.1**) and $[Mn^{II}$(sal-aebmz-H(sal-aebmz)] (**4.2**). In set shows spectra of visible region 450 – 900 nm.

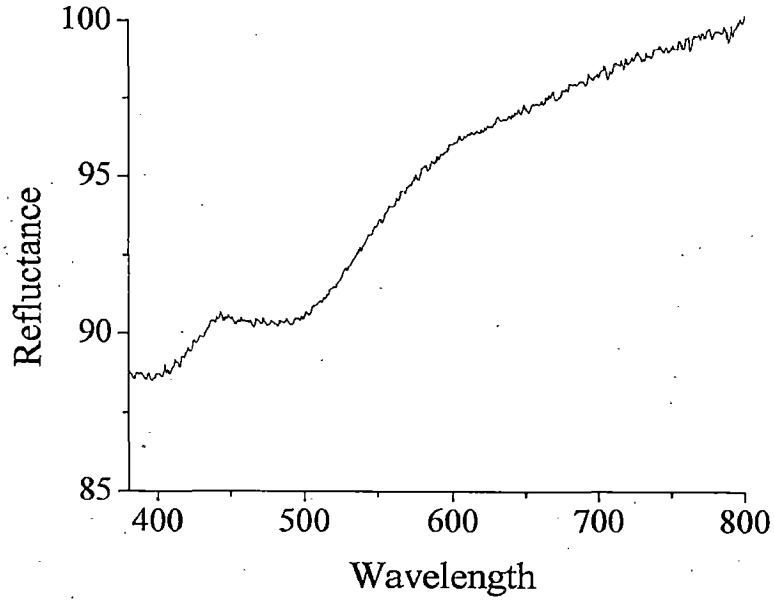

Figure 4.5. Diffused reflectance spectrum of [Mn(sal-aebmz)$_2$].

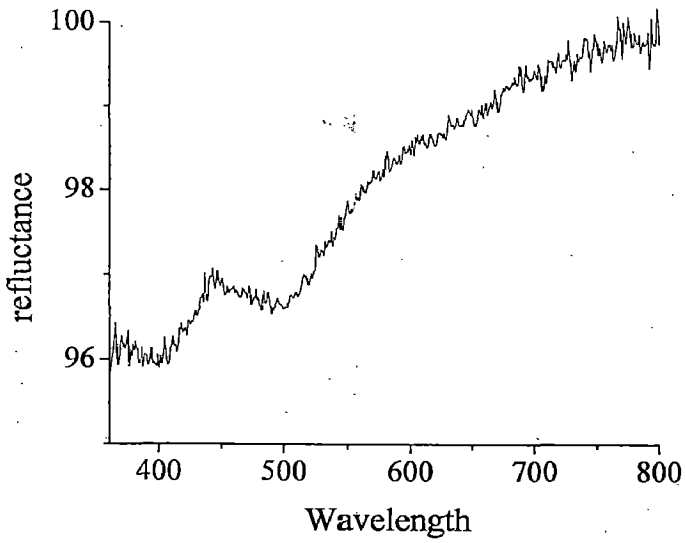

Figure 4.6. Diffused reflectance spectrum of [Mn(sal-aebmz-H)(sal-aebmz)].

Table 4.4. Electronic spectral data of ligand and complexes.

Compound	Solvent	λ_{max}(nm)/ ε(litre mol^{-1} cm^{-1})
Hsal-aebmz	MeOH	317, 281, 275, 254, 206
4.1	MeOH	618(259), 482(576), 367(535), 324(1023), 280(3159), 272(3682), 241(3884), 205(7813)
	Reflectance	~615, 450
4.2	MeOH	619(352), 485(865), 367(815), 324(1874), 281(6221), 272(7252),241(7755), 208(15050)
	Reflectance	~620, 450

4.3.5. Electrochemical studies

The cyclic voltammograms of two complexes were recorded over a potential range of –0.3 to 0.6 V in DMF (dried over molecular sieves), using 0.1 M tetrabutylammonium perchlorate (TBAP) as a supporting electrolyte. The shapes of the cyclic voltammograms of both the complexes are similar (Figure. 4.7), showing their similar nature in solution. Same conclusion has also been inferred while studying UV-vis spectral studies. The observed one-electron redox wave at $E_{½}$ = 0.114 (for **1**) and 0.131V (for **4.2**) vs. Ag/AgCl corresponds to the Mn^{III}–Mn^{II} redox couple [193,83]. A peak-to-peak separation (ΔE) value of ca. 0.51 V for both the complexes is relatively large but can still be considered small which suggests that both have reversible to quasireversible behaviour [193,83].

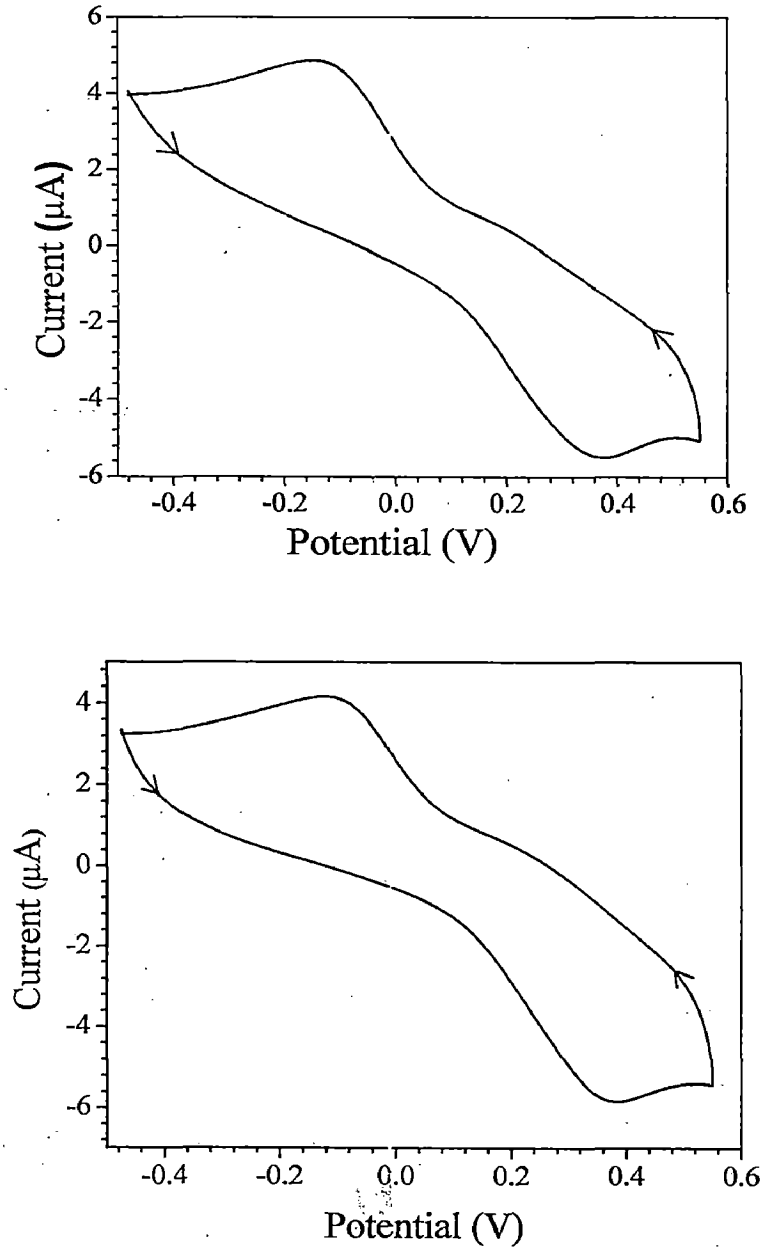

Figure. 4.7. Cyclic voltammogram of $[Mn^{III}(sal\text{-}aebmz)_2]ClO_4$ (**4.1**) (above) and of $[Mn^{III}(sal\text{-}aebmz\text{-}H)(sal\text{-}aebmz)]$ (**4.2**) (below) in DMF solution (1 mM), Ag/ AgCl as reference electrode, glassy carbon as working electrode and platinum wire as auxiliary electrode. Scan rate: 0.1 V/s.

4.3.6. Reactivity of Mn^{III}(sal-aebmz-H)(sal-aebmz)] (4.2) with H_2O_2 in methanol

The behaviour of the methanolic solution of [Mn^{III}(sal-aebmz-H)(sal-aebmz)] (**4.2**) upon addition of H_2O_2 was monitored by electronic absorption spectroscopy. Thus the stepwise additions of two drops portions of 30% H_2O_2 (0.305 g, 2.96 mmol) dissolved in 5 mL of MeOH to 5 mL of ca. 3.1×10^{-4} M solution of [Mn^{II}(sal-aebmz)$_2$] in MeOH results in the decrease in intensities of the 367 and 324 nm bands and emerge as a weak shoulder band at ca.350 nm; inset of Figure. 4.8(A). Simultaneously the two UV bands appearing at 281 and 272 nm improve their intensity while bands appearing at 241 and 208 nm increase in intensity and finally disappear (Figure. 4.8(A)). The d-d bands appearing at 619 and 485 nm recorded with more concentrated solutions slowly decrease their intensities and finally 619 nm band almost disappears while 485 nm one appears as a weak shoulder (Figure. 4.8(B)). This spectral change may correspond to the formation of active oxidized manganese species [185,194,195] which is responsible for the oxidative bromination. Similar spectral changes have also been observed for complex **4.1** (see Figure. 4.9). Interestingly, solutions of all complexes acquire original spectral patterns on keeping for long time.

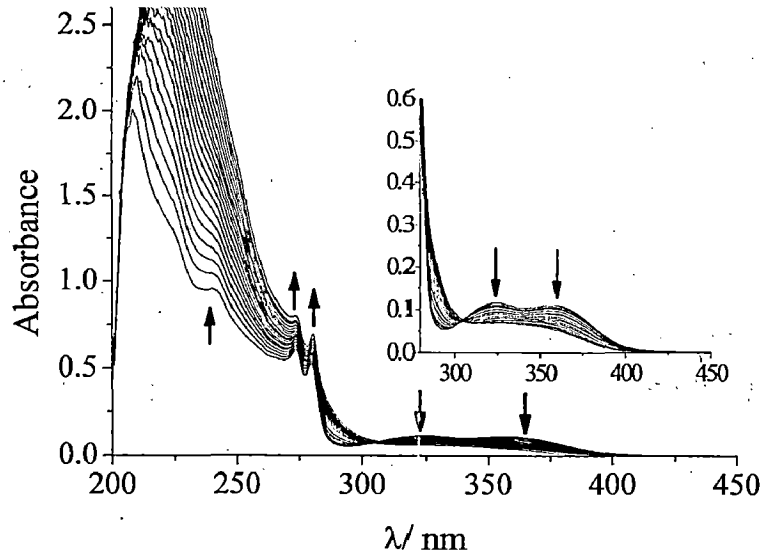

Figure 4.8. (A) UV-Vis spectral changes observed during titration of [Mn^{III}(sal-aebmz-H)(sal-aebmz)] (**4.2**) with H_2O_2. The spectra were recorded after stepwise additions of two drops portions of 30% H_2O_2 (0.305 g ,2.96 mmol) dissolved in 5 mL of MeOH to 5 mL of 3.1×10^{-4} M solution in MeOH.

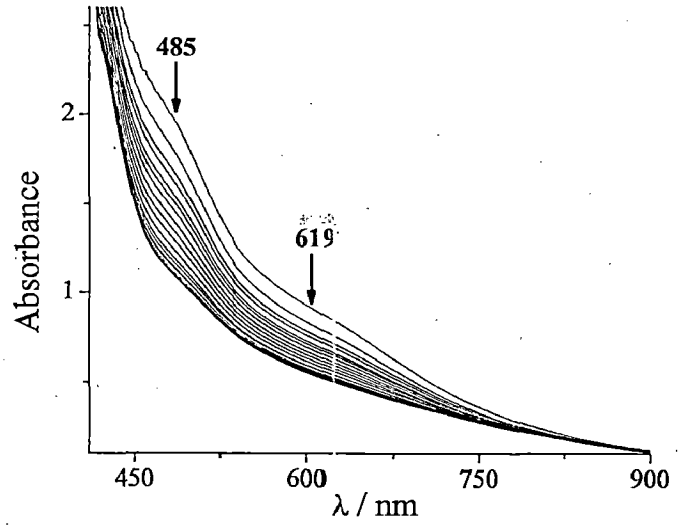

Figure 4.8. (B) UV-Vis spectral changes observed during titration of [Mn^{III}(sal-aebmz-H)(sal-aebmz)] (**4.2**) with H_2O_2. The spectra were recorded after stepwise additions of two drops portions of 30% H_2O_2 (0.305 g ,2.96 mmol) dissolved in 5 mL of MeOH to 25 mL of 2.32×10^{-3} M solution of **4.2** in MeOH.

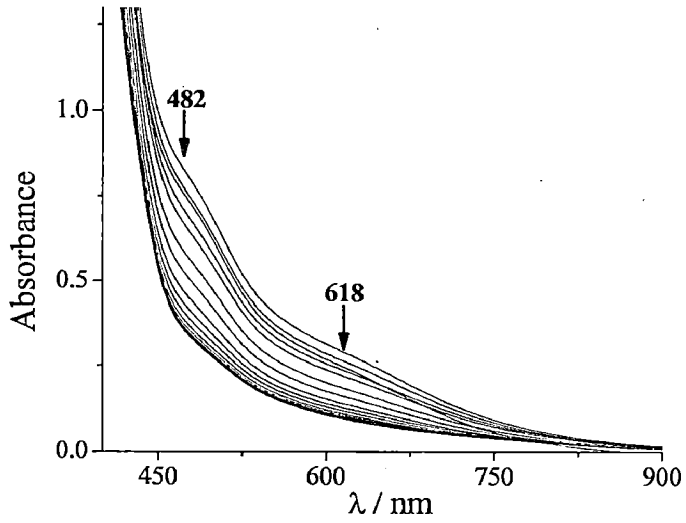

Figure 4.9. UV-Vis spectral changes observed during titration of $[Mn^{II}(sal\text{-}aebmz)_2]\cdot ClO_4$ (**4.1**) with H_2O_2. The spectra were recorded after stepwise additions of two drops portions of 30% H_2O_2 dissolved in 10 mL of MeOH to 20 mL of 1.23×10^{-3} M solution in MeOH.

4.3.7. Oxidative bromination of styrene

Oxidative bromination of styrene under a two-phase system, using $[Mn^{III}(sal\text{-}aebmz\text{-}H)(sal\text{-}aebmz)]$ (**4.2**) as catalyst in the presence of KBr, $HClO_4$ and H_2O_2 gave mainly three products namely, (a) 1,2-dibromo-1-phenylethane, (b) 2-bromo-1-phenylethane-1-ol and (c) 1-phenylethane-1,2-diol; Scheme **4.2.** Addition of $HClO_4$ in four equal portions was required to obtain better oxidative bromination. All products were separated/ isolated by column chromatography and the content of each fraction was confirmed by ^1H NMR as well as GC-MS. The obtained products are the same as those reported by Conte *et al.* [112,113] and others [163]. The formation of other minor products as obtained earlier, was ignored.

The following parameters were studied to optimize the reaction conditions for the maximum oxidative bromination of styrene taking **4.2** as catalyst precursor: (i) catalyst amount, (ii) oxidant amount, (iii) potasium bromide amount and (iv) perchloric acid amount.

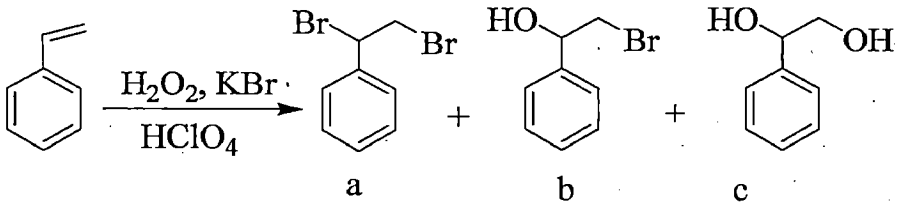

Scheme 4.2. Main products obtained by oxidative bromination of styrene. (a) 1,2-dibromo-1-phenylethane (dibromide), (b) 2-bromo-1-phenylethane-1-ol (a bromohydrin) and (c) 1-phenylethane-1,2-diol.

Three different amounts of **4.2** viz. 0.002, 0.004 and 0.006 g of catalyst precursor were used while keeping the fixed amount of styrene (1.04 g, 10 mmol), KBr (3.57 g, 30 mmol), 30 % H_2O_2 (3.405 g, 30 mmol), aqueous 70 % $HClO_4$ (5.72 g, 40 mmol) in a 40 mL CH_2Cl_2–water (50% v/v) mixture at room temperature. As presented in Figure 4.10, a maximum of 96 % conversion was obtained after 1 h of reaction time with 0.002 g catalyst precursor while 0.004 and 0.006 g catalyst precursor gave nearly the same conversion. Therefore, 0.002 g of catalyst was set as optimum. During the reaction, addition of $HClO_4$ was made in four equal portions, one immediately after the catalyst precursor (reaction time = 0), and the three other portions with 15 min. intervals.

The effect of amount of aqueous 30% H_2O_2 was studied considering substrate to oxidant ratios of 1 : 1, 1 : 2 and 1 : 3 for a fixed amount of styrene (1.04 g, 10 mmol), amount of catalyst precursor (0.002 g), KBr (3.57 g, 30 mmol) and $HClO_4$ (5.72 g, 40 mmol) in CH_2Cl_2-H_2O (40 mL, 50% v/v), and reaction was monitored at room temperature for 1 h (Figure 4.11). Increasing the substrate to oxidant ration from 1:1 to 1:2 not only increases the % conversion but also changes the products selectivity. Thus, 1:1, substrate to oxidant ratio gives 88% conversion with mono bromo derivative 42 % and di-ol derivative 57 %. But at substrate to oxidant of 1:2, 95 % product conversion is observed with monobromo derivative 7 % , dibromo derivative 20 % and diol derivative 72 %. Further increasing the oxidant amount gives almost same product conversion with slightly different product selectivity i.e. mono bromo derivative 3 %, dibromo derivative 13 % and

diol derivative 83 %. Therefore, substrate to oxidant ratio of 1:2 was considered the best for the optimum condition.

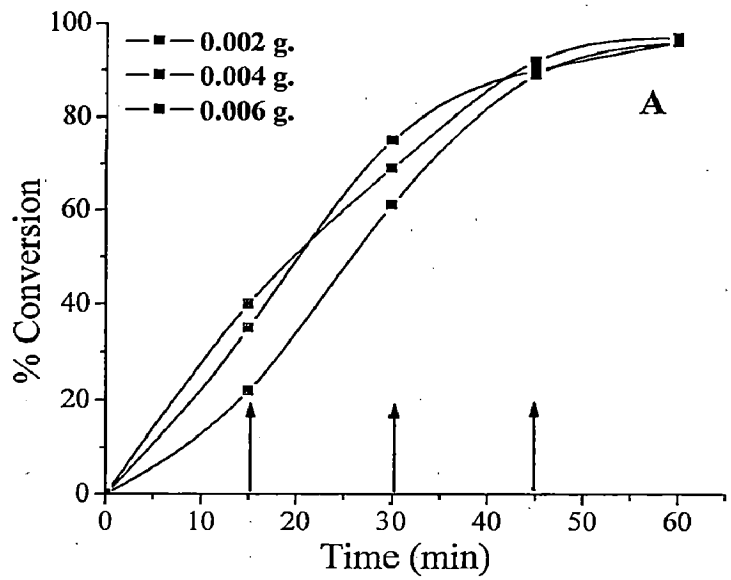

Figure 4.10. Effect of amount of catalyst on the oxidative bromination of styrene at room temperature for 1 h.

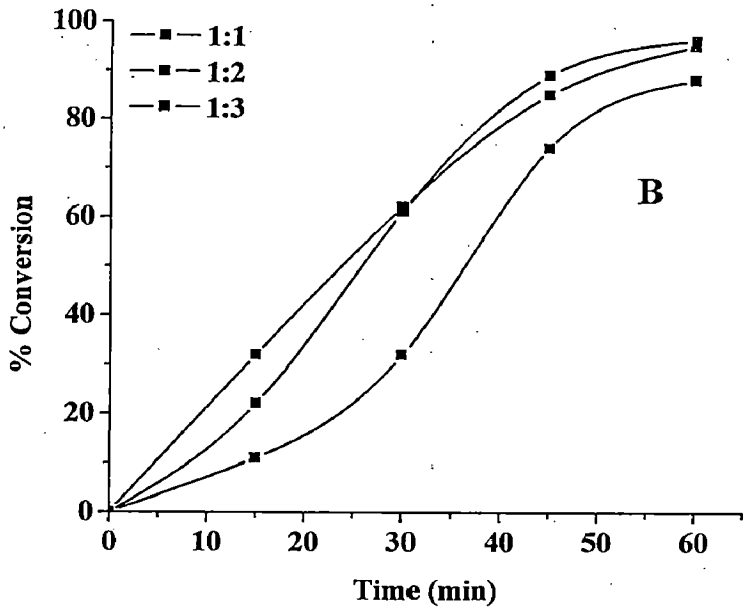

Figure 4.11. Effect of the amount of H_2O_2 on the oxidative bromination of styrene.

Similarly three different substrate to KBr ratios were considered. Substrate to KBr ratio 1:1 gives 62 % product conversion with dibromo derivative as a major product (87 %) along with a small amount of diol derivative (13 %) but no monobromo derivative was found in this reaction time (Figure 4.12). Substrate to KBr ratio 1:2 shows 97 % conversion with monobromo derivative 25 % , dibromo derivative 8 % and diol derivative 66 % while 1:3 shows 95 % conversion with monobromo derivative 7 % , dibromo derivative 20 % and diol derivative 72 %. Thus 1:2 substrate to KBr ratio was set as optimum.

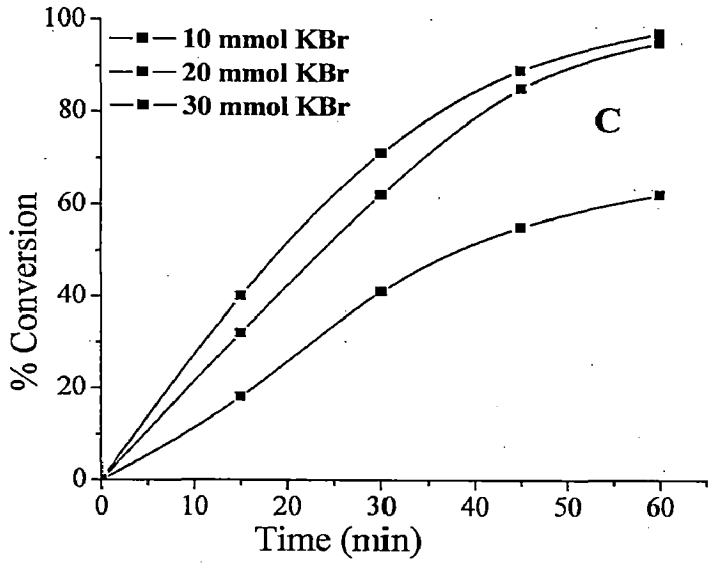

Figure 4.12. Effect of the amount of KBr on the oxidative bromination of styrene.

To optimize the amount of $HClO_4$, three different amounts of 70% $HClO_4$ were used for a fixed amount of styrene (1.04 g, 10 mmol), amount of catalyst precursor (0.002 g), KBr (2.38 g, 20 mmol), 30 % H_2O_2 (2.27 g, 20 mmol) and CH_2Cl_2-H_2O (40 mL, 50% v/v) at room temperature for 1 h (Figure 4.13). Addition of extra $HClO_4$ has an effect on % conversion and on product selectivity. One equivalent extra addition of $HClO_4$ gives 80 % conversion with exclusively dibromo derivative as a major product (66 %) and small amount of diol derivative (33 %). Two equivalent extra addition of $HClO_4$ increases the conversion from 80 % to 96 % with mono bromo derivative 39 %, dibromo derivative 3 % and diol derivative 57 %. Further increament of extra addition of $HClO_4$ does not improve

the product conversion only selectivity changes. Hence two equivalent extra addition of $HClO_4$ (a total of 30 mmol) was the best.

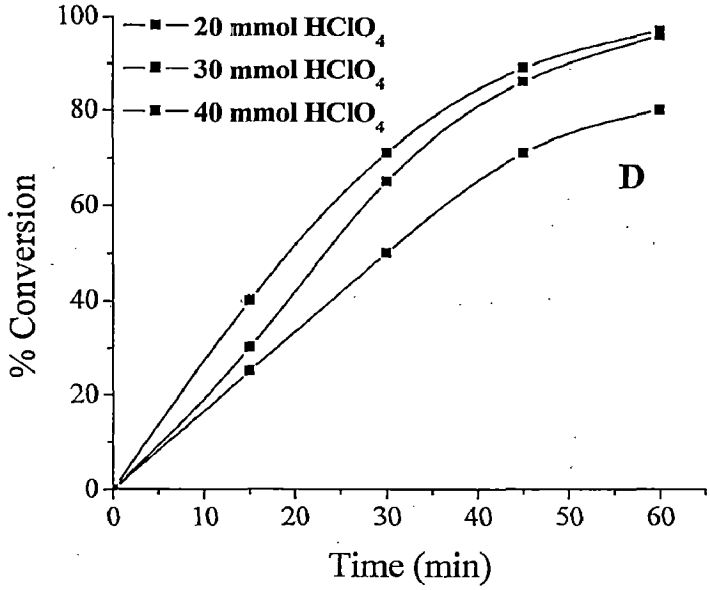

Figure 4.13. Effect of the amount of perchloric acid on the oxidative bromination of styrene.

Table 4.5 presents summary of the oxidative bromination of styrene obtained under various reaction conditions applied. Thus, the optimised reaction conditions concluded for the oxidative bromination of 10 mmol of styrene are: catalyst precursor (0.002 g), KBr (2.38 g, 20 mmol), 30% H_2O_2 (2.27 g, 20 mmol) and 70% $HClO_4$ (4.29 g, 30 mmol) in CH_2Cl_2-H_2O (40 mL, 50% v/v). Under this condition, a maximum of 96% oxidative bromination of styrene has been achieved with monobromo derivative 39%, dibromo derivative 3% and diol derivative 57%.

The most acceptable mode of action of vanadium-dependent bromoperoxidase enzymes (V-BrPOs) involves the presence of vanadium in their active sites [163,154-157]. The vanadium in the presence of hydrogen peroxide forms a peroxido vanadium derivative that oxidizes a bromide ion, thus forming a bromine equivalent intermediate. Such an intermediate may then either brominate an appropriate organic substrate or react with another molecule of Br^- to form bromine. The bromine generated may further react with substrate to brominate.

The oxidized active manganese intermediate species formed by the interaction of H_2O_2 (vide supra) may oxidise the bromide ion, similar to haloperoxidases. This then transfers to the organic phase (CH_2Cl_2) where the bromination of the styrene takes place [112,113].

Table 4.5. Results of oxidative bromination of styrene using [Mn^{III}(sal-aebmz-H)(sal-aebmz)] (**4.2**) as catalyst precursor. Conversion data obtained after 1 h.

Entry No.	Styrene	KBr	H_2O_2	$HClO_4$	Catalyst	Solvent (DCM/H_2O)	% Conversion
1.	1.04 g (10 mmol)	3.57 g (30 mmol)	3.405 g (30 mmol)	5.72 g (40 mmol)	0.002 g	20/20	96
2	1.04 g (10 mmol)	3.57 g (30 mmol)	3.405 g (30 mmol)	5.72 g (40 mmol)	0.004 g	20/20	97
3	1.04 g (10 mmol)	3.57 g (30 mmol)	3.405 g (30 mmol)	5.72 g (40 mmol)	0.006 g	20/20	96
4	1.04 g (10 mmol)	3.57 g (30 mmol)	1.135 g (10 mmol)	5.72 g (40 mmol)	0.002 g	20/20	88
5	1.04 g (10 mmol)	3.57 g (30 mmol)	2.27 g (10 mmol)	5.72 g (40 mmol)	0.002 g	20/20	95
6	1.04 g (10 mmol)	1.19 g (10 mmol)	2.27 g (10 mmol)	5.72 g (40 mmol)	0.002 g	20/20	62
7	1.04 g (10 mmol)	2.38 g (20 mmol)	2.27 g (10 mmol)	5.72 g (40 mmol)	0.002 g	20/20	97
8	1.04 g (10 mmol)	2.38 g (20 mmol)	2.27 g (10 mmol)	2.86 g (20 mmol)	0.002 g	20/20	80
9	1.04 g (10 mmol)	2.38 g (20 mmol)	2.27 g (10 mmol)	4.29 g (30 mmol)	0.002 g	20/20	96

4.4. Conclusions

Neutral [Mn^{III}(sal-aebmz-H)(sal-aebmz)] (**4.2**) with monobasic tridentate 2-[2-(1H-(benzo[d]imidazol-2-yl)ethylimino)methyl]phenol (Hsal-aebmz, **4.I**) has been isolated where intermolecular hydrogen bonding between protonated and deprotonated non-coordinated benzimidazole nitrogen atoms stabilize the neutal species and control the molecular packing. The usual ionic complex [Mn^{III}(sal-aebmz)$_2$]·ClO_4 (**4.1**) has also been isolated. In solid phase they are different but their solution behaviours are nearly same. Complex **4.2** is shown to be a functional mimic of vanadium-dependent haloperoxidases and satisfactorily catalyses the oxidative bromination of styrene where the selectivity of the products follows the order: 1-phenylethane-1,2-diol > 2-bromo-1-phenylethane-1-ol > 1,2-dibromo-1-phenylethane.

Chapter-5

◈ Copper(II) complex of monobasic tridentate ONN donor ligand: Synthesis, encapsulation in zeolite-Y, characterization and catalytic activity

---

This work is published in *J. Coord. Chem.*, 64, 2995–3011, 2011.

Copper(II) complex of monobasic tridentate ONN donor ligand: Synthesis, encapsulation in zeolite-Y, characterization and catalytic activity

5.1. Introduction

Coordination chemistry of monobasic tridentate ONN ligands has been studied considerably due to their interesting structural, magnetic and other properties [196-203]. One of the coordination sites of such ligands is mostly involved in bridging with other metal centre producing dinuclear or polynuclear species [196-203]. Dimerization through X bridging in complexes of formula [MLX] (M = Cu^{II}, Ni^{II}, Zn^{II}, Mn^{III} , Cd^{II}, etc., L = ONN monobasic tridentate ligands and X = N_3^-, Cl^-, NCO^-, NCS^- etc.) are also known [199-203]. However, mononuclear complexes, in the presence of suitable oxidant, may form facile intermediate by expanding the coordination number which can facilitate catalytic oxidation reaction. Importance of mononuclear complexes we earlier prepared mononuclear complexes e.g. [V^VO_2(sal-ambmz)] and [Cu^{II}(sal-ambmz)Cl] upon encapsulation in the nano cavity of the zeolite-Y in catalytic reactions has been presented earlier[151]. Such zeolite encapsulated metal complexes (ZEMC) have provided the opportunity to develop catalytic processes for the selective oxidation of various substrates and are able to produce important intermediates as well as most industrial products [204-207,33]. In this chapter, we report mononuclear copper(II) complex of (Z)-2-(1-(2-(1H-benzo[d]imidazol-2-yl)ethylimino) ethyl)phenol (Hhap-aebmz, **5.I**; Scheme 5.1), its characterization by single crystal X-ray study and encapsulation in the nano cavity of zelite-Y. Catalytic activities of encapsulated complex have been studied for the oxidation of cyclohexene and phenol. Its catalytic potential has also been compared with the corresponding neat analogue.

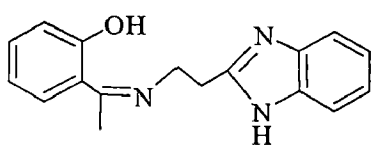

Scheme 5.1. Structure of (Z)-2-(1-(2-(1H-benzo[d]imidazol-2-yl)ethylimino)ethyl) phenol (Hhap-aebmz, **5.I**).

5.2. Experimental

5.2.1. Materials and methods

All chemicals and solvents were of AR grade and used without purifications. Copper content in zeolite-Y complex was obtained by Atomic Absorption Spectroscopy. IR spectra were recorded as KBr pellet on a Nicolet NEXUS Aligent 1100 FT-IR spectrometer after grinding the sample with KBr. Electronic spectra of ligand and complex were recorded in methanol on shimadzu 1601 PC UV–VIS spectrophotometer. Electronic spectrum of zeolite-Y encapsulated complex was recorded in Nujol by layering the mull of the sample to inside of one of the cuvettes while keeping the other one layered with Nujol as reference. ^{1}H NMR and ^{13}C NMR spectra were obtained in $CDCl_3$ on a Bruker Avance III 400 MHz spectrometer with the common parameter settings. The magnetic susceptibility of the complex was measured at 298 K with vibrating sample magnetometer model 155, using nickel metal with saturation magnetization of 55 emu/g as standard. X-ray powder diffractograms of zeolite related samples were recorded using a Bruker AXS D8 advance X-ray powder diffractometer with a Cu-Kα target. Scanning electron micrograph (SEM) of zeolite-Y having encapsulated complex was recorded on a Leo instrument model 435VP. The energy dispersive X-ray analysis (EDX) was obtained on a FEI Quanta 200 FEG. The sample was dusted on alumina and coated with thin film of gold to prevent surface charging and to protect the surface material from thermal damage by electron beam. In all analyses, a uniform thickness of about 0.1 mm was maintained. Other details are presented in chapter 2.

5.2.2. Preparations

5.2.2.1. Hhap-aebmz (5.I)

An aqueous solution of aebmz·2HCl (4.680 g, 20 mmol in 15 ml water) was neutralized by adding aqueous Na_2CO_3 solution (2.120 g, 20 mmol). A methanolic solution of *o*-hydroxyacetophenone (2.72 g, 20 mmol in 20 ml) was added drop-

wise to the above solution with stirring. A yellow solid slowly separated out from the solution within 2 h which was filtered, washed thoroughly with water followed by petroleum ether and dried in vacuum at room temp. Finally it was recrystallized from acetonitrile. Yield: 4.24 g (75.9 %). Anal. calc. for $C_{17}H_{17}N_3O$ (279.34) : C, 73.1; H, 6.1; N, 15.0 %. Found : C, 72.7; H, 6.2; N, 15.1 %. ^{1}H NMR ($CDCl_3$, δ/ppm): 7.5(b, 2H, –OH and -NH). 7.47(d, 1H), 7.3(d, 1H), 7.26(s, 2H), 7.19(q, 2H), 6.9(d, 1H), 6.7(t, 1H, aromatic), 4.09(t, 2H, $–CH_2$), 3.38(t, 2H, $–CH_2$), 2.3(s, 3H, $–CH_3$). ^{13}C NMR ($CDCl_3$, δ/ppm): 14.7 (CH_3), 30.4 (CH_2CH_2N), 47.3 (CH_2CH_2N), 152.1(NH–*C*=N, benzimidazole), 164.8 (ph–*C*–OH), 173.5 (C=N, imine), 117.1, 118.7, 119.0, 122.3, 128.3, 133.3 (aromatic).

5.2.2.2. [Cu^{II}(hap-aebmz)Cl] (5.1)

A solution of $CuCl_2·2H_2O$ (0.852 g, 5 mmol) dissolved in methanol (8 ml) was added to a hot solution of Hhap-aebmz (1.396 g, 5 mmol) in methanol (15 ml) and the reaction mixture was kept under stirring for 5 h. The dark green solid of [Cu^{II}(hap-aebmz)Cl] slowly separated out. This was filtered off, washed with petroleum ether and dried in vacuum over silica gel. Yield: 1.26 g (67.0 %). Anal. calc. for $C_{17}H_{16}N_3OClCu$ (377.33) : C, 54.1; H, 4.3 % ; N, 11.1 %, Found : C, 53.8; H, 4.4; N, 11.2 %.

5.2.2.3. [Cu^{II}(hap-aebmz)Cl]-Y (5.2)

A methanolic solution of Hhap-aebmz (2.0 g) was mixed with copper-exchanged zeolite-Y ([Cu^{II}]-Y, 3.0 g) [151] suspended in methanol (50 ml) and the reaction mixture was refluxed for 14 h in an oil bath with stirring. This was filtered off, washed with methanol and again suspended in methanol to remove excess ligand present in the cavities as well as on the surface of the zeolite along with neat complex if any using Soxhlet extractor. The remaining uncomplexed metal ions in zeolite were removed by stirring with aqueous 0.01M NaCl (200 ml) for 8 h.

Finally it was washed with double distilled water and dried at ca. 120 °C for several hours. Found : Cu, 2.4 %.

5.2.3. X-ray Crystal Structure Determination

Three-dimensional X-ray data for Hhap-aebmz (**5.I**) and [Cu^{II}(hap-aebmz)Cl] (**5.1**) were collected on a Bruker SMART Apex CCD diffractometer at 100(2) K, using a graphite monochromator and Mo-K_α radiation (λ = 0.71073 Å) by the ϕ-ω scan method. Reflections were measured from a hemisphere of data collected of frames each covering 0.3 degrees in ω. Of the 14777 and 26444 reflections measured, all of which were corrected for Lorentz and polarization effects, and for absorption by semi-empirical methods based on symmetry-equivalent and repeated reflections, 3060 and 3186 independent reflections exceeded the significance level $|F|/\sigma(|F|) > 4.0$. Complex scattering factors were taken from the program package SHELXTL [166]. The structures were solved by direct methods and refined by full-matrix least-squares methods on F^2. The non-hydrogen atoms were refined with anisotropic thermal parameters in all cases. All hydrogen atoms were left to refine freely in the two compounds, except the hydrogen atom H(2N) of the benzimidazole group which was located from a difference electron density map and fixed to 0.90 to the corresponding heteroatom, in **5.I**. A final difference Fourier map showed no residual density outside; minimum and maximum final electron density: 0.417 and –0.486 for **5.I** and 0.735 and –0.366 for **5.1** e.$Å^{-3}$. Crystal data and details of the data collection and refinement for the new compounds are collected in Table 5.1.

Table 5.1. Crystal data and structure refinement for Hap-aebmz (**5.I**) and for [Cu^{II}(hap-aebmz)Cl] (**5.1**).

	5.I	**5.1**
Formula	$C_{17}H_{17}N_3O$	$C_{17}H_{16}ClCuN_3O$
Formula weight	279.34	377.32
T, *K*	100(2)	100(2)
Wavelength, *Å*	0.71073	0.71073
Crystal system	Monoclinic	Monoclinic
Space group	C2/c	$P2_1/c$
a/Å	27.9320(9)	8.0432(4)
b/Å	6.5521(2)	10.1802(5)
c/Å	19.5644(6)	18.7209(9)
β/°	127.6270(10)	99.175(3)
V/$Å^3$	2835.80(15)	1513.28(13)
Z	8	4
F_{000}	1184	772
D_{calc}/g cm^{-3}	1.309	1.656
μ/mm^{-1}	0.084	1.627
θ/ (°)	2.63-28.46	2.28-28.41
R_{int}	0.0289	0.0502
Crystal size/ mm^3	0.40 x 0.19 x 0.18	0.35 x 0.12 x 0.09
Goodness-of-fit on F^2	1.083	1.054
R_1 [a]	0.0433	0.0322
wR_2 (all data) [b]	0.1204	0.0731
Largest differences peak and hole ($eÅ^{-3}$)	0.417 and -0.486	-0.366 and 0.735

[a] $R_1 = \Sigma \| |F_o| - |F_c| \| / \Sigma |F_o|$. [b] $wR_2 = \{\Sigma[w(\| |F_o|^2 - |F_c|^2 |)^2] / \Sigma[w(F_o^4)]\}^{1/2}$

5.2.4. Catalytic reactions

5.2.4.1. Oxidation of cyclohexene

The catalytic reaction was carried out in a glass reactor of 50 ml capacity equipped with a reflux condenser. Cyclohexene (0.82 g, 10 mmol) was dissolved in acetonitrile (5 ml) and to this was added an aqueous 30 % H_2O_2 (2.27 g, 20 mmol) and [Cu^{II}(hap-aebmz)Cl]-Y (0.005 g). The reaction was carried out in an oil bath with continuous stirring while maintaining the reaction temperature at 80 °C. The progress of the reaction was monitored by withdrawing the sample at definite time intervals and analyzing quantitatively through thermo electron gas chromatograph equipped with HP-1 capillary column (30 × 0.25 mm × 0.25 μm) and FID detector. The identities of the products were confirmed by GC-MS model Perkin-Elmer, Clarus 500 by comparing the fragments of each product with the library available.

5.2.4.2. Oxidation of Phenol

In a typical reaction, aqueous 30 % H_2O_2 (2.27 g, 20 mmol) and phenol (1.88 g, 20 mmol) were mixed in 5 ml of acetonitrile and the reaction mixture was heated at 80 °C with continuous stirring in an oil bath. Catalyst [Cu^{II}(hap-aebmz)Cl]-Y (0.010 g) was added to the reaction mixture and the reaction was considered to begin. During the reaction, the products were analyzed and their identities confirmed as mentioned above by withdrawing small aliquots after specific interval of time.

5.3. Results and discussion

Synthesis of ligand Hhap-aebmz is straight forward. Elemental analysis, IR, ^1H and ^{13}C NMR spectral data, and single crystal X-ray study (discussed later) confirm its structure.

Most [Cu^{II}(ONN)X] (where ONN = coordinating atoms of monobasic tridentate ligands, X = Cl^-, Br^-, SCN^-, N_3^- etc.) type complexes exist as dimmer / polymer where each unit has square pyramidal structure through X^- bridging [199-203]. The green complex [Cu^{II}(hap-aebmz)Cl] (**5.1**), synthesized here by reacting Hhap-aebmz with $CuCl_2$, exists in its monomeric form with distorted square planar

structure (vide infra). Magnetic moment value of 1.72 μB also suggests its magnetically dilute nature and existence in its monomeric form. Encapsulation of **5.1** in the nano cavity of the zeoite-Y involved the interaction of $[Cu^{II}]$-Y with excess Hhap-aebmz in methanol where ligand slowly enters into the cavity of zeolite-Y due to its flexible nature and interacts with metal ions. Soxhlet extraction using methanol finally purified the impure complex. The remaining uncomplexed metal ions in zeolite were removed by exchanging with aqueous 0.1 M NaCl solution. As one extra anionic ligand would be required to balance the overall charges on the Cu^{II}, Cl^- of NaCl used during exchanged process fulfills this requirement. The presence of chloride ion has been confirmed qualitatively. Thus, the formula of Cu^{II} complex may be written as $[Cu^{II}$(hap-aebmz)Cl]-Y (**5.2**). As impure **5.2** was extracted well with methanol, the presence of 2.4 % copper is only due to the encapsulation of metal complex in the super cages of the zeolite-Y. About 10 Å diagonal distance of $[Cu^{II}$(hap-aebmz)Cl] (**5.1**) allows its encapsulation in the super cages of zeolite-Y without any strain. Similarity in the spectral properties of neat as well as encapsulated complex (vide infra) suggests a similar distorted square planar structure for encapsulated complex as well.

5.3.1. Description of structures of Hhap-aebmz, (5.I) and $[Cu^{II}$(hap-aebmz)Cl](5.1)

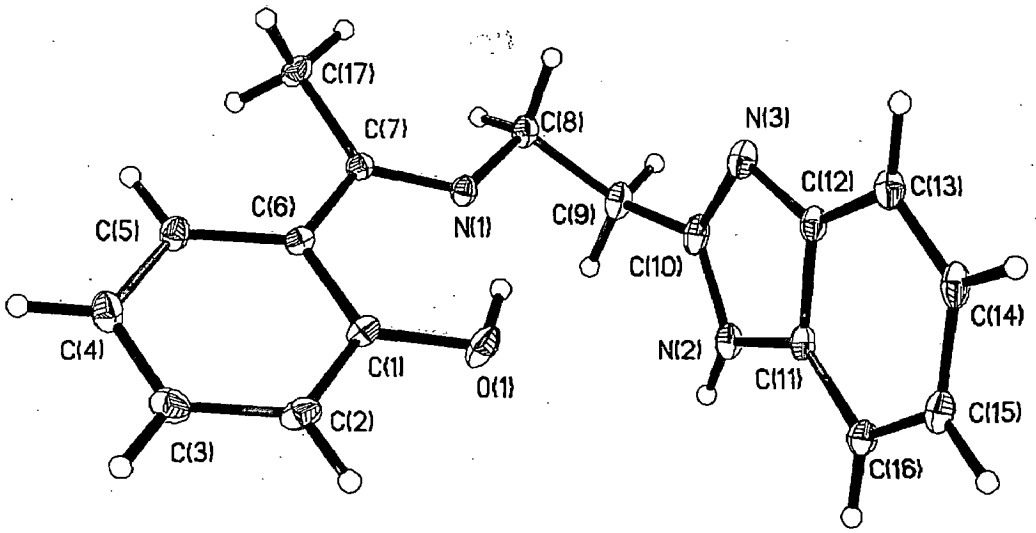

Figure 5.1. ORTEP plot of Hhap-aebmz (**5.I**) ligand. All the non-hydrogen atoms are represented by their 30 % probability ellipsoids. Hydrogen atoms are included.

Light orange crystals of Hhap-aebmz (**5.I**) ligand were grown by slow evaporation of methanolic solution at room temperature. Figure **5.1** shows ORTEP representation of Hhap-aebmz (**5.I**). Table 5.2 presents bond lengths and angles while Table 5.3 provides distances and angles of hydrogen bonds.

Structure of [Cu^{II}(hap-aebmz)Cl] complex was grown by slow evaporation of methanolic solution at room temperature. The ORTEP plot of the complex is shown in Figure 5.2. The polyhedron is a much distorted square plane. Phenolic oxygen, azomethine nitrogen, benzimidazolic nitrogen and Cl atoms constitute the distorted square plane. The mean deviation from planarity of the plane containing the four donor atoms amounts to 0.4685(9) Å (see Figure 5.3). All the atoms coordinated to Cu(II) are within 1.9 – 2.2 Å. Angles O(1)-Cu(1)-N(1): 91.44(7)°; N(1)-Cu(1)-N(2): 89.74(7)°; O(1)-Cu(1)-Cl(1): 92.41(5)° and N(2)-Cu(1)-Cl(1): 97.75(5)° are closer to expected 90°. Selected bond lengths and angles for the complex are presented in Table 5.5.-The difference of the current structure from the literature is its existence as supramolecular form through hydrogen bonding while other reported structures are dimeric where two chlorine atoms of two units bridge together [199-203]. Strong intermolecular hydrogen bonding exists between hydrogen of NH group of benzimidazole and bonded phenolic oxygen (See Table 5.3) as shown in Figure 5.4 and this is responsible for its existence as supramolecular assembly. Short contacts between Cu---Cl and N---Cl atoms of the different complexes appear in the supramolecular structure (see Figure 5.5). The interaction between chlorine and copper atoms of different complex is weak [Cl(1)---Cu(1): 2.974 Å). Chlorine and nitrogen atoms [Cl(1)---N(1): 3.258 Å] of different complex show short contacts interactions between them too [208].

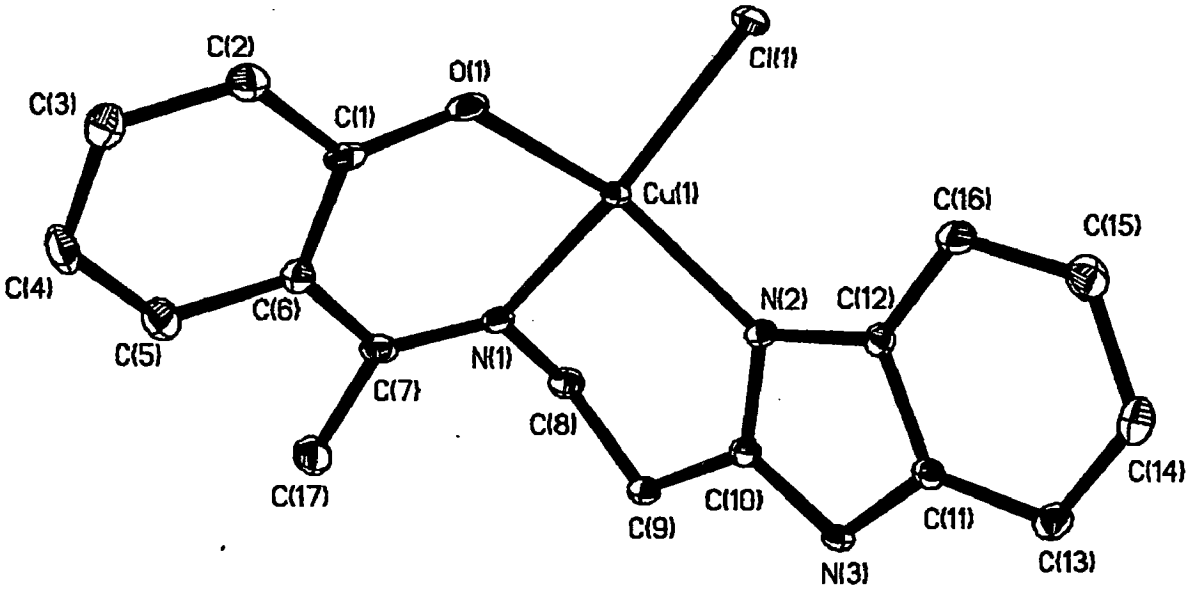

Figure 5.2. ORTEP plot of [Cu^{II}(hap-aebmz)Cl]. All the non-hydrogen atoms are represented by their 50 % probability ellipsoids. Hydrogen atoms are omitted for clarity.

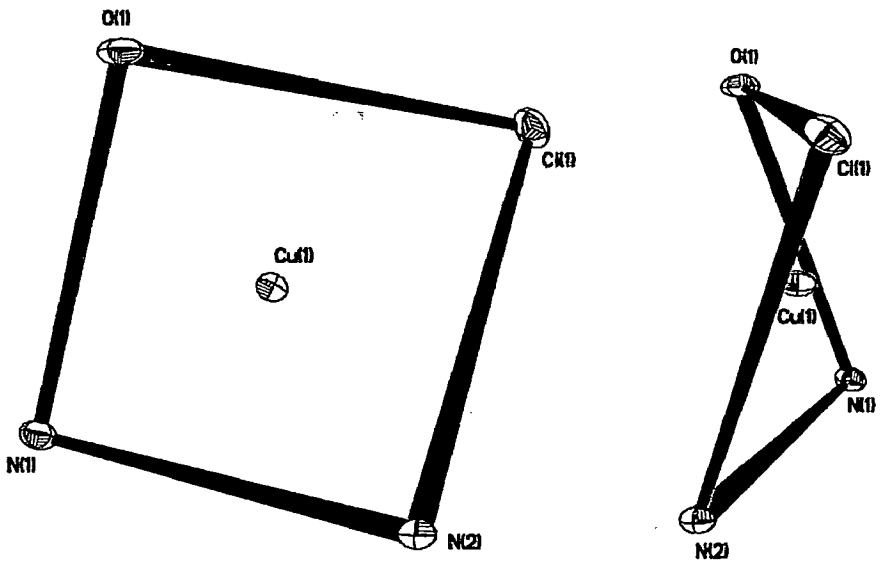

Figure 5.3. Coordination polyhedron around the Cu(II) ion (two different views) in the complex [Cu^{II}(hap-aebmz)Cl].

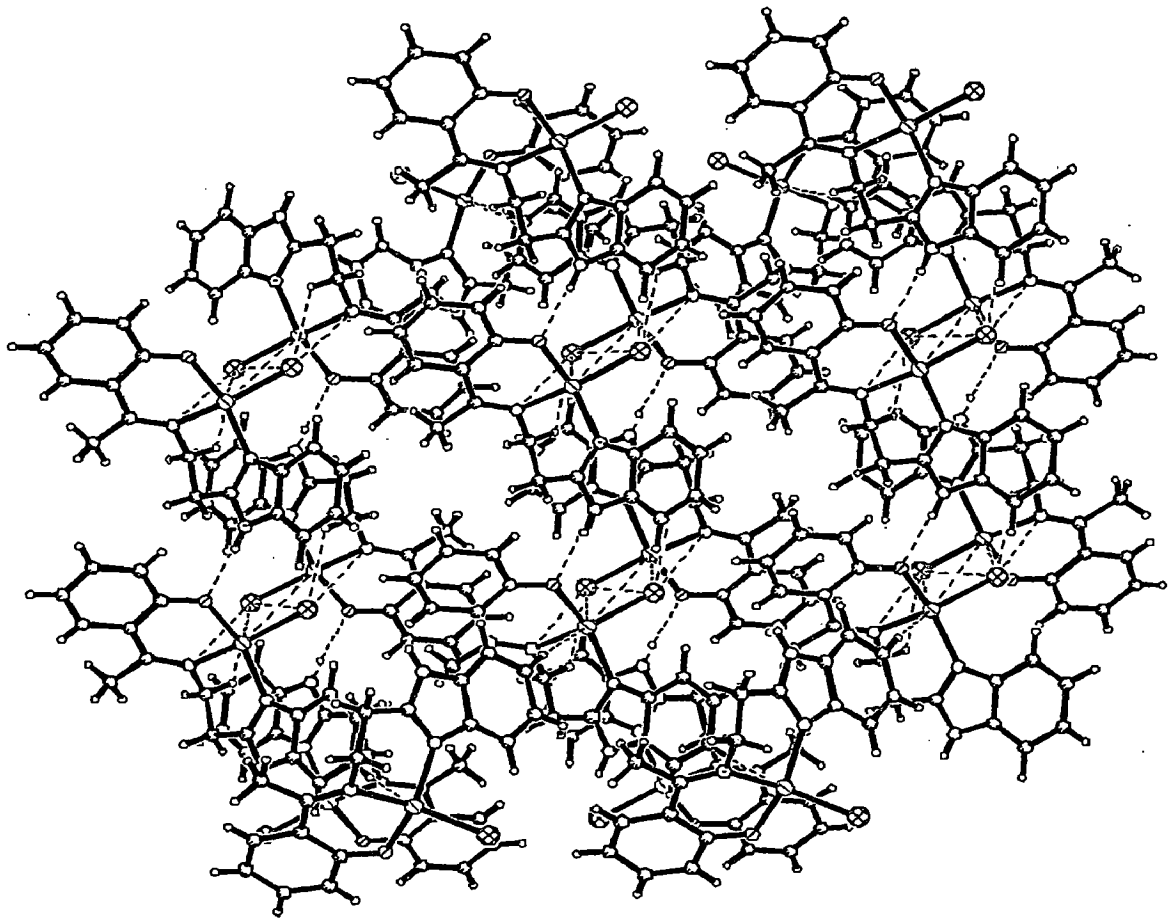

Figure 5.4. Supramolecular assembly showing intermolecular hydrogen bonding.

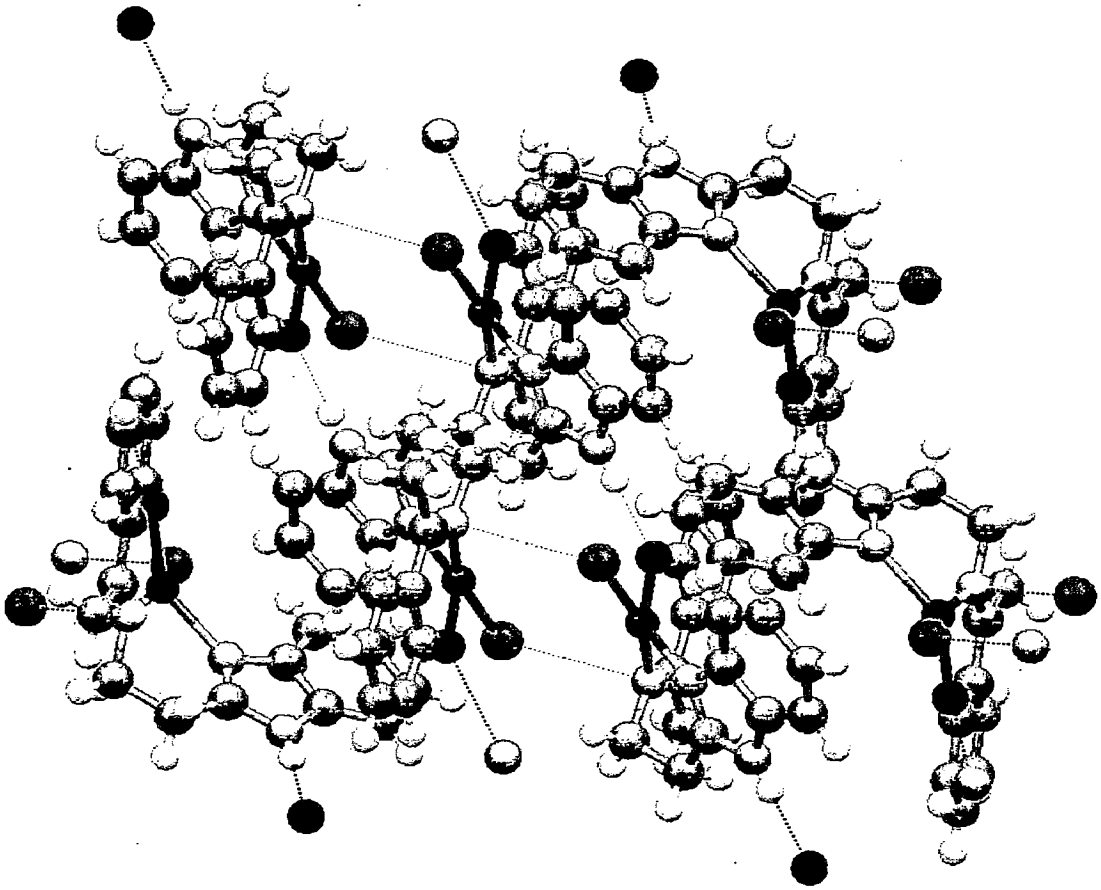

Figure 5.5. Crystal packing view of the complex [Cu^{II}(hap-aebmz)Cl], (**5.1**). We can see the intermolecular hydrogen bonds between N(3)···O(1) and short contacts between Cl(1)---N(1).

Table 5.2. Bond lengths and angles for (hap-aebmz) (**5.I**) and for [Cu^{II}(hap-aebmz)Cl] (**5.1**).

Bond lengths [Å]			
5.I		**5.1**	
N(1)-C(7)	1.2852(16)	Cu(1)-O(1)	1.9293(15)
N(1)-C(8)	1.4590(16)	Cu(1)-N(1)	1.9549(18)
O(1)-C(1)	1.3446(16)	Cu(1)-N(2)	2.0511(17)
N(2)-C(10)	1.3372(18)	Cu(1)-Cl(1)	2.2480(6)
N(2)-C(11)	1.3889(16)	N(1)-C(7)	1.296(3)
N(3)-C(10)	1.3422(18)	N(1)-C(8)	1.474(3)
N(3)-C(12)	1.3870(17)	O(1)-C(1)	1.292(3)
Bond angles [°]			
C(7)-N(1)-C(8)	122.69(11)	O(1)-Cu(1)-N(1)	91.44(7)
O(1)-C(1)-C(2)	117.98(11)	O(1)-Cu(1)-N(2)	143.96(7)
O(1)-C(1)-C(6)	122.05(11)	N(1)-Cu(1)-N(2)	89.74(7)
C(10)-N(2)-C(11)	106.11(11)	O(1)-Cu(1)-Cl(1)	92.41(5)
C(10)-N(3)-C(12)	105.91(11)	N(1)-Cu(1)-Cl(1)	161.36(5)
N(1)-C(7)-C(6)	117.06(11)	N(2)-Cu(1)-Cl(1)	97.75(5)
N(1)-C(7)-C(17)	123.91(11)	C(7)-N(1)-Cu(1)	128.47(15)
N(1)-C(8)-C(9)	108.55(10)	C(8)-N(1)-Cu(1)	108.92(13)
N(1)-C(7)-C(17)	123.91(11)	C(1)-O(1)-Cu(1)	126.50(13)
N(1)-C(8)-C(9)	108.55(10)	C(10)-N(2)-Cu(1)	124.52(14)
N(2)-C(10)-N(3)	113.10(12)	C(12)-N(2)-Cu(1)	127.77(13)

Table 5.3. Distances [Å] and angles [°] of hydrogen bonds in compounds (hap-aebmz) (**5.I**) and in [CuCl(hap-aebmz)] (**5.1**).

Compound	D-H···A	D-H	H···A	D···A	D-H···A
5.I	O(1)-H(1O)···N(1)	0.99(3)	1.61(3)	2.5267(15)	152(2)
5.I	N(2)-H(2N)···N(2)_$1	0.92	2.03	2.942(2)	169.1
5.1	N(3)-H(3N)...O1_$1	0.81(3)	1.98(3)	2.786(2)	174(3)

$1 for **5.I**, -x, -y, -z+1
$1 for **5.1**, x+1, y, z

5.3.2. IR Spectral Studies

IR spectrum of **5.I** exhibits two sharp bands at 1615 and 1634 cm^{-1} due to υ(C=N) (azomethine / ring) stretch. These bands move towards lower wave number (1610 cm^{-1}) on coordination of azomethine / ring nitrogen to the metal. The presence of hydrogen bonding between NH of benzimidazile and other electronegative atoms in ligand is indicated by the appearance of several medium intensity bands in the range 2500 – 2700 cm^{-1}. These bands are also present in **5.1** indicating the presence of hydrogen bonding. The coordination of the phenolic oxygen could not be ascertained unequivocally due to the appearance of a weak band at ca. 3400 cm^{-1}. However, structurally characterized complex e.g. [VO_2(sal-aebmz)](Hsal-aebmz = Schiff base derived from salicylaldehyde and 2-aminoethylbenzimidazole) [46] and [Cu^{II}(hap-aebmz)Cl] discussed in this chapter, confirms the monobasic tridentate ONN behaviour of **5.I**. In addition, the far IR region the complex exhibits three sharp bands at 570, 530 and 315 cm^{-1} due to υ(Cu–O), υ(Cu–N) and υ(Cu–Cl) modes, respectively. Complex **5.2** exhibits these bands at 1612 cm^{-1} (C=N), 570 cm^{-1} (Cu–O), 455 cm^{-1} (Cu–N) and 315 cm^{-1} (Cu–Cl).

5.3.3. Electronic Spectral Studies

Table **5.3** presents electronic spectral data of ligand and complexes. The UV spectrum of the ligand is exactly similar to that of Hsal-aebmz reported earlier

[46]. All these bands are also present in the complex **5.1** with slight variations. A band at 452 nm is assigned due to the ligand-to-metal charge transfer (LMCT) from the phenolate oxygen to an empty d orbital of copper. In addition, a broad band at ca. 700 nm also appears due to d – d transition of Cu^{II} ion. Encapsulated complex **5.2** displays only two bands at 225 and 297 nm in Nujol in the UV region and LMCT band at 500 nm in the visible region. The d-d transition band could not be located due to poor loading of **5.1** in the zeolite-Y.

Table 5.4. Electronic spectral data of ligand and complexes

Compounds	Solvent	$\lambda_{max/nm}$ (ε / L mol^{-1} cm^{-1})
Hhap-aebmz (**5.I**)	MeOH	204(5839), 248(1575), 274(1539), 281(1498), 320(328), 388(251)
$[Cu^{II}$(hap-aebmz)Cl] (**5.1**)	MeOH	212(2366), 235(1251), 271(912), 277(821)), 357(201), 299(198), 452(173), 700(47)
$[Cu^{II}$(hap-aebmz)Cl]-Y (**5.2**)	Nujol	225, 297, 390, 500

5.3.4. Field emission-scanning electron micrograph (FE-SEM) and energy dispersive X-ray analysis (EDX) study

Accurate information on the morphological changes in terms of exact orientation of ligands coordinated to the metal ion has not been possible due to poor loading of the metal complex. However, it is clear from the micrograph that zeolite-Y having encapsulated complex has well defined crystals free from any shadow of the metal ions or complex present on its external surface. The micrograph of $[Cu^{II}$(hap-aebmz)Cl]-Y is presented in Figure **5.6** along with the energy dispersive X-ray analysis (EDX) profile. Energy dispersive X-ray analysis plot, evaluated semi-quantitatively, support this conclusion as no copper or nitrogen contents were noted on the spotted surface on the micrograph of $[Cu^{II}$(hap-aebmz)Cl]-Y. Thus, complex is present in the nano cavities of the zeolite-Y.

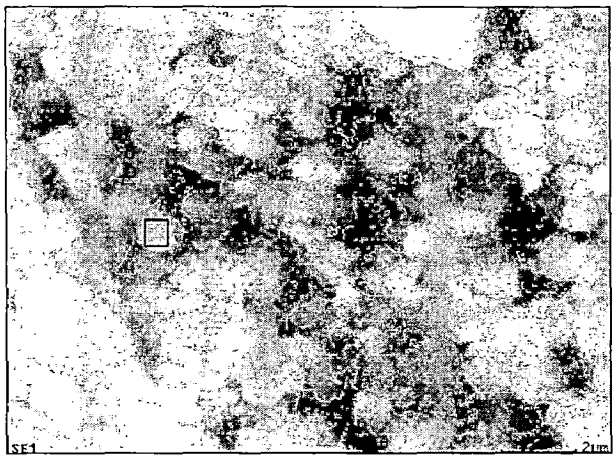

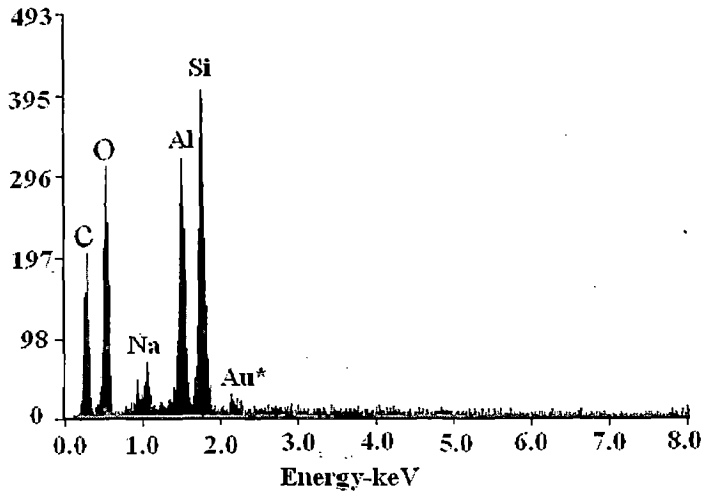

Figure 5.6. Scanning electron micrograph of [Cu^{II}(hap-aebmz)Cl]-Y (left) and Energy dispersive X-ray analysis (EDX) profile of [Cu^{II}(hap-aebmz)Cl]-Y(right).

5.3.5. Powder X-ray diffraction study

The powder X-ray diffraction patterns of Na-Y, [Cu^{II}]-Y and [Cu^{II}(hap-aepy)Cl]-Y (Figure 5.7) were recorded at 2θ values between 5 and 70° to compare their crystalline nature and to ensure encapsulation of complex inside the cavity. Essentially similar diffraction patterns in encapsulated complex, [Cu^{II}]-Y and Na-Y were noticed except a slightly weaker intensity of the zeolite having metal complex encapsulated. These observations indicate that the framework of the zeolite has not undergone any significant structural change during incorporation of the catalyst i.e. crystallinity of the zeolite-Y is preserved during encapsulation. No new peaks due to encapsulated complex were detected in the complex encapsulated sample possibly due to very low percentage loading of metal complex. However, the copper content found (see experimental) after encapsulation is only due to the presence of copper(II) complex in the cavities of the zeolite-Y.

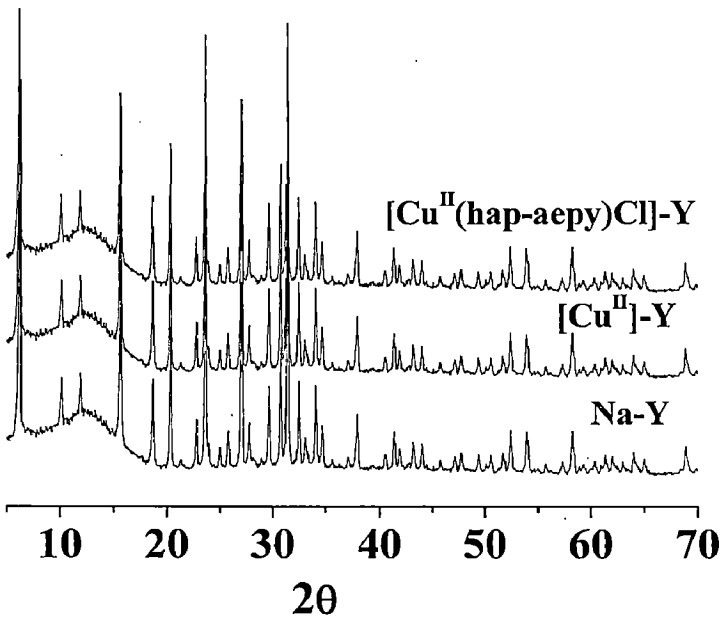

Figure 5.7. XRD patterns of Na-Y, [Cu^{II}]-Y and [Cu^{II}(hap-aebmz)Cl]-Y.

5.3.6. Catalytic reactions

5.3.6.1. Oxidation of cyclohexene

Complex [Cu^{II}(hap-aebmz)Cl]-Y catalyzes the oxidation of cyclohexene by H_2O_2 efficiently to give cyclohexene epoxide, 2-cyclohexene-1-one, 2-cyclohexene-1-ol, and cyclohexane-1,2-diol as presented in Scheme 5.2.

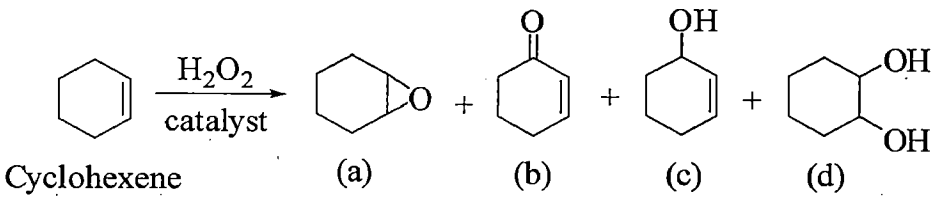

Scheme 5.2. Reaction products of cyclohexene. (a) = cyclohexene epoxide, (b) = 2-cyclohexene-1-one, (c) = 2-cyclohexene-1-ol and (d) = cyclohexane-1,2-diol.

Reaction conditions have been optimized for the maximum oxidation of cyclohexene by varying different parameters viz. the effect of amount of oxidant (moles of H_2O_2 per mole of cyclohexene), catalyst (amount of catalyst per mole of cyclohexene), temperature and solvent amount of the reaction mixture.

Three different cyclohexene to aqueous 30% H_2O_2 molar ratios viz 1:1, 1:2 and 1:3 were considered while keeping the fixed amount of cyclohexene (0.82 g, 10 mmol) and catalyst (0.004 g) in 10 ml of MeCN and the reaction was carried out at 80 °C. The percentage conversion of cyclohexene as a function of time is presented in Figure 5.8. A maximum of 85.0 % conversion was obtained at a cyclohexene/ aqueous H_2O_2 molar ratio of 1:1 in 6 h of reaction time. This conversion reached to 91.0% and 95.0% at cyclohexene/ H_2O_2 ratio of 1:2 and 1:3, respectively. As cyclohexene/ aqueous H_2O_2 ratio of 1:3 showed increment of only 4 % as compared to that of 1:2, a 1:2 molar ratio was considered suitable to obtain the optimum cyclohexene conversion of 91.0% in 6 h reaction time.

The effect of amount of catalyst on the oxidation of cyclohexene is shown in Figure 5.9. Three different amounts of catalyst viz. 0.003, 0.004 and 0.005 g were considered while keeping the fixed amount of cyclohexene (0.82 g, 10 mmol), aqueous H_2O_2 (2.27 g, 20 mmol) in MeCN (10 ml) and reaction was

carried out at 80 °C. It is clear from the plot that 0.005 g catalyst is the best one to obtain the highest conversion (96 %) of cyclohexene.

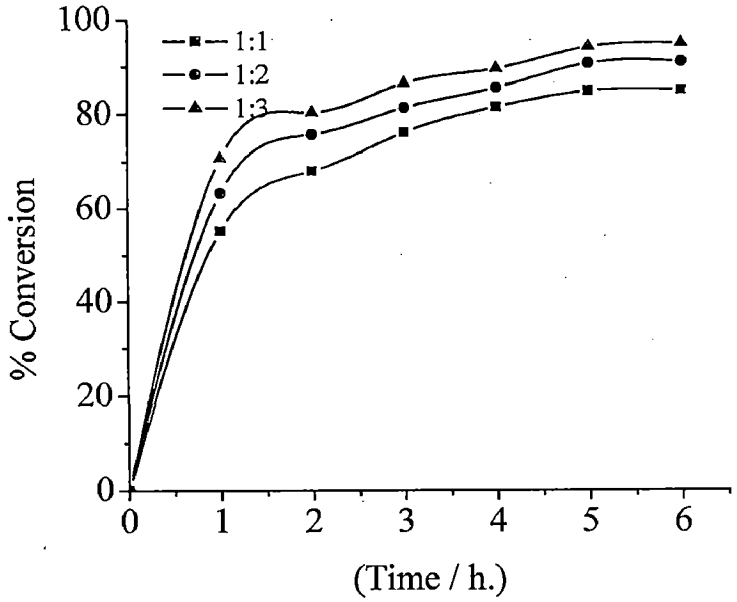

Figure 5.8. Effect of oxidant concentration on cyclohexene oxidation. Reaction conditions: cyclohexene (0.82 g, 10 mmol), catalyst (0.004 g), acetonitrile (10 ml) and temp. (80 °C).

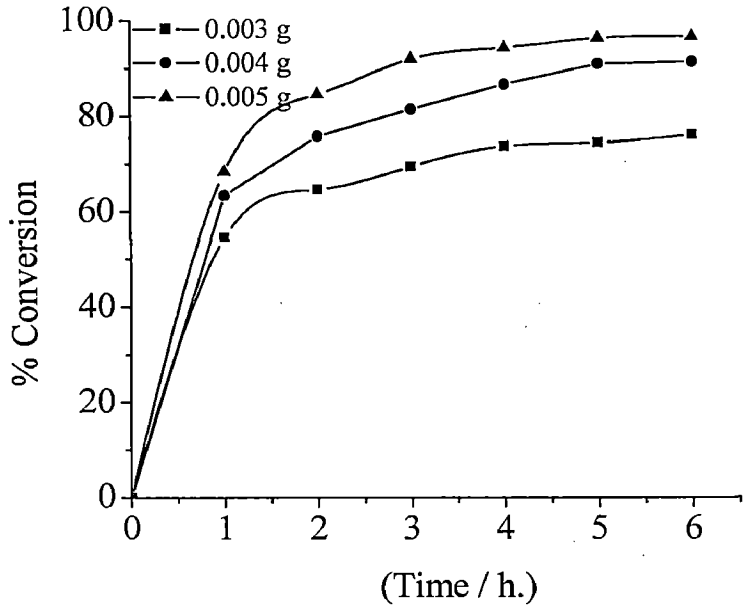

Figure 5.9. Effect of catalyst amount on the cyclohexene oxidation. Reaction conditions: cyclohexene (0.82 g, 10 mmol), H_2O_2 (2.27 g, 20 mmol) and acetonitrile (10 ml) and temp. (80 °C)

Figure 5.10 illustrates the oxidation of cyclohexene at three different volumes (5, 10 and 15 ml) while keeping the optimized conditions of catalyst (0.005 g), cyclohexene (0.82 g, 10 mmol) and H_2O_2 (2.27 g, 20 mmol), and running the reaction at 80 °C. It is evident from the plot that the performance of the reaction in 5 ml solvent amount is most suitable to obtain nearly quantitative oxidation (99.6%) of cyclohexene. Similarly we have also observed that conducting the catalytic reaction at 80 °C is most suitable to maximize the oxidation of cyclohexene.

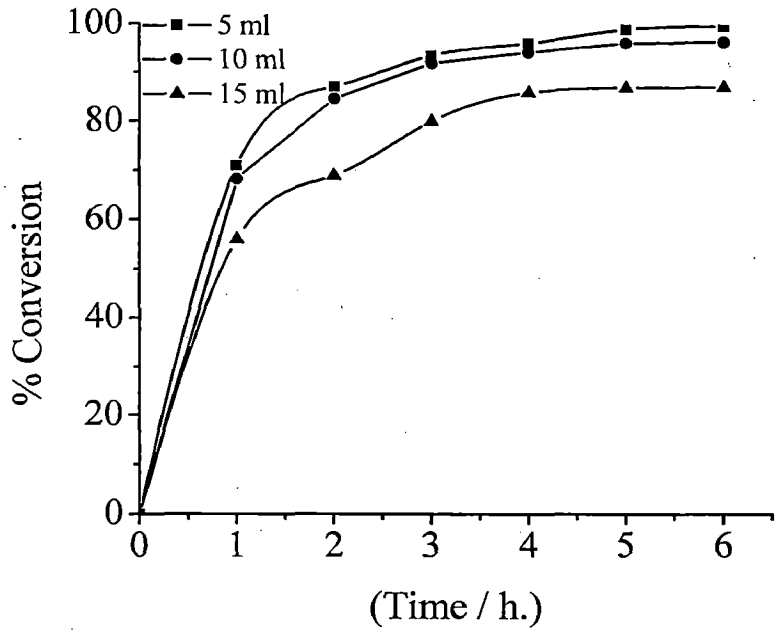

Figure 5.10. Effect of solvent amount on cyclohexene oxidation. Reaction conditions: Cyclohexene (0.82 g, 10 mmol), catalyst (0.005 g), H_2O_2 (2.27 g, 20 mmol) and temp. (80 °C).

Thus, for the maximum oxidation of 10 mmol (0.82 g) of cyclohexene, the other required conditions as concluded were: $[Cu^{II}$(hap-aebmz)Cl]-Y (0.005 g), H_2O_2 (2.27 g, 20 mmol), acetonitrile (5 ml) and temperature (80 °C). Under this condition nearly quantitative oxidation (99.6%) of cyclohexene was achieved where the selectivity of different products followed the order: 2-cyclohexene-1-ol (44%) > 2-cyclohexene-1-one (40%) cyclohexene epoxide (12%) > cyclohexane-1, 2-diol (4%). A maximum of 90 % conversion with neat catalyst precursor

[Cu^{II}(hap-aebmz)Cl] was obtained under similar conditions where products selectivity varied in the order: 2-cyclohexene-1-ol (33%)> 2-cyclohexene-1-one (32%) > cyclohexane-1,2-diol (23%) > cyclohexene epoxide (8%). Thus, encapsulated catalyst performs better and catalyses the oxidation of cyclohexene almost quantitatively.

Catalytic potential of the encapsulated complex presented here compares well with similar encapsulated complexes. For example, [Cu(2-pyrazinecarboxylate)$_2$]-Y exhibited as high as 90.5 % conversion of cyclohexene at a substrate to oxidant (30 % H_2O_2) ratio of 1:2 where no formation of cyclohexene epoxide was observed and the selectivity of the other oxidation products varied in the order: 2-cyclohexene-1-one (51%)> 2-cyclohexene-1-ol (42.4%) > cyclohexane-1,2-diol (6.6%) [209]. Complex [Cu(sal-oaba)(H_2O)]-Y, however, exhibited only 45.8% conversion with the formation of only two products, 2-cyclohexene-1-one and 2-cyclohexene-1-ol [210]. Cyclohexene was oxidized very slowly by *tert*-butylhydroperoxide using similar catalyst [Cu(pan)Cl)]-Y (where Hpan = 1-(2-pyridylazo)-2-naphthol) under aerobic conditions and only 28% conversion was obtained Here, the percent selectivity of products varied in the order: 1-*tert*-butylperoxy-2-cyclohexene 89% > 2-cyclohexene-1-one (11%) [211].

The reaction mixture of [Cu^{II}(hap-aebmz)Cl]-Y, cyclohexene and solvent taken under above optimized conditions after a contact time of 6 h at 80 °C was filtered and after activating the catalyst by washing with acetonitrile and drying at ca. 120 °C, it was subjected to further catalytic reaction under similar conditions. A maximum conversion of 98 % suggests that complex is still present in the cavity of the zeolite-Y. The filtrate collected after separating the used catalyst was placed into the reaction flask and the reaction was continued after adding fresh oxidant for another 2 h. The gas chromatographic analysis showed no change in conversion and this confirms that the reaction did not proceed upon removal of the solid catalyst. The reaction was, therefore, heterogeneous in nature.

5.3.6.2. Oxidation of phenol

The catalysts based on zeolite encapsulated metal complexes have played excellent role in the oxidation of phenol and a wide range of products selectivity has been reported [212,213,94]. Oxidation of phenol, catalyzed by [Cu^{II}(hap-aebmz)Cl]-Y using H_2O_2 as an oxidant gave two major products catechol and hydroquinone with a mass balance of ca. 97%. These are the only expected products based on the directing group of phenol. Gas chromatographic analysis also indicated a minor product, which may possibly be benzoquinone formed by partial oxidation of hydroquinone (Scheme 5.3) but it was ignored. Slight colouration of reaction mixture, which is not detectable by GC under the condition used herein, is possibly due to polymeric materials.

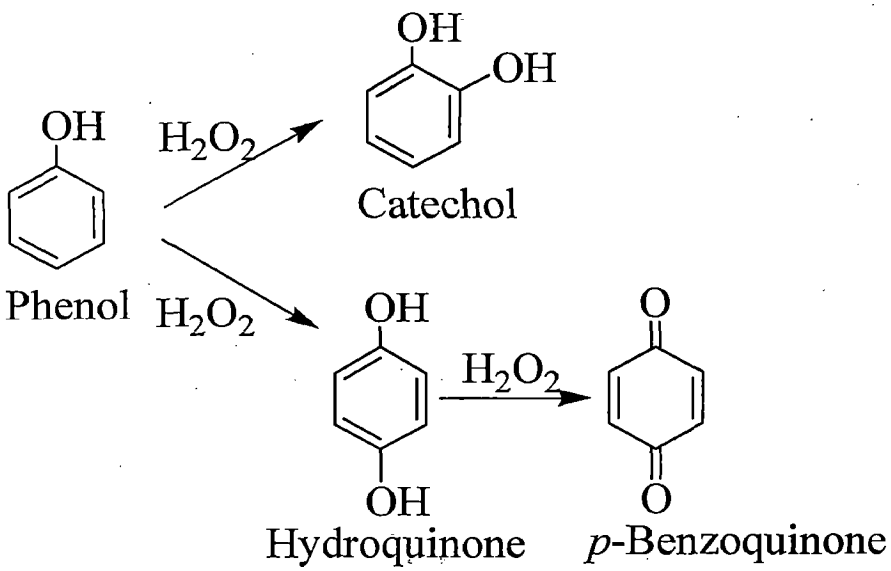

Scheme 5.3. Oxidation products of phenol.

In order to achieve suitable reaction conditions for the maximum oxidation of phenol, the effect, (i) amount of catalyst per mole of phenol, (ii) H_2O_2 concentration (moles of H_2O_2 per mole of phenol, (iii) volume of solvent and (iv) temperature of the reaction mixture were also studied here.

The effect of amount of catalyst on the oxidation of phenol is shown in Figure. 5.11. Increasing the catalyst amount from 0.005 g to 0.010 g at the fixed

amount of phenol (1.88 g, 20 mmol), aqueous 30% H_2O_2 (2.27 g, 20 mmol), acetonitrile (5 ml) and temperature (80 °C) increases the conversion from 40.3% to 43.3%. Further increasing the catalyst amount to 0.015 g initiates the reaction quickly but over all conversion of phenol reaches to only 37.1%. As 0.010 g catalyst shows only 3 % increment of conversion compared to 0.005 g of catalyst, an amount of 0.005 g is considered the best to bring optimum conversion of phenol in 6 h of reaction time.

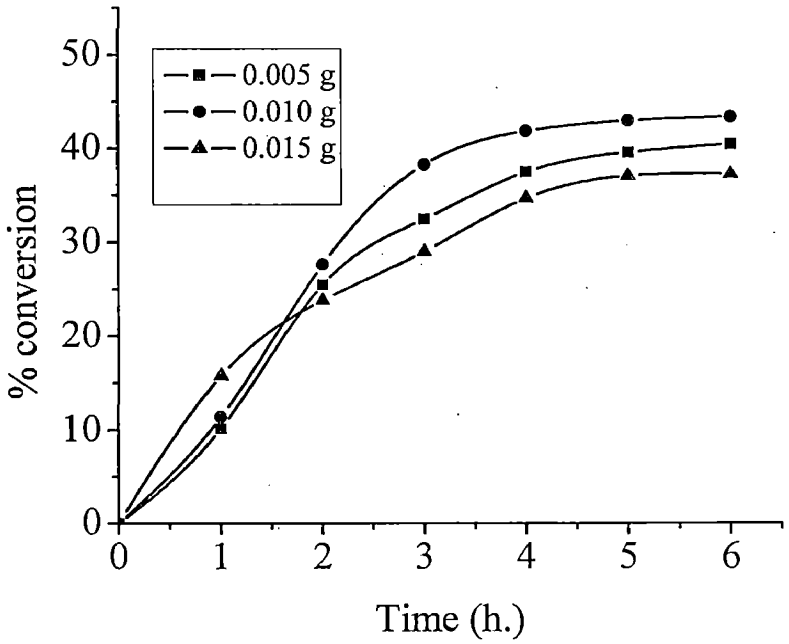

Figure 5.11. Effect of catalyst amount on phenol oxidation. Reaction conditions: Phenol (1.88 g, 20 mmol), H_2O_2 (2.27 g, 20 mmol), acetonitrile (5 ml) and temp. (80 °C).

Using three different phenol to H_2O_2 molar ratios viz. 1 : 1, 1 : 2 and 1 : 3 for a fixed amount of phenol (1.88 g, 20 mmol), [Cu^{II}(hap-aebmz)Cl]-Y (0.005 g), MeCN (5 ml) and temperature (80 °C), the obtained percentage conversion of phenol were 40.3%, 48.3% and 65.7%, respectively. It is clear from the plot presented as a function of time (Figure 5.12) that the phenol to aqueous 30% H_2O_2 molar ratio of 1 : 3 is the best ratio to obtain maximum oxidation of phenol

(65.7%) at 80 °C while 1 : 1 and 1 : 2 molar ratios gave lower conversions. About 6 h was required to establish the equilibrium.

Variation in the volume of the solvent was also studied by taking 5, 10 and 15 ml of acetonitrile; Figure 5.13. It was observed that for 1.88 g (20 mmol) of phenol, catalyst (0.005 g), H_2O_2 (7.98 g, 60 mmol), acetonitrile (5 ml) and reaction temperature (80 °C) were sufficient enough to carry out the reaction for good transformation (65.7%) of phenol. The temperature of the reaction medium also influences the reaction rate. It was inferred that 80 °C was the best suited temperature for the maximum oxidation of phenol under the above reaction conditions. At this temperature, a maximum of 65.7% conversion of phenol was achieved in 6 h of contact time. Lowering the temperature lowers the conversion of phenol. Catalytic results under all reaction conditions are presented in Table 5.5.

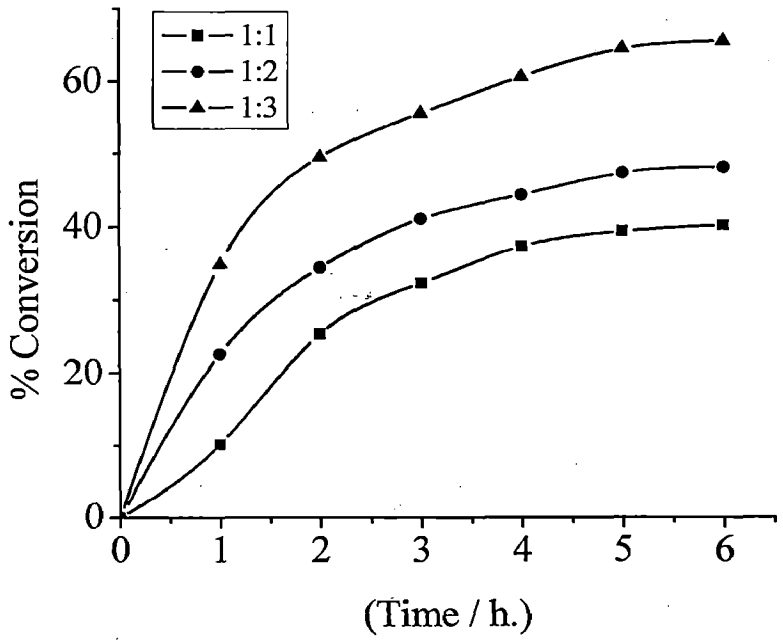

Figure 5.12. Effect of oxidant concentration on phenol oxidation. Reaction conditions: Phenol (1.88 g, 20 mmol), catalyst (0.005 g), acetonitrile (5 ml) and temp. (80 °C).

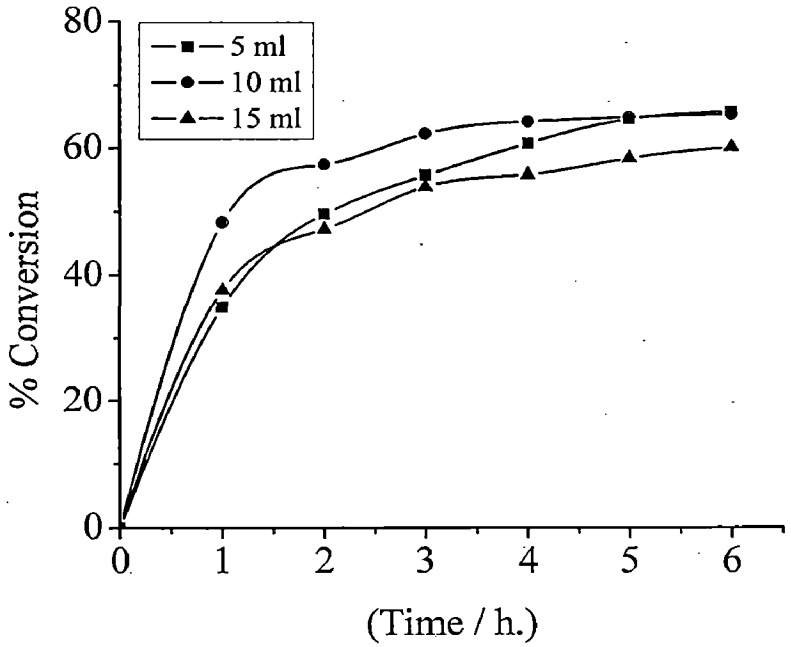

Figure 5.13. Effect of solvent on phenol oxidation. Reaction conditions: phenol (1.88 g, 20 mmol), catalyst (0.005 g), H_2O_2 (6.81 g, 60 mmol) and temp. (80 °C).

Table 5.5. Conversion of phenol (1.88 gm, 20 mmol) using $[Cu^{II}(hap\text{-}aebmz)Cl]$-Y as catalyst in 6 h of reaction time under different reaction conditions.

Entry No.	Catalyst (g)	H_2O_2 (g, mmol)	Temp. (° C)	MeCN (ml)	Conv. %	Selectivity %		
						Cat	Hq	Unidentified
1	0.005	2.27, 20	80	5	40.3	70.6	27.0	2.4
2	0.010	2.27, 20	80	5	43.3	60.1	36.5	3.4
3	0.015	2.27, 20	80	5	37.2	69.7	29.9	0.4
4	0.005	4.54, 40	80	5	48.3	66.7	32.3	1.0
5	0.005	6.81, 60	80	5	65.7	66.1	32.9	1.0
6	0.005	6.81, 60	80	10	65.4	66.6	33.2	0.2
7	0.005	6.81, 60	80	15	60.1	66.4	33.5	0.1
8	0.005	6.81, 60	75	5	62.9	67.2	32.8	-

Thus, optimized operating reaction conditions for the maximum oxidation of phenol were fixed as follows: phenol (1.88 g, 20 mmol), [Cu^{II}(hap-aebmz)Cl]-Y (0.005 g), 30% H_2O_2 (6.81 g, 60 mmol), acetonitrile (5 ml) and reaction temperature (80 °C). Under this condition, [Cu^{II}(hap-aebmz)Cl]-Y exhibits 65.7 % conversion where the selectivity of major product catechol was 66.1 % and of hydroquinone was 32.9 %. The performance of the neat complex [Cu^{II}(hap-aebmz)Cl], considering same mole concentration as was used for encapsulated one, under the above reaction conditions is low (44%) with 66% selectivity of the major product. Thus, encapsulation of the complex [Cu^{II}(hap-aebmz)Cl] in zeolite-Y enhances its catalytic activity. The overall performance of encapsulated complex is also better along with the higher turn over frequency (TOF) than the corresponding neat one.

The catalytic performance of the encapsulated complex reported here is better than the data reported in the literature. For example, the observed conversions for zeolite-Y encapsulated complexes are: [Cu(sal-ambmz)Cl]-Y (42.0%) [151], [Cu(salpn)]-Y (H_2salpn = N,N′-bis(salicylidene)propane-1,3-diamine) (31%) [214], Cu(saldien)]-Y (46%) [215], [VO(salen)]-Y (32.6 %) [103]. Catalyst NH_4[VO(sal-inh)]-Y (H_2sal-inh = Schiff base derived from salicylaldehyde and isonicotinic acid hydrazide) exhibits only 26.5 % conversion [216]. The selectivity towards the formation of catechol in all cases is always higher than hydroquinone.

5.3.7. Reaction of [Cu^{II}(hap-aebmz)Cl] with H_2O_2 and possible reaction pathway of the catalyst

At least three types of intermediates having a copper–oxygen interaction viz. side-on Cu^{III}–(μ-η^2-peroxido)–Cu^{III}, bis(μ-oxido–Cu^{III}) and Cu^{III}–O–O–H (copperhydroperoxide) have been reported in the literature during the catalytic action [217,218]. We have studied the interaction of **5.1** with H_2O_2 in methanol by electronic absorpt ion spectroscopy to have idea of the possible intermediate during catalytic activity. Thus the addition of one-drop portions of 30% H_2O_2 dissolved in methanol to ca.10^{-3} M methanolic solution of [Cu^{II}(hap-aebmz)Cl] results in the

gradual weakening of the 700 nm band. The band at 452 nm also weakens along with increase in intensity and shifts to ca. 445 nm (see inset of Figure 5.14). Addition of H_2O_2 to a diluted solution (ca.10^{-4} M) resulted in the increment of the intensities of 357 and 299 nm bands (Figure 5.14) along with their conversion into weak shoulders. Two bands appearing at 271 and 277 nm remain almost unchanged while bands at 212 and 235 nm slightly gain intensity.

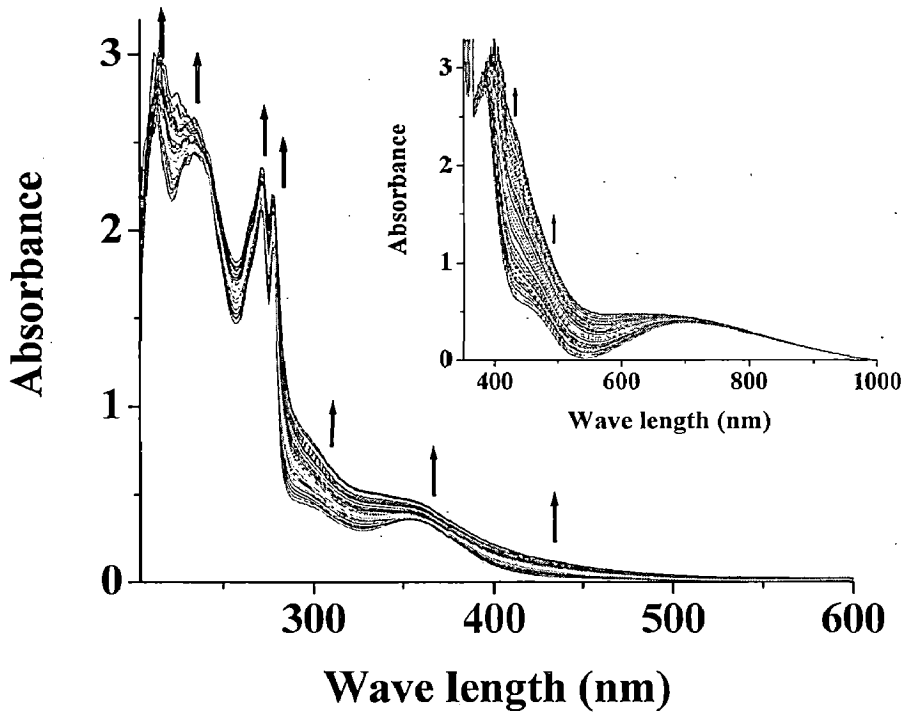

Figure 5.14. Spectral changes observed during the titration of a methanolic solution of [Cu^{II}(hap-aebmz)Cl] (ca. 10^{-4} M) with 30% H_2O_2 dissolved in minimum amount of methanol. Spectra were recorded after successive addition of 2 drops portion of H_2O_2 solution. In set shows similar titration with higher concentration of complex (ca. 10^{-3} M).

All these suggest the interaction of H_2O_2 with Cu^{II} centre. As complex [Cu^{II}(hap-aebmz)Cl] is expected to remain in its monomeric form in the nano cavity of the zeolite-Y, the facile formation of intermediate [(HOO)-Cu^{III}(hap-aebmz)Cl] is expected because of its possibility to expand the coordination number even in the cavity of zeolite-Y. The expansion of coordination number of Cu^{II} complexes having monobasic tridentate ONN donor ligands through

dimerization/polymerization is very common [199-203]. Such (L)Cu^{III}–O–O–H complexes are known to exhibit a charge transfer band at ca. 600 nm [219]. The decrease in the intensity of 700 nm band without any isosbestic point in complex may possibly be due to the merging of this additional charge transfer band with d–d transition. The peroxide intermediate finally transfers coordinated oxygen atoms to the substrate to give the products.

5.4. Conclusions

By using Schiff base Hhap-aebmz, an ONN donor ligand, complex [Cu^{II}(hap-aebmz)Cl] has been prepared. Structures of ligand as well as complex have been confirmed by single crystal X-ray study. Complex [Cu^{II}(hap-aebmz)Cl] has been encapsulated in the cavity of zeolite-Y and its catalytic activity for the oxidation of cyclohexene has been evaluated. Nearly quantitative conversion with the selectivity of different products of the order, 2-cyclohexene-1-ol (44 %) > 2-cyclohexene-1-one (40 %) cyclohexene epoxide (12 %) > cyclohexane-1,2-diol (4%) has been obtained. The recyclability of the catalyst is an added advantage. Oxidation of cyclohexene proceeds through intermediate [(HOO)-Cu^{III}(hap-aebmz)Cl] species, formation of which has been demonstrated by electronic absorption spectroscopy.

References

References

1. N. D. Chasteen, "The biochemistry of vanadium", Struc. Bond., 53, 105 – 138, 1983.

2. L. C. Cantley, L. Josephson, R. Warner, M. Yanaisawa, C. Lechene and G. Guidotti, "Vanadate is a potent (Na, K)-ATPase inhibitor found in ATP derived from muscle", J. Biol. Chem., 252, 7421 – 7423, 1977.

3. L. Josephson and L. C. Cantley, "Isolation of a potent (Na-K) stimulated ATPase inhibitor from striated muscle", Biochem., 16, 4572 – 4578, 1977.

4. B. Venugopal and T. D. Luckey, "Metal toxicity in mammals. 2. Chemical toxicity of metals and metalloids", New York, Plenum Press, pp. 220 – 226, 1978.

5. Y. Sheehter and A. Shisheva, "Vanadium salts and the future treatment of diabetes", Endeavour, 17, 27 – 31, 1993.

6. D. Gambino, "Potentiality of vanadium compounds as anti-parasitic agents", Coord. Chem. Rev., 255, 2193– 2203, 2011.

7. H. Sakurai, Y. Kojima, Y. Yoshikawa, K. Kawabe and H. Yasui, "Antidiabetic vanadium(IV) and zinc(II) complexes", Coord. Chem. Rev., 226, 187 – 198, 2002.

8. K. H. Thompson, J. H. McNeill and C. Orvig, "Vanadium compound as insulin mimics", Chem. Rev., 99, 2561 – 2571, 1999.

9. D. C. Crans, "Chemistry and insulin–like properties of vanadium(IV) and vanadium(V) compounds", J. Inorg. Biochem., 80, 123 – 131, 2000.

10. L. H. Gao, W. P. Liu, B. L. Wang, L. Li, M. J. Xie, Y. R. Li, Z. H. Chen and X. Z. Chen, "Effects of bis(α–furancarboxylato)oxovanadium(IV) on non–diabetic and streptozotocin–diabetic rats", Clin. Chim. Acta, 368, 173 – 178, 2006.

11. M. Yamaguchi, K. Wakasugi, R. Saito, Y. Adachi, Y. Yoshikawa, H. Sakurai and A. Katoh, "Syntheses of vanadyl and zinc(II) complexes of 1–hydroxy–4,5,6– substituted 2(1H)–pyrimidinones and their insulin–mimetic activities", J. Inorg. Biochem., 100, 260 – 269, 2006.

12. D. Rehder, J. C. Pessoa, C. F. G. C. Geraldes, M. M. C. A. Castro, T. Kabanos, T. Kiss, B. Meier, G. Micera, L. Pettersson, M. Rangel, A. Salifoglou, I. Turel and D. Wang, "In vitro study of the insulin–mimetic behaviour of vanadium(IV,V) coordination compounds", J. Biol. Inorg. Chem., 7, 384 – 396, 2002.

13. H. Vilter, "Peroxidases from phaeophyceae: A vanadium(V)-dependent peroxidase from Ascophyllum nodosum", Phytochem., 23, 1387 – 1390, 1984.

14. U. Kusthardt, B. Hedman, K. O. Hodgson, R. Hahn and H. Vilter, "High-resolution XANES studies on vanadium-containing haloperoxidase: pH-dependence and substrate binding", Federation Eur. Biochem. Soc., 329, 5 – 8, 1993.

15. M. Weyand, H. J. Hecht, M. Kiesz, M. F. Liaud, H. Vilter and D. Schomburg, "X-ray structure determination of a vanadium-dependent haloperoxidase from

Ascophyllum nodosum at 2.0 Å Resolution", J. Mol. Biol., 293, 595 – 611, 1999.

16. M. I. Isupov, A. R. Dalby, A. Brindley, Y. Izumi, T. Tanabe, G. N. Murshudov and J. A. Littlechild, "Crystal structure of vanadium dependent bromoperoxidase from Corallina officinalis", J. Mol. Biol., 299, 1035 – 1049, 2000.

17. A. Messerschmidt and R. Wever, "X-ray structure of a vanadium-containing enzyme: Chloroperoxidase from the fungus Curvularia inaequalis", Proc. Natl. Acad. Sci. U.S.A., 93, 392 – 396, 1996.

18. C. Dong, F. Huang, H. Deng, C. Schaffrath, J.B. Spencer, D. O'Hagan and H.J. Naismith, "Crystal structure and mechanism of a bacterial fluorinating enzyme", Nature, 427, 561 – 565, 2004.

19. A. Messerschmidt, L. Prade, and R.Wever, "Implications for the catalytic mechanism of the vanadium-containing enzyme chloroperoxidase from the fungus Curvularia inaequalis by X-ray structures of the native and peroxide form", Biol. Chem., 378, 309 – 315, 1997.

20. B. H. Simons, P. Barnett, E. G. M. Vollenbroek, H. L. Dekker, A. O. Muijsers, A. Messerschmidt and R. Wever, "Primary structure and characterization of the vanadium chloroperoxidase from the fungus Curvularia inaequalis", Eur. J. Biochem.,229, 566 – 574, 1995.

21. M. P. J. van Deurzen, I. J. Remkes, F. van Rantwijk and R. A. Sheldon, "Chloroperoxidase catalyzed oxidations in t-butyl alcohol/water mixtures", J. Mol. Catal. A: Chem., 117, 329–337, 1997.

22. M. P. J. van Deurzen, F. van Rantwijk and R. A. Sheldon, "Selective oxidations catalyzed by peroxidases", Tetrahedron, 53, 13183–13220, 1997.

23. W. Hemrika, R. Renirie, H L. Dekker, P. Barnett and R. Wever, "From phosphatases to vanadium peroxidases: A similar architecture of the active site", Proc. Natl. Acad. Sci. U.S.A., 94, 2145–2149, 1997.

24. A. F. Neuwald, "An unexpected structural relationship between integral membrane phosphatases and soluble haloperoxidases", Protein Sci., 6, 1764–1767, 1997.

25. H. B. ten Brink, H. E. Schoemaker and R. Wever, "Sulfoxidation mechanism of vanadium bromoperoxidase from Ascophyllum nodosum: Evidence for direct oxygen transfer catalysis", Eur. J. Biochem., 268, 132–138, 2001.

26. N. Jayme, Carter-Franklin, and A. Butler, "Vanadium bromoperoxidase-catalyzed biosynthesis of halogenated marine natural products", J. Am. Chem. Soc., 126, 15060–15066, 2004.

27. D. Wischang, O. Brucher and J. Hartung, "Bromoperoxidases and functional mimica as catalysts for oxidative bromination-a sustainable synthetic approach", Coord. Chem. Rev., 255, 2204 – 2217, 2011.

28. D. Rehder, "The coordination chemistry of vanadium as related to its biological functions", Coord. Chem. Rev., 182, 297 – 322, 1999.

29. D. Rehder, "Metal ions in biological systems: Vanadium and its role in life", (Eds.: H. Sigel, A. Sigel), Marcel Dekker Inc., New York, chapter 1. 1995.

30. M. R. Maurya, "Development of the coordination chemistry of vanadium through bis(acetylacetonato)oxovanadium(IV): synthesis, reactivity and structural aspects", Coord. Chem. Rev., 237, 163-181, 2003.

31. M. R. Maurya, "Structural models of vanadate-dependent haloperoxidases and their reactivity", J. Chem. Sci., 118, 503-511, 2006.

32. M. R. Maurya, "Structural models of vanadate-dependent haloperoxidases, their reactivity, immobilization on polymer support and catalytic activities", J. Chem. Sci., 123, 215-228, 2011.

33. M. R. Maurya, A. Kumar and J. Costa Pessoa, "Vanadium complexes immobilized on solid supports and their use as catalysts for oxidation and functionalization of alkanes and alkenes", Coord. Chem Rev., 255, 2315–2344, 2011.

34. C. R. Cornman, J. Kampf, M. S. Lah and V. L Pecoraro, "Modeling vanadium bromoperoxidase: Synthesis, structure, and spectral properties of vanadium(IV) complexes with coordinated imidazole", Inorg. Chem., 31, 2035 – 2043, 1992.

35. C. R. Cornman, G. J. Colpas, J. D. Hoeschele, J. Kampf and V. L. Pecoraro, "Implications for the spectroscopic assignment of vanadium biomolecules: Structural and spectroscopic characterization of monooxovanadium(V) complexes containing catecholate and hydroximate based noninnocent ligands", J. Am. Chem. Soc., 114, 9925 – 9933, 1992.

36. C. R. Cornman, J. Kampf and V. L. Pecoraro, "Structural and spectroscopic characterization of Vanadium(V)–oxoimidazole complexes", Inorg. Chem., 31, 1981 – 1983, 1992.

37. M. Sivák, D. Joniaková and P. Schwendt, "Nitrilotriacetato–monoperoxo complexes of vanadium(V): Formation in aqueous solution, synthesis and structure", Trans. Met. Chem., 18, 304 – 309, 1993.

38. L. Kuchta, M. Sivak and F. Pavelcik, "Synthesis, characterization and crystal structure of barium(nitrilotriacetato)oxoperoxovanadate(V) trihydrate", J. Chem. Res. (S), 393– 394, 1993.

39. F. W. B. Einstein, R. J. Batchelor, S. J. Angus–Dunne and A. S. Tracey, "A product formed from glycylglycine in the presence of vanadate and hydrogen peroxide: The (glycylde–N–hydroglycinato–κ^3N^2,N^N,O^1)oxoperoxovanadate(V) Anion", Inorg. Chem., 35, 1680– 1684, 1996.

40. M. Cásny, M. Sivák and D. Rehder, "Monoperoxo–vanadium(V) complexes of R,S–N–(carboxymethyl)aspartate", Inorg. Chim. Acta, 355, 223– 228, 2003.

41. V. Conte, O. Bortolini, M. Carraro and S. Moro, "Models for the active site of vanadium–dependent haloperoxidases: Insight into the solution structure of peroxo vanadium compounds", J. Inorg. Biochem., 80, 41– 49, 2000.

42. M. R. Maurya, S. Khurana, C. Schulzke and D. Rehder, "Dioxo- and oxovanadium(V) complexes of biomimetic hydrazone ONO donor ligands: Synthesis, characterisation, and reactivity", Eur. J. Inorg. Chem., 779 – 788, 2001.

43. M. R. Maurya, S. Agarwal, C. Bader, M. Ebel and D. Rehder, "Synthesis, characterisation and catalytic potential of hydrazonatovanadium(V) model complexes with $[VO]^{3+}$ and $[VO_2]^{+}$ cores", Dalton Trans., 537– 544, 2005.

44. W. Plass, A. Pohlmann and H.K. Yozgatli, "N-salicylidenehydrazides as versatile tridentate ligands for dioxovanadium(V) complexes", J. Inorg. Biochem., 80, 181– 183, 2000.

45. M. R. Maurya, S. Agarwal, C. Bader and D. Rehder, "Dioxovanadium(V) complexes of ONO donor ligands derived from pyridoxal and hydrazides: Models of vanadate-dependent haloperoxidases", Eur. J. Inorg. Chem., 147 – 157, 2005.

46. M. R. Maurya, A. Kumar, M. Ebel and D. Rehder, "Synthesis, characterization, reactivity, and catalytic potential of model vanadium(IV,V) complexes with benzimidazole-derived ONN donor ligands", Inorg. Chem., 45, 5924 – 5937, 2006.

47. M. R. Maurya, A. Arya, U. Kumar, A. Kumar, F. Avecilla and J. Costa Pessoa, "Polymer-bound oxidovanadium(IV) and dioxidovanadium(V) complexes: synthesis, characterization and catalytic application for the hydroamination of styrene and vinyl pyridine", Dalton Trans., 9555 – 9566, 2009.

48. M. R. Maurya, A. Arya, A. Kumar, M. L. Kuznetsov, F. Avecilla and J. Costa Pessoa, "Polymer-bound oxidovanadium(IV) and dioxidovanadium(V) complexes as catalysts for the oxidative desulfurization of model fuel diesel", Inorg. Chem., 49, 6586 – 6600, 2010.

49. M. R. Maurya, A. Arya, A. Kumar and J. Costa Pessoa, "Polystyrene bound oxidovanadium(IV) and dioxidovanadium(V) complexes of histamine derived ligand for the oxidation of methyl phenyl sulfide, diphenyl sulfide and benzoin", Dalton Trans., 2185 – 2195, 2009.

50. M. J. Xie, Y. Ping, L. D. Zheng, J. Z. Hui and C. Peng, "{2-[2-(N,N'-Dimethylamino)ethyliminomethyl]phenolato-κ3N,N',O}dioxovanadium(V)", Acta Crystallogr. Sect., E60(10), m1382-m1383, 2004.

51. D. Rehder, C. Weidemann, A. Duch and W. Priebsch, "Vanadium-51 shielding in vanadium(V) complexes: A reference scale for vanadium binding sites in biomolecules", Inorg. Chem., 27, 584 – 587, 1988.

52. M. R. Maurya, A. A. Khan, A. Azam, S. Ranjan, N. Mondal, A. Kumar and J. Costa Pessoa, "Dinuclear oxidovanadium(IV) and dioxidovanadium(V) complexes of 5,5-methylenebis(dibasic tridentate) ligands: Synthesis, spectral characterisation, reactivity, and catalytic and antiamoebic activities", Eur. J. Inorg. Chem., 5377–5390, 2009.

53. M. R. Maurya, A. A. Khan, A. Azam, S. Ranjan, N. Mondal, A. Kumar and F. Avecillam J. Costa Pessoa, "Vanadium complexes having $[V^{IV}O]^{2+}$ and $[V^{V}O_2]^{+}$ cores with binucleating dibasic tetradentate ligands: Synthesis, characterization, catalytic and antiamoebic activities", Dalton Trans.,1345–1360, 2010.

54. G. J. Colpas, B.J. Hamstra, J.W. Kampf and V.L. Pecoraro, "Functional models for vanadium haloperoxidase: Reactivity and mechanism of halide oxidation", J. Am. Chem. Soc., 118, 3469 – 3478, 1996.

55. N. D. Chasteen in "Biological Magnetic Resonance", (Ed.: J. Reuben), Plenum, New York, p. 53, 1981.

56. D. Rehder, "Bioinorganic Vanadium Chemistry", John Wiley & Sons, New York, 2008.

57. A. Butler in J. Reedijk, E. Bouwman (Eds.), Bioinorganic Catalysis, Marcel Dekker, New York , 2nd ed. (Chapter 5), 1999.

58. C. Slebodnick, B. J. Hamstra and V. L. Pecoraro, "Modeling the biological chemistry of vanadium: Structural and reactivity studies elucidating biological function", Struct. Bonding (Berlin), 89, 51 – 107, 1997.

59. M. R. Maurya, M. Kumar and A. Arya, "Model dioxovanadium(V) complexes through direct immobilization on polymer support, their characterization and catalytic activities", Catal. Commun., 10, 187 – 191, 2008.

60. M. R. Maurya, H. Saklani and S. Agarwal, "Oxidative bromination of salicylaldehyde by potassium bromide / H_2O_2 catalysed by dioxovanadium(V) complexes encapsulated in zeolite–Y: A functional model of haloperoxidases", Catal. Commun., 5, 563–568, 2004.

61. A Butler, "Mechanistic considerations of the vanadium haloperoxidases", Coord. Chem. Rev., 187, 17 – 35, 1999.

62. Vanadium compounds: Chemistry, biochemistry and therapeutic applications, (Eds. V. L. Pecoraro, C. Slebodnick, B. Hamstra, D. C. Crans and A. S. Tracy), ACS Symposium Series, Ch. 12. 1998.

63. M.R. Maurya, A. Kumara, P. Manikandanb and S. Chand, "Synthesis, characterisation and catalytic potential of oxovanadium(IV) based coordination polymers having a bridging methylene group", Appl. Catal. A: Gen., 277, 45–53, 2004.

64. M. R. Maurya, S. Sikarwar, T. Joseph, P. Manikandan and S. B. Halligudi, Synthesis, "Characterisation and catalytic potentials of polymer anchored copper(II), oxovanadium(IV) and dioxomolybdenum(VI) complexes 2-(-hydroxymethyl)benzimidazole", React. Funct. Polymer, 63, 71 – 83, 2005.

65. R. Ando, T. Yagyu and M. Maeda, "Characterization of oxovanadium(IV)–Schiff–base complexes and those bound on resin, and their use in sulfide oxidation", Inorg. Chim. Acta, 357, 2237 – 2244, 2004.

66. R. Ando, S. Mori, M. Hayashi, T. Yagyu and M. Maeda, "Structural characterization of pentadentate salen–type Schiff–base complexes of oxovanadium(IV) and their use in sulfide oxidation", Inorg. Chim. Acta, 357, 1177 – 1184, 2004.

67. R. Ando, H. Inden, M. Sugino, H. Ono, D. Sakaeda, T. Yagyu and M. Maeda, "Spectroscopic characterization of amino acid and amino acid ester–Schiff–base complexes of oxovanadium and their catalysis in sulfide oxidation", Inorg. Chim. Acta, 357, 1337 – 1344, 2004.

68. Q. Zeng, W. Weng and X. Xue, "Sulfide oxidation catalyzed vanadyl complexes of N-salicylidene a-amino acids at low catalyst loading", Inorg. Chim. Acta, 388, 11–15, 2012.

69. V. Conte, A. Coletti, B. Floris, G. Licini and C. Zonta, "Mechanistic aspects of vanadium catalysed oxidations with peroxides", Coord. Chem. Rev., 255, 2165– 2177, 2011.

70. D. W. Christianson, "Structural chemistry and biology of manganese metalloenzymes", Prog. Biophys. Molec. Biol. 67, 217–252, 1997.

71. Y. Kono and I. Fridovich, "Isolation and characterization of the pseudocatalase of Lactobacillus plantarum. A new manganese-containing enzyme", J. Biol. Chem. 258, 6015–6019, 1983.

72. W. F. Beyer Jr. and I. Fridovich, "Pseudocatalase from Lactobacillus plantarum: evidence for a homopentameric structure containing two atoms of manganese per subunit", Biochemistry 24, 6460–6467, 1985.

73. V. V. Barynin, P. D. Hempstead, A. A. Vagin, S. V. Lamzin, P. M. Harrison and P. J. Artymyuk, "The three-dimensional structure of the di-Mn catalase, and the environment of the di-Mn sites in different redox states", J. Inorg. Biochem. 67, 196, 1997.

74. G. S. Allgood and J. J. Perry, "Characterization of a manganese-containing catalase from the obligate thermophile Thermoleophilum album", J. Bacteriol. 168, 563–567, 1986.

75. G. C. Dismu, "The Organization and Function of Manganese in the Water-Oxidizing Complex of Photosynthesis", Academic: New York, Chapter 16, p 275, 1986.

76. J. D. Crowley, D. A. Traynor and D. C. Watherburn, "Manganese and its role in biological processes", Vol. 37, Marcel Dekker,Inc., New York, 2000.

77. R. Hage, "Oxidation catalysis by biomimetic manganese complexes", Recl. Trav. Chim. Pays-Bas, 115, 385–395, 1996.

78. T. Katsuki, "Catalytic asymmetric oxidations using optically active (salen)manganese(III) complexes as catalysts", Coord. Chem. Rev, 140, 189–214, 1995.

79. E. N. Jacobsen, "Asymmetric catalytic epoxidation of unfunctionalized olefins", in Catalytic Asymmetric Synthesis, Ed., I. Ojima, VCH: New York, p.159, 1993.

80. E. N. Jacobsen, "Transition metal-catalysed oxidations: Asymmetric epoxidations", in Comprehensive Organometallic Chemistry II, Eds. E.W. Abel, F.G.A. Stone and G. Wilkinson, Pergamon: New York, Vol. 12, p. 1097, 1995.

81. N. A. Law, M. T. Caudle and V. L. Pecoraro, "Manganese redox enzymes and model systems: properties, structures, and reactivity", Adv. Inorg. Chem. 46, 305–440, 1998.

82. L. Canali and D. C. Sherrington, "Utilisation of homogeneous and supported chiral metal(salen) complexes in asymmetric catalysis", Chem. Soc. Rev. 28, 85 – 93, 1999.

83. M. Maneiro, M.R. Bermejo, M. I. Fernández, E. Gómez-Fórneas, A. M. González-Noya and A. M. Tyryshkin, "A new type of manganese-Schiff base complex, catalysts for the disproportionation of hydrogen peroxide as peroxidase mimics", New J. Chem. 27, 727–733, 2003.

84. M. R. Maurya, P. Saini, C. Haldar and F. Avecilla, "Synthesis, characterisation and catalytic activities of manganese (III) complexes of pyridoxal-based ONNO donor tetradenatate ligands", Polyhedron, 31, 710–720, 2012.

85. A. P. A. Ganeshpure, G.L. Tembe and S. Satish, "Oxidation of cyclohexane by tert-butylhydroperoxide catalyzed by manganese(II) N,N'-ethylene bis(salicylideneaminato) and analogous complexes", J. Mol. Catal. A: Chem., 113, L423–L425, 1996.

86. P. Das, I. Kúzniarska-Biernacka, A. R. Silva, A. P. Carvalho, J. Pires and C. Freire, "Encapsulation of chiral Mn(III) salen complexes into aluminium pillared clays: Application as heterogeneous catalysts in the epoxidation of styrene", J. Mol. Catal. A: Chem., 248, 135–143, 2006.

87. A. Berkessel, M. Frauenkron, T. Schwenkreis, A. Steinmetz, G. Baum and D. Fenske, "Pentacoordinated manganesec (III) dihydrosalen complexes as biomimetic oxidation catalysts", J. Mol. Catal. A: Chem., 113, 321–342, 1996.

88. A. Guha, K. S. Banu, A. Banerjee, T. Ghosh, S. Bhattacharya, E. Zangrando and D. Das, "Bio-relevant manganese(II) compartmental ligand complexes: Syntheses, crystal structures and studies of catalytic activities", J. Mol. Catal. A: Chem., 338, 51–57, 2011.

89. C. Lu, Z. Fu, Y. Liu, F. Liu, Y. Wu, J. Qin, X. He and D. Yin, "A moderate and efficient method for oxidation of ethylbenzene with hydrogenperoxide catalyzed by 8-quinolinolato manganese(III) complexes", J. Mol. Catal. A: Chem., 331, 106–111, 2010.

90. M. Cavazzini, G. Pozzi, S. Quici and I. Shepperson, "Fluorous biphasic oxidation of sulfides catalysed by (salen)manganese(III) complexes", J. Mol. Catal. A: Chem., 204–205, 433–441, 2003.

91. S. Tangestaninejad, M. Moghadam, V. Mirkhani, I. Mohammadpoor-Baltork and M.S. Saeedi, "Efficient epoxidation of alkenes with sodium periodate catalyzed by reusable manganese(III) salophen supported on multi-wall carbon nanotubes", Appl. Catal. A: Gen., 381, 233–241, 2010.

92. F. Bedioui, "Zeolite-encapsulated and clay-intercalated metal prophyrin, phtahlocyanine and Schiff-base complexes as models for biomimetic oxidation catalysts: An overview", Coord. Chem. Rev., 144, 39 – 68, 1995.

93. K. J. Balkus Jr. and A. G. Gabrielov, "Zeolite encapsulated metal complexes", J. Incl. Phenom. Mol. Recog. Chem., 21, 159 – 184, 1995.

94. S. P. Verkey, C. Ratnasamy and P. Ratnasamy, "Zeolite-encapsulated manganese(III) salen complexes", J. Mol. Catal. A: Chem., 135, 295 – 306, 1998.

95. S. P. Verkey, C. Ratnasamy and P. Ratnasamy, "Selective oxidation over copper and manganese salens encapsulated in zeolites", Micropor. Mesopor. Mater, 22, 465 – 474, 1998.

96. S. P. Verkey, C. Ratnasamy and P. Ratnasamy, "Oxidation of p-xylene over zeolite-encapsulated copper and manganese complexes", Appl. Catal. A: Gen., 182, 91 – 96, 1999.

97. S. Deshpande, D. Srinivas and P. Ratnasamy, "EPR and catalytic investigation of Cu(salen) complexes encapsulated in zeolites" J. Catal., 188, 261 – 269, 1999.

98. S. Chavan, D. Srinivas and P. Ratnasamy, "Structure and catalytic properties of dimeric copper(II) acetate complexes encapsulated in zeolite-Y", J. Catal., 192, 286 – 295, 2000.

99. S. A. Chavan, D. Srinivas and P. Ratnasamy, "Selective oxidation of para-xylene to terephthalic acid by μ_3-oxo-bridged Co/Mn cluster complexes encapsulated in zeolite-Y", J. Catal., 204, 409 – 419, 2001.

100. C. R. Jacob, S. P. Varkey and P. Ratnasamy, "Zeolite-encapsulated copper (X_2-salen) complexes", Appl. Catal. A: Gen., 168, 353– 364, 1998.

101. C. R. Jacob, S. P. Varkey and P. Ratnasamy, "Selective oxidation over copper and manganese salens encapsulated in zeolites", Microporous Mesoporous Mat., 22, 465– 474, 1998.

102. K. J. Balkus Jr., A. K. Khanmamedova, K. M. Dixon and F. Bedioui, "Oxidations catalyzed by zeolite ship-in-a-bottle complexes", Appl. Catal. A: Gen., 143, 159– 173, 1996.

103. M. R. Maurya, M. Kumar, S. J. J. Titinchi, H. S. Abbo and S. Chand, "Oxovanadium (IV) Schiff base complexes encapsulated in zeolite-Y as catalyst for the liquid phase hydroxylation of phenol", Catal. Lett., 86, 97– 105, 2003.

104. V. K. Bansal, P. P. Thankachan and R. Prasad, "Oxidation of benzyl alcohol and styrene using H_2O_2 catalyzed by tetraazamacrocycle complexes of Cu(II) and Ni(II) encapsulated in zeolite-Y" , Appl. Catal. A: Gen., 381, 8–17, 2010.

105. M. S. Niasari and A. Sobhani, "Ship-in-a-bottle synthesis, characterization and catalytic oxidation of cyclohexane by Host (nanopores of zeolite-Y)/guest (Mn(II), Co(II), Ni(II) and Cu(II) complexes of bis(salicyaldehyde)oxaloyldihydrazone) nanocomposite materials", J. Mol. Catal. A: Chem., 285, 58–67, 2008.

106. K. K. M. Yusuff and J. Mathew, "Ascorbic acid oxidation by a new zeolite encapsulated copper(II) complex", Indian J. Chem., 36A, 303–306, 1997.

107. T. H Bennur, D. Srinivas and S. Sivasanker, "Oxidation of ethylbenzene over "neat" and zeolite-Y encapsulated copper tri- and tetraaza macrocyclic complexes", J. Mol. Catal. A: Gen., 207, 163–171, 2004.

108. A. Butler and C. J. Carrano, "Coordination chemistry of vanadium in biological systems", Coord. Chem. Rev., 109, 61–105, 1991.

109. A. Butler, M. J. Clague and G.E. Meister, "Vanadium Peroxide Complexes", Chem. Rev., 94, 625–638, 1994.

110. D. Gambino, "Potentiality of vanadium compounds as anti-parasitic agents", Coord. Chem. Rev., 255, 2193– 2203, 2011.

111. V. Conte and B. Floris, "Vanadium catalyzed oxidation with hydrogen peroxide", Inorg. Chim. Acta., 363, 1935–1946, 2010.

112. V. Conte, A. Coletti, B. Floris, G. Licini and C. Zonta, "Mechanistic aspects of vanadium catalyzed oxidations with peroxides", Coord. Chem. Rev. 255, 2165–2177, 2011.

113. J. A. L. da Silva, J. J. R. Fraústo da Silva and A. J. L. Pombeiro, "Oxovanadium complexes in catalytic oxidations", Coord. Chem. Rev., 255, 2232–2248, 2011.

114. M. R. Maurya and J. Costa Pessoa, "Polymer-bound metal complexes as catalysts: Synthesis, characterization, reactivity and catalytic activity in E-H bond activation", J. Organomet. Chem., 696, 244–254, 2011.

115. I. Correia, S. Aksu, P. Adão, J. Costa Pessoa, R. A. Sheldon, and I. W. C. E. Arends, "Vanadate substituted phytase: Immobilization, structural characterization and performance for sulfoxidations", J. Inorg. Biochem., 102, 318–329, 2008.

116. V. Vergopoulos, W. Priebsch, M. Fritzsche and D. Rehder, "Binding of L-histidine to vanadium. Structure of exo-[VO_2{N-(2-oxidonaphthal)-His}]", Inorg. Chem. 32, 1844–1849, 1993.

117. L. J. Calviou, J. M. Arber, D. Collison, C. D. Garner and W. Clegg, "A structural model for vanadyl-histidine interactions: structure determination of [VO(1-vinylimidazole)$_4$Cl]Cl by a combination of x-ray crystallography and x-ray absorption spectroscopy", J. Chem. Soc., Chem. Commun., 654–656, 1992.

118. A. D. Keramidas, S. M. Miller, O. P. Anderson and D. C. Crans, "Vanadium(V) Hydroxylamido Complexes: Solid State and Solution Properties", J. Am. Chem. Soc., 119, 8901–8915, 1997.

119. S. Samanta, S. K. Dutta and M. Chaudhury, "Utilization of LVO2- species (L2- is a tridentate ONS donor) as an inorganic analogue of carboxylate group: a journey to a new domain of coordination chemistry", J. Chem. Sci., 118, 475–486, 2006.

120. S. K. Dutta, S. Samanta, S. Mukhopadhyay, P. Burckel, A. A. Pinkerton and M. Chaudhury, "Spontaneous Assembly of a Polymeric Helicate of Sodium with LVO_2 Units Forming the Strand: Photoinduced Transformation into a Mixed-Valence Product", Inorg. Chem., 41, 2946–2952, 2002.

121. S. Samanta, D. Ghosh, S. Mukhopadhyay, A. Endo, T. J. R. Weakley and M. Chaudhury, "Oxovanadium(IV) and -(V) Complexes of Dithiocarbazate-Based Tridentate Schiff Base Ligands: Syntheses, Structure, and Photochemical Reactivity of Compounds Involving Imidazole Derivatives as Coligands", Inorg. Chem., 42, 1508–1517, 2003.

122. S. Rayati, N. Sadeghzadeh and H. R. Khavasi, "A new di-μ-oxo bis[oxovanadium(V)] complex containing Schiff base ligand derived from 1,2-diaminopropane and 2'-hydroxy-4'-methoxyacetophenone: Synthesis, structure and catalytic properties", Inorg. Chem. Commun., 10, 1545–1548, 2007.

123. S. Rayati, N. Torabi, M. Koliaei, F. Ashouri, S. Mohebbi, A. Wojtczak and A. Kozakiewicz, "Oxovanadium(IV) Schiff base complexes derived from 2,2'-dimethylpropandiamine: A homogeneous catalyst for cyclooctene and styrene oxidation", Appl. Catal. A: Gen., 346, 65–71, 2008.

124. S. Rayati, N. Torabi, A. Ghaemi, S. Mohebbi, A. Wojtczak and A. Kozakiewicz, "Vanadyl tetradentate Schiff base complexes as catalyst for C-H bond activation of olefins with tert-butylhydroperoxide: Synthesis, characterization and structure", Inorg. Chim. Acta, 361, 1239–1248, 2008.

125. S. Mohebbi, D.M. Boghaei, A.H. Sarvestani and A. Salimi, "Oxovanadium(IV) complexes as homogeneous catalyst - aerobic epoxidation of olefins", Appl. Catal. A: Gen., 278, 263–267, 2005.

126. M. R. Maurya, A. K. Chandrakar and S. Chand, "Oxovanadium(IV) and copper(II) complexes of 1,2-diaminocyclohexane based ligand encapsulated in zeolite-Y for the catalytic oxidation of styrene, cyclohexene and cyclohexane", J. Mol. Catal. A: Chem., 270, 225–235, 2007.

127. M. R. Maurya, A. Arya, U. Kumar, A. Kumar, F. Avecilla and J. Costa Pessoa, "Polymer-bound oxidovanadium(IV) and dioxidovanadium(V) complexes: synthesis, characterization and catalytic application for the hydroamination of styrene and vinyl pyridine", Dalton Trans., 9555 – 9566, 2009.

128. M. R. Maurya, S. Sikarwar and P. Manikandan, "Oxovanadium(IV) complex of 2-(α-hydroxyethyl)benzimidazole covalently bonded to chloromethylated polystyrene for oxidation of benzoin", Appl. Catal. A: Gen., 315, 74–82, 2006.

129. A. A. Khan, Ph. D. Thesis, "Synthesis, characterisation and potential application of vanadium complexes" Indian Institute of Technology Roorkee, Roorkee, India, 2010.

130. M. A. Ali and M. T. H. Tarafder, "Metal complexes of sulfur and nitrogen-containing ligands: complexes of S-benzyldithiocarbazate and a Schiff base

formed by its condensation with pyridine-2-carboxaldehyde", J. Inorg. Nucl. Chem., 39, 1785–1791, 1977.

131. M. Das and S.E. Livingstone, "Metal chelates of dithiocarbazic acid and its derivatives. IX. Metal chelates of ten new Schiff bases derived from S-methyldithiocarbazate" , Inorg. Chim. Acta, 19, 5–10, 1976.

132. C. S. Marvel and N. Tarkoy, "Heat-stability studies on chelates from Schiff bases of salicylaldehyde derivatives", J. Am. Chem. Soc., 79, 6000–6002, 1957.

133. M. R. Maurya, D. C. Antony, S. Gopinathan and C. Gopinathan, "Binuclear dioxomolybdenum(VI) complexes of flexibly-bridged hexadentate tetraanionic Schiff's bases derived from methylene- or dithio-bis(salicylaldehyde) and S-methyldithiocarbazate or S-benzyldithiocarbazate", Bull. Chem. Soc. Japan, 68, 554–565, 1995.

134. A. Rockenbauer and L. Korecz, "Automatic computer simulations of ESR spectra", Appl. Magn. Reson., 10, 29–43, 1996.

135. M. R. Maurya, S. Khurana, Shailendra, A. Azam, W. Zhang and D. Rehder, "Synthesis, characterisation and antiamoebic studies of dioxovanadium(V) complexes containing ONS donor ligands derived from S-benzyldithiocarbazate" , Eur. J. Inorg. Chem., 1966–1973, 2003.

136. M. R. Maurya, S. Agarwal, C. Bader and D. Rehder, "Dioxovanadium(V) complexes of ONO donor ligands derived from pyridoxal and hydrazides: Models of vanadate-dependent haloperoxidases", Eur. J. Inorg. Chem., 147–157, 2005.

137. M. R. Maurya, S. Khurana, W. Zhang and D. Rehder, "Vanadium(IV/V) complexes containing $[VO]^{2+}$, $[VO]^{3+}$, $[VO_2]^{+}$ and $[VO(O_2)]$+ cores with ligands derived from 2-acetylpyridine and S-benzyl- or S-methyldithiocarbazate", Eur. J. Inorg. Chem., 1749–1760, 2002.

138. K. Wüthrich, "E.S.R. (electron spin resonance) investigation of VO^{2+} complex compounds in aqueous solution. II", Helv. Chim. Acta, 48, 1012–1017, 1965.

139. A. J. Tasiopoulos, A. N. Troganis, A. Evangelou, C. P. Raptopoulou, A. Terzis, Y. Deligiannakis and T. A. Kabanos, "Synthetic analogs for oxovanadium(IV) - glutathione interaction: an EPR, synthetic and structural study of oxovanadium(IV) compounds with sulfhydryl-containing pseudopeptides and dipeptides", Chem. Eur. J., 5, 910–921, 1999.

140. I. Cavaco, J. Costa Pessoa, M. T. Duarte, R. T. Henriques, P. M. Matias and R. D. Gillard, "Crystal and molecular structure of $[V_2O_3(sal\text{-}L\text{-}val)_2(H_2O)]$ (sal-L-val = N-salicylidene-L-valinate) and spectroscopic properties of related complexes", J. Chem. Soc. Dalton Trans., 1989–1996, 1996.

141. J. Costa Pessoa, I. Cavaco, I. Correia, D. Costa, R.T. Henriques and R. D. Gillard, "Preparation and characterisation of new oxovanadium(IV) Schiff base complexes derived from salicylaldehyde and simple dipeptides", Inorg. Chim. Acta, 305, 7–13, 2000.

142. M. R. Maurya and A. Kumar, "Oxovanadium(IV) based coordination polymers and their catalytic potentials for the oxidation of styrene, cyclohexene and trans-stilbene", J. Mol. Catal. A: Chem., 250, 190–198, 2006.

143. D. Rehder, G. Santoni, G. M. Licini, C. Schulzke and B. Meier, "The medicinal and catalytic potential of model complexes of vanadate-dependent haloperoxidases", Coord. Chem. Rev., 237, 53–63, 2003.

144. M. R. Maurya, M. Kumar, A. Kumar and J. Costa Pessoa, "Oxidation of p-chlorotoluene and cyclohexene catalysed by polymer-anchored oxovanadium(IV) and copper(II) complexes of amino acid derived tridentate ligand", Dalton Trans., 4220–4232, 2008.

145. M. R. Maurya, U. Kumar and P. Manikandan, "Synthesis and characterisation of polymer-anchored oxidovanadium(IV) complexes and their use for the oxidation of styrene and cumene", Eur. J. Inorg. Chem., 2303–2314, 2007.

146. B. J. Hamstra, G. J. Colpas and V. L. Pecoraro, "Reactivity of Dioxovanadium(V) Complexes with Hydrogen Peroxide: Implications for Vanadium Haloperoxidase", Inorg. Chem., 37, 949–955, 1998.

147. I. Cavaco, J. Costa Pessoa, M. T. Duarte, R. T. Henriques, P. M. Matias and R. D. Gillard, "Crystal and molecular structure of $[V_2O_3(sal\text{-}L\text{-}val)_2(H_2O)]$ (sal-L-val = N-salicylidene-L-valinate) and spectroscopic properties of related complexes", J. Chem. Soc. Dalton Trans., 1989–1996, 1996.

148. J. Costa Pessoa, I. Cavaco, I. Correia, D. Costa, R.T. Henriques and R.D. Gillard, "Preparation and characterisation of new oxovanadium(IV) Schiff base complexes derived from salicylaldehyde and simple dipeptides", Inorg. Chim. Acta, 305, 7–13, 2000.

149. I. Cavaco, J. Costa Pessoa, S. Luz, M. T. L. Duarte, P. M. Matias, R. T. Henriques and R. D. Gillard, "N-Salicylideneamino-acidate complexes of

oxovanadium(IV)-II. Synthesis, characterization and deamination of an N-salicylideneglycylglycinato complex", Polyhedron, 14, 429–439, 1995.

150. M. R. Maurya, A. K. Chandrakar and S. Chand, "Oxidation of phenol, styrene and methyl phenyl sulfide with H2O2 catalyzed by dioxovanadium(V) and copper(II) complexes of 2-aminomethylbenzimidazole-based ligand encapsulated in zeolite-Y", J. Mol.Catal. A: Chem., 263(1-2), 227–237, 2007.

151. M. R. Maurya, U. Kumar, I. Correia, P. Adão and J. Costa Pessoa, "A polymer-bound oxidovanadium(IV) complex prepared from an L-cysteine-derived ligand for the oxidative amination of styrene", Eur. J. Inorg. Chem., 577–587, 2008.

152. K. Fukui, H. Ohya-Nishiguchi and H. Kamada, "Electron Spin-Echo Envelope Modulation Study of Imidazole-Coordinated Oxovanadium(IV) Complexes Relevant to the Active Site Structure of Reduced Vanadium Haloperoxidases", Inorg. Chem., 37, 2326–2327, 1998.

153. D. C. Crans, J. J. Smee, E. Gaidamauskas and L. Yang, "The Chemistry and Biochemistry of Vanadium and the Biological Activities Exerted by Vanadium Compounds", Chem. Rev., 104, 849–902, 2004.

154. M. J. Clague, N. L. Keder and A. Butler, "Biomimics of vanadium bromoperoxidase: Vanadium (V)-Schiff base catalyzed oxidation of bromide by hydrogen peroxide", Inorg. Chem., 32, 4754–4761, 1993.

155. G. Zampella, P. Fantucci, V. L. Pecoraro and L. De Gioia, "Reactivity of Peroxo Forms of the Vanadium Haloperoxidase Cofactor. A DFT Investigation", J. Am. Chem. Soc., 127, 953–960, 2005.

156. O. Bortolini, M. Carraro, V. Conte and S. Moro, "Models for the active site of vanadium-dependent haloperoxidases: insight into the solution structure of peroxo vanadium compounds", J. Inorg. Biochem., 80, 41–49, 2000.

157. J. Littlechild, E. Garcia-Rodriguez, E. Coupe, A. Watts, M. Isupov in Vanadium: The Versatile Metal, (Eds. K. Kustin, J. Costa Pessoa, D.C. Crans), ACS Series Book, 974, 136–147, 2007.

158. O. Bortolini, C. Chiappe, V. Conte and M. Carraro, "Direct synthesis of stable adamantylideneadamantane bromonium salts", Eur. J. Org. Chem., 3237–3239, 1999.

159. P. Adão, M.R. Maurya, U. Kumar, F. Avecilla, R.T. Henriques, M.L. Kusnetsov, J. Cost Pessoa, and I. Correia, "Vanadium-salen and -salan complexes: Characterization and application in oxygentransfer Reaction", Pure Appl. Chem., 81, 1279–1296, 2009.

160. S. K. Dutta, S. Samanta, S. B. Kumar, O. H. Han, P. Burckel, A. A. Pinkerton and M. Chaudhury, "Mixed-Oxidation Divanadium(IV,V) Compound with Ligand Asymmetry: Electronic and Molecular Structure in Solution and in the Solid State", Inorg Chem. 1999, 38, 1982–1988.

161. G. Ambrosi, M. Formica, V. Fusi, L. Giorgi and M. Micheloni, "Polynuclear metal complexes of ligands containing phenolic units", Coord. Chem. Rev., 252, 1121–1152, 2008.

162. A. Mondal, S. Sarkar, D. Chopra, T. N. G. Row, K. Pramanik and K. K. Rajak, "Family of Mixed-Valence Oxovanadium(IV/V) Dinuclear Entities

Incorporating N_4O_3-Coordinating Heptadentate Ligands: Synthesis, Structure, and EPR Spectra", Inorg. Chem. 44, 703–708, 2005.

163. M. R. Maurya, C. Haldar, A. A. Khan, A. Azam, A. Salahuddin, A. Kumar and J. Costa Pessoa, "Synthesis, Characterization, Catalytic and Antiamoebic Activity of Vanadium Complexes of Binucleating Bis(dibasic tridentate ONS donor) Ligand Systems", Eur. J. Inorg. Chem., 15, 2560–2577, 2012.

164. R. A. Rowe and M. M. Jones, "Vanadium (IV) oxy(acetylacetonate)", Inorg. Synth., 5, 113–116, 1957.

165. R. R. Gagne, C. L. Spiro, T. J. Smith, C. A. Hamann, W. R. Thies and A. D. Shiemke, "The synthesis, redox properties, and ligand binding of heterobinuclear transition-metal macrocyclic ligand complexes. Measurement of an apparent delocalization energy in a mixed-valent copper(I)-copper(II) complex", J. Am. Chem. Soc., 103 (14), 4073–4081, 1981.

166. G. M. Sheldrick, SHELXL-97: An Integrated System for Solving and Refining Crystal Structures from Diffraction Data (Revision 4.1); University of Göttingen, Germany, 1997.

167. N. R. Sangeetha, V. Kavita, S. Wocadlo, A. K. Powell and S. Pal, "Vanadium(V) complexes of O,N,O-donor tridentate ligands containing the $\{V^{V}O(OMe)\}^{2+}$ unit: syntheses, structures and properties", J. Coord. Chem., 51, 55–66, 2000.

168. M. Moon, M. Pyo, Y. C. Myoung, C. I. Ahn and M. S. Lah, "Square pyramidal dialkoxo-bound monooxo-vanadium(V) complex and its behavior in solution", Inorg. Chem., 40, 554–557, 2001.

169. W. Plass, A. Pohlmann and H.-P. Yozgatli, "N-salicylidenehydrazides as versatile tridentate ligands for dioxovanadium(V) complexes", J. Inorg. Biochem., 80, 181–183, 2000.

170. D. Wang, M. Ebel, C. Schulzke, C. G□uning, S. K. S. Hazari and D. Rehder, "Vanadium(IV and V) complexes containing SNO (dithiocarbonylhydrazone; thiosemicarbazone) donor sets", Eur. J. Inorg. Chem., 935–942, 2001.

171. H. Schmidt, M. Bashirpoor and D. Rehder, "Structural characterization of possible intermediates in vanadium-catalyzed sulfide oxidation", J. Chem. Soc., Dalton. Trans., 3865–3870, 1996.

172. D. Rehder, C. Weidemann, A. Duch and W. Priebsch, "Vanadium-51 shielding in vanadium(V) complexes: a reference scale for vanadium binding sites in biomolecules", Inorg. Chem., 27, 584–587, 1988.

173. D. Rehder, Transition Metal Nuclear Magnetic Resonance (Ed.: P. S. Pregosin), Elsevier, New York, p. 1, 1991.

174. O. W. Howarth, "Vanadium-51 NMR", Progr. Magn. Reson. Spectrosc., 22(5), 453–485, 1990.

175. K. L. Brown, "Chemistry and Enzymology of Vitamin B_{12}", Chem. Rev., 105, 2075–2149, 2005.

176. F. H. Zelder, C. Buchwalder, R. M. Oetterli and R. Alberto, "One-pot synthesis of the metal-free AD and BC Fragments of Vitamin B_{12}", Chem. Eur. J., 16, 6155–6158, 2010.

177. R. Kumar, K. Mahiya and P. Mathur, "Synthesis, spectral and structural characterization of Cu(II) complexes of a tridentate NNO donor Schiff base carrying a pendant benzimidazolyl arm", Indian J. Chem., 50A, 775 – 780, 2011.

178. D. P. Riley, "Functional mimics of superoxide dismutase enzymes as therapeutic agents", Chem. Rev., 99, 2573–2587, 1999.

179. K. Ghosh, N. Tyagi, P. Kumar, U. P. Singh and N. Goel, "Stabilization of Mn(II) and Mn(III) in mononuclear complexes derived from tridentate ligands with N_2O donors: Synthesis, crystal structure, superoxide dismutase activity and DNA interaction studies", J. Inorg. Biochem., 104, 9–18, 2010.

180. H. Sigel, A. Sigel, in Metal Ions in Biological Systems, (Eds: H. Sigel, A. Sigel), Marcel Dekker, Inc. 2000.

181. G. C. Dismukes, "Manganese Enzymes with Binuclear Active Sites", Chem. Rev., 96, 2909–2926, 1996.

182. M. S. Lah, M. M. Dixon, K. A. Pattridge, W. C. Stallings, J. A. Fee and M. L. Ludwig, "Structure-function in Escherichia coli iron superoxide dismutase: Comparisons with the manganese enzyme from Thermus thermophilus", Biochemistry., 34, 1646–1660, 1995.

183. J. E. Penner-Hahn, "Metal Sites in Proteins and Models", (Eds: H. A. O. Hill, P. J. Sadler, A. J. Thomson), Springer-Verlag, p. 1, 1998.

184. J. Limburg, V. A. Szalai and G. W. Brudvig, "A mechanistic and structural model for the formation and reactivity of a MnV:O species in photosynthetic water oxidation", J. Chem. Soc., Dalton Trans. 1353–1362, 1999.

185. L. A. Ceson and A. R. Day, "Preparation of some benzimidazolylamino acids. Reactions of amino acids with o-phenylenediamines", J. Org. Chem., 27, 581 – 586, 1962.

186. R. L. Dutta, A. Syamal, Elements of Magnetochemistry, Affiliated East-West Press, New Delhi, 2nd edn., p.8, 1993.

187. C. E. Hulme, M. Watkinson, M. Haynes, R. G. Pritchard, C. A. McAuliffe, N. Jaiboon, B. Beagley, A. Sousa, M. R. Bermejo and M. Fondo, "Structurally diverse manganese(III) complexes of tetradentate N_2O_2 Schiff-base ligands with ancillary carboxylate donors", J. Chem. Soc., Dalton Trans., 1805–1814, 1997.

188. S. Biswas, K. Mitra, C. H. Schwalbe, C. R. Lucas, S. K. Chattopadhyay and B. Adhikary, "Synthesis and characterization of some Mn(II) and Mn(III) complexes of N,N'-o-phenylenebis(salicylideneimine) (LH_2) and N,N'-o-phenylenebis(5-bromosalicylideneimine) (L_1H_2). Crystal structures of [Mn(L)(H_2O)(ClO_4)], [Mn(L)(NCS)] and an infinite linear chain of [Mn(L)(OAc)]", Inorg. Chim. Acta., 358, 2473–2481, 2005.

189. M. J. Baldwin, J. W. Kampf, M. L. Kirk and V. L. Pecoraro, "Structural and Magnetic Studies of Manganese(II) Complexes of the Imidazole-Containing Ligand 5-NO_2-salimH [5-NO_2-salimH_2 = 4-(2-((5-nitrosalicylidene)amino)ethyl)imidazole] with Varying Nuclearity", Inorg. Chem., 345252–5260, 1995.

190. L. K. Woo and M. R. Maurya, "Rational design of linear trinuclear metal complexes", Inorganic Chemistry., 30, 4671–4673, 1991.

191. L. J. Boucher and C. G. Coe, "Manganese Schiff base complexes: Synthesis and circular dichroism of optically active tetradentate chelates of manganese(III) and of μ-oxo-μ-hydroxo-dimanganese(III,IV) dimers", Inorg. Chem., 15, 1334–1340, 1976.

192. S. B. Kumar, S. Bhattacharyya, S. K. Dutta, E. T. Tiekink and M. Chaudhury, "Mononuclear manganese(III) complexes of a heterodonor (N_2OS) ligand containing thiolate-type sulfur: synthesis, structure, redox and spectroscopic properties", J. Chem. Soc., Dalton Trans., 16, 2619–2626, 1995.

193. J. Lin, C. Tu, H. Lin, P. Jiang, J. Ding and Z. Guo, "Crystal structure and superoxide dismutase activity of a six-coordinate manganese(III) complex", Inorg. Chem. Commun., 6, 262–265, 2003.

194. P. P. Knops-Gerrits, D. E. de Vos and P. A. Jacobs, "Oxidation catalysis with semi-inorganic zeolite-based Mn catalysts", J. Mol. Catal. A: Chem., 117, 57–70, 1997.

195. K. Srinivasan, S. Perrier and J. K. Kochi, "Dual pathways for manganese catalysis of olefin oxidation with alkyl hydroperoxides", J. Mol. Catal., 36, 297–317, 1986.

196. R. Vicente, A. Escuer, E. Peñalba, X. Solans and M. Font-Bardía, "Synthesis and crystal structure determination of a one-dimensional end-to-end cyanate-bridged copper(II) compound", J. Chem. Soc. Dalton Trans., 3005–3008, 1994.

197. A. Escuer, M. Font-Bardia, E. Penñalba, X. Solans and R. Vicente, "Versatility of the cyanato ligand: structure and magnetic properties of four new copper(II)-cyanato compounds derived from tridentate amines", Inorg. Chim. Acta., 286, 189–196, 1999.

198. C. R. Choudhury,S. K. Dey, R. Karmakar, C.-D. Wu, C.-Z. Lu, M.S. El Fallah and S. Mitra. "First report of singly phenoxo-bridged copper(II) dimeric complexes: synthesis, crystal structure and low-temperature magnetic behaviour study", New J. Chem., 27, 1360–1366, 2003.

199. P. Talukder, A. Datta, S. Mitra, G. Rosair, M.S. El Fallah and J. Ribas. "End-to-end single cyanato and thiocyanato bridged Cu(II) polymers with a new tridentate Schiff base ligand: Crystal structure and magnetic properties", Dalton Trans., 4161–4167, 2004.

200. S. K. Dey, N. Mondal, M. S. El Fallah, R. Vicente, A. Escuer, X. Solans, M. Font-Bardía, T. Matsushita, V. Gramlich and S. Mitra, "Crystal Structure and Magnetic Interactions in Nickel(II) Dibridged Complexes Formed by Two Azide Groups or by Both Phenolate Oxygen-Azide, -Thiocyanate, -Carboxylate, or -Cyanate Groups", Inorg. Chem., 43, 2427–2434, 2004.

201. S. Sen, P. Talukder, S. K. Dey, S. Mitra, G. Rosair, D. L. Hughes, G. P. A. Yap, G. Pilet, V. Gramlich and T. Matsushita, "Ligating properties of a potentially tetradentate Schiff base $[(CH_3)_2NCH_2CH_2N{:}CHC_6H_3(OH)(OMe)]$ with zinc(II), cadmium(II), cobalt(II), cobalt(III) and manganese(III) ions: synthesis and structural studies", Dalton Trans., 1758–1767, 2006.

202. S. Basak, S. Sen, S. Banerjee, S. Mitra, G. Rosair and M. T. G. Rodríguez, "Three new pseudohalide bridged dinuclear Zn(II) Schiff base complexes: Synthesis, crystal structures and fluorescence studies.", Polyhedron, 26, 5104–5112, 2007.

203. S. Basak, S. Sen, C. Marschner, J. Baumgartner, S. R. Batten, D. R. Turner and S. Mitra, "Synthesis, crystal structures and fluorescence properties of two new di- and polynuclear Cd(II) complexes with N_2O donor set of a tridentate Schiff base ligand", Polyhedron, 27, 1193–1200, 2008.

204. J. M. Fraile, J. I. Garcia and J. A. Mayoral, "Basic solids in the oxidation of organic compounds", Catal. Today, 57, 3-16, 2000.

205. R. A. Sheldon, I. W. C. E. Arends and A. Dijksman, "New developments in catalytic alcohol oxidations for fine chemical synthesis", Catal. Today, 57, 157–166, 2000.

206. G. J. Hutchings, "New approaches to rate enhancement in heterogeneous catalysis", Chem. Commun., 301–306, 1999.

207. M. R. Maurya, S. J. J. Titinchi and S. Chand, "Catalytic activity of chromium(III), iron(III) and bismuth(III) complexes of 1,2-bis(2-hydroxybenzamido)ethane (H_2hybe) encapsulated in zeolite-Y for liquid phase hydroxylation of phenol", J. Mol. Catal. A: Chem., 214, 257-264, 2004.

208. J. P. M. Lommerse, A. J. Stone, R. Taylor and F.H. Allen, "The Nature and Geometry of Intermolecular Interactions between Halogens and Oxygen or Nitrogen", J. Am. Chem. Soc., 118, 3108–3116, 1996.

209. P. Chutia, S. Kato, T. Kojima and S. Satokawa, "Synthesis and characterization of Co(II) and Cu(II) supported complexes of 2-pyrazinecarboxylic acid for cyclohexene oxidation", Polyhedron, 28, 370–380, 2009.

210. M. R. Maurya, A. K. Chandrakar and S. Chand, "Zeolite-Y encapsulated metal complexes of oxovanadium(VI), copper(II) and nickel(II) as catalyst for the oxidation of styrene, cyclohexane and methyl phenyl sulfide", J. Mol. Catal. A: Chem., 274, 192–201, 2007.

211. I. Kuźniarska-Biernacka, K. Biernacki, A.L. Magalhães, A.M. Fonseca and I.C. Neves, "Catalytic behavior of 1-(2-pyridylazo)-2-naphthol transition metal complexes encapsulated in Y zeolite", J. Catal., 278, 102–110, 2011.

212. R. Raja and P. Ratnasamy, "Selective oxidation with copper complexes incorporated in molecular sieves", Stud. Surf. Sci. Catal.,101, 181–190, 1996.

213. S. Seelan, A. K. Sinha, D. Srinivas, S. Sivasanker, "Hydroxylation of phenol with H_2O_2 catalyzed by metal phthalocyanine complexes encapsulated in zeolite-Y" Bull. Catal. Soc. India, 1, 29–37, 2002.

214. M. R. Maurya, S. J. J. Titinchi and S. Chand, "Spectroscopic and catalytic activity study of N,N'-bis(salicylidene)propane-1,3-diamine copper(II) encapsulated in zeolite-Y", Appl. Catal. A: Gen., 228, 177–187, 2002.

215. M. R. Maurya, S. J. J. Titinchi and S. Chand, "Oxidation of phenol with H_2O_2 catalyzed by Cu(II), Ni(II) and Zn(II) complexes of N,N'-bis(salicylidene)diethylenetriamine (H_2saldien) encapsulated in Y-zeolite", J. Mol. Catal. A: Chem., 201, 119–130, 2003.

216. M. R. Maurya, H. Saklani, A. Kumar and S. Chand, "Dioxovanadium(V) Complexes of Dibasic Tridentate Ligands Encapsulated in Zeolite-Y for the Liquid Phase Catalytic Hydroxylation of Phenol Using H_2O_2 as Oxidant", Catal. Lett., 93, 121–127, 2004.

217. E. I. Solomon, P. Chen, M. Metz, S.-K. Lee and A. E. Palner, "Oxygen binding, activation, and reduction to water by copper proteins", Angew. Chem. Int. Ed., 40, 4570–4590, 2001.

218. J. P. Klinman, "Mechanisms Whereby Mononuclear Copper Proteins Functionalize Organic Substrates", Chem. Rev., 96, 2541–2561, 1996.

219. K. D. Karlin, J. C. Hayes, Y. Gultneh, R. W. Cruse, J. W. McKown, J. P. Hutchinson and J. Zubieta, "Copper-mediated hydroxylation of an arene: model system for the action of copper monooxygenases. Structures of a binuclear copper(I) complex and its oxygenated product", J. Am. Chem. Soc., 106, 2121–2128, 1984.

Summary & Conclusion

In the active center of vanadate-dependent haloperoxidases (VHPO) vanadium is in a trigonal-bipyramidal environment where it is covalently linked to three non-protein oxo groups in the equatorial plane, to the protein back bone through N_ε of an imidazole moiety of a proximal histidine, and to an axial OH group *trans* to the histidine, further hydrogen bonded to a distal (catalytic) histidine and water molecules. The binucleating hydrazones, $CH_2(H_2sal\text{-}sbdt)_2$ (**2.I**) and $CH_2(H_2sal\text{-}smdt)_2$ (**2.II**) derived from 5,5'-methylenebis(salicylaldehyde) [$CH_2(Hsal)_2$] and S-benzyldithiocarbazate or S-methyldithiocarbazate form $V^{IV}O$- and $V^{V}O_2$-complexes. The complexes are binuclear in the solid state as well as in solution, but they do not interact to each other and thus present two independent vanadium centers with trigonal bipyramidal structures. The $V^{V}O_2$-complexes partly model the active site of VHPO. These model characters extend to functional similarities, in that they catalyze the oxidative bromination of styrene in the presence of KBr, $HClO_4$ and H_2O_2 in biphasic aqueous/ CH_2Cl_2 solution. The formation of several intermediate species namely $[CH_2\{V^{V}O(O_2)(L)\}_2]^{2-}$ and $[CH_2\{V^{V}O(OH)(L)\}_2]$ were established, some of them probably being involved in a the catalytic processes studied. On addition of acid (HCl) the V^{V} species present are partly reduced/ hydrolysed, yielding several species, namely the oxidohydroxido complex.

The binucleating hydrazones [$H_3dfmp(inh)_2$ (**3.I**), $H_3dfmp(nah)_2$ (**3.II**) and $H_3dfmp(bhz)_2$ (**3.III**); inh = isonicotinoylhydrazide, nah = nicotinoylhydrazide and bhz = benzoylhydrazide] provide only mononuclear $V^{IV}O$-, $V^{V}O$- and $V^{V}O_2$-complexes. Theoretical studies clearly show that more electron density lies in only one of the arms. Hence, vanadium ion preferentially binds to that coordinating arm which has more electron cloud while other arm remains silent. The isolated complexes with these ligands have very interesting reactivity. Oxidovanadium(IV) complexes oxidizes in methanol slowly and gives oxidomethoxidovanadium(V) complexes of the type [VO(OMe)(MeOH)L] (where L = ligand). In the molecular structure of $[V^{V}O(OMe)\{Hdfmp(bhz)_2\}(MeOH)]$, the vanadium center adopts a

distorted six-coordinated octahedral geometry with the ($Hdfmp(bhz)_2$) ligand coordinated through the one $O_{hydroxyl}$, one $N_{hydrazone}$, and one O_{keto} atoms; the oxo and, two oxygen (one of methoxy group and one of methanol group) atoms complete the coordination sphere. The presence of additional coordination site in inh based ligand results in the formation of polynuclear dioxidovanadium complex $[V^VO_2\{H_2dfmp(inh)_2\}]$ where pyridinic nitrogen from second ligand participates in coordination with vanadium while pyridinic nitrogen of first ligand is simply protonated. Ligand $H_3dfmp(nah)_2$ **(3.II)** has no effect of having addition functional group and behaves similar to that of $H_3dfmp(bhz)_2$ **(3.III)**. These V^VO- and V^VO_2-complexes also catalyze the oxidative bromination of sryrene.

Synthesis of coordination compounds has further been extended to manganese with the idea if they would serve good functional models of haloperoxidases. While complex $[Mn^{III}(sal\text{-}aebmz)_2]ClO_4$ (where Hsal-aebmz is a Schiff base derived from salicylaldehyde and 2-aminoethylbenzimidazole) is the expected one, complex $[Mn^{III}(sal\text{-}aebmz\text{-}H)(sal\text{-}aebmz)]$ is a neutral species stabilized, in the solid state, through inter molecular hydrogen bonding between NH groups of the two benzimidazole moieties after losing one of the hydrogen atoms. However, their behaviors in solution are similar. Complex $[Mn^{III}(sal\text{-}aebmz\text{-}H)(sal\text{-}aebmz)]$ is shown to be a functional mimic of vanadium-dependent haloperoxidases and satisfactorily catalyses the oxidative bromination of styrene where the selectivity of the products follows the order: 1-phenylethane-1,2-diol > 2-bromo-1-phenylethane-1-ol > 1,2-dibromo-1-phenylethane.

At the end, looking at the importance of zeolite-Y encapsulated metal complexes (ZEMC) where these complexes are suggested as model compounds for enzyme mimicking, copper(II) complex has been prepared and encapsulated in the cavity of zeolite-Y to study its catalytic activity. Thus complex $[Cu^{II}(hap\text{-}aebmz)Cl]$ (where Hhap-aebmz is a Schiff base derived from *o*-hydroxyacetophenone and 2-aminoethylbenzimidazole) has been prepared using Hhap-aebmz, an ONN donor

ligand. Complex [Cu^{II}(hap-aebmz)Cl] has been encapsulated in the cavity of zeolite-Y and its catalytic activity for the oxidation of cyclohexene has been evaluated. Nearly quantitative conversion with the selectivity of different products of the order, 2-cyclohexene-1-ol (44 %) > 2-cyclohexene-1-one (40 %) cyclohexene epoxide (12 %) > cyclohexane-1,2-diol (4%) has been obtained. The recyclability of the catalyst is an added advantage. Oxidation of cyclohexene proceeds through intermediate [(HOO)-Cu^{III}(hap-aebmz)Cl] species, formation of which has been demonstrated by electronic absorption spectroscopy.

Thus, syntheses, characterization, reactivity and catalytic activities of vanadium, manganese and copper complexes presented in the thesis contribute considerably to the existing knowledge.

*****